ALGERICAN DEMOCRATIC AND POPULAR REPUBLIC

MINISTRY OF HIGH EDUCATION AND SCIENTIFIC RESEARCH

UNIVERSITY OF SAAD DAHLAB BLIDA 1

INSTITUTE OF AERONAUTICAL AND SPACE STUDIES

AIRCRAFT CONSTRUCTION DEPARTEMENT

Final study master's dissertation

Option : AIRCRAFT PROPULSION

Theme :

«Numerical simulation of turbulent methane combustion process in can-type combustors »

Realized by:

REMMAL Hamama

Supervised by:

Dr. R. RENANE

Dr. R. ALLOUCHE

Defence date : .. / .. / 2024

Member of the jury :

Mr. NECH	Jury's president
Mr. CHEGRANI	examiner
Mr. BEKHTI	examiner
Mr. OULED BESSI	examiner
Dr. R. RENANE	supervisor
Dr. R. ALLOUCHE	supervisor

Academic year : 2023/2024

إهداء

أرى رحلتي الجامعية قد شارفت على الإنتهاء بالفعل، من بعد تعب ومشقة لوقت طويل، وها أنا اليوم أختم بحث تخرجي بكل مالدي من همة ونشاط وبداخلي كل تقدير وامتنان لكل شخص كان له الفضل في مسيرتي وقدم لي المساعدة ولو باليسر .

(وآخر دعواهُمْ أَنِ الْحَمْدُ لِلَّهِ رَبِّ الْعَالَمِينَ)

اشكر الله عز وجل أولاً وأخيراً ، له الحمد وله الفضل ، ما كنت لأفعل لولا فضل الله ، فالحمد الله عند البدء وعند الختام ، الحمد لله ما انتهى درب ولا تحتم جهد ولا تم سعي إلا بفضله الحمد لله على التمام وعلى لذة الإنجاز.

إلى من حبهم يعلو فوق كل حب إلى من أنارو لي طريق العلم وساندوني ووفرو لي سبل السعادة والنجاح.

إلى والدي العزيز حفظه الله –

معلمي الأول وسندي الثابت في كل خطوات حياتي ، مصدر فخري وسعادتي الذي لا أرى الدنيا إلا به .

إلى أمي الغالية أدامها الله –

أيام عظيمة تلك التي سهرتي بها من أجلي و علمتيني بأن الحياة عقبات كلما اخترتها كلما خطوت خطوه إلى النجاح.

إلى رفقاء دربي الذين أمدوني دائماً بالقوة وكانوا موضع الاتكاء في كل عثراتي وكانو لي حضناً وسنداً ومناره و زرعو لي التفاؤل في دربي.

Gifting

I humbly dedicate this work to my dear parents, who have been my pillars, my inspiration, and my motivation throughout this journey. To my father for his unwavering support, and to my mother for her light, her unconditional love, and her infinite patience. May their love and guidance continue to lead me on the path of success and fulfillment. I am forever grateful for their sacrifices and unwavering belief in me. This achievement is as much theirs as it is mine, and I hope to continue making them proud in all that I do.

To my sisters Meriem, Assia, and Chaima, who have been my accomplices, my confidants, and my best supporters. Your presence has been a constant comfort. I am endlessly grateful for your love and encouragement. I am truly fortunate to have such incredible sisters by my side. I love you all more than words can express.

To the memory of my aunt, Sabiha, and my grandfather, Your memory remains alive in my heart, and your absence leaves an immense void. Your guidance and support have shaped me into the person I am today, and I carry your lessons with me always. I miss you both dearly, but I find comfort in knowing that you are watching over me from above. You will forever hold a special place in my heart.

To my extended family, to my aunts, uncles, cousines Ikram, Imene, Maissa, Amira…, and cousins, whose support and encouragement have been a source of strength and courage, and I am forever grateful for the bond we share.

To my friends, Khadija, Ziana, Bouchra, Feriel, Raounak, Amina and sara, who shared my joys, my sorrows, and my successes. Your friendship is a treasure that I will always cherish. I am grateful for the laughter and the tears we have shared, and the support we have given each other through thick and thin. Distance may separate us, but our bond remains strong.

For that special person who has been there for me in my hardest time , I am eternally grateful. Their unwavering support and love have truly been a beacon of light in my darkest days. I don't know how I would have made it through without

them by my side, and I will always cherish and appreciate everything they have done for me. They have shown me the true meaning of care, and I am so blessed to have them in my life.

To my ultimaty friend, Imene Mazouzi, you were such a great bond that I will always cherish. Thank you for always being there for me, through the good times and the bad. I am grateful to have you as one of my friends.

To the entire propulsion team promotion, I look forward to the day when we will all be successful. Thank you all for being such wonderful friends and companions during all this years.

Acknowledgements

First and foremost, I am grateful to Allah, the Almighty, for giving us the bravery and determination to do this work. Without His guidance and blessings, I would not have been able to accomplish all that I have.

As I reflect on the completion of my final master's thesis, I am overwhelmed with gratitude towards my professors **Dr. RENANE** and **Dr. ALLOUCHE** who have guided and supported me throughout this journey. Their expertise, dedication, and encouragement have been invaluable in shaping my research and academic growth. I am forever thankful for their mentorship and believe that their contributions have been instrumental in my success.

I also want to express my profound gratitude to the president and the jury members who have decided to honor our work by being present. Their support and recognition mean so much to me, and I am truly grateful for their time and effort in evaluating my work. I am humbled by this acknowledgment and will continue to strive for excellence in our future endeavors. Thank you once again for this incredible honor.

Lastly, I would like to express my gratitude to all of the instructors and professors at the aeronautical institute who helped us with our formation, all of my friends and fellow promoters, and everyone else who helped make this project a reality, no matter how far away they were.

A special acknowledgement to my hidden pair, ZEKRI Feriel, for her support and encouragement in the hardest times during the realization of this project. I know that you will shine even more in the near future.

ملخّص

الهدف من هذه الدراسة هو المحاكاة العددية لعملية الاحتراق المضطرب للميثان في غرف الاحتراق ، باستخدام برامجيات Ansys-Fluent.النموذج الرياضي مبني على معادلات Navier-Stokesمع نموذج اضطراب RANS k-ε realizable ويؤخذ في الاعتبار تحليل دقيق لعمليات الاحتراق، والنمذجة الرياضية للظواهر، والمحاكاة العددية للعملية .وهناك مقارنة بين مشعلين :المفرق التقليدي والمفرق الهوائي العكسي .ويستخدم هذا الأخير مفهوماً لتحقيق الاحتراق غير المختلط، مع مختلف بارامترات مجالات الاحتراق المضطرب، بما في ذلك درجة الحرارة والضغط الساكنين، والتغيرات في مختلف البارامترات، بما في ذلك الكثافة، والكسر الكتلي، ودرجة حرارة التسخين المسبق .وبالإضافة إلى ذلك، يُنظر في أثر إضافة الهيدروجين إلى احتراق الميثان من أجل تحسين كفاءة الطاقة عن طريق زيادة القيمة الحرارية وخفض انبعاثات ثاني أكسيد الكربون وثاني أكسيد الكربون، فضلاً عن تشجيع الاحتراق الأنظف مع انخفاض انبعاثات وجزيئات أكسيد النيتروجين .

الكلمات الرئيسية :احتراق غير مسبق، Ansys-Fluent، Navier-Stokes، نموذج اضطراب RANS k-ε realizable ، غرفة الاحتراق التقليدي، غرفة الاحتراق بالهواء العكسي، الاحتراق المضطرب، النمذجة الرياضية، انبعاثات وجزيئات أكسيد النيتروجين NOx.

Abstract

The aim of this study is to numerically simulate the turbulent combustion process of methane in can-type burners, using Ansys-Fluent software. The mathematical model is based on the Navier-Stokes equations with the RANS k- ε realizable turbulence model. A thorough analysis of the combustion processes, mathematical modeling of the phenomena, and numerical simulation of the process are taken into account. A comparison is made between two burners: the conventional combustor and the reverse air combustor. The latter utilizes a concept to achieve non-premixed combustion, with different turbulent combustion flow fields parameters, including static temperature and pressure... and changes in various parameters, including density, mass fraction, and preheating temperature. Additionally, the effect of hydrogen addition to methane combustion is considered in order to improve energy efficiency

by increasing calorific value and reducing CO2 and CO emissions, as well as promoting cleaner combustion with a decrease in nitrogen oxide (NOx) emissions and particles.

Key words: non-premixed combustion, Ansys-Fluent, Navier-Stokes, RANS, k-ε realizable turbulence model, conventional combustor, reverse air combustor, turbulent combustion, mathematical modeling, NOx emissions.

Résumé

L'objectif de cette étude est de simuler numériquement le processus de combustion turbulente du méthane dans des brûleurs de type canal, en utilisant le logiciel Ansys-Fluent. Le modèle mathématique est basé sur les équations de Navier-Stokes avec le modèle de turbulence RANS k-ε réalisable. Une analyse approfondie des processus de combustion, la modélisation mathématique des phénomènes et la simulation numérique du processus sont pris en compte. Une comparaison est effectuée entre deux brûleurs : le brûleur conventionnel et le brûleur d'air inverse. Ce dernier utilise un concept pour atteindre une combustion non prémélangée, avec différents champs de flux de produits de combustion turbulents, incluant la température statique et la pression... ainsi que des variations de divers paramètres, notamment la densité, la fraction massique et la température de préchauffage. De plus, l'effet de l'ajout d'hydrogène à la combustion du méthane est considéré afin d'améliorer l'efficacité énergétique en augmentant la valeur calorifique et en réduisant les émissions de CO2 et CO, tout en favorisant une combustion plus propre avec une diminution des émissions d'oxydes d'azote (NOx) et des particules.

Mots-clés : combustion non pré-mélangée, Ansys-Fluent, Navier-Stokes, RANS, modèle de turbulence k- ε réalisable, brûleur conventionnel, brûleur d'air inverse, combustion turbulente, modélisation mathématique, les émissions NOx.

Table of contents

List of figures

List of tables

Nomenclature

Chapter 01	
n_i	mole number of species i
n	total mole number
m	mass
w_i	mass fraction
m_i	Mass of species i
M_i	mass of one mol of species i
x_i	mole fractions
ρ	density
c	concentration
$\bar{M}$	mean molar mass
R	universal gas constant
λ	theoretical air coefficient
ϕ	equivalence ratio
$k^{\frac{1}{2}}$	turbulence velocity
l_t	turbulence characteristic length
s_l	Propagation speed of the laminar flame
e_l	laminar flame thickness
η_k	Kolmogorov Length scale
τ_k	Small time scales according to Kolmogorov
τc	Chemical time
τ_T	Turbulence time scale
Ka	Number of Karlovitz
Da	Number of Damköhler
δ_p	preheating area of thickness
δ_r	reaction area of thickness
τ_k^{-1}	turbulence's stretch rate
Re	Reynolds number
Re_t	Turbulent Reynolds number

Re_t*	Critical turbulent Reynolds number
K	Speed constant of a reaction
A	per-exponential factor
E_a	Activation energy
A	Perfect gas constant
μ(T)	molecular viscosity of the mixture
μ_0	reference viscosity
P_r	Prandtl number
D_k	molecular diffusiveness
S_c	Schmidt number
v	kinematic viscosity
D_{th}	thermal diffusion
L_e	Lewis number
Chapter 02	
Y_K	mass fraction of the species k
Y_{DK}	propagation speed of the species k
$\dot{W}_K$	mass production rate per unit of volume of the species k
ϕ	Flow property
ϕ_i	Instantaneous value of flow property
$\bar{\phi}_i$	Mean component of ϕ_i
ϕ_i'	Fluctuating component of ϕ_i
ε	Turbulence dissipation rate
ν	Kolmogorov velocity scale
ΔT	Time interval
u,v,w	Components of flow velocity U in x, y and z directions
u', v', w'	Fluctuations in flow velocities
CFD	Computational fluid dynamics
ω	Specific dissipation rate
RANS	Reynolds average Navier-Stokes
μ_t	Turbulent dynamic viscosity

$\bar{v}$	turbulent kinematic viscosity modified
k	Turbulent kinetic energy
K	Mean kinetic energy
p_b	production of turbulent kinetic energy due to volume forces.
v_t	turbulent viscosity
$\bar{\Omega}_{ij}$	average tensor of the velocity of rotation
δ	thickness of the boundary layer
w_i	reaction rate
W_i	average reaction rate
$Y_j^f(Z)$	rate of stretching
PDF	Probability density function
ξ^*	quantities on a fine scale
C_ξ	Volume fraction constant
Chapter 03	
EDP	partial derivative differential equation
DFM	Finite difference methods
FEM	Finite elements methods
SM	Spectral methods
FVM	Finite volume methods
VC	Control volume
φ	gradient of the quantity
SIMPLE	(Semi-Implicit Method for Pressure-Linked Equation
SIMPLER	SIMPLE Revised
SIMPLEC	SIMPLE-Consistent
PISO	Pressure Implicit with Splitting of Operators
u_i	component of the velocity following the direction x_i
Γ	The diffusion coefficient
S	source term

PRESTO	pressure straggling option
$r_i^{(k)}$	Residual for equation i after iteration (k)
Chapter 04	
D	Diameter
R	Radius
3D	3 dimensions
TIT	Turbine inlet temperature
BC	Boundary condition
AFR	Air fuel ratio
$\dot{m}_{tot}$	Total mass flow rate
$A_{inlet\ swirler}$	Inlet swirler area
$A_{primary\ air}$	Primary air area
$A_{secondary\ air}$	Secondary air area
A_{tot}	Total area
$\dot{m}_{fuel\ inlet\ combustor}$	Inlet fuel combustor mass flow rate
$\dot{m}_{primary\ air}$	Primary air mass flow rate
$\dot{m}_{inlet\ swirler}$	Inlet swirler mass flow rate
$\dot{m}_{secondary\ air}$	Secondary air mass flow rate
k	Thermal conductivity
C_p	Specific heat
ρ	Density
L_c	characteristic length
h	convective heat transfer coefficient
NO ppm	NOx emissions parts per million

Introduction

Introduction

One method of energy conversion is combustion, which produces thermal energy. Combustion is a highly exothermic and irreversible process that occurs in a container called a burning chamber, involving a fuel and a combustion fuel. The aviation industry is eager to learn more about this process. Manufacturers and researchers are primarily focused on understanding the behavior of various thermodynamic factors to achieve environmentally friendly and efficient combustion processes. Numerical simulation, based on the analysis of models and hypotheses, is the result of extensive research and testing, which is both time-consuming and expensive.

Whether it is for space exploration, aviation, land transportation, or power generation, combustion remains one of the primary methods of energy production used today. The majority of this energy is derived from finite fossil fuels. Moreover, burning these hydrocarbons releases pollutants into the atmosphere on a local and global scale. Carbon dioxide contributes to global warming, while nitrogen oxides deplete the ozone layer. Within this broader context, the energy and transportation industries are working towards enhancing their combustion processes to minimize fuel consumption and reduce pollutant emissions. Achieving these goals is challenging and requires both basic and technological research.

Researchers recognize that the turbulent nature of discharges significantly impacts combustion in engines and industrial installations such as gas turbines and turbo-reactors. Therefore, studies focus on examining the relationships between various physical phenomena occurring in combustion chambers. These include the complex interaction between the flow of the air-fuel mixture (fluid mechanics), heat discharge and convection phenomena (thermal), and the combustion reaction itself (combustion chemistry). Since the turn of the century, researchers have particularly focused on the relationship between combustion and turbulence, resulting in a wide range of ongoing studies at the experimental, theoretical, and numerical levels.

Additionally, the combustion chamber must withstand extreme strains. First and foremost, it must ensure complete fuel combustion, minimize pollutant emissions, reduce charge loss caused by excessive compression, maintain a stable turbine input temperature, and occupy the smallest possible volume while facilitating adequate wall cooling.

The study of turbulent combustion has undergone a revolutionary change due to computational methods and experimental data. These techniques enable the simulation of complex setups, such as combustion in gas turbines. To avoid the expense of experimental measurements, numerous industrial groups and academic organizations have developed software for numerical simulation. However, accurate modeling is necessary to ensure proper simulation, considering the significant scale differences between various physical events and the configurations being considered. Ansys-Fluent is a popular tool used to simulate various energy events in combustion chambers. Simulating these events directly requires substantial memory and computation time. Models must account for the physical aspects of small-scale combustion chambers, including gas mixing and reactive fuel-air combinations. Ansys-Fluent Code has become a widely used and popular simulation tool for studying these phenomena in industry and research.

The present work utilizes Ansys-Fluent, a computational fluid dynamics (CFD) software that uses the RANS k-ε realizable turbulence model. The study includes a thorough analysis of combustion processes, mathematical modeling of combustion phenomena, and a numerical simulation of the combustion process. The objective of the study is to compare two types of combustors: conventional and reverse air combustors. Both combustors use the concept of non-premixed combustion and have different flow fields for turbulent combustion products, including static temperature and pressure. Various parameters, such as density and mass fraction, are also analyzed. The study evaluates the influence of variations in air fuel ratio and preheat temperature. Specifically focusing on the performance of the reverse air combustor.

This study is divided into five chapters:

Chapter 1 provides essential definitions necessary to understand the main phenomena of the study, such as "combustion," different types of flames, and the effect of hydrogen addition to the methane and air mixture. Additionally, we have identified the geometries that will be studied, and previous works and research have been presented.

In Chapter 2, we mathematically model a viscous, turbulent, reactive flow. First, we present the equations that govern this type of flow. We then cover various turbulence models, boundary layers, and wall functions and provide an overview of turbulent combustion modeling in detail.

In Chapter 3, we define the solvers and discretization patterns for the finite volume method, as well as different numerical resolutions. We also provide a reminder of the various numerical methods and present the Ansys-fluent code.

Chapter 4 focuses on modeling the combustors that will be studied, including all dimensions. We also estimate and calculate the boundary conditions as well as the mass flow rate for different sections. Additionally, a mesh study and quality assessment have been conducted. Furthermore, we define all the simulation steps under ANSYS-Fluent, including models, boundary conditions, solution methods, and control.

In Chapter 5, we discuss the results of the simulation using the ANSYS-Fluent software, specifically regarding combustion. We also compare the performance of both combustors in different cases. Finally, the conclusion provides a summary of the main findings of this study, along with the study's limitations and recommendations for future research.

CHAPTER 01:

General Overview

Summary :

Chapter 01: General overview

1.1 Introduction

Combustion, the oldest technology ever employed by humans, has been in use for over a million years. Currently, combustion provides over 90% of the energy support needed worldwide, including heating, electrical power generation, and transportation. Therefore, it is crucial to have a clear understanding of the process.

In the past, combustion research focused on fluid mechanics, which involves chemical reactions that release heat globally. While thermodynamics-based explanations of heat release were somewhat useful for developing stationary combustion processes, they are inadequate for addressing transient events like ignition and quenching, or when pollutant production is involved. This is because they assume infinitely fast chemical reactions.

This chapter presents different knowledge about combustion and flames to help us better understand these phenomena.

1.2 Fundamental definitions

To conduct a comprehensive quantitative study of combustion processes, it is essential to have a solid foundation of understanding concepts and terms. This section will delve into these concepts in detail. Additionally, we will analyze previous work and the state of the art chronologically. We will also present the two geometric models of combustion chambers that are the focus of this study.

1.2.1 Mole Fraction

The mole fraction x_i of the species i denotes the ratio of the mole number n_i of species i to the total mole number $n = \sum n_i$ of the mixture (x_i=n_i /n).

1.2.2 Mass Fraction

The mass m is a fundamental property of matter (units of kg in the SI system). The mass fraction w_i is the ratio of the mass m_i of the species i and the total mass $m = \sum m_i$ of the mixture (w_i=m_i /m).

1.2.3 Molar Mass

The molecular weight (now outdated) The mass of one mol of species i is denoted by M_i (units of, say, g/mol).It is common practice to represent mass fractions w_i and mole fractions x_i as percentages. Simple computations may be used to confirm the following relations (1.1) and (1.2), where S stands for the number of distinct compounds:

$$w_i = \frac{M_i n_i}{\sum_{j=1}^{S} M_j n_j} = \frac{M_i x_i}{\sum_{j=1}^{S} M_j x_j} \tag{1.1}$$

$$x_i = \frac{w_i}{M_i}\bar{M} = \frac{w_i/M_i}{\sum_{j=1}^{S} w_j/M_j} \tag{1.2}$$

Densities are independent of a system's size or scope. These variables are referred to as intense properties, and their definition is the system volume V divided by the equivalent extensive characteristics, which are dependent on the system's extent. Intense qualities include, for example:

mass density (density): $\rho = m/V$ (in e.g., $\mathrm{kg/m^3}$) (1.3)

molar density (concentration): $c = n/V$ (in e.g., $\mathrm{mol/m^3}$) (1.4)

It follows that the mean molar mass is given by the expression (1.5):

$$\frac{\rho}{c} = \frac{m}{n} = \bar{M} \tag{1.5}$$

In chemistry, concentrations c of chemical species defined in this way are usually denoted by species symbols in square brackets (e.g., $c_{\mathrm{H_2O}} = [\mathrm{H_2O}]$).

For gases and gas mixtures in combustion processes, an equation of state relates the temperature, pressure, and density of the gas. For many conditions, it is satisfactory to use the ideal gas equation of PV = nRT.

where p denotes the pressure (in units of Pa), V the volume (in m^3), n the mole number (in mol), T the absolute temperature (in K), and R the universal gas constant ($R = 8.314$ J.mol $^{-1} \cdot K^{-1}$). It follows that in relation (1.6):

$$c = \frac{p}{RT} \text{ and } \rho = \frac{p\bar{M}}{RT} = \frac{p}{RT\sum_{i=1}^{S} \frac{w_i}{M_i}}. \quad (1.6)$$

The ideal gas equation of state provides an insufficient prediction of concentration or density when temperatures are close to or below the critical temperature or when pressures are close to or above the critical pressure. It is more accurate to think of the system as a genuine gas.

1.3 Combustion

1.3.1 Definition

Combustion is a chemical reaction that occurs when oxygen in the air, fuel, and a heat source combine. Combustion is an exothermic reaction (exothermic reaction). It is manufactured in an "open" system or a "closed" system (i.e. no heat and mass exchange with the external environment). Overall, this is a chemical reaction that only occurs when chemical species interact or are willing to modify each other. Combustion is also a reaction in which combustible substances are oxidized by oxygen (combustibles), the products of which are called smoke or unburned.**[1]**

1.3.2 Combustion propagation

Two important combustion regimes can be distinguished

1.3.2.1 Deflagration (very fast)

This is a quick process that takes less than a millisecond to complete 80 percent of the way. It is distinguished by the existence of a flame that spreads across the

mixture that hasn't burned. A flame is characterized by a fast chemical reaction that takes place in an extremely thin fluid layer, together with sharp temperature and species concentration gradients and luminescence. The flame front can be viewed as an interface between the unburned mixture and the burned gases from a macroscopic perspective.

The burned gases have a significantly higher volume, temperature, and density than the unburned combination.

In air-fuel mixes, deflagration waves often travel at rates less than one meter per second. This group includes all flame activities that take place in the gas turbine combustion chambers.**[2]**

1.3.2.2 Detonation (instant)

A shock wave that is coupled to and supported by a zone of chemical reaction is the hallmark of the detonation. Explosion waves move between one and four kilometers per second, or supersonic speeds. They can't happen in the traditional air-fuel mixtures employed in gas turbine combustors, but they might in circumstances where oxygen injection is utilized to help with acceleration and ignite. the engine. The military is currently interested in pulse detonation engines, which use detonation waves in their combustion chambers.**[2]**

1.3.3 Combustion reaction classifications

1.3.3.1 Combustion reaction

$$C_xH_Y + \left(x + \frac{y}{4}\right) O_2 \rightarrow xCO_2 + \frac{Y}{2} H_2O \qquad (1.7)$$

Burnt gases contain fully oxidized products, while actual combustion generates intermediate products. Air, typically used as the oxidizer, is composed of 21% oxygen, 78% nitrogen, and 1% argon, which are crucial for pollution issues as shown above in equation (1.7).

For the sake of simplicity, we will assume that the final two chemicals are inert. We will also presume that air is made up of 79% "atmospheric nitrogen" and 21%

oxygen, with argon being explained by the presence of a fictional molar mass. Thus, a hydrocarbon's combustion reaction with air becomes as shown in equation (1.8):

$$C_xH_Y + \left(x + \frac{y}{4}\right) O_2 + \frac{79}{21}\left(x + \frac{y}{4}\right) N_2 \rightarrow xCO_2 + \frac{Y}{2}H_2O + \frac{79}{21}\left(x + \frac{y}{4}\right) N_2 \qquad (1.8)$$

The combustion reaction is called a reactionary mechanism, i.e., it takes place in several chain reactions.

1.3.3.2 Stiochiometry

The conservation rules directly yield the stoichiometric relationships between the amounts of reactants consumed and the products generated. The equation for the reaction balance is used to calculate them.

Theoretical combustion calculations are based on stoichiometric combustion. By comparing the actual combustion findings with those of neutral combustion, analyses conducted on a fuel with a known composition will allow us to properly characterize it. Thus, we can define the following in terms of theory:

- Combustion with excess air.
- Combustion in the absence of air.

1.3.3.3 Theoretical air

Strictly essential air, also known as theoretical air, is the minimal amount of air needed for a fuel to burn completely. An exact combination would be necessary for theoretical air to completely burn. In actuality, some surplus air is needed to guarantee full combustion. The theoretical air calculated with the expression (1.9):

$$\lambda = \frac{\text{used air}}{\text{theoretical air}} \qquad (1.9)$$

The equation for complete combustion of a hydrocarbon with excess air becomes the equation (1.10) and the excess air is determined by the relation (1.11).

$$C_xH_Y + \lambda\left(x + \frac{y}{4}\right)O_2 + \lambda\frac{79}{21}\left(x + \frac{y}{4}\right)N_2 \rightarrow xCO_2 + \frac{Y}{2}H_2O + \frac{79}{21}\left(x + \frac{y}{4}\right)N_2 + E\left(x + \frac{y}{4}\right)O_2 \quad (1.10)$$

$$E = 1 - \lambda \quad (1.11)$$

The air-fuel ratio is also used to characterize the reactant mixture.

λ< 1,combustion is not complete. Carbon monoxide is shown to develop when there is a small air deficit. Unburned hydrocarbons or carbon in the form of graphite (black smoke) may persist in areas with severe air shortages.

1.3.3.4 Equivalence ratio

Equivalence ratio is a non-dimensional number that is equal to 1 when the mix is stoichiometric, a mixture rich in fuel, i.e., φ > 1. The combustion of a rich mixture leads fatally to incomplete burning, the corresponding term (1.12) is used to calculate the equivalence ratio for a mixture.

$$\phi = \frac{\left(\frac{\text{fuel quantity}}{\text{air quantity}}\right)_{\text{actual}}}{\left(\frac{\text{fuel quantity}}{\text{air quantity}}\right)_{\text{stiochiometric}}} \quad (1.12)$$

1.3.3.5 Complete combustion

During complete combustion, the reagents react with the oxidizing agent to form products that can no longer be oxidized by the oxidizing agent. These products have reached a level of stability that cannot be altered by the combustion reaction. **[2]**

1.3.3.6 Incomplete combustion

Incomplete combustion occurs when there is not enough oxidizer to completely react the fuel or when the contact time at temperatures where combustion is possible is too short. It therefore produces combustion residues and smoke in the form of ash, some of which are highly toxic to humans and the environment, such as carbon monoxide (a deadly gas), pure carbon particles (soot, tar, and ash), nitrogen oxides,

hydrocarbons (carcinogens such as benzene or highly toxic substances such as polycyclic aromatic hydrocarbons), and volatile organic compounds. **[2]**

1.4 Flames characterization

The notion of flame encompasses different processes and can be characterized using different parameters which have the advantage of allowing classification. The three main parameters are:

The nature and number of reagents;

The mode of introduction of the reagents;

The gas flow regime in the reaction medium.**[2]**

1.4.1 Flames classification

Examples of combustion systems ordered with respect to premixedness and flow type are shown in figure (1.1).

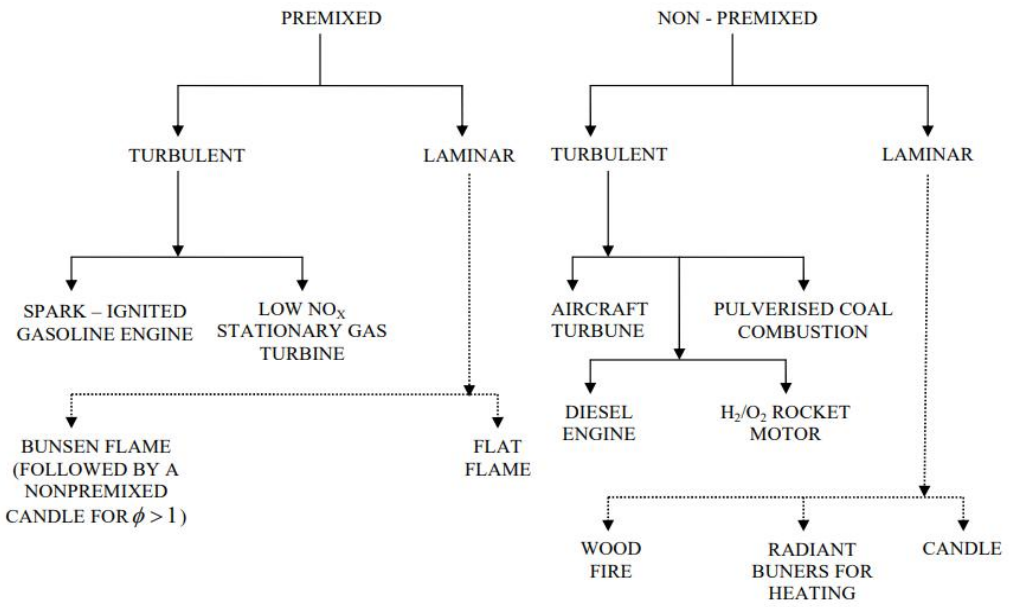

Figure 1.1 different types of combustion system. [3]

In combustion processes, fuel and oxidizer (typically air) are mixed and burned. It is useful to identify several combustion categories based upon whether the fuel and

oxidizer are mixed first and burned later (premixed) or whether combustion and mixing occur simultaneously (non-premixed).

1.4.1.1 The premixed combustion

Figure (1.2) represents the premixd flame, for which the reactants are previously mixed before the introduction and initiation of combustion at the level of the burner, In these flames controlled by chemical and thermal processes, the rate of propagation is determined by the oxidation reactions that occur in the flame front. This mode is often used in a lean mixture, thus increasing efficiency and reducing the production of NOx. This type of flame increases the risk of explosion, which comes from the storage mode of the reactive mixture. **[4]**

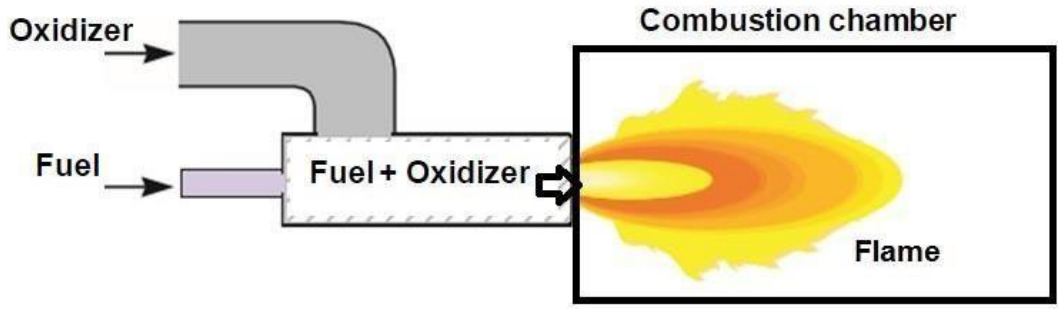

Figure 1.2 premixed combustion. [4]

1.4.1.2 The non premixed combustion(diffusion flame)

The diffusion flame as shown in figure (1.3), for which fuel and oxidizer injected differently. In these process-managed flame physics of material transfer, the speed of propagation is controlled mainly by molecular diffusion phenomena. The resulting flame front is positioned in the meeting zone of the two currents. Easier to master. These flames have the disadvantage of producing a large quantity of pollutants because the temperatures reached on the flame fronts are generally high **[4]**. The instantaneous thermochemical state of the fluid is related to a conserved scalar quantity known as the mixing fraction. The mixing fraction can be written in terms of the mass fraction as follows. **[5]**

Non-premixed flames include more complex chemistry than premixed ones, because the equivalence ratio ϕ covers the whole range from 0 (air) to ∞ (pure fuel).

Rich combustion occurs on the fuel side, lean combustion on the air side. The flame front, which is usually characterized by intense luminescence, is fixed to regions near the location of the stoichiometric composition ϕ=1, since this is where the temperature is highest.

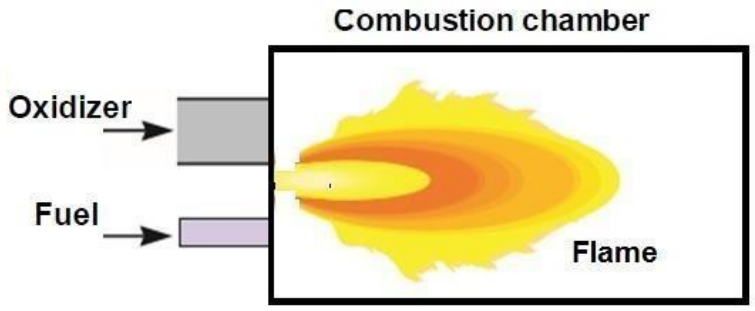

Figure 1.3 non-premixed combustion. [4]

1.4.1.3 The partially premixed combustion

In terms of mixing, there are two extremes: premixed combustion, where the fuel and oxidizer are completely mixed before they enter the combustion chamber, and non-premixed combustion, where the fuel and oxidizer enter separately. We have dealt with these two cases in the two preceding paragraphs. In technical applications, however, the optimum is often somewhere between the two extremes, trying to take advantage of the advantageous characteristics of both while avoiding their negative effects. If the fuel and the oxidizer enter separately but partially mix under the effect of turbulence, the combustion takes place in a stratified medium once the mixture is ignited. The principe of this type of combustion is represented in figure (1.4) below. **[4]**

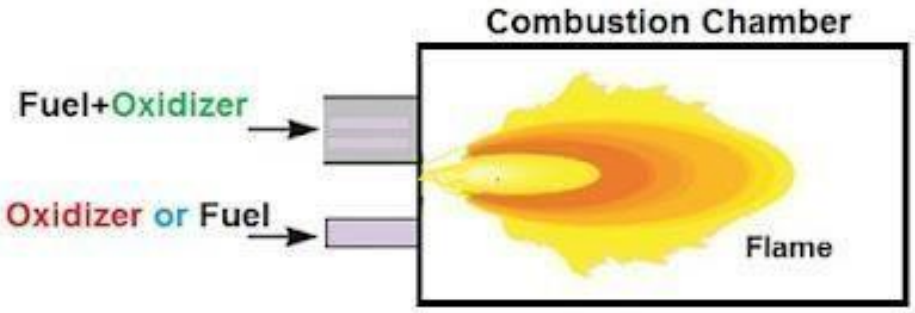

Figure 1.4 partially premixed combustion. [4]

1.4.2 Flame structure

The temperature, species concentration, and velocity distribution in space within a flame are referred to as its "flame structure". The kind of combustion as well as the properties of the fuel and oxidant determine the flame structure shown in figure (1.5). A reaction zone, where the fuel and oxidant react, a preheat zone, where the reactants are heated to their ignition temperature, and a post-flame zone, where the reaction products are cooled, make up the flame structure in general. **[60]**

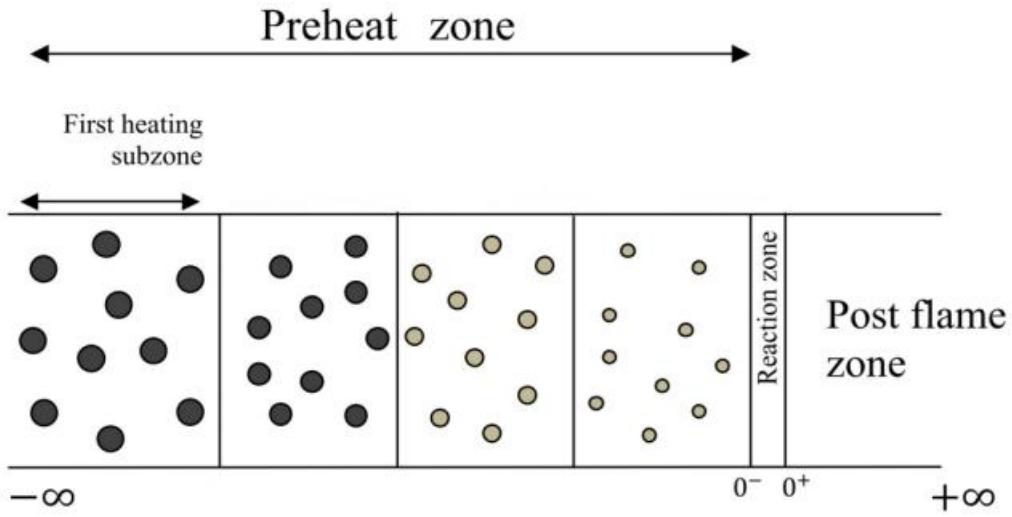

Figure 1.5 flame structure phases. [59]

1.4.3 Flame regimes

Usually, a number of variables, such as the fuel-air mixture, flow conditions, turbulence intensity, and combustion system architecture, influence the flame regime. These elements affect how turbulence and combustion interact, resulting in various flame behaviors and structures.

It is possible to distinguish between various flame regimes using theoretical analysis, numerical simulations, and experimental measurements. Laminar flames, cellular flames, turbulent flames with wrinkled structures, and flamelet regimes are a few types of flames that are widely known. Flame form, propagation speed, flame stability, and the existence of turbulence-generated eddies or flame surface wrinkling are just a few of the distinctive traits that each regime displays.

Borghi proposed the most widely used classifications of turbulent flames, which are referred to as flame regime diagrams. Peter made modifications to this schematic. Dimensionless parameters (Re_t*, Da, Ka), turbulent parameters (u', L_t), and flame parameters (S_L, δ_L) define the diagram. Additionally, the mass diffusivity and heat diffusivity were assumed to be equal in this diagram. The Schmidt number is, therefore, unity. A visual depiction of several flame regimes is shown in the figure (1.6) below. **[67]**

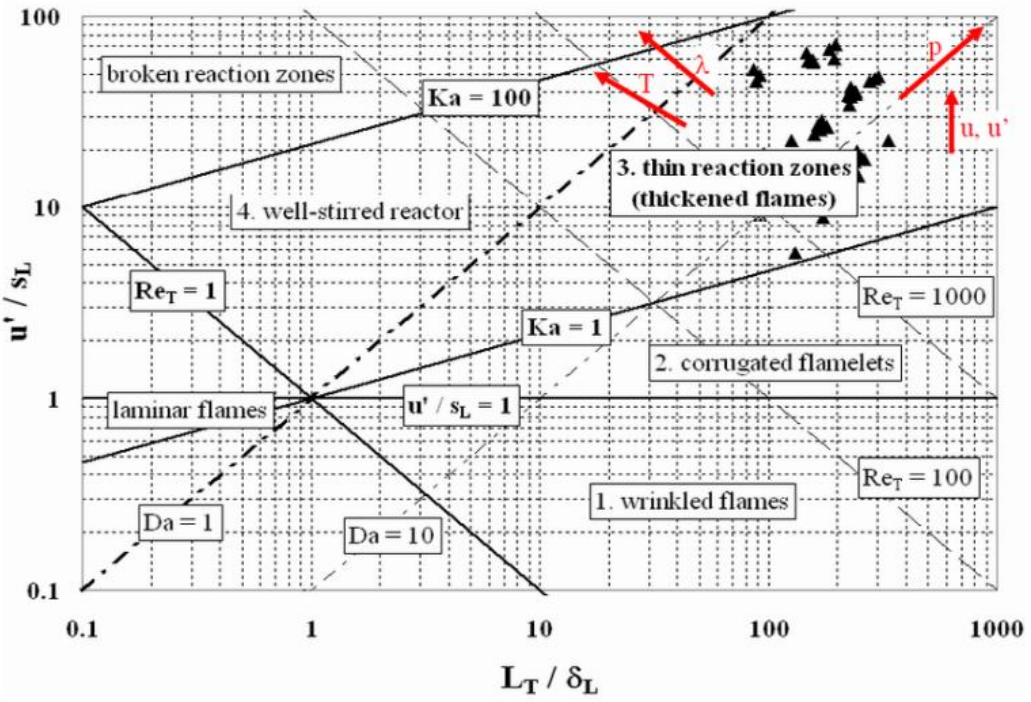

Figure 1.6 flames regime according to Borghi and Peter. [67]

According to Damköhler, the regime boundaries of turbulent combustion can be identified by comparing the spatial scales of turbulence and turbulence velocity $k^{\frac{1}{2}}$, turbulence characteristic length l_t, laminar flame thickness e_l, or the propagation speed of the laminar flame s_l in the mixture under consideration. The two characteristic numbers are $\frac{k^{\frac{1}{2}}}{s_l}$ and $\frac{l_t}{e_l}$ **[6]**. We define the Kolmogorov scale as the combustion and turbulence scales in table 1. **[2]**

Table 1-1 scales of flames classification according to Damköhler. [2]

Length scale	$\eta_{\mathrm{k}} = \left(\frac{\gamma l_t}{k^{\frac{1}{2}}}\right)^{\frac{3}{4}}$
Small time scales according to Kolmogorov	$\tau_{\mathrm{k}} = \left(\frac{\gamma l_t}{k^{\frac{3}{2}}}\right)^{1/2}$
Laminar flame thickness	$\mathrm{e}_1 = \sqrt{\mathrm{D}\tau_{\mathrm{c}}}$
Chemical time	$\tau \mathrm{c} = \frac{s_{\mathrm{l}}}{\mathrm{e}_1}$
Turbulence time scale	$\tau_{\mathrm{T}} = (ltk)1/2$
Number of Karlovitz	$\mathrm{Ka} = \frac{\tau_{\mathrm{c}}}{\tau \mathrm{k}}$
Number of Damköhler	$\mathrm{Da} = \frac{\tau_{\mathrm{T}}}{\tau \mathrm{c}}$

1.4.3.1 Damköhler Number (Da)

The Damköhler numbers (Da) are non-dimensional quantities employed in chemical engineering to establish a connection between the timescale of chemical reactions (reaction rate) and the rate of transport phenomena taking place within a system. as expressed by the relation (1.13) **[7]**:

$$\mathrm{Da} = \frac{reaction\ rate}{convective\ mass\ transport\ rate} \tag{1.13}$$

In its commonly used version, the Damköhler number connects the convection time frame inside a reactor to the timescale of a chemical reaction. The volumetric flow rate through the reactor in the case of semi-batch chemical processes or continuous processes (such as plug flow or stirred tank) determines this relation:

A useful estimate of the possible degree of conversion that could be achieved in a chemical process is provided by the value of the Damköhler number (Da). Generally speaking, the conversion usually stays below 10% when the value of Da is less than

0.1. On the other hand, a conversion rate of more than 90% is anticipated when Da is greater than 10.

Da >> 1: very fast chemistry slow combustion time is greater than the characteristic turbulence time.

Da << 1: slow chemistry; combustion time is less than the characteristic turbulence time.

Ka < 1: even the smallest structures cannot alter the flame structure: "flammelettes" regime. **[6]**

1.4.3.2 Premixed laminar flame

When lighting a gas mixture where the fuel and oxidant are initially mixed in advance, a flame front separates the fresh gas (product) from the burned gas (reactive) **[8]** by a thickness δ_L that may be divided into two distinct zones.

– a preheating area of thickness δ_p, in which mass and heat diffusion are the two dominant processes and where chemical reactions are considered to be negligible;
– a reaction area of thickness δ_r, a very thin area in which heat is released due to chemical reactions. In this area, the conduction phenomena are then negligible compared to those of diffusion. **[9]**

Thus The thickness of this laminar flame may be similar to the distance traveled by the heat released by the reaction over timeτ_c and how long this reaction lasts. Thus, by intervening with the thermal diffusion coefficient α.

The fuel-air mixture's richness and propagation speed, influenced by the nature of reagents, mixture richness, and fresh gas temperature, determine the propagation of two zones perpendicular to the flame front, ranging from 0.1 to 1 m/s. **[2]**

the figure (1.7) shows the schematic concept of a laminar premixed flame.

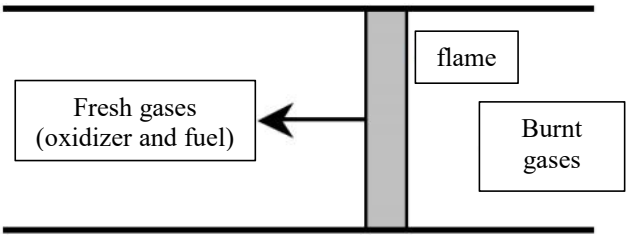

Figure 1.7 laminar premixed flame schematic representation. [10]

1.4.3.3 Non-premixed laminar flame

The combustion can be carried out in the form of a laminar diffusion flame when it occurs between an oxidizing medium and a combustible medium that is not premixed. **[2]**

Its main feature, called diffusion, is to present a reaction area separating the reagents, fuel, and oxidant. **[11]**

In this type of flame as represented in figure (1.8), the chemical reactions are very fast compared to convection phenomena, and combustion is controlled by the spread of species and heat. **[8]**

Diffusion flames develop from reaction phenomena and heat and mass diffusion, producing on both sides of the reactive zone. Convection phenomena are more important for bringing the reagents and carrying the products more effectively than just diffusion.**[2]**

The rate of reaction of this type of flame is mainly controlled by the molecular diffusion that governs the supply of reagents to the flames.

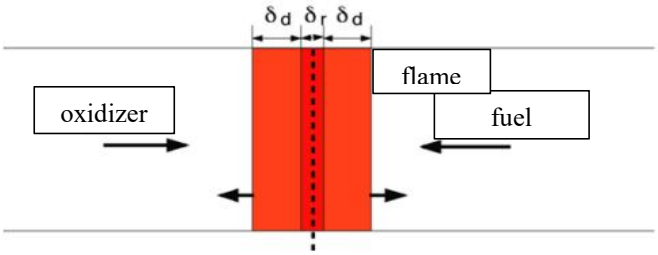

Figure 1.8 laminar non-premixed flame schematic representation. [12]

1.4.3.4 Turbulent premixed flames

The classification of the turbulent combustion regimes of premix flames dates back to Damköhler (1947), who adopted the idea that a large-scale turbulence only folds the flame without significant modification of its internal structure, whereas a small-scale Turbulence affects the transfer processes in the internal structure of the laminar flame. Three types of flames are distinguished.

- The flames folded.
- The flames thickened.
- The flames folded-thick.
- **The flamelets folded:**

Ka <1,flaming regime even small structures cannot modified the structure of the flame.

Da <1,slow chemistry.

$\frac{k^{\frac{1}{2}}}{s_l}$< 1, the intensity of the turbulence is negligible. This type of flame consists of flaming flames of the laminar type that are accompanied by turbulence.

- **The flamelets folded with pockets**

Ka <1, flame thrower even small structures cannot alter the flame structure.

Da < 1, slow chemistry,

$\frac{k^{\frac{1}{2}}}{s_l} > 1$, The intensity of the turbulence becomes significant, leading to the formation of gas pockets.

- **The folded flames – thick**

Ka > 1, we don't see any more flammelettes.

Da < 1, slow chemistry.

Turbulence increases kinetic energy, leading to more frequent interactions between flames. The curvature radius of flames can be around e_l, resulting in a flame structure that gradually changes. However, the turbulence's stretch rate, which is of the order of τ_k^{-1}, can reduce this thickness in some places. This stretch rate becomes greater as the turbulence's kinetic energy increases. This can result in the extinction of contact reaction zones. Excessive stretching of the flamethrower, indicating strong kinetic energy turbulence, can lead to the local extinction of flames.

- **The thick flames**

Ka >100, Da >1 fast chemistry.

This regime is an extension of the previous regime. When you increase the turbulent kinetic energy, there comes a time when there is only one flame, not curved but very thick, much thicker than in the other direction, where the reaction is even more distributed in space. In this regime, there can be no wave or flame folding, and it is better to speak of a "reaction zone" than a flame with a defined thickness. This diet is called the "thick flames" regime$\eta_k < e_l$.

The figure (1.9) shows the different types of premixed turbulent flame.

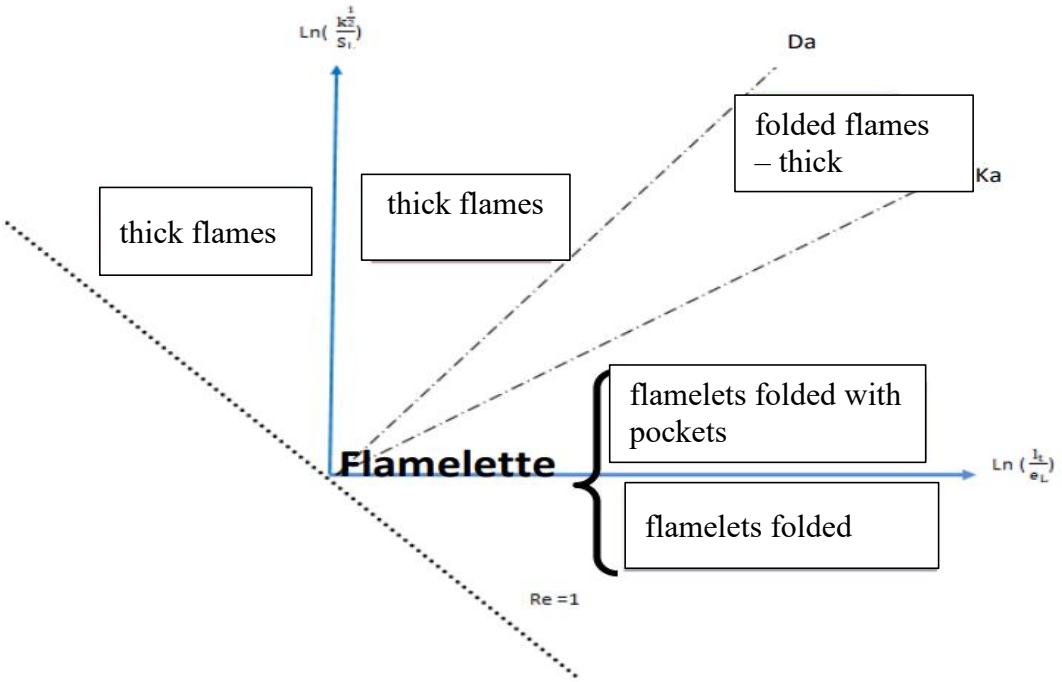

Figure 1.9 turbulent premixed flame types. [2]

1.4.3.5 Non-premixed turbulent flames

- **Folded Flamelets**

Re_t= 1 When the turbulence is not too strong, the structure of the diffusion flame is that of a folded flame; it is then composed of a long flamelets (laminar diffuse flame) continuously. Folded, stretched, and compressed alternately by turbulent movements.

- **Flamelets Domain with Extinction**

When the turbulence becomes strong enough, $1<Re_t<Re_t*$ is the flammelettes domain.

The large scales will interact with two parts quite far away, and this will form flammelettes loops.

Small spatial scales close to the thickness of the flame thrower will lead to local thickening. The reaction zone closes on itself.

- **Flame field in chemical equilibrium $Re_t>Re_t*$**

The area where it is no longer possible to distinguish flamelets in the proper sense of the term is the flame field in chemical equilibrium with a structure that resembles the one of small spatial scales in flammelettes domain with extinction, but only the calculation that takes place along the reaction zones is no more simple.

- **Pseudo-Laminar Flame Domain**

There are relatively few turbulent temperature and concentration variations in the flame. Before any significant chemical event, they had time to dissolve (this does not imply that the speed fluctuations are minimal, as they are, by hypothesis, constantly replenished). Then, we find ourselves in the middle of a raging flame that may be classified as pseudo-laminar. Strong turbulent fluctuations occur on a very tiny scale, resulting in a nearly constant diffusion flame with broad diffusion-convection zones encircling a reaction area, much like in a typical laminar flame.

Figure (1.10) shows all the types of non-premixed turbulent flame types.

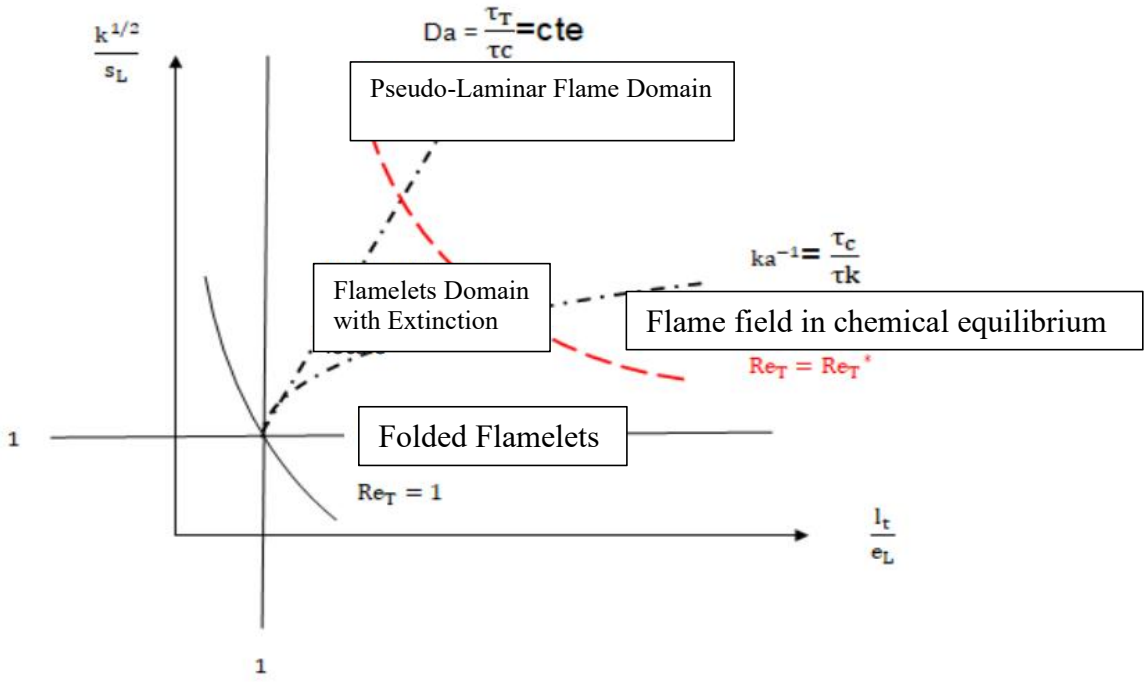

Figure 1.10 non-premixed turbulent flame types. [2]

1.5 Chemical kinetics

1.5.1 Definition

Chemical kinetics is the study of the speed of chemical reactions. It consists of tracking the evolution of chemical reactions (the appearance of a product, the disappearance of a reactive) according to time. The reactions are classified into two groups:

-Homogeneous reactions that take place entirely in a single phase

-Heterogeneous reactions where the transformation takes place on the surface of a catalyst or on the walls of a container.

1.5.2 Arrhenius Law

This law gives an expression of the speed constant (k) of the reaction in the form (1.14) **[13]**:

$$\mathrm{K} = \mathrm{A} \cdot \mathrm{e}^{\frac{-\mathrm{E_a}}{\mathrm{RT}}} \qquad (1.14)$$

A: per-exponential factor;

E_a: Activation energy in J/mol;

R: Perfect gas constant;

T: Temperature in K.

This law is independent of concentrations and time, depending on the reaction studied and the temperature.

The unit of the speed constant depends on the overall order of the reaction.

Global order $\mathbf{n = 0}$: $k = \frac{V}{[A]^0[B]^0} \Rightarrow k$ en mol L $^{-1}\boldsymbol{s}^{-1}$;

Global order $\mathbf{n = 1}$: $k = \frac{V}{[A]^1[B]^0} \Rightarrow kens^{-1}$;

Global order $\mathbf{n = 2}$: $k = \frac{V}{[A]^1[B]^1} \Rightarrow k$ en L mol m^{-1} s^{-1}.

The idea of a molecular shock's efficiency can be understood thanks to this expression of k. The shocks that genuinely cause a reaction, that is, that enable molecules to go from the reactive to the produced state, are known as effective shocks. When a shock is ineffective, the molecules depart the shock site without changing chemically.

In order for molecules to transition from the reactive state to the generated state during a shock, they need to have enough kinetic energy and speed to cross the energy barrier. The molecules' thermal agitation is the source of this energy.

1.5.3 Transport coefficients

The molecular viscosity of the mixture is expressed in the expression (1.15) according to the temperature with a Sutherland law. **[14]**:

$$\mu(T) = \mu_0(T/T_0)^{3/2}(T_0 + S/T + S) \quad (1.15)$$

μ_0 is the known reference viscosity at the reference temperature T0.

Godel shows in his thesis that the Sutherland law, for mixtures, allows for satisfactory results. **[15]**

The thermal conductivity of the mixture is defined using a Prandtl number in the below relation (1.16).

$$\lambda = \mu c_p / P_r \quad (1.16)$$

Molecular diffusiveness in a multispecies gas is a challenging topic to solve; most combustion algorithms employ simplified patterns (often Fick's law) and so do not require such detailed diffusivity modeling.

The molecular diffusiveness is then simplified and expressed according to a Schmidt $S_{c,k}$, number associated with the species j and assumed constant:

$$D_k = \frac{\mu}{\rho S_{c,k}} \quad (1.17)$$

P_r and $S_{c,k}$: assumptions constant in time and space.

1.5.4 Feature Numbers

The kinematic viscosity homogeneous to a diffusivity of quantity of motion is:

$$v = \mu/\rho \tag{1.18}$$

The Prandtl number corresponds to the ratio of kinematic viscosity and thermal diffusion:

$$P_r = \frac{\mu}{\rho}/\frac{\lambda}{\rho c_p} = \frac{\mu c_p}{\lambda} \tag{1.19}$$

Where, thermal diffusion is given by:

$$D_{th} = \lambda/\rho c_p \tag{1.20}$$

The Schmidt number compares kinematic viscosity and molecular diffusion:

$$S_c = v/D \tag{1.21}$$

Finally, the Lewis number is the ratio between thermal diffusion and molecular diffusion:

$$L_e = \lambda/(\rho c_p D) = S_c/p_r \tag{1.22}$$

1.6 Influence of hydrogen blending combustion

Hydrogen is a high-energy-density, carbon-free material that is frequently added to natural gas or methane in gas turbines. The technique of combining hydrogen fraction with methane has the advantage of partially eliminating carbon emissions from the system, maintaining a clean atmosphere, extending the restrictions on flammability, and lowering the overall cost of the fuel mixture.

1.6.1 Methane and hydrogen combustion

Because of their unique qualities, methane and hydrogen are two fuels that are frequently researched. Carbon dioxide and water vapor are the main byproducts of the burning of methane and hydrogen, which makes them appealing alternatives for lowering greenhouse gas emissions.

Research has demonstrated that methane flames can exhibit a variety of flame structures, such as turbulent and laminar flames. While turbulent flames feature a wrinkled flame front and greater flame speeds, laminar flames are characterized by smooth flame fronts and moderate flame rates. A number of parameters, such as the fuel-air mixture, temperature, pressure, and flow rate, affect how quickly methane flames spread.

The addition of hydrogen to methane/air flames has been studied as a potential method for improving combustion efficiency and reducing emissions. Studies have shown that adding hydrogen to methane/air flames can change the flame structure and propagation characteristics. The addition of hydrogen can increase the flame speed, widen the flammability range, and reduce the lean flammability limit. The combustion efficiency of the mixture can also be improved by adding hydrogen, as hydrogen has a higher combustion efficiency compared to methane. **[16]**

1.6.2 Chemistry of methane and hydrogen

The combustion of methane and hydrogen is an exothermic reaction, which means that it releases energy in the form of heat. The amount of heat released during combustion is proportional to the amount of fuel burned and can be calculated using the heat of combustion equation shown in formula (1.30). **[17]**

$$\Delta H_{\text{combustion}} = \sum n\Delta H_{f(\text{products})} - \sum m\Delta H_{f(\text{reactants})} \qquad (1.23)$$

The general Methane/Hydrogen combustion equation is written as the equation (1.24) **[18]**:

$$(\alpha CH4 + \beta H2) + (2\alpha + \beta 2) \rightarrow \alpha CO2 + (2\alpha + \beta)H2O + (2\alpha + \beta 2)N2 \quad (1.24)$$

In comparison to the reference situation of pure methane-air combustion, the mole fraction of CO2 increases across the combustor as hydrogen is added, while the mole fraction of CH4 decreases. The chemical kinetic effect and a decrease in the molar fraction of the CH4 reactant are the causes of the change in the number of carbon-related species in the flame. The following is an identification and presentation of the main chemical processes that produce CH4 represented in table 2 **[60-61].**

Table 1-1 chemical process of CH4 production with Arrhenius's constants. [61]

reactions	A (kg, cm, K, mol)	n	E_a(cal/mol)
CH4 + OH => CH3 + H2O	1.60000E+06	2.1	2460
CH4 + H => CH3 + H2	2.20000E+04	3	8750
O+CH4 => OH+CH3	1.020E+09	1.500	8600.00
CO + OH => CO2 + H	1.51000E+07	1.3	-758

1.7 Overview of gas turbine combustion chambers

A gas turbine combustor is a device for raising the temperature of the incoming air stream from the compressor by the addition and combustion of fuel **[19]**. In order to do this, the combustor needs to meet a number of contradictory requirements. It needs to be able to capable of quickly starting an ignition and need to function steadily in a variety of circumstances. It must fundamentally allow for full fuel combustion at all operating stages while reducing the production and release of unwanted contaminants.Enough mixing must be accomplished in the combustor to produce a suitable exit gas temperature distribution in order to prevent damage to the turbine. In order to sustain excellent overall performance, the combustor must also run with the least amount of pressure loss possible. Ultimately, each of these tasks needs to be carried out in a configuration that is as small, light, and inexpensive as possible, while still being strong enough to have a respectable working life.

1.8 Can-type combustors

1.8.1 Conventional can-type combustor (backward swirl combustor)

the conventional combustor is a model of a gas turbine combustor of the Can type, around three or four scale. It is representative of the Rolls-Royce Tay gas turbine combustor **[20]**. The traditional combustor fuel injector, swirler, hemispherical head (dome), one row of primary holes, one row of secondary holes on a cylindrical barrel, and a circular to rectangular nozzle . The fueling device is a fuel injector with a conical form and 90° cone-shaped fuel jets.

Ten 1.7 mm diameter holes arranged circumferentially on the pitch circle diameter of a 90° cone in the center at the upstream end of the hemispherical head are used to inject gaseous fuel. A swirler positioned before the primary zone with 10 around the fuel injector on the combustor head, flat vanes are positioned at a 45° angle to the flow. In conventional combustor, one row of primary holes and one row of secondary holes are located in the intermediate barrel section. The typical combustor has six main holes and twelve dilution holes, each with a diameter of 10 mm, piercing through the liner surface. The original combustor geometry has been taken from the works of McGuirk et. al. **[21,22,23]**. They have performed extensive

experimentation on a model can type combustor to understand the velocity field and streamline pattern for the same.

Figures (1.11) and (1.12) below show the original combustor geometry considered for experimentation and the schematic conception of the conventional combustor.

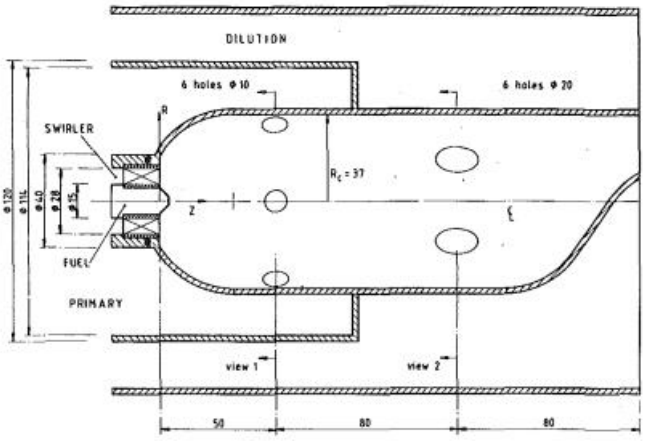

Figure 1.11 original can-type combustor experimentation conception. [23]

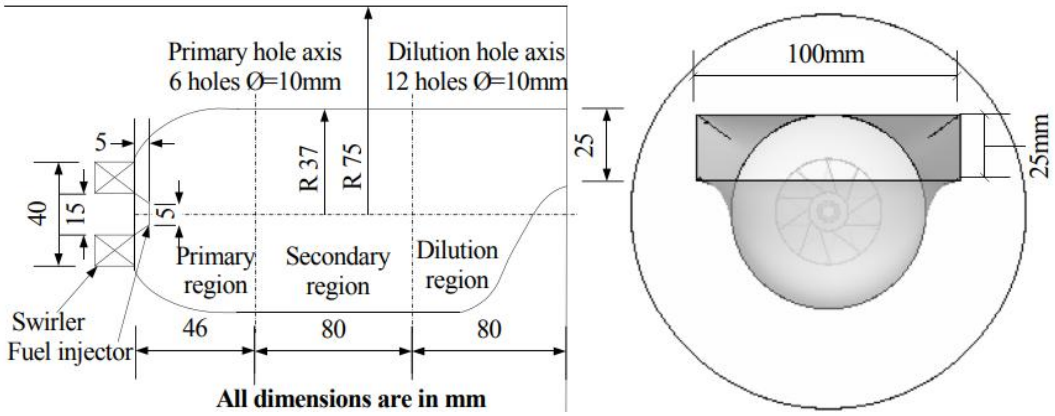

Figure 1.12 schematic conception for conventional combustor. [24]

Later on, possible changes in the original geometry are suggested. Upon employing the said changes, a new geometry of the combustor is obtained 'reverse air can-type combustor'.

1.8.2 Reverse air can-type combustor(upward swirl combustor)

Reverse air can-type combustor is a can combustor geometry produced with an upward swirl configuration. The swirler is positioned between the primary and secondary zones in an upward swirl arrangement. Through a swirler, the main air needed for combustion enters the combustion chamber and moves upstream toward the fuel injector, which is positioned in the center. A conical-shaped fuel injector with

ten 1.7 mm diameter fuel holes positioned in a 90° cone at the dome region's center and upstream end is used to inject fuel into the combustion chamber. On the liner wall of the combustor barrel in the dilution zone, there is one row of dilution air holes.

The concept used here is taken from the work of Timohiko et. al. **[25]**. Here a peripheral entry from the dome for the primary air has been considered eventually eliminating the primary holes and the swirler from the design.The modified geometry indicates a possible reduction in turbulence in the primary zone. But if flow is effectively controlled, this geometry generates adequate turbulence only where necessary so that the flame front may propagate inside the combustor until it reaches the nozzle end.

Figures (1.13) and (1.14) below show the first conception and the schematical design of this combustor:

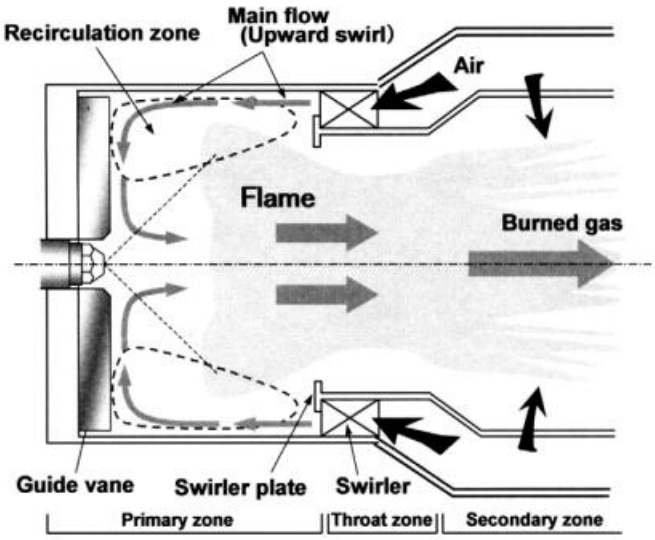

Figure 1.13 first conception of reverse air combustor concept. [25]

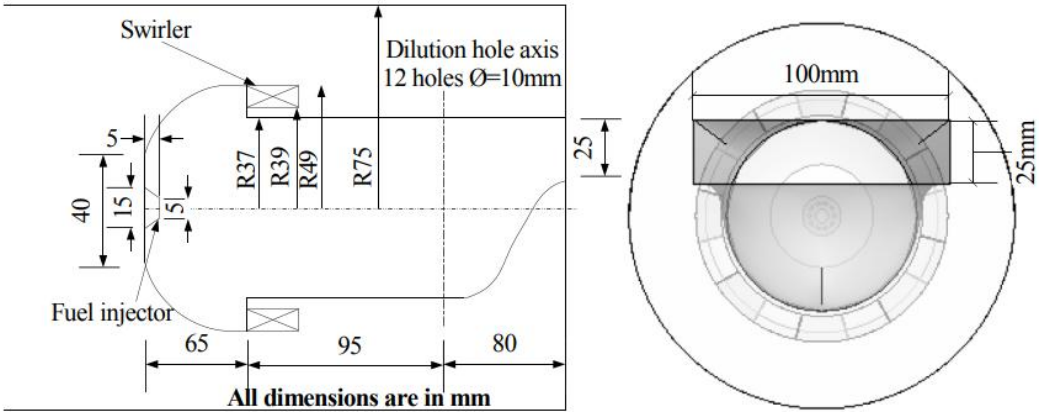

Figure 1.14 schematic conception for reverse air combustor. [24]

1.8.3 Experimental procedure

Figure (1.15) shows a schematic diagram of this experimental setup. The test setup is equipped with fuel lines, airlines, and the measurement system. A pictorial view of an experimental combustion system is shown in figure (1.16). A blower supplies the air required for combustion. A variable-frequency drive is used to control the airflow rate by controlling the blower motor speed. An orifice flange assembly along with a differential pressure transmitter is fitted in the airline for measurement of airflow. The uncertainty in air flow measurement is 0.25%. The fuel flow is metered through a calibrated fuel flow controller and a meter with an accuracy of ± 0.4% of the reading and 0.2% of the full scale. The temperature distribution at the exit of the combustor is measured by L-shaped K-type thermocouples of 3 mm in diameter, as shown in figure (1.17).

The schematic diagram of the exit section of the combustor in figure (1.17) demonstrates the positions of different thermocouples at the exit of the combustor. The axial heat conduction losses are accounted for in the thermocouple measurements.The measurement error for temperature is 4-5 °C for the maximum temperature and 1-2 °C for the minimum temperature if heat conduction losses are limited. A thermal imaging camera is used to capture a thermographic image of the outer wall of the combustor. The temperature measurement range of the thermal camera is -30 to 350 °C. The measurement accuracy of the thermal imager is ± 2 °C. **[26]**

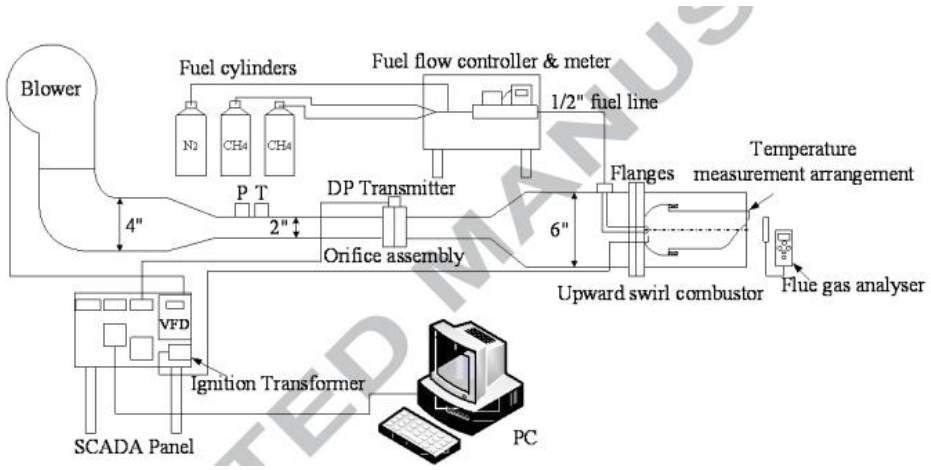

Figure 1.15 schematic diagram of test setup. [26]

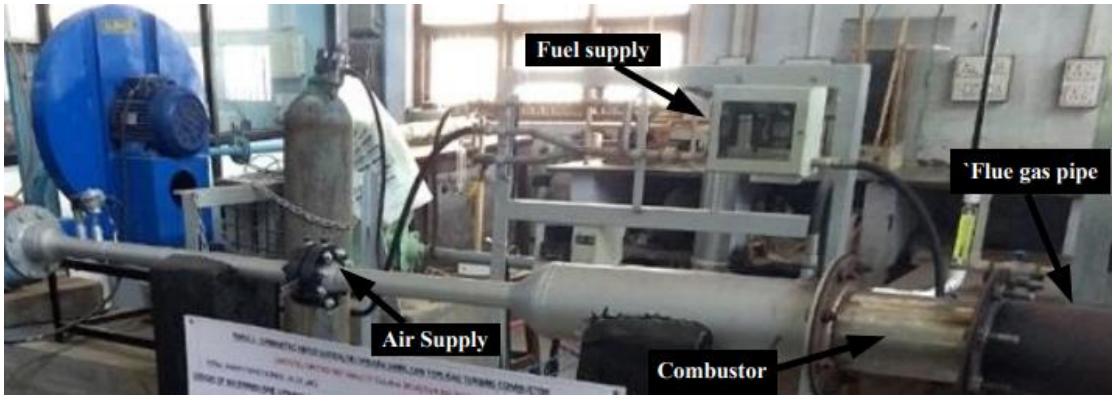

Figure 1.16 view of experimental setup. [26]

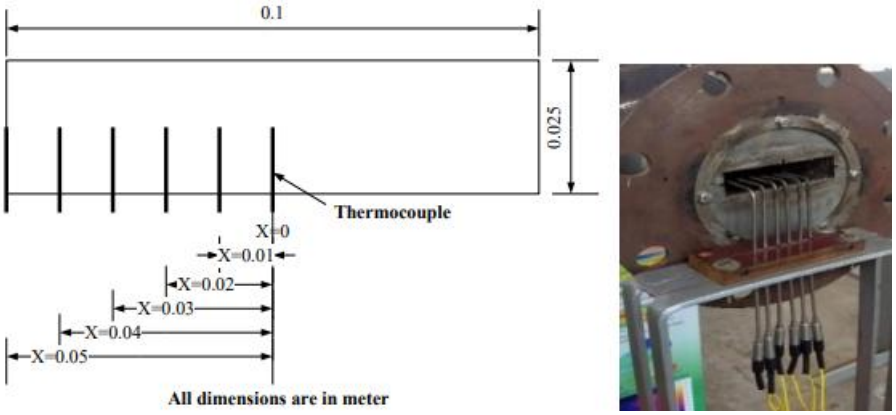

Figure 1.17 exit section of combustor(thermocouples placement). [26]

1.9 Previous works and findings about the combustors

An overview of important literature referred during the investigation is presented here. They are as follows:

1.9.1 Previous works about the conventional can-type combustor

1. The article titled "**Investigation of Swirler/Dilution Jet Flow Split on Primary Zone Flow Patterns in a Water Model Can-Type Combustor**" by **P. Koutmos and J.J. McGuirk (February 1985)** utilized Laser Doppler anemometry (LDA) measurements to study the flow field in a water model of a can-type gas turbine combustion chamber. The combustor geometry consisted of a swirl-driven primary zone, annulus-fed rows of primary and secondary jets, and an exit contraction. Variations in flow split between the swirler and dilution holes

affected the flow pattern in the primary zone. Despite these changes, the flow pattern downstream of the secondary jets remained consistent due to strong mixing. **[27]**

2. In a publication by **J. McGuirk1** and **J. M. L. M. Palma** in **July 1993** titled "**The Flow Inside a Model Gas Turbine Combustor: Calculations**," the authors evaluated the capability of the k-ε turbulence model to calculate flow inside gas turbine combustors. They compared the results obtained from a cylindrical coordinate system and hybrid differencing with velocity measurements. The study found larger discrepancies in the primary region, where there was an under-prediction of maximum negative axial velocity and turbulence kinetic energy. However, the model showed acceptable results in other combustion regions and provided correct flow predictions. **[23]**
3. In a publication by **Gopinath** and **V. Ganesan** (**1994**) titled "**Numerical investigation of the combined effect of swirler and primary jets on the recirculation zone of a can-type combustor by means of an orthogonal array technique**," the authors used an orthogonal array technique to investigate the effects of swirler and primary jets on the recirculation zone of a can-type gas turbine combustor. The study found that the flow rate through the swirler and the size of the primary injection hole have a greater influence on the characteristics of the recirculation zone than the swirl number and hub diameter. There may be a critical point beyond which the swirl number and swirler geometry dominate the effect of primary jets in determining the recirculation zone characteristics. The recirculation ratio initially decreases due to weakening primary jets, but increases after reaching the critical point. **[28]**
4. In his research article titled "**Combustion of Syngas Fuel in Gas Turbine Can Combustor**," published in **September 2010**, **Chaouki Ghenai** investigates the combustion of syngas fuel mixture in a gas turbine can combustor. The study focuses on the impact of fuel composition and heating value on combustion performance and emissions. Mathematical models are used to analyze the effects of syngas fuel composition and lower heating values on flame shape, gas temperature, carbon dioxide mass, and nitrogen oxides per unit of energy generation. **[29]**

5. In their article titled **"Numerical Investigation of the Combustion of Methane Air Mixture in Gas Turbine Can-Type Combustion Chamber"** (**November 2012**), **Firoj H. Pathan, Nikul K. Patel, and Mihir V. Tadvi** investigated the combustion of methane air mixture in a gas turbine can-combustor using computational fluid dynamics (CFD) with the CFX solver. The objective was to gain a better understanding of combustion phenomena and emissions, given the difficulties in mechanical design due to high cycle temperatures. The study examined the impact of parameters such as air-fuel ratio, swirler angle, and axial position on combustion chamber performance and emissions. The findings will assist in determining the optimal combustion chamber geometry for reducing emissions. **[30]**
6. In their research paper accepted in **April 2015**, titled "**Thermal and emission characteristics of a CAN combustor**," **Rupesh Shah and Jyotirmay Banerjee** conducted experimental research to determine the thermal and emission properties of a CAN catalyst. They recorded temperature and emission levels at the compressor exit for different swirler vane orientations and air fuel ratios (AFR), using methane as The results showed that an increase in AFR and swirler vane orientation reduces carbon monoxide emissions. However, an AFR of 45 leads to higher NOX emissions. **[31]**
7. In a study conducted by **Firoj H. Pathan, Dinesh K. Dabhi**, and **Nikul K**. Patel in **May 2016**, a comparative analysis of the combustion in a gas turbine can-type combustion chamber was performed. The researchers used CFD software with CFX solver to analyze the combustion of methane-air mixture. The objective of the study was to gain a better understanding of combustion phenomena and emissions, as mechanical design is challenging due to high cycle temperatures. Non-premixed gas combustion was simulated using PDF Flamelet and Eddy Dissipation Combustion Models. **[32]**
8. In **November 2018**, **Shreekala N. and N. Sridhara** examined the flow and emission characteristics of gasoline and Jet-A fuel in a can combustor using turbulent non-premixed flamelet combustion. Their study, titled "Combustion Characteristics in a Can Combustor Fueled with Surrogates of Gasoline and Jet-A Using Numerical Methods," used numerical simulations to analyze compressor efficiency, pressure loss factor, and emission levels. The results showed that gasoline combustion resulted in a four-fold higher pressure loss. **[33]**

1.9.2 Previous works about reverse air can-type combustor

1. In a study conducted by Masataka ARAI, Shunsuke AMANO, and Tomohiko FURUHATA (2007), the combustion characteristics of a prototype microgas turbine gas combustor with an induced recirculation zone were examined. The use of a swirler was implemented to enhance recirculation in the primary combustion zone. The combustor demonstrated strong potential for lean combustion and wide flame holding. Additionally, the forced recirculation and turbulent shear flow resulted in low NOx emissions. **[34]**
2. In their **2007** article titled "**Development of a can-type low NOx combustor for microgas turbines (fundamental characteristics in a primary combustion zone with upward swirl)**," **Tomohiko Furuhata, Shunsuke Amano, Kousaku Yotoriyama,** and **Masataka Arai** proposed a low NOx combustor for kerosene-fueled microgas turbines. This combustor features primary and secondary combustion zones connected by a throat, with a swirler placed between them to enhance gas recirculation. The authors investigated the optimal configuration of the combustor to achieve high stability and low emissions, considering fundamental combustion characteristics such as lean combustion limit, flame luminosity, exhaust gas composition, and combustion gas temperature. **[25]**
3. In their study,**Shah and Banerjee** (**2014**) developed a prototype of the can-type upward swirl combustor. The combustion tests involved the use of a conventional can-type combustor, a backward swirl combustor, and an upward swirl can-type combustor. The results showed that when the primary air enters the combustor in an upward swirl arrangement, the flame is confined toward the combustor axis. As a result, the liner wall remains significantly colder compared to using the backward swirl can combustor. Experimental results also indicate that NOx emissions from an upward swirl combustor are substantially lower than those from a backward swirl combustor. However, there are several major challenges that need to be addressed in order to ensure the adoption of upward swirl combustion, including low combustion efficiency and increased CO emission output. **[35]**
4. In a paper accepted in **November 2017**,**Parag Rajpara, Ankit Dekhatawala, Rupesh Shah**, and **Jyotirmay Banerjee** explored the influence of fuel injection

methods on the performance of upward swirl can-type combustors **[26]**. They also conducted another study in December 2017, titled "**Combustion characteristics of can combustor with different fuel injector configurations**" **[36]**. In this research, they evaluated a new concept of reverse fuel injection in an upward swirl can-type gas turbine combustor. The analysis involved varying the length of the injector as a design variable. The researchers utilized Large Eddy Simulations (LES) and Discrete Ordinates (DO) methods for radiation modeling, and the presumed shape Probability Density Function (PDF) approach for modeling the turbulence-chemistry interaction. The results demonstrated that reverse fuel injection enhances near-field mixing and fuel penetration, thereby improving combustion efficiency and reducing CO emissions without adversely affecting NOx emissions.

5. The research conducted by **Parag Rajpara, Rupesh Shah**, and J**yotirmay Banerjee** in **2018** focuses on the "**Effect of hydrogen addition on combustion and emission characteristics of methane-fueled upward swirl can combustor**". This study examines the use of hydrogen as a supplementary fuel in methane-fueled gas turbine combustion engines. Large-eddy simulations are utilized to analyze the impact of hydrogen enrichment on flame characteristics and chemical kinetics. The results indicate that higher concentrations of hydrogen lead to increased flame velocity, temperature, and CO emissions, while reducing NOx emissions. **[37]**

1.9.3 Previous works with both conventional and reverse air can-type combustor

Parag Rajpara, Ankit Dekhatawala, Rupesh Shah, and **Jyotirmay Banerjee** conducted a study published in December 2017 in the International Journal of Thermal Sciences (**2018**) titled "**Thermal and emission characteristics of reverse air flow CAN combustor**" **[24]**. In another work, **Parag Rajpara, Rupesh Shah**, and **Jyotirmay Banerjee** published a study in **2022** in Advances in Energy and Combustion (Safety and Sustainability) called "Performance Evaluation of Upward Swirl Combustor with Reverse Fuel Injector and Hydrogen Blending" **[38]**. These studies compared the thermal and emission characteristics of conventional and reverse air flow CAN type gas turbine combustors using Large Eddy Simulations (LES). The results revealed that the conventional combustor liner wall is dominated by hot

combustion gases, while the reverse air flow combustor has a relatively lower wall side temperature. This configuration eliminates hot spots, reduces NOx emission levels, and minimizes the need for wall-cooling. The LES model was used to analyze radiative heat transfer and turbulence-chemistry interactions. However, it was found that the upward swirl arrangement in the combustor resulted in lower combustion efficiency and higher CO emission levels, despite the reduced NOx emissions.

To simplify the experimentation process, the researchers did not consider the effect of the nozzle. The combustor models primarily consisted of the swirler stage and the fuel injector. These designs were chosen as they provided sufficient turbulence and mixing for complete fuel combustion within the domain.

1.10 Conclusion

At the end of the chapter, we identified the main phenomenon: combustion. By understanding the chemical behavior and identifying the geometries of the two types of can-type combustors (conventional and reverse air), we can study the phenomena inside them. From this, we can conclude that the type of flame present in our study is a turbulent non-premixed flame.

To fully comprehend our study, it is important to understand the governing equations and the significance of turbulence, as it plays a significant role in our research. These topics will be explored in the next chapter.

CHAPTER 02:

Mathematical modeling

Summary :

Chapter 02: Mathematical modeling

2.1 Introduction

Basic nonlinear equations, such as the Navier-Stokes equations, are essential for theoretical research in the field of combustion. These equations address unresolved fluid dynamics issues. Consequently, numerical techniques are necessary for studying these equations.

High levels of turbulence are a distinguishing characteristic of the flow regime inside a gas turbine's combustion chamber. The primary and dilution holes are intentionally designed to create turbulence within the chamber to meet its requirements, as discussed in Chapter 1. Efficient fuel and air mixing require a turbulent flow, which can be achieved to some extent.

Therefore, understanding the characteristics of turbulent flows and the challenges of managing turbulence in CFD (computational fluid dynamics) becomes crucial.

2.2 The fundamental equations of fluid dynamics

These equations are the mathematical expression of three fundamental physical principles on which the entire dynamics of fluids is based:

- The mass is preserved;
- Movement quantity preservation ;
- Energy is preserved.

2.2.1 Equation of continuity

The continuity equation, developed in the 19th century by French mathematician and physicist Agustin-Louis Cauchy, is a fundamental principle in fluid dynamics that expresses the conservation of mass within a fluid flow. It states that the rate at which mass enters or exits a control volume must be balanced by the rate at which mass changes within the volume.

the continuity equation (2.1) in a non-conservative for:

$$\frac{\partial \rho}{\partial t} + \frac{\partial (\rho u_i)}{\partial x_i} = 0 \tag{2.1}$$

the continuity equation of chemical species (partial mass balance) **[39]**:

$$\nabla.(\rho Y_K Y_{DK}) = \dot{W}_K \tag{2.2}$$

Y_K is the mass fraction of the species k.

Y_{DK} is the propagation speed of the species k.

$\dot{W}_K$ is the mass production rate per unit of volume of the species k.

Or it can be written with the form of the expression (2.3) :

$$\frac{\partial \rho Y_k}{\partial t} + \frac{\partial}{\partial x_i}\left(\rho(u_i + V_{k,i})Y_k\right) = \dot{\omega}_k \text{ for } k = 1, N \tag{2.3}$$

where $V_{k,i}$ is the i- component of the diffusion velocity V_k of species k and $\dot{\omega}_k$ is the reaction rate of species k. By definition:

$$\sum_{k=1}^{N} Y_k V_{k,i} = 0 \text{ and } \sum_{k=1}^{N} \dot{\omega}_k = 0 \tag{2.4}$$

2.2.2 Momentum equation

The Navier-Stokes equations, which is the momentum equation in fluid dynamics, is frequently represented in its differential form. The pressure gradient, viscous forces, and external forces acting on the fluid are all related to the acceleration of fluid particles in the equation. It is possible to write it as the relation (2.5):

$$\frac{\partial (\rho u_i)}{\partial t} + \frac{\partial (u_j u_i)}{\partial x_i} = -\frac{\partial p}{\partial x_i} + \frac{\partial T_{ij}}{\partial x_j} \tag{2.5}$$

2.2.3 Energy equation

A key idea in fluid dynamics and thermodynamics is the conservation of energy, sometimes known as the energy equation. Based on the fundamental law of thermodynamics ($\Delta U = Q - W$), it has been developed and derived over many years by different scientists.

$$\frac{\partial}{\partial t}\left[\rho\left(e+\frac{1}{2}u_i u_i\right)\right]+\frac{\partial}{\partial x_i}\left[\rho u_j\left(h+\frac{1}{2}u_i u_i\right)\right]=\frac{\partial u_i \tau_{ij}}{\partial x_j}-\frac{\partial q_j}{\partial x_j} \quad (2.6)$$

e: specific internal energy;

h: specific Enthalpy;

$$\mathrm{h}=\mathrm{e}+\frac{\mathrm{p}}{\rho} \quad (2.7)$$

$$\tau_{ij}=2\mu s_{ij}+\beta\frac{\partial u_k}{\partial x_k}\delta_{ij} \quad (2.8)$$

s_{ij}: symmetrical part of velocity gradient tensor.

δ_{ij}: Kronecker's symbol.

β: thermal conductivity.'

the heat flow vector q_j appearing in the energy equation which is generally calculated from the Fourier law.

$$q_j=-\lambda\frac{\partial T}{\partial x_j} \quad (2.9)$$

λ: thermal conductivity.

2.2.4 State Equation

State equation is a basic fluid dynamics relationship that defines a fluid's thermodynamic state.It connects a fluid's temperature (T), density (ρ or specific volume v), and pressure (p) in this equation:

$$P=\rho rT \quad (2.10)$$

2.3 Turbulence

2.3.1 overview

Turbulent flows are characterized by fluctuating velocity fields **[40]**. In addition to causing the transported amounts to fluctuate, these fluctuations also mix transported quantities including momentum, energy, and species concentration. These fluctuations are too computationally expensive to directly mimic in real-world engineering computations since they can occur at small scales and high frequencies. Alternatively, the small scales can be eliminated from the instantaneous (precise) governing equations by temporal averaging, ensemble averaging, or other manipulations that provide a modified set of equations that require less computing power to solve.

2.3.2 Characteristics of Turbulent flows

The major characteristics of a turbulent flow regime are:

- Diffusivity
- Irregularity
- Large Reynolds number
- 3D vorticity fluctuations
- Dissipation
- Continuum

The instantaneous value ϕ , of any flow property (velocity, temperature, pressure etc.) can be expressed as the sum of a mean component and a fluctuating component. Hence any flow variable is given as the expression (2.1):

$$\phi_i = \bar{\phi}_i + \phi_i' \qquad (2.11)$$

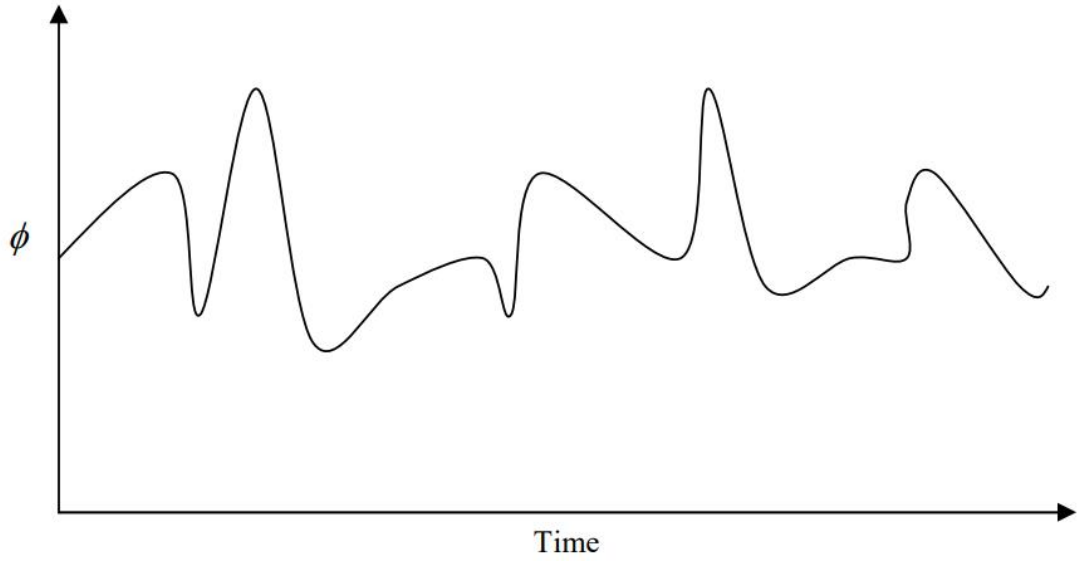

Figure 2.1 transient fluctuations in a flow property in a turbulent flow. [41]

2.3.3 Scales in turbulence

Turbulent flow experiences fluctuations at both the largest and smallest scales. Larger scales are influenced by flow field dimensions, while the smallest scales are governed by molecular viscosity's diffusivity action. Viscosity smooths velocity fluctuations at the smallest scales, preventing infinitely small scales of motion.

Rate of energy supplied ≡Rate of energy dissipated

Parameters governing small scale motion

There are two major parameters which account for the small scales motions:

- The Dissipation rate, ε ($m^2 sec^{-3}$), which is the rate of dissipation of Turbulence Kinetic energy inside the domain.

- The Kinematic viscosity, ν ($m^2 sec^{-1}$), which is the rate at which momentum diffuses inside the domain.

The figure (2.2) shown the Kolmogorov's microscales.

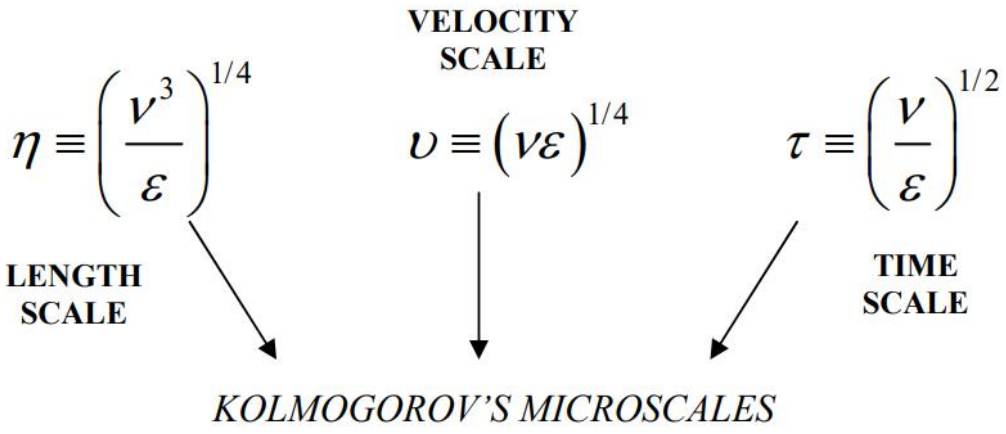

Figure 2.2 Kolmogorov's microscales. [41]

2.4 Effect of turbulence on time averaged Navier-Stokes equations

Turbulent flows depict eddying motions over a wide variety of length scales, constituting a key contrast from laminar flow visualizations. Turbulent flows with a high Reynolds number and a 0.1 by 0.1 m flow domain have eddies as small as 10 to 100μm. In order to characterize processes at all length scales, this calls for computational meshes of 109 to 1012 points.

Significant advances in computer hardware are needed to solve the time-dependent Navier-Stokes equations of completely turbulent flows at high Reynolds numbers, which is an amazing computing challenge.

2.4.1 Reynolds equations

The mean Φ of a flow property ϕ is given by the relation (2.12):

$$\Phi = \frac{1}{\Delta t}\int_0^{\Delta t} \phi(t)dt \qquad (2.12)$$

Theoretically, Δt should approach infinity; nonetheless, Δt is sufficiently long if it is greater than the time scales of the property ϕ slowest changes (caused by the biggest eddies). For stable mean flows, this definition of a flow property's mean is sufficient. In time-dependent flows, the so-called ensemble average—the mean of a

property at time t is determined by averaging the instantaneous values of the property over a significant number of repeated experiments.

The flow property ϕ is time dependent and can be thought of as a sum of a steady mean component Φ and a time-varying fluctuating component ϕ' with zero mean value; hence;

$$\phi(t) = \Phi + \phi'(t) \tag{2.13}$$

Or writing in an implicit manner: $\phi = \Phi + \phi'$ (2.14)

The time average of the fluctuations ϕ' is, by definition, zero:

$$\phi' = \frac{1}{\Delta t}\int_0^{\Delta t} \phi'(t)dt \equiv 0 \tag{2.15}$$

The kinetic energy k (per unit mass) associated with turbulence is defined as:

$$k = \frac{1}{2}\left(\overline{u'^2} + \overline{v'^2} + \overline{w'^2}\right) \tag{2.16}$$

The turbulence intensity T_i is linked to the kinetic energy and a reference mean flow velocity U_{ref} as follows:

$$T_i = \frac{(2/3k)^{1/2}}{U_{\text{ref}}} \tag{2.17}$$

To investigate the effects of fluctuations the flow variables $\vec{u}$, p, ρ, h and e are replaced by the sum of a mean and a fluctuating component. Thus:

$$\rho = \bar{\rho} + \grave{\rho}, \quad u_i = \tilde{u}_i + \grave{u}_i, \; P = \bar{P} + P', \quad h = \tilde{h} + \grave{h}, \quad e = \tilde{e} + \grave{e}$$

The above equations indicate the new terms that were added as a result of time averaging. Because of the velocity variations, these words entail products of variable velocities and represent convective momentum transfer. These terms are typically positioned on the right side of the aforementioned equations to represent their function as extra turbulent stresses on the U, V, and W mean velocity components.

Hence the equations (2.1), (2.5), (2.6) and (2.10) and get modified to:

$$\frac{\partial \bar{\rho}}{\partial t} + \frac{\partial(\bar{\rho}\tilde{u}_i)}{\partial x_i} = 0 \tag{2.18}$$

$$\frac{\partial(\bar{\rho}\,\tilde{u}_i)}{\partial t}+\frac{\partial\left(\bar{\rho}\tilde{u}_i\tilde{u}_j\right)}{\partial x_i}=-\frac{\partial \bar{p}}{\partial x_i}+\frac{\partial\widetilde{(T_{ij})}}{\partial x_j}-\frac{\partial\overline{\rho\acute{u}_i\grave{u}_j}}{\partial x_j} \tag{2.19}$$

$$\frac{\partial\left[\bar{\rho}\left(\tilde{e}+\frac{\tilde{u}_l\tilde{u}_l}{2}\right)+\frac{\overline{\rho\acute{u}_i\grave{u}_i}}{2}\right]}{\partial t}+\frac{\partial\left[\rho u_j\left(\tilde{h}+\frac{\tilde{u}_l\tilde{u}_l}{2}\right)+\frac{\overline{\rho\acute{u}_i\grave{u}_i}}{2}\right)\right]}{\partial x_i}= \tag{2.20}$$

$$\frac{\partial\left[-\bar{q}_J-\overline{\rho\acute{u}_j\grave{h}}+\overline{\acute{u}_i\tau_{lJ}}-\frac{\overline{\rho\acute{u}_j\acute{u}_i\acute{u}_i}}{2}\right]}{\partial x_i}+\frac{\partial\left[\tilde{u}_l\left(\widetilde{\tau_{lj}}-\rho\acute{u}_i\acute{u}_i\right)\right]}{\partial x_j}$$

$$\bar{P}=\bar{\rho}r\tilde{T} \tag{2.21}$$

The extra terms:

$\overline{\rho\acute{u}_i\grave{u}_j}$, reynolds tensor stress;

$\frac{\overline{\rho\acute{u}_i\grave{u}_i}}{2}$, turbulent kinetic energy;

$\overline{\rho\acute{u}_j\grave{h}}$, turbulent heat flux;

$\overline{\acute{u}_i\tau_{lJ}}$, molecular diffusion;

$\frac{\overline{\rho\acute{u}_j\acute{u}_i\acute{u}_i}}{2}$, turbulent transport energy.

2.4.2 Closure problem-the need of turbulence modeling-

The instantaneous continuity and Navier-Stokes equations, involving four unknowns, have not been solved directly, indicating their complexity and potential for future research.

Momentum equations involve time-averaging operations, removing instantaneous fluctuations, resulting in six additional unknowns, Reynolds stresses. Turbulence modeling aims to develop computational procedures with sufficient accuracy and generality to predict Reynolds stresses and scalar transport terms, addressing the complexity of turbulence.

2.5 Turbulence models

A computer process to conclude the system of mean flow equations and solve a relatively large range of flow issues is known as a turbulence model. Generally, in engineering, one just looks for turbulence's impacts on the mean flow. In a general-purpose CFD code, a turbulence model needs to be accurate, easy to use, low computational cost, and have a broad range of applications. Below is a classification of the several turbulence models used in CFD:

BASED ON RANS (CLASSICAL MODELS)-REYNOLDS AVERAGE NAVIER-STOKES-

- Zero equation-Mixing length model.
- One equation Spalart-Allmaras model.
- Two equation – The k-ε and k-ω models.
- Seven equation – Reynolds stress model.

2.5.1 Navier-Stokes Medium Equations Simulation (RANS)

RANS simulations are used to solve the mediated Navier-Stokes equations, which fully represent turbulence in this context. However, it is important to note that the outcomes may not accurately reflect reality, especially in complex simulated scenarios such as reactive situations. Nevertheless, these simulations are valuable in determining the general magnitude of temperature, pressure, and speed in average flow. As a result, they serve as the basis for many industrial codes currently in use. Additionally, the computational costs for these simulations are relatively low (measured in CPU time), allowing for the simulation of intricate structures on finely-tuned grids. **[44]**

2.6 RANS model

Two Equation Models

To describe l, the length scale is to write a transport equation for that quantity or for another quantity to describe it in an indirect way.

The two-equation models involve transport equations for pairs:k-ε ; k-ω; k-τ

$k-\varepsilon \rightarrow \varepsilon \sim k^{\frac{3}{2}} l$, it is the specific dissipation of turbulent kinetic energy.

$k-\omega \rightarrow \omega = \frac{\varepsilon}{k} \sim \frac{k^{\frac{1}{2}}}{l}$, it is the specific dissipation of turbulent kinetic energy.

$k-\tau \rightarrow \tau = \frac{k}{\varepsilon} k^{\frac{-1}{2}} l$, this is the typical time of turbulence.

2.6.1 The k-ε standard model

This model emphasizes the mechanisms affecting turbulent kinetic energy based on the modeling of two transport equations. The first is that of the turbulent kinetic energy (κ), and the second is its viscous dissipation rate (ε).

$$\frac{\partial(\overline{\rho}k)}{\partial t} + \frac{\partial(\bar{\rho}\bar{u}_j k)}{\partial x_j} = 2\tau_{RIJ}\frac{\partial \widetilde{U_L}}{\partial xj} - \bar{\rho}\varepsilon + \left(\frac{\mu_t}{\sigma_k} + \mu\right)\frac{\partial K}{\partial x_j} + p_b \quad (2.22)$$

$$\frac{\partial(\overline{\rho}\varepsilon)}{\partial t} + \frac{\partial(\bar{\rho}u_j\varepsilon)}{\partial x_j} = c_{\varepsilon 1}\frac{\bar{\rho}\varepsilon}{k}\tau_{RIJ}\frac{\partial \widetilde{U_L}}{\partial xj} - c_{\varepsilon 2}\frac{\bar{\rho}\varepsilon^2}{k} + \left(\frac{\mu_t}{\sigma_\varepsilon} + \mu\right)\frac{\partial K}{\partial x_j} + c_{\varepsilon 1}c_{\varepsilon 3}\frac{\varepsilon}{k}\frac{\bar{\rho}\varepsilon}{k}p_b \quad (2.23)$$

Thus, the turbulent dynamic viscosity μ_t is calculated by **[45]**:

$$u_t = \rho C_u \frac{k^2}{\varepsilon} \quad (2.24)$$
$$C_\mu = 0.09$$

p_b, the production of turbulent kinetic energy due to volume forces.

$$p_b = \beta'' g_a \frac{\mu_s}{pr_t}\frac{\partial T}{dx_s} \quad (2.25)$$

g_i, is the component of the vector gravity in direction i.

$pr_t = 0.85$, for the model k epsilons standard and realizable.

$c_{\varepsilon 1}\frac{\bar{\rho}\,\varepsilon}{k}\tau_{RIJ}\frac{\partial \bar{U}_L}{\partial xj}$, dissipation production deadline.

$2\tau_{RIJ}\frac{\partial \tilde{U}_i}{\partial xj}$, term of production of turbulent kinetic energy.

$c_{\varepsilon 1}\frac{\bar{\rho}\varepsilon^2}{k}$, dissipation term.

$\bar{\rho}\,\varepsilon$, Dissipation term turbulent kinetic energy.

$\left(\frac{\mu_2}{\sigma_k}+\mu\right)\frac{\partial K}{\partial x_j}$, Term of the sum of turbulent kinetic energy diffusion and transport.

Table 2-1 standard k-epsilon model closing coefficients. [42]

$c_{\varepsilon 1}$	$c_{\varepsilon 2}$	c_{μ}	σ_k	σ_c
1.44	1.92	0.09	1	1.3

The robustness of the model, as well as its savings in calculation time, is a reasonable accuracy for a wide range of turbulent flows.

2.6.2 The k-ε RNG model

The RNG model κ−ε, developed by Yakhot and Orszag, considers turbulent scales to determine energy transport and dissipation. This model, based on renormalization group methods, produces transport equations similar to the standard κ−ε model, with constants calculated theoretically.

The relations presented below are those of a recent version developed by Yakhot and Orszag. **[46]**

$$\frac{\partial\left(\rho U_j^k\right)}{\partial x_j}=\frac{\partial}{\partial x_j}\left[\rho\sigma_k v_{eff}\frac{\partial k}{\partial x_j}\right]+\rho v_t\left[\frac{\partial U_i}{\partial x_j}+\frac{\partial U_j}{\partial x_i}\right]\frac{\partial U_j}{\partial x_i}-\rho\varepsilon \quad (2.26)$$

$$\frac{\partial\left(\rho U_j^2\right)}{\partial x_j}=\frac{\partial}{\partial x_j}\left[\rho\sigma_\varepsilon v_{eff}\frac{\partial \varepsilon}{\partial x_j}\right]+C_{\varepsilon 1}\frac{\varepsilon}{k}\rho v_t\left[\frac{\partial U_i}{\partial x_j}+\frac{\partial U_j}{\partial x_i}\right]\frac{\partial U_i}{\partial x_j}-C_{\varepsilon 2}\rho\frac{\varepsilon^2}{k}-R \quad (2.27)$$

2.6.3 The k-ε Realizable model

The last model in the κ−ε family differs from the standard model mainly by two important things:

• A new formulation for turbulent viscosity;

• A new equation for the dissipation rate ε.

"Realizable" refers to a model that satisfies specific mathematical restrictions on the Reynolds limits, which makes sense given the principles of turbulent flow physics. As a result, this model forecasts the jets' spread rate more precisely. Additionally, it performs better in flow scenarios involving separation, recirculation, rotation, and boundary layers under high negative pressure gradients. Given the aforementioned enhancements, these final two turbulence models (κ−ε RNG and Realizable) produce

better results than the standard model. However, the weakest link in the entire κ–ε family continues to be the discharges, which have a strong anisotropy of turbulent restrictions. **[43]**

So the transport equations of this model are:

$$\frac{\partial\left(\rho U_j^k\right)}{\partial x_j} = \frac{\partial}{\partial x_j}\left[\rho\sigma_k v_{eff}\frac{\partial k}{\partial x_j}\right] + \rho v_t\left[\frac{\partial U_i}{\partial x_j} + \frac{\partial U_j}{\partial x_i}\right]\frac{\partial U_j}{\partial x_i} - \rho\varepsilon \tag{2.28}$$

$$\frac{\partial\left(\rho U_j^2\right)}{\partial x_j} = \frac{\partial}{\partial x_j}\left[\rho\sigma_\varepsilon v_{eff}\frac{\partial \varepsilon}{\partial x_j}\right] + C_{\varepsilon 1}\frac{\varepsilon}{k}\rho v_t\left[\frac{\partial U_i}{\partial x_j} + \frac{\partial U_j}{\partial x_i}\right]\frac{\partial U_i}{\partial x_j} - C_{\varepsilon 2}\rho\frac{\varepsilon^2}{k} - R \tag{2.29}$$

With the turbulent viscosity determined by:

$$v_t = C_\mu\frac{k^2}{\varepsilon} \tag{2.30}$$

C_μ is calculated by:

$$C_\mu = \frac{1}{A_0 + A_s\frac{kU^*}{\varepsilon}} \tag{2.31}$$

$$U^* = \sqrt{S_{ij}S_{ij} + \tilde{\Omega}_{ij}\tilde{\Omega}_{ij}} \tag{2.32}$$

$$\tilde{\Omega}_{ij} = \bar{\Omega}_{ij} - \varepsilon_{ijk}\omega_k - 2\varepsilon_{ijk}\omega_k \tag{2.33}$$

$\bar{\Omega}_{ij}$ is the average tensor of the speed of rotation and ω_k is the angular speed.The constants A0 and As are determined as follows:

$$A_0 = 4\ A_s = \sqrt{6}\cos\varphi \tag{2.34}$$

$$\varphi = \frac{1}{3}\text{Arccos}\left(\min(\max(\sqrt{6}w, -1), 1\right) \tag{2.35}$$

$$w = \frac{S_{ij}S_{jk}S_{ki}}{\bar{S}^2} \tag{2.36}$$

$C_{1\varepsilon}$ is defined as:

$$C_{1\varepsilon} = \max\left(\frac{\eta}{5+\eta}, 0.43\right) \tag{2.37}$$

$$\eta = S\left(\frac{k}{\varepsilon}\right) \tag{2.38}$$

The constants C_2,σ_k, σ_ε were specified by Shih and are defined as follows:

$$C_2=1.9,\ \sigma_k=1.0,\ \sigma_\varepsilon=1.2$$

Table 2-2 k-epsilon realizable model closing coefficients. [42]

A_0	A_s	Φ	W
4.04	$\sqrt{6}\cos\phi$	$\frac{1}{3}\cos^{-1}(\sqrt{6}\,W)$	$\frac{S_{ij}S_{jk}S_{ki}}{\sqrt{S_{ij}S_{ij}}}$

2.7 Boundary layer

A boundary layer is a low-thick region formed by the flow of a viscous fluid in the presence of an obstacle. It is classified as laminar if the Reynolds Re number is less than a critical value, about 3×10^5, or turbulent if it exceeds this value. The boundary layer is formed due to non-slip and non-penetration conditions that impose zero speed on the wall. The flow becomes almost one-dimensional, with a large scale of variation in tangential directions before the normal speed. The idealization of a boundary layer is an infinitely thin, semi-infinite flat plate immersed in a uniform flow. Walls significantly influence turbulent flows, with viscosity effects reducing tangential speed fluctuations in areas close to the walls.

2.7.1 The Internal Region

The numerical simulation of near-wall areas has a significant impact due to the strong gradient of turbulent flow variables, which are primarily influenced by the presence of walls, ensuring accurate calculations of turbulent flows away from walls.

The kinematic sizes in the vicinity of the wall are often associated with the internal parameters of the limit layer, namely U_τ, the friction velocity at the wall, and the cinematic viscosity; we then define the addimensional mean sizes, $\bar{U}^+$ and y^+, as follows:

$$\bar{U}^+ = \bar{U}/u_\tau \text{ et } y^+ = yu_\tau/v \qquad (2.39)$$

This region is denominated as a viscous sub-layer and the second region or the internal region of the turbulent boundary layer corresponds to the zone y≤0.2δ.

2.7.1.1 The viscous sub-layer

Because of the zone's higher viscous tension than turbulent tension and linear average speed profile:

$$\bar{U}^{+}=y^{+} \text{ where, } 0< y^{+}<5 \tag{2.40}$$

2.7.1.2 A Second Region

The production and dissipation of turbulent kinetic energy is dominant. It consists of:

Buffer layer, $5\leq y^{\pm}<30$:

Though they are not entirely insignificant, the viscous effects in this region diminish before the turbulent friction.

Logarithmic Zone, $30\leq y^{\pm}<200$:

When friction reaches the buffer zone, it becomes essentially turbulent. The molecular viscosity's contribution vanishes in the face of the turbulence cutting pressure, and as a result, the speed of friction takes on the appearance of a distinctive speed fluctuation scale. Since molecular viscosity is no longer relevant in this context, an expression that specifies this context by must be constructed via dimensional analysis.

$$\bar{U}^{+}=\frac{1}{K}\,\text{Ln}\; y^{+}+\text{B} \tag{2.41}$$

k =0.41 is the universal constant of Von Karman

B is a neighboring constant of 5.

2.7.2 The external region

In this region, other parameters may intervene such as δ the thickness of the boundary layer which is valid for y/δ≥ 0.2 and U_{∞} the outflow speed.

Thus the average speed profile, where the flow structure is fully controlled by turbulence. In this region, we speak of deficit speed law which is given by:

$$\frac{U_{\infty}-\bar{U}}{u_{\tau}}=\Phi\left(\frac{y}{\delta}\right) \tag{2.42}$$

Where,

$U_\infty - \bar{U}$, shows the speed deficit relative to the external speed.

The function Φ , is not universal because it can be influenced by many parameters such as the pressure gradient, the number of Reynolds, or the development conditions of the upper limit layer of the x abscess.

2.8 Combustion modeling

Flames are dynamic phenomena that involve the transport of gases through convection and diffusion. Gases escape at a specific speed due to reservoir pressure, creating a reaction zone in the mixture. This zone is formed when gases and air mix continuously. As gases escape, heat is released, and the gas escape and heat released also mix. This process is explained by thermodynamics laws, mathematical models, and the impact of turbulence on combustion and the impact of burning on turbulentness.

2.8.1 Aerothermochemistry equation [42]

2.8.1.1 The reaction rate

the rate of appearance or extinction of the species i :

$$w_i = \frac{dn_i}{dt} \tag{2.43}$$

2.8.1.2 The Mass Conservation Equation

$$\frac{\partial \rho}{\partial t} + \sum_{\alpha=1}^{3} \frac{\partial \rho v_\alpha}{\partial x_\alpha} = 0 \tag{2.44}$$

2.8.1.3 The Transportation Equation of Chemical Species

$$\frac{\partial \rho y_i}{\partial t} + \sum_{\alpha=1}^{3} \frac{\partial (\rho v_\alpha y_i)}{\partial x_\alpha} = \sum_{\alpha=1}^{3} \frac{\partial \left(- j_{i,\alpha}\right)}{\partial x_\alpha} + \rho w_i \tag{2.45}$$

2.8.1.4 The energy equation

$$\frac{\partial \rho u_t}{\partial t} + \sum_{\alpha=1}^{3} \frac{\partial(\rho v_\alpha v_\beta)}{\partial x_\alpha} = \sum_{\alpha=1}^{3} \frac{\partial\left(-j_{q,\alpha} - \sum_{i=1}^{n} j_{i,\alpha} + \sum_{\beta=1}^{3} v_\beta \tau_{\alpha\beta}\right)}{\partial x_\alpha} + \sum_{\beta=1}^{3} v_\beta F_\beta \quad (2.46)$$

The molecular diffusion flux equation $j_{i,\alpha}$, the diffusion of mas $j_{q,\alpha}$, the quantity of movement $\tau_{\alpha\beta}$, must be expressed with their aforementioned expressions the energy equation can also be written by showing the reaction rate to process the reactive flow.

$$\mathrm{h} = \bar{c_p} T + \sum_{1}^{n} y_i h_{i,0} \quad (2.47)$$

$$u = \bar{c_v} T + \sum_{1}^{n} y_i u_{i,0} \quad (2.48)$$

The energy equation becomes:

$$\frac{\partial}{\partial t}\left(\rho\left(\bar{c_v} T + \sum_{1}^{3} \frac{\partial(\rho v_\beta v_\beta)}{2}\right)\right) + \sum_{1}^{3} \sum_{1}^{3} \frac{\partial}{\partial x_\alpha}\left(\rho v_\alpha\left(\left(\bar{c_p} T + \sum_{1}^{3} \frac{\partial(\rho v_\beta v_\beta)}{2}\right)\right)\right) = \sum_{\alpha=1}^{3} \frac{\partial\left(-j_{q,\alpha} - \sum_{i=1}^{n} (h_i - h_{i,0}) j_{i,\alpha} + \sum_{\beta=1}^{3} v_\beta \tau_{\alpha\beta}\right)}{\partial x_\alpha} + \sum_{\beta=1}^{3} v_\beta F_\beta - \rho \sum_{1}^{n} h_{i,0} w_i \quad (2.49)$$

2.8.1.5 The momentum equation

$$\frac{\partial \rho v_\beta}{\partial t} + \sum_{\alpha=1}^{3} \frac{\partial (\rho v_\alpha h_t)}{\partial x_\alpha} = -\frac{\partial p}{\partial x_\beta} + \sum_{\alpha=1}^{3} \frac{\partial (\tau_{\alpha\beta})}{\partial x_\alpha} + F_\beta \qquad (2.50)$$

2.9 Simulation models of combustion

It must be underlined once more that a predictive calculation can only address average amounts in the statistical sense, much like with turbulent premixed flames and any turbulence discharge.

2.9.1 PDF model (probability density function)

Mix fraction modeling (PDF formulation) involves solving transport equations for a single preserved scalar (the mix fraction). Transport equations for specific species are not solved by this method. The individual concentration component for the species of interest is derived from the distribution of the predicted mixture fraction. Mechanisms of reaction that may be unknown or extremely complex are not explicitly defined. Instead, the reactive system is treated using either chemical balance calculations or “what is mixed is burned." The physical properties of chemical species and balance data are obtained from the chemical database. Finally, the interaction of turbulence and chemistry is considered using the probability density function (PDF) **[47]**.

The formulation of a chemical equilibrium model is enhanced by the use of mix fraction modeling, which simulates turbulent diffusion flames and other reaction processes. This method allows for rigorous interaction between turbulence and chemistry, enabling better estimates of average flow density.

2.9.2 Species transport

ANSYS FLUENT predicts the local mass fraction of each chemical species, Y_i by solving a convection-diffusion equation specific to the i_{th} species. This equation represents the conservation of mass and has a general form:

$$\frac{\partial}{\partial t}(\rho Y_i) + \nabla \cdot (\rho \vec{v} Y_i) = -\nabla \cdot \vec{J}_l + R_i + S_i \qquad (2.51)$$

where Y is the rate of creation by addition from the scattered phase plus any user-defined sources, and N is the net rate of formation of species Y through chemical reaction. For N− 1 species, an equation of this type will be solved, where N is the total number of fluid phase chemical species in the system. The N_{th} mass fraction is calculated as one minus the sum of the N − 1 solved mass fractions since the mass fraction of the species must add up to unity. To reduce numerical inaccuracy, the species with the biggest mass fraction overall, such as N − 2 in the case of air as the oxidant, should be chosen as the N_{th} species. **[48]**

2.9.2.1 Laminar finite rate

In this model, reaction rates determined by the Arrhenius kinetic expression and the effects of turbulent fluctuation are ignored. This model is exact for laminar flow, but it produces inaccurate results for turbulent flows. However, this laminar rate modeling may be acceptable in some cases where the chemistry is very slow or there is a there is a slow turbulent-chemistry interaction, such as in supersonic flames. This model is computationally cheaper than the EDC (Eddy Dissipation Concept) model but more expensive than the Eddy Dissipation model.

2.9.2.2 Eddy dissipation model

This work deals with the problem of non-premixed turbulent flames (diffusion). This model was therefore used for the modeling of reaction rates. The eddy dissipation model is based on the work of Magnussen and Hjertager, in which chemistry is considered very fast relative to turbulence. In this case, combustion, which is controlled only by turbulence, transports the mixture of fresh gases and hot products into the reaction zone where chemical kinetics is rapidly carried out. The latter can therefore be neglected. **[49]**

The reaction rate $R_{i,r}$ of the species i of the reaction is given by the minimum of the following expressions:

$$R_{i,r} = v'_{i,r} M_{w,i} A\rho \frac{\varepsilon}{k} \min\left(\frac{Y_R}{v'_R M_{w,R}}\right)$$

$$R_{i,r} = v'_{i,r} M_{w,i} AB\rho \frac{\varepsilon}{k}\left(\frac{\sum pY_p}{\sum_J^N v''_{j,r} M_{w,j}}\right) \quad (2.52)$$

Where:

Y_p: is the mass fraction of a species p in the products; Yr: is the mass fraction of a species r in the reagents;

A and B: are empirical constants with values 4 and 5 respectively;

$M_{w,i}$: is the molar mass of the species i.

2.9.2.3 Eddy dissipation concept model

The Eddy Dissipation Concept model is an extension of the turbulent dissipation model to include the detailed chemical mechanisms in turbulence flows. **[50]**

This model assumes that reactions occur in a small, turbulent structure called the fine scale. In ANSYS FLUENT, the length fraction of the fine scale is modeled by:

$$\xi^* = C_\xi \left(\frac{v\varepsilon}{k^2}\right)^{1/4} \quad (2.53)$$

ξ^*: refers to quantities on a fine scale;

C_ξ: volume fraction constant = 2,1377;

v: kinematic viscosity.

The volume fraction of the fine scale is calculated as $(\xi^*)^3$. Species are supposed to react in the fine structure of volume $(\xi^*)^3$ on the time scale defined by:

$$\tau^* = C_\tau \left(\frac{v}{\varepsilon}\right)^{1/2} \quad (2.54)$$

C_τ is the constant of the time scale, equal to 0.4082. Arrhenius's reactions are supposed to take place in a finite volume $(\xi^*)^3$ over time τ^*. Finally, the reaction speed was modeled by:

$$R_i = \frac{\rho(\xi^*)^2}{\tau^*[1-(\xi^*)^3]}(Y_i^* - Y_i) \qquad (2.55)$$

Where Y_i^* is the mass fraction of the species i after reaction in the fine structure over time τ^*. This model may incorporate a detailed kinetic mechanism, but typical mechanisms are invariably rigid, and their solutions are very expensive to calculate.

2.10 Conclusion

This chapter focuses on analyzing the governing equations and phenomena of turbulence in the system, highlighting the complexity of reactive turbulent flows. Various numerical simulation approaches for turbulent flows are considered, with a particular focus on Reynolds-Averaged Navier-Stokes (RANS) models. Based on this analysis, the RANS turbulence model with the k−ϵ and k−ϵ realizable formulation, is selected for studying the system, as well as we identified the different combustion models that are used for combustion modeling, and we will use the PDF model for the modeling of the main phenomena of this study. The next step involves determining an appropriate resolution for the numerical simulation of the system.

CHAPTER 03:

Numerical resolution

Summary:

Chapter 03: Numerical resolution

3.1 Introduction

In the previous chapter, we discussed a mathematical system that needs to be solved. In this chapter, we will explore suitable methods to resolve our system. We have all the necessary knowledge to understand the numerical behavior of our study, as well as the computational fluid dynamics code that we will utilize to analyze our phenomena.

3.2 Numerical resolution methods

The mathematical model, which consists of a partial derivative differential equation (PDE) or a system of PDE's, is transformed into an algebraic equation system using a discretization method. The most well-known discretization methods are:

Finite Difference Methods (FDM) ;
Finite Elements Methods (FEM);
Spectral methods (SM);
Finite Volume Methods (FVM).

3.3 Finite Volume Method

The method was first described by Patankar and Spalding in 1971 and published in 1980 in "Numerical Heat Transfer and Fluid Flow" The conservation equations involving partial derivatives are discretized using the finite volume approach, which transforms them into algebraic equations with numerical solutions. To derive the discretized equations that preserve all physical quantities within a control volume (CV), the control volume technique involves integrating the partial derivative equations over each control volume. The transport equation for a scalar quantity F can be used to illustrate this discretization principle.

- The method was developed as a special formulation of the finite difference The digital algorithm consists of the following steps:
- The computational domain is divided into finite volumes (mesh generation).
- Equations are integrated overall control volumes
- Discretization involves replacing the various types of finite difference approximations for terms representing convection, diffusion, and source terms. This results in the conversion of integrals into an algebraic equation system.
- The system of algebraic equations is solved using an iterative method.
- The method has several advantages:

-It allows for straight forward derivation of algebraic equations

-It expresses the principle of conservation in a control sub-volume in the same way that a differential equation expresses it in a control volume.

-The solution obtained ensures the preservation of all quantities (displacement, energy, etc.) within a group of control volumes or the entire computational domain.

-It can handle complex geometries.

-It directly calculates pressure, which is an important parameter.

The finite volume approach is based on dividing the computational domain into adjacent control volumes. Each control volume contains a "primary" node where the differential equation is incorporated. **[43]**

3.3.1 Finite Volume Method Applied to Coupling Treatment (Velocity-pressure)

PDE's, can be transformed into an algebraic equation system using a discretization method. The most well-known discretization methods are as follows:

The first challenge lies in the non-linearity of the convective term in the equations for conservation of momentum.

The second challenge arises from the fact that the pressure field is unknown in the source term, and there is no governing equation for the pressure field itself. The

pressure is indirectly specified by the continuity equation. The correct pressure field is the one that, when inserted into the equation for conservation of momentum, yields a corresponding velocity field that satisfies the continuity equation. All three equations are interrelated, as each component of velocity appears in all three equations. If the pressure gradient is known, the pressure field becomes part of the overall solution to the problem; however, the pressure gradient is typically not known.

Within Fluent, two solvers are known: "density-based explicit and implicit" and "pressure-based implicit."

3.4 Density based solver

If the flow is compressible, the density-based solver solves the equations governing continuity, quantity of motion, and transport of energy and species simultaneously, in the form of a set or vector of equations. The equations governing additional scales are solved sequentially. There are two algorithms available to solve the coupled set of equations: the explicit-coupled formulation and the implicit-coupled formula. **[42]**

Each iteration consists of the following steps:

1. Adjust the fluid's characteristics based on the available solution. (If the computation is still in progress, the initialized solution will be used to update the fluid properties.)
2. Solve the equations for continuity, quantity of motion, and, if relevant, energy and species at the same time.
3. If necessary, use previously updated values of other variables to solve equations for scales such as radiation and turbulence.
4. Use a discrete phase trajectory calculation to update the source terms in the relevant continuous phase equations when inter-phase coupling needs to be included.
5. Verify the convergence of the equation set. **[43]**

3.5 Pressure based solver

Density remains constant and independent of pressure in the case of an incompressible flow. In this scenario, the coupling of pressure and velocity affects the

solution of the flow field, and the resulting velocity field satisfies the continuity equation when the appropriate pressure field is substituted into the conservation equations for momentum. **[42]**

The pressure-based solver allows you to solve your flow problem separately or in a coupled manner. Different algorithms are used depending on the case. These five pressure-velocity coupling algorithms are: SIMPLE, SIMPLER, SINGLE, PISO, and Coupled.

3.5.1 SIMPLE algorithm (Semi-Implicit Method for Pressure-Linked Equation)

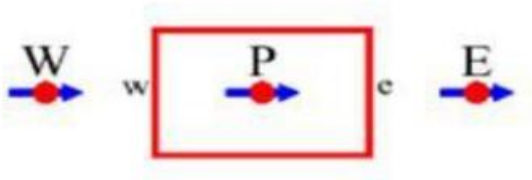

Figure 3.1 finite volume discretion. [51]

Here we take the stationary transport equation of a variable Φ by convection diffusion in its general form:

$$\frac{\partial}{\partial x_i}(\rho u_i \phi) = \frac{\partial}{\partial x_i}\left(\Gamma \frac{\partial \phi}{\partial x_i}\right) + S \qquad (3.1)$$

Where,

u_i , is the component of the velocity following the direction x_i.

ρ , The volume mass.

Γ , The diffusion coefficient.

S , the source term.

The integration of the previous equation (3.1) into finite volume gives :

$$a_e u_e = \sum a_{nb} u_{nb} + b + A_e\left(P_p - P_E\right) \qquad (3.2)$$

$$a_{nb} u_{nb} = a_c u_e$$

Is an initial pressure field p^*. The provisional solution of the previous equation (3.2) will be noted u^* (note that u^* does not verify the continuity equation).

$$a_e {u_e}^* = \sum a_{nb} {u_{nb}}^* + b + A_e\left(P_p^* - P_E^*\right) \qquad (3.3)$$

At this stage, neither of the two variables is correct. Both require correction.

$$U = u' + u^* \tag{3.4}$$

$$\mathrm{p} = \mathrm{p}' + \mathrm{p}^* \tag{3.5}$$

Where, u' and p' are the correction to estimate.

By introducing (3.4) and (3.5) in (3.2) we will get:

$$u_e = u_e^* + d_e\left(P_p' - P_E'\right) \tag{3.6}$$

We obtained the velocity correction equation: $d_e = \frac{A_e}{a_e}$.

Note here that for linear equations, the term $\sum$ has simply been neglected. Normally, this term must be deleted when the procedure converges. That is, this omission does not affect the final result, but it somewhat distorts the temporary result. This is the only simplification made in the SIMPLE algorithm. It has been corrected in the more advanced variants (SIMPLER et SIMPLEC).

the pressure correction equation from introducing the equation (3.6) in (3.2), to be written as follows:

$$a_p p_p = a_E p_E' - a_w p'_w + b \tag{3.7}$$

The following is a summary of the SIMPLE algorithm:

1. Select the pressure range p* for the start;

2. To determine a speed field u*, solve the transport equation;

3. resolve equations for pressure correction;

4. Accurate speed and pressure fields;

5. Resolve additional transport equations pertaining to different problem scalars, like temperature or turbulent characteristics;

6. To return to step 2, swap out the old pressure field for the new one.

Calculations should be repeated until all variables converge.

3.5.6 Pressure interpolation choice [42]

- The standard scheme is used in a very large number of applications.

- The second-order technique is selected for compressible flows, and it can even increase the accuracy of compressible flows.
- For high turbine flow, the PRESTO scheme (pressure straggling option) is appropriate. a rapid rate of rotation.
- The suggested body-forced weighted scheme is crucial for flow or volume forces.

3.6 Meshing

3.6.1 Mesh Definition

A mesh is created by dividing a physical domain into smaller, typically convex sub-domains. An EDP is resolved by it.

There are two main categories of numerical simulation codes in fluid mechanics. The two classes, structure mesh and non-structure mesh, are equivalent to the types of mesh utilized in simulations. Each of these two mesh types has benefits and drawbacks.

3.6.2 Structured mesh

A structured mesh is a line of mesh or a mesh by space direction such that, in dimensions 2 and 3, each node of the mesh can be uniquely identified by a double (x, y) or a triple (x, y, z). The table below enumerates this mesh's benefits and drawbacks.

Table 3-1 advantages and disadvantages of structured mesh.

Advantages	Disadvantages
-Their description is light, and with a small number of parameters, it is possible to define a whole mesh. -Their modification is very easy, on the one hand because of the few parameters to modify and, on the other hand, because of the possibility of using projection algorithms.	-Human expertise is necessary. A structured mesh must meet a specific specification for the charges. -They do not allow complex geometries to be woven into a single block. For example, it is impossible to mesh a disk through a single-block structure mesh. -Its implementation is difficult.

-Calculations are generally faster in a structured mesh than in an unstructured mesh.	

3.6.3 Non-structured mesh

An unstructured mesh is constructed with at least the following elements:

• The number of nodes in the grid, and each node being identified by the coordinates (xi; yi; zi).

• The number of volumes in the mesh, with each volume being defined by the N tops of the cell, and this is the connectivity table of the elements of the mesh.

The advantages and disadvantages of this mesh are listed in the table below:

Table 3-2 advantages and disadvantages of non structured mesh.

Advantages	Disadvantages
-Their generation is more automatic. -They are adapted to complex shapes without the operator having to interfere too much. -They require fewer points compared to structured mesh.	-They increase errors, at least locally. -The calculation time is generally longer, and it is more difficult to store the calculation data. -It is difficult to locally control mesh density.

3.7 Under relaxation

Convergence is not always satisfactory, and in this case, the solution should not be used for an analysis of the actual flow **[44]**. This may be the case when the boundary conditions are not suitable, when the mesh is too rough and therefore requires refinement in areas involving large gradients, or when dynamic effects are significant, making the solution unstable. One solution is then to “slow down” the operation of the digital resolution by introducing relaxation coefficients, α, in the

previous equations. Thus, the solution at iteration (k) is estimated from only one part of the solution estimated at iteration (k − 1):

$$x_i^{(k)} = x_i^{(k-1)} + \alpha\left(\sum_{j=1}^{N}\left(-\frac{A_{ij}}{A_{ii}}\right)x_j^{(k-1)} + \frac{b_i}{A_{ii}}\right) \tag{3.8}$$

The under-relaxation approach is applied when the coefficient value is $0 < \alpha < 1$, while the over-relaxation technique is applied when $\alpha > 1$ ~a. for an extremely fast flow via an endless number of circular cylinders that are aligned (using a periodicity constraint in this scenario). When an under-relaxation is put on the solution's evolution, an acceptable convergence of them is attained; otherwise, the calculation is halted by the calculation code. Thus, it is seen that under-relaxation enables convergent solutions with a higher number of iterations in challenging circumstances.

3.8 Convergence judgment

For most problems, the convergence criterion requires defined scaled residues to decrease to 10^{-3} for all equations except for energy and P-1 equations, for which the criteria is 10^{-6}.

Sometimes, however, this criterion may not be appropriate. Typical situations are listed below. **[44]**

- A large-scale residue for the continuity equation might result from an initial continuity residue that is extremely modest if the flow field is initially estimated accurately. Examining the uncalibrated residue and comparing it to a suitable scale, such as mass flow at the input, is helpful in such a scenario.
- High-scale factors can be the outcome of an inaccurate starting estimate for some equations, like turbulence quantities. Scaled residues in these situations will begin low, rise with the accumulation of nonlinear sources, and then fall. Therefore, it is best practice to assess convergence based on both the residue's behavior and value. Before declaring that the solution has converged, you have to ensure that the residue keeps becoming smaller (or stays weak) for a number of iterations (let's say 50 or more).

A further popular method for assessing convergence is to demand a three-order-of-magnitude drop in unscaled residues. Both pressure-based solvents and density-based solvers have defined residues. The convergence condition for this method is that the unscaled standardized residues must approach 10^{-3}. But in many situations, this criterion might not be appropriate:

-If you provide a very good initial estimate, the residues may not fall by three orders of magnitude. In an almost isothermic discharge, for example, energy residues may not fall by three orders if the initial temperature estimate is very close to the final solution.
-If the main equation contains non-linear source terms that are null at the beginning of the calculation and accumulate slowly during the computation, the residues may not fall by three orders of magnitude. In the case of natural convection in a container, for example, the residues of the initial movement quantity may be very close to zero because the initial estimate of the uniform temperature does not generate floatability. In such a case, the initial residue close to zero is not a good scale for the residue.
-If the interest variable is almost zero everywhere, the residues may not fall by three orders of magnitude. In a fully developed flow in a pipe, for example, the transverse speeds are zero. If these speeds were initialized at zero, the initial (and final) residues are both close to zero, and a three-order drop cannot be expected.

Before declaring that the solution has converged in such circumstances, it is prudent to keep an eye on the integrated quantities, such as traction or the overall heat transfer coefficient. Examining unstaged, non-standardized residue to see if it is modest in relation to the right scale might also be helpful.

On the other hand, it is plausible that a three-order residual drop may not ensure convergence if the first estimate is really low and the initial residues are very high. This holds true for k equations, for which it is challenging to make reasonable initial assumptions. Once more, it is helpful to examine the total integrated amounts that specifically catch your attention.

3.9 Computational fluid dynamics

Through computer-based simulation, systems including fluid flow, heat transport, and related phenomena like chemical reactions are analyzed in computational fluid dynamics, or CFD **[63]**. The method has a broad variety of industrial and non-industrial application sectors and is highly powerful.

The primary cause of CFD's lag is the underlying behavior's extreme complexity, which makes it impossible to describe fluid flows in a way that is both sufficiently complete and inexpensive.

Fluent is a CFD software capable of modeling fluid flows involving complex physical phenomena such as turbulence, thermal transfer, chemical reactions, and multiphase flows in complex geometry areas. It is widely used in the aerospace industry. It offers a simple interface, allowing the user access to the functions required for the calculation of the solution and the display of the results **[44]**.

The numerical techniques that can solve fluid flow issues are the foundation of CFD codes. All commercial CFD packages feature sophisticated user interfaces for entering problem parameters and examining outcomes, making their solution capabilities easily accessible.

Thus, there are three primary components to all codes:

- Preprocessor;
- Solver;
- post-processor.

3.9.1 Preprocessor

Preprocessing is the process of entering a flow problem into a CFD program through an operator-friendly interface and then transforming that input into a format that the solver can use. During the preprocessing phase, the user does the following **[41]**:

-The computational domain is the defined geometry of the area of interest.
-Grid creation is the process of breaking the domain up into several more manageable, non-overlapping sub-domains: a mesh or grid of cells, also known as control volumes or elements.
-choosing the chemical and physical phenomena that require modeling.
-Fluid property definition.
-defining suitable border conditions at cells that contact or coincide with the domain boundary.

The generation of the mesh is carried out in Gambit, which is the software offered with Fluent. It allows to represent the geometry of the system and define the types of conditions at the boundaries of the domain **[44]**.

At nodes within each cell, the solution to a flow problem (temperature, pressure, velocity, etc.) is defined. The number of cells in the grid determines how accurate a CFD solution is. More cells generally translate into more accurate solutions. The fineness of the grid affects a solution's accuracy as well as its cost in terms of required computer hardware and computation time. Optimal meshes are frequently not consistent, being coarser in regions with little change and finer in areas with significant fluctuations from point to point. **[41]**

3.9.2 Solver

The numerical solution techniques can be divided into three categories, as we saw in the beginning of the chapter: spectral methods, finite element methods, and finite difference methods. The following actions are taken by the numerical techniques that serve as the solver's foundation in outline **[41]**:

-The unknown flow variables are approximated using basic functions.
-Discretization through further mathematical manipulations and approximation substitution into the controlling flow equations.
-the algebraic equation’s solution.

The discretization procedures and the approximation of the flow variables are linked to the primary distinctions among the three distinct streams.

The solver allows numerically to define the operating conditions (gravity, pressure) in which the simulation is performed, as well as the specification of the conditions at the limits, the definition of the properties of the fluid, and the type of material. Finally, it allows you to choose the iterative process for the calculation. It also provides an interface for monitoring the progress of calculations at any time **[44]**.

3.9.3 Post-processor

Similar to preprocessing, post-processing has seen a significant surge in development activity recently. The most popular CFD software now comes with flexible data visualization tools because engineering workstations, many of which have exceptional graphics capabilities, are becoming more common. **[41]**

The component that enables you to see the domain's geometry and grid is the post-processor; it is primarily responsible for displaying the outcomes. This enables the visualization of all other sizes computed on a segment, a domain part, or the complete domain, as well as the speed vector fields, pressure, and turbulence fields. Additionally, it provides the ability to visualize particle trajectories, current lines, and curves.

These features have evolved more recently to incorporate animation for dynamic result display, data export capabilities for additional manipulation outside of the code, and reliable alphanumeric output from all codes in addition to graphics.

3.10 Solving problem using CFD

CFD simulation is crucial in solving fluid flow problems due to the complex underlying physics. It involves identifying and formulating the flow problem in terms of physical and chemical phenomena. Decisions include modeling in two or three dimensions, excluding ambient temperature or pressure variations, and solving turbulent flow equations or neglecting them. The results generated by a CFD code are at best as good as the underlying physics and operator.

The quality of the information produced by CFD is, at least in part, determined by how appropriate the simplifications made at this point are, so the user must

constantly be aware of all the assumptions—both explicit and implicit—that have been made. **[52]**

The numerical method employs mathematical concepts such as convergence, consistency, and stability to produce an exact solution. Convergence involves a numerical method producing solutions that approach the exact solution as the grid spacing approaches zero. Consistency involves consistent numerical schemes that produce algebraic equations equivalent to the governing equation. Stability involves damping errors, preventing wild oscillations or divergence if the technique is not stable. **[53]**

The finite volume approach guarantees local conservation of a fluid property ϕ for each control volume. When numerical schemes have the conservativeness property, the fluid property is globally conserved over the whole domain. This is accomplished by using consistent expressions for fluxes of ϕ through the cell faces of neighboring control volumes, and it is obviously significant physically [58].The Boundedness property, which is related to stability, stipulates that the maximum and minimum boundary values of the flow variable must limit the solution of a linear problem without sources. Restrictions on the magnitude and signs of the algebraic equations' coefficients can be used to create boundedness. Despite the fact that flow problems are non-linear, it is crucial to understand the boundedness of a finite volume scheme when dealing with linearly linked problems. **[54]**

Finally, convection and diffusion have an impact on all flow processes. A change in temperature at one site affects the temperature in all directions surrounding it in roughly equal measure when diffusive phenomena, such as heat conduction, are present. The directionality of influence must be taken into consideration in finite volume schemes with the transportiveness attribute in terms of the relative intensity of diffusion and convection. **[53]**

Conservativeness, boundedness and transportiveness are designed into all finite volume schemes and have been widely shown to lead to successful CFD simulations.

Different kinds of operator abilities are needed to complete the CFD computation itself. The primary tasks at the input stage are the specification of the domain

geometry and grid design; the user then needs to acquire a successful simulation result. Such a solution is characterized by two factors: grid independence and convergence of the iterative process. The iterative nature of the solution process results in very few so-called residuals, or measurements of the overall conservation of flow properties, in a converged solution. **[52]**

Understanding the predicted features of the flow is crucial for designing a good first grid **[55]**. It is undoubtedly helpful to have prior knowledge of the fluid dynamics of the specific problem, and gridding experience with related situations is also quite beneficial **[56]**. The sole method to get rid of errors caused by the coarseness of the grid is to carry out grid dependence research, which is a process of gradually fine-tuning a coarse grid until some important outcomes remain the same. After that, there is no grid in the simulation.**[52]**

It is evident that there are best practices recommendations that might help a CFD code user, and regular validation is essential as the last line of defense against errors. But experience and a solid grasp of the principles of numerical algorithms as well as the physics of fluid flows are the key components of success in computational fluid dynamics (CFD). **[52]**

3.11 Conclusion

In conclusion of this chapter, we have determined that for our study, we will use the finite volume method with the pressure-based solver to solve the mathematical system. In addition, considering the complexity of the geometries in our study and the advantages discussed in this chapter, we will adopt a non-structured mesh for our simulation.

Now that we have identified the numerical code to be used in our simulation and understand all its components, including the steps for solving a problem with this code, we can proceed to the main part of our project. This will involve the geometries and simulation modeling, which will be discussed in the next chapter.

CHAPTER 04:

Combustors modeling and simulation setup

Summary:

Chapter 04: combustors modeling and fluent setup

4.1 Introduction

A brief overview of both the reverse air combustor and conventional combustor geometries has already been discussed in Chapter 1. In this chapter, we will focus on the detailed modeling of these geometries and their respective uses.

These chamber designs can be greatly improved by making appropriate changes to the overall geometry. However, this cannot be achieved without a thorough understanding of the flow physics within the entire domain. Therefore, the present work aims to perform extensive cold flow simulations for two can-type combustor geometries using the CFD processor FLUENT.

4.2 Main parts of can-type combustor

4.2.1 Dome

The combustion chamber dome forms the primary zone where the initial flame structure and subsequent propagation are determined.

The dome region mainly experiences the formation of a toroidal recirculation zone, which aids in anchoring the flame in the primary zone. However, excessive turbulence generated in this region can sometimes cause flame rupture, leading to a degradation in overall combustor performance. Therefore, it is crucial to carefully control the turbulence in this area by adjusting the dome's geometry. **[41]**

4.2.2 Fuel injector

The injector has a trapezoidal shape (a frustum in 3D). It has an external diameter of 15 mm and an internal diameter of 5 mm. As mentioned, there are ten fuel holes distributed around the perimeter of the injector. Each hole has a diameter of 1.7 mm. In the reverse air combustor, the holes are located on the center line of the injector, while in the conventional combustor, they are positioned along the pitch **[24]**. The 5 mm extent of the injector in the flow direction has been taken into

consideration. To ensure effective fuel and air mixing in the primary zone, fuel is only emitted from the peripheral holes and not from the injector tip.

4.2.3 Combustor barrel (cylinder)

The central part of the combustion chamber is known as the barrel region. It includes the primary and dilution holes, as well as the cylindrical body of the chamber. The flow of gases within the barrel is primarily governed by the turbulence generated by the radially penetrating jets of primary and dilution air. The majority of the flow does not effectively carry the primary jets along with it. As a result, most of the flow returns to the primary zone and forms the toroidal wakes discussed earlier. However, due to the acceleration provided by the nozzle at the rear, the dilution jets are pulled along with the bulk flow. **[21]**

4.2.4 Swirler

For the reverse air swirler, its geometry consists of 8 vanes, while the conventional one has been designed with 10 vanes, slanted 45 degrees toward the swirler's axis **[25]**. This configuration of the vanes causes the incoming air flow to develop a characteristic swirl as it enters the primary zone. The swirl ensures the efficient mixing of air and fuel.

4.2.5 Convergent nozzle

The nozzle section guides the hot gases from the combustor to the gas turbine stage. The nozzle needs to ensure an even temperature distribution at the outlet of the combustor to prevent thermal stress on the turbine vanes. Achieving an even temperature distribution is challenging in a configuration where flame dynamics and turbulence dominate most of the physics. **[41]**

The nozzle is designed as a circular to rectangular convergent type. Under combustion conditions, hot gases reach high velocities inside the nozzle, which makes it necessary to include this portion in the simulation. It should be noted that there is significant complexity involved in modeling this stage due to the large discrepancy in the sections at both ends (circular to rectangular).

4.3 Combustors modeling:

Both SOLIDWORKS and workbench ANSYS design-modeler have been used for modeling the parts of the combustor.

4.3.1 Conventional can-type combustor

4.3.1.1 Dome and cylinder

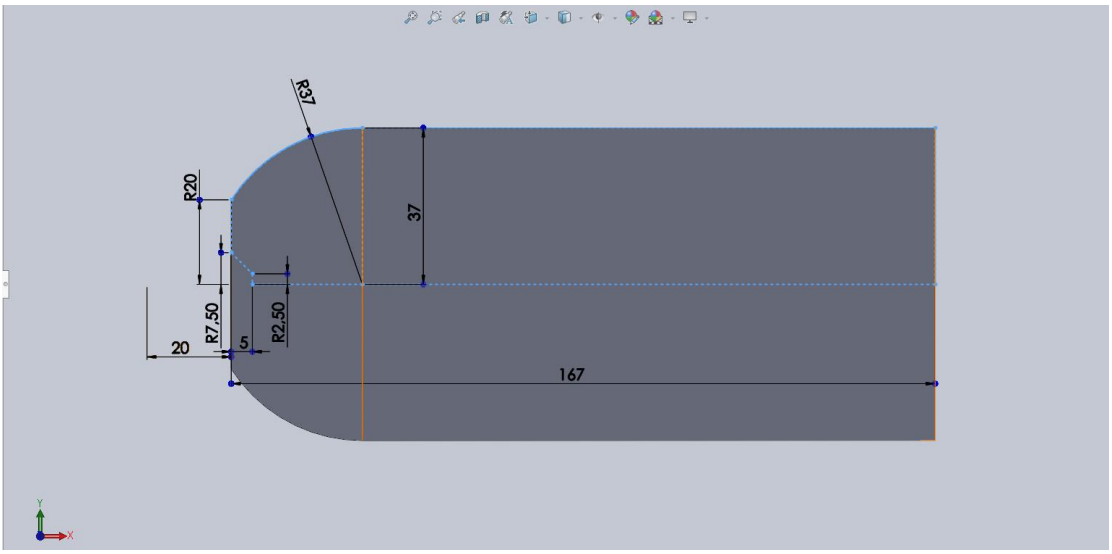

Figure 4.1 conventional combustor dome and cylinder dimensions and conception in SOLIDWORKS.

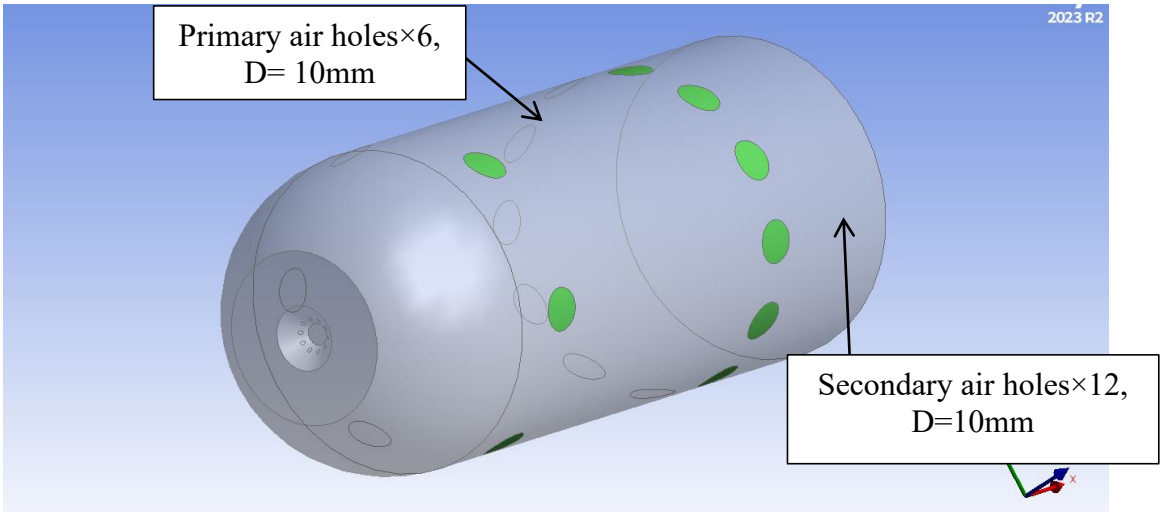

Figure 4.2 conventional combustor dome and cylinder 3D view, primary and secondary air holes dimensions

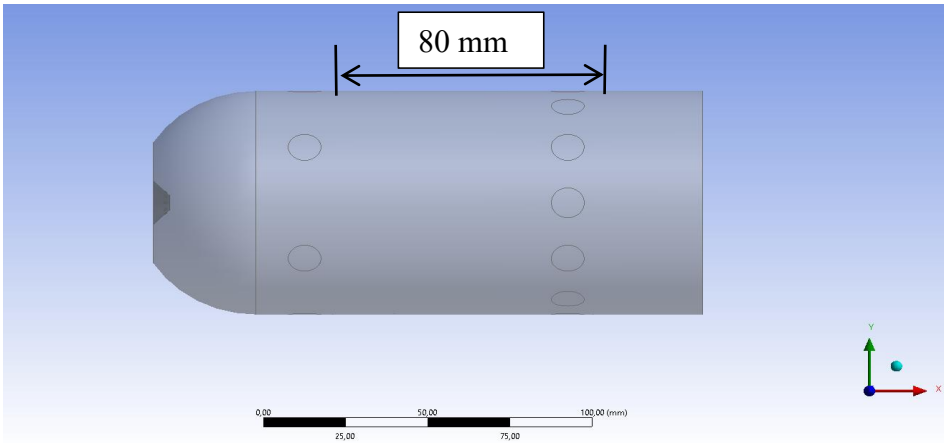

Figure 23: conventional combustor dome and cylinder front face.

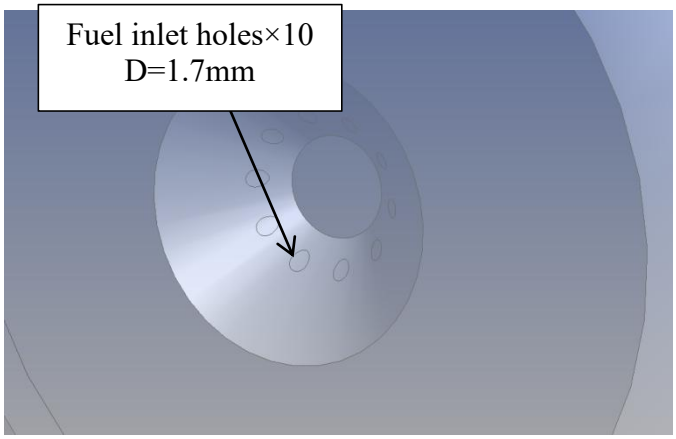

Figure 4.4 conventional combustor fuel injector with fuel inlet holes.

4.3.1.2 Swirler

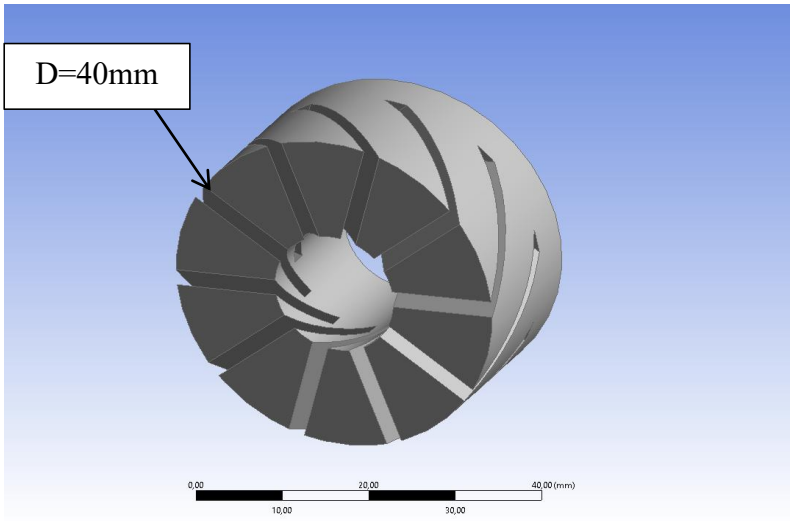

Figure 4.5 conventional combustor swirler 3D view

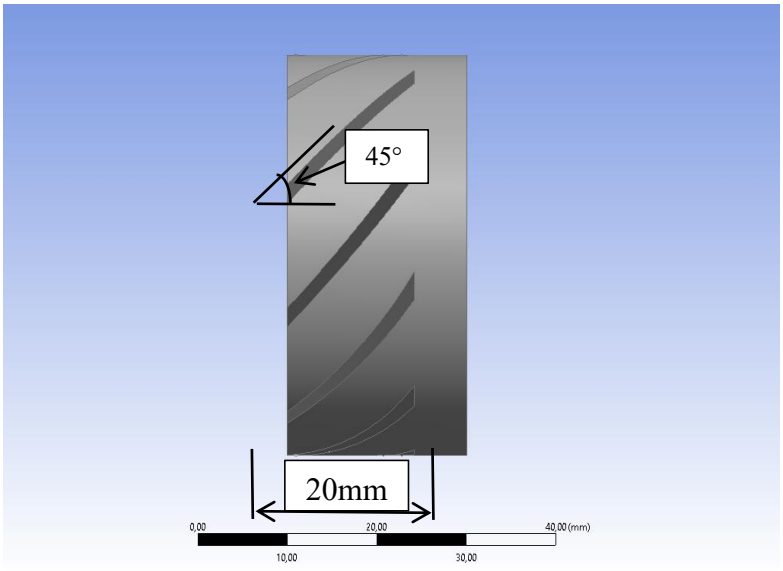

Figure 4.6 conventional combustor front view, vanes inclination.

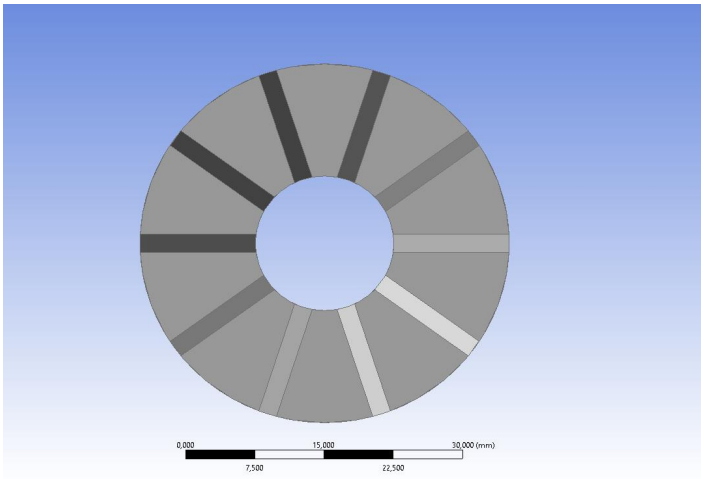

Figure 4.7 conventional combustor left view, vanes thickness (2mm)

4.3.2 Reverse air can-type combustor

4.3.2.1 Dome

The main advantage of this type of design is that the majority of the flow occurs inside the primary zone in a forward direction. This is not the case for the conventional combustor dome, where primary jets that penetrate radially cause the majority of the flow to recirculate inside the dome. Additionally, there are no areas of strong turbulence that could hinder the spread of flames inside the chamber. As a result, this design increases the likelihood of forming a stable flame with a hot core.

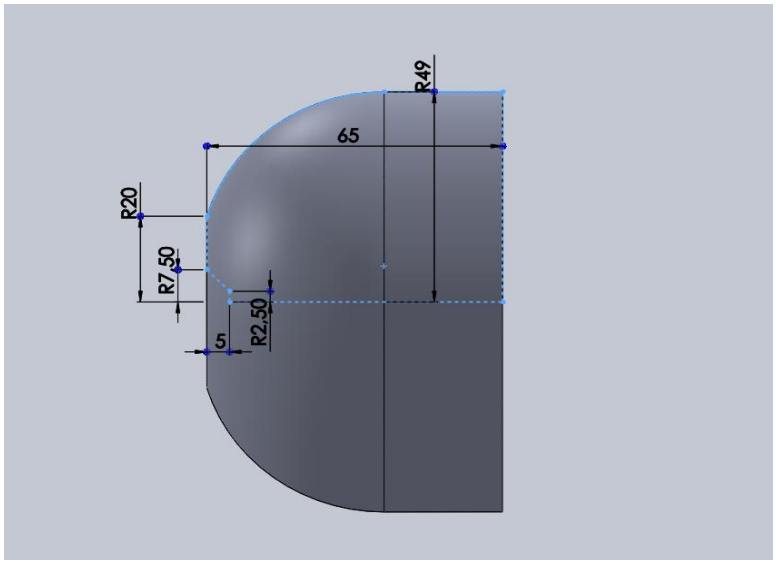

Figure 4.8 reverse air combustor dome dimensions in SOLIDWORKS.

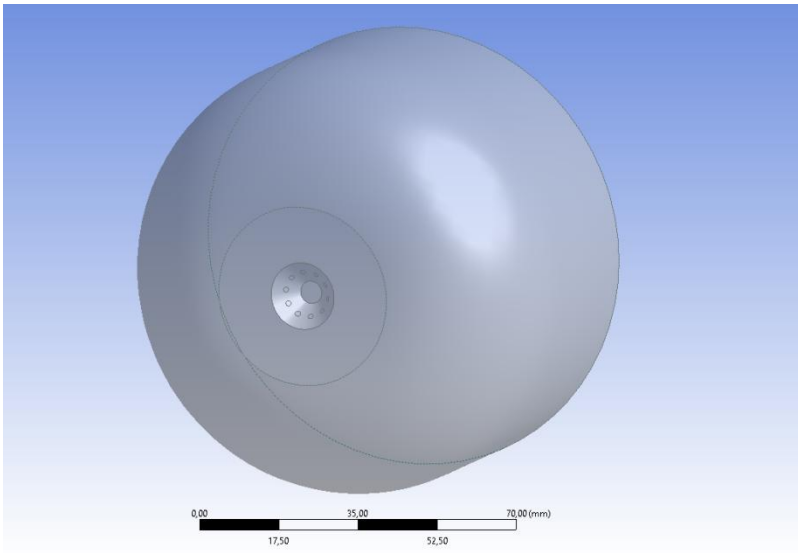

Figure 4.9 reverse air combustor 3D view

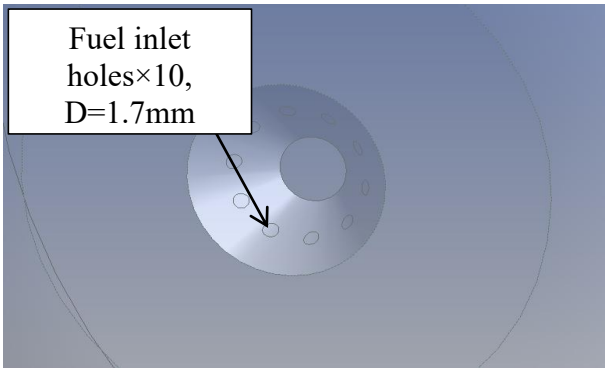

Figure 4.10 reverse air combustor-fuel inlet dimensions.

4.3.2.2 Cylinder barrel

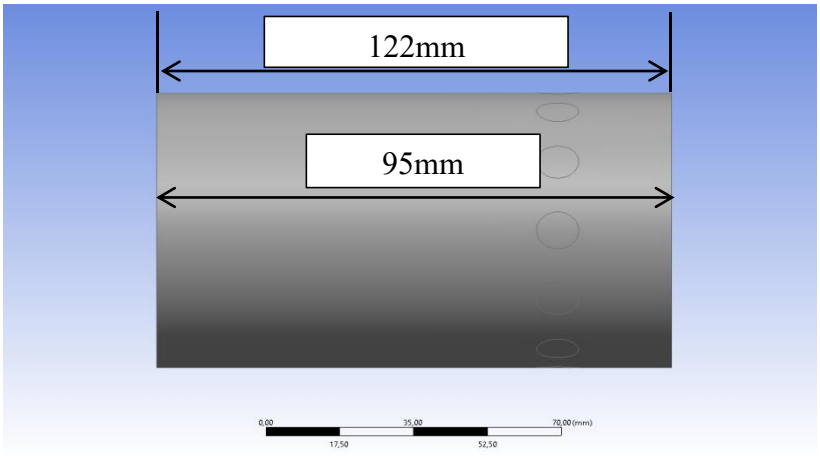

Figure 4.11 reverse air combustor cylinder front face-dimensions.

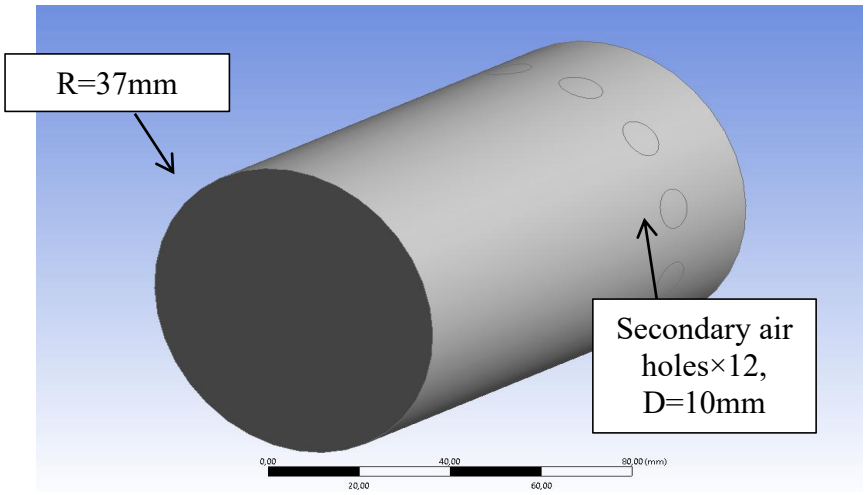

Figure 4.12 reverse air combustor cylinder 3D view.

4.3.2.3 Swirler

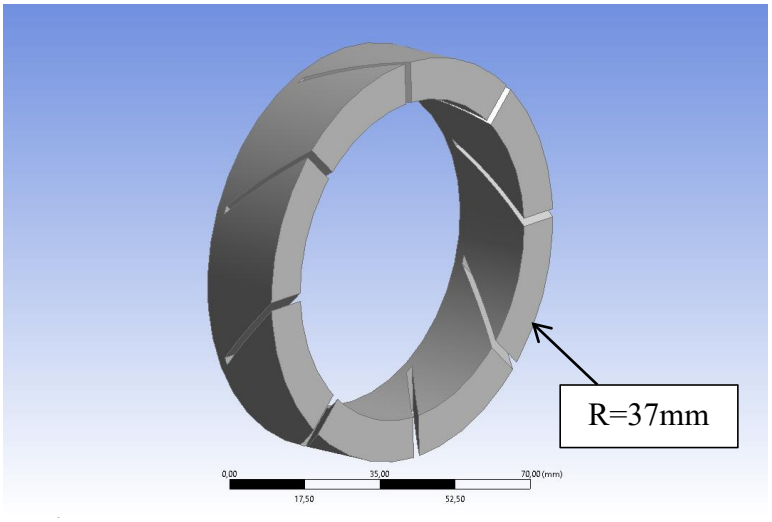

Figure 4.13 reverse air combustor swirler 3D view.

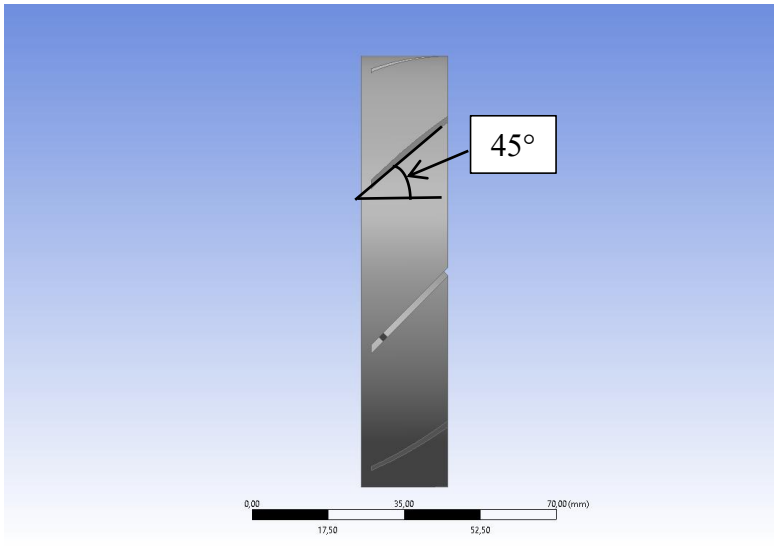

Figure 4.14 reverse air combustor swirler front view, vanes inclination.

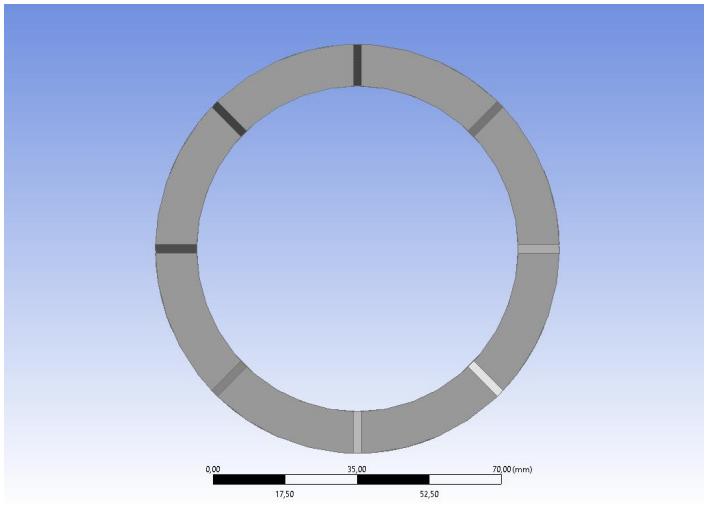

Figure 4.15 reverse air combustor swirler right view, thickness of vanes 2mm.

4.3.2.4 Convergent nozzle:

The nozzle conception stays the same for the both combustors.

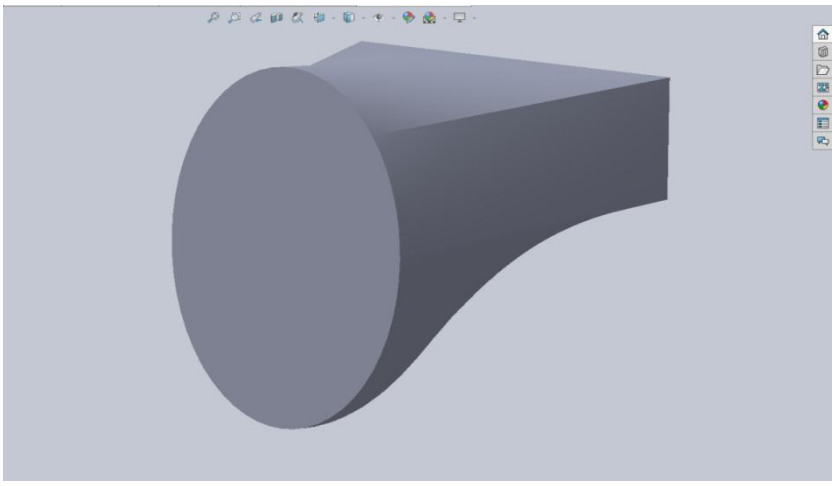

Figure 4.16 convergent nozzle 3D view in SOLIDWORKS.

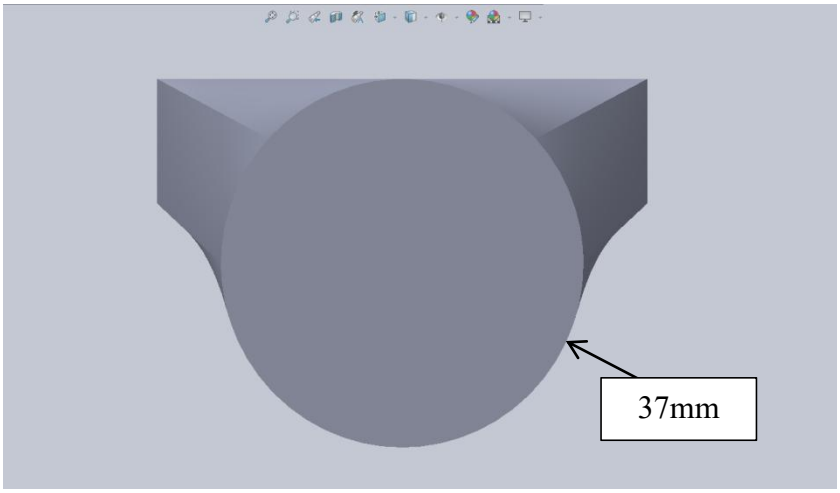

Figure 4.17 convergent nozzle left view.

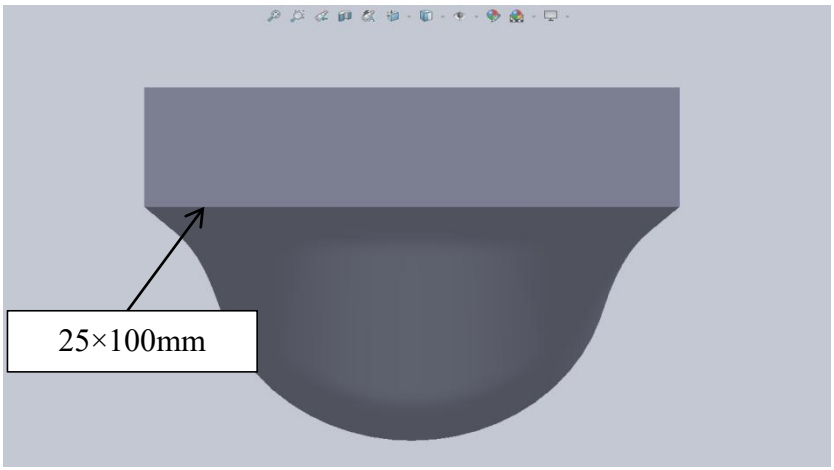

Figure 4.18 convergent nozzle right view.

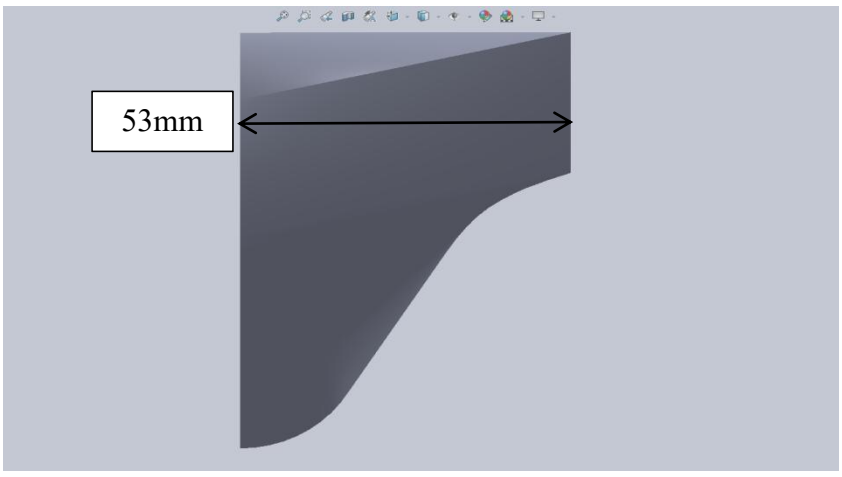

Figure 4.19 convergent nozzle front view.

4.4 Assembling the combustors

4.4.1 Conventional can-type combustor

By assembling all the components described above, the design of the conventional combustion chamber is complete. The combination of swirling flow with radially penetrating primary jets facilitates the generation of a significant amount of turbulence inside the primary zone. However, the wakes generated near the wall region may act as additional sources for anchoring the flame. This can result in undesirable overheating of the walls of the combustor.

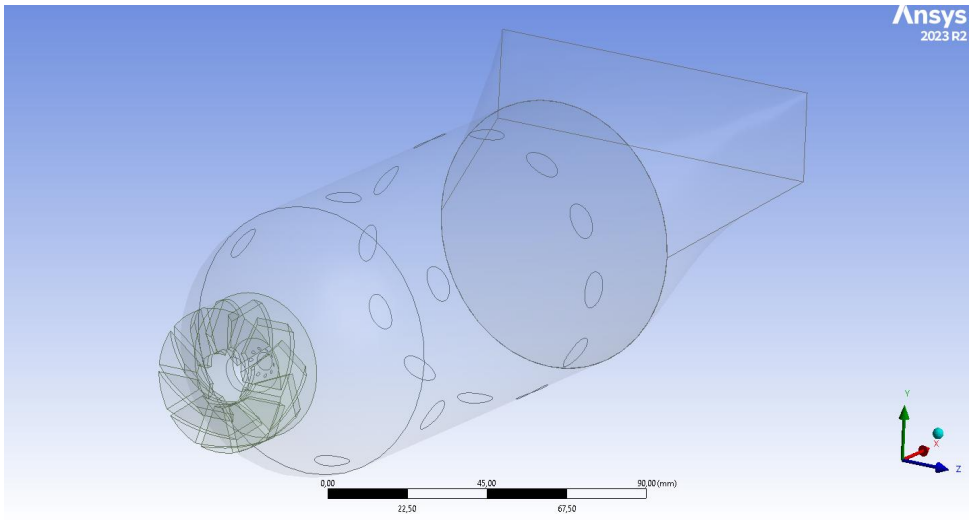

Figure 4.20 conventional combustor 3D front view.

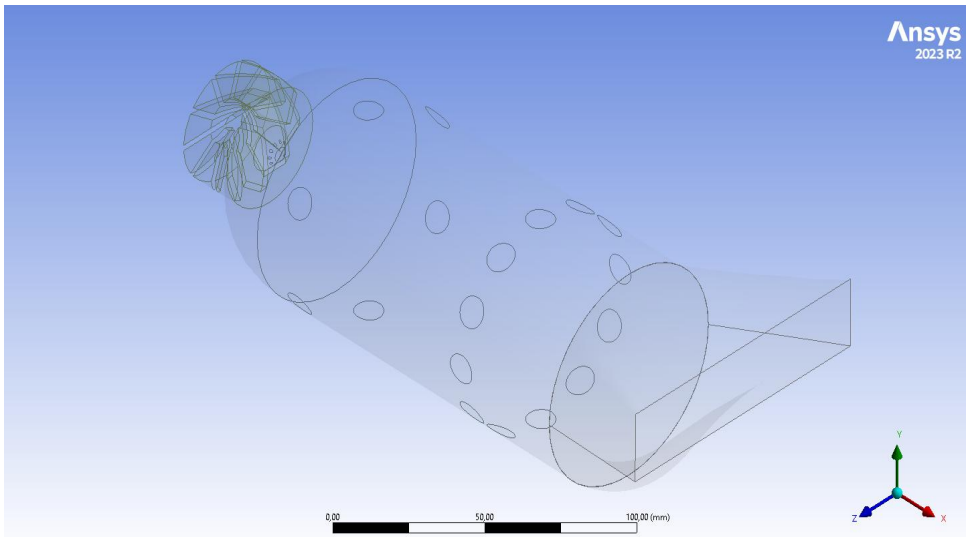

Figure 4.21 conventional combustor 3D back view.

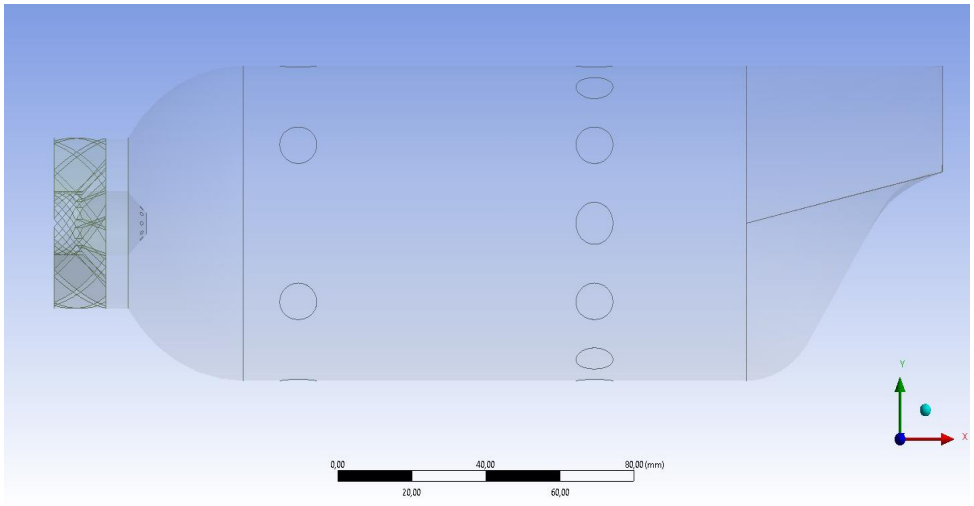

Figure 4.22 conventional combustor front view.

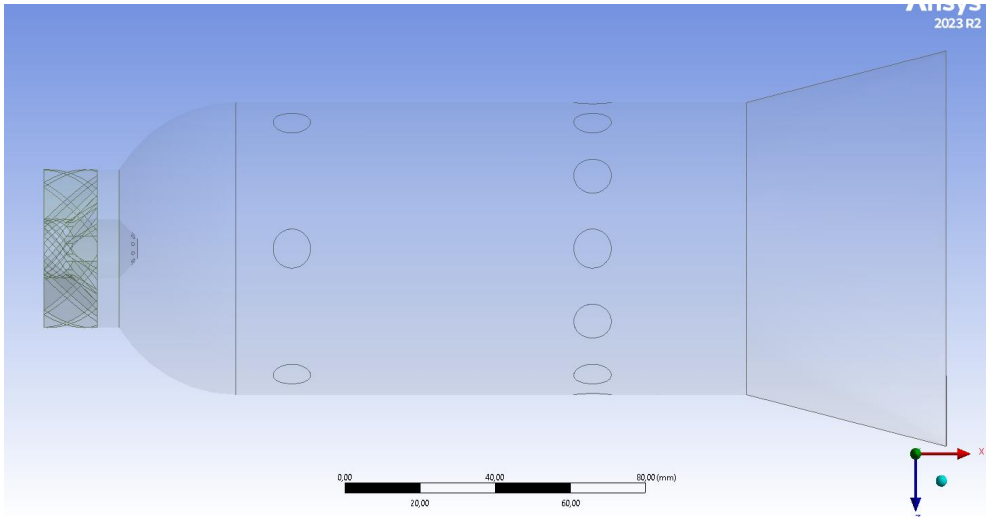

Figure 4.23 conventional combustor top view.

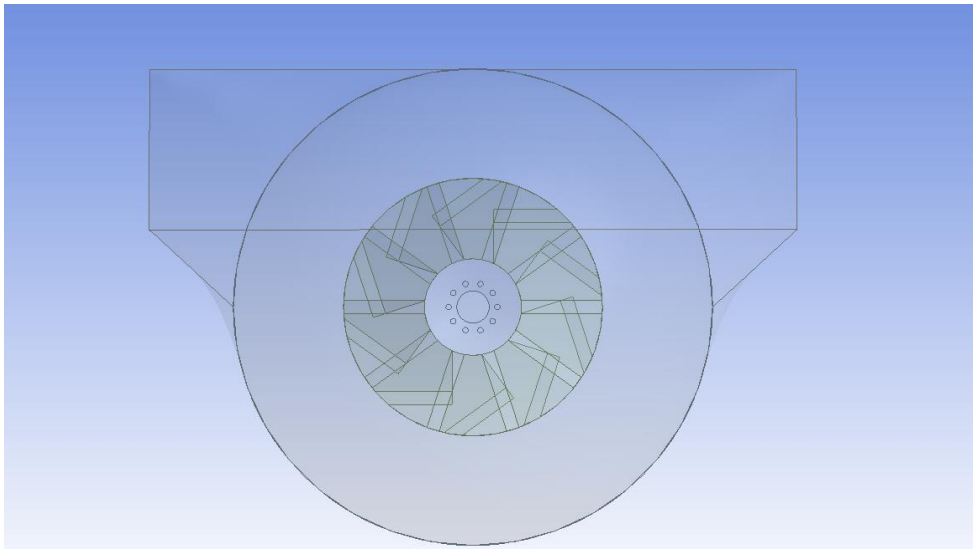

Figure 4.24 conventional combustor left view.

4.4.2 Reverse air can-type combustor

In this combustor, the mixing in the dome region is controlled by the effectiveness of fuel injection and the turbulence generated by the primary air entering the dome in a peripheral manner. There is a global change in the behavior of the flow within this geometry. The toroidal recirculation zone is reduced in size, resulting in a forward-moving flow regime within the primary zone. Steady flame dynamics can be expected from such a design.

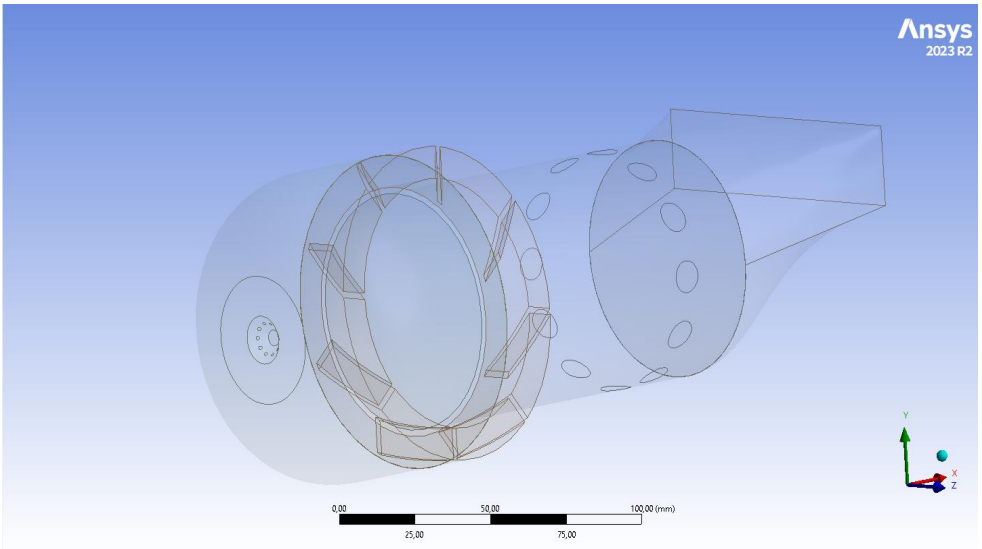

Figure 4.25 reverse air combustor 3D front view

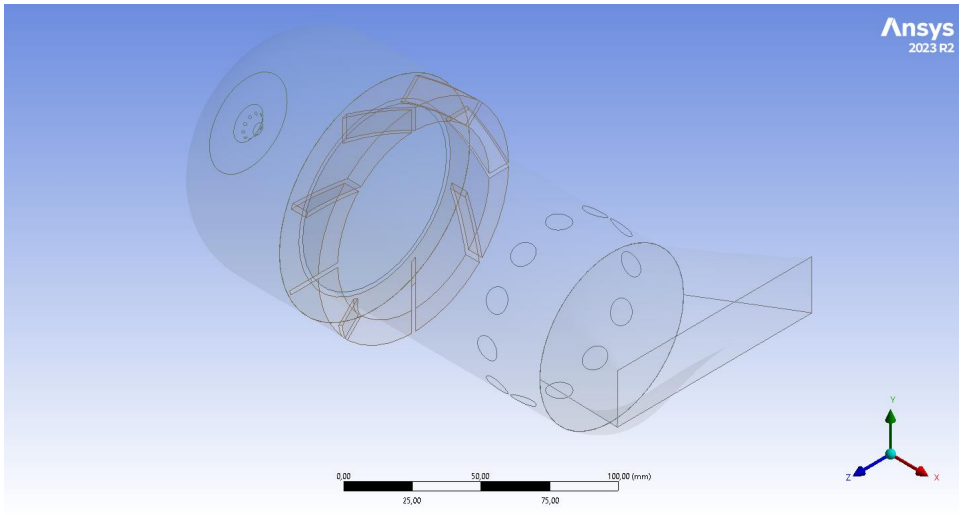

Figure 4.26 reverse air combustor 3D back view.

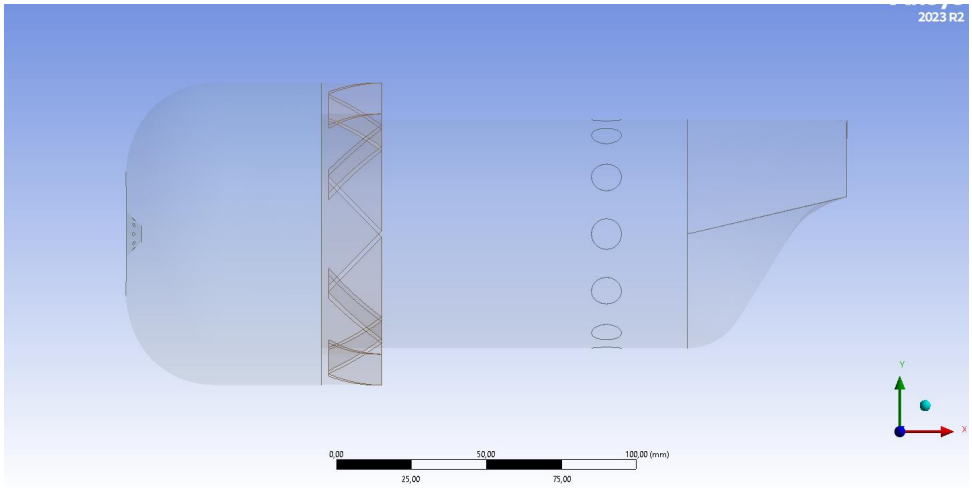

Figure 4.27 reverse air combustor front view.

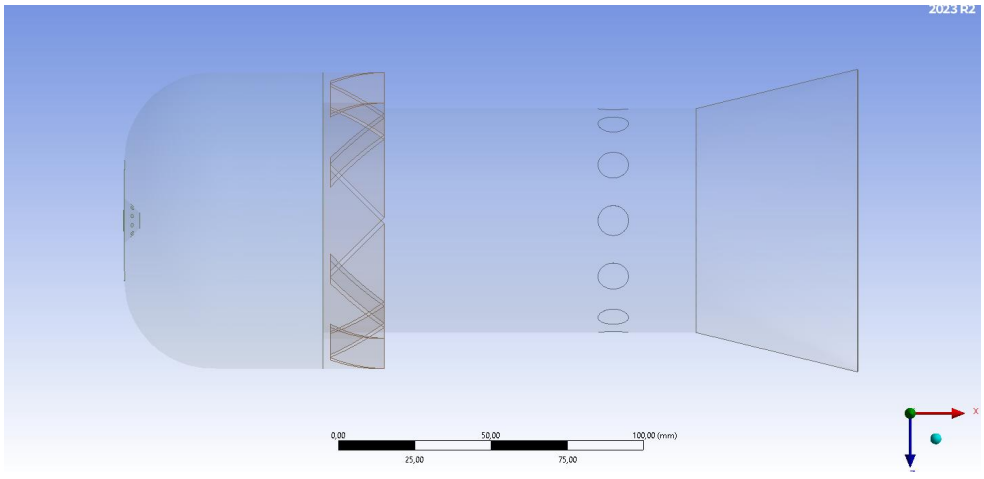

Figure 4.28 reverse air combustor top view.

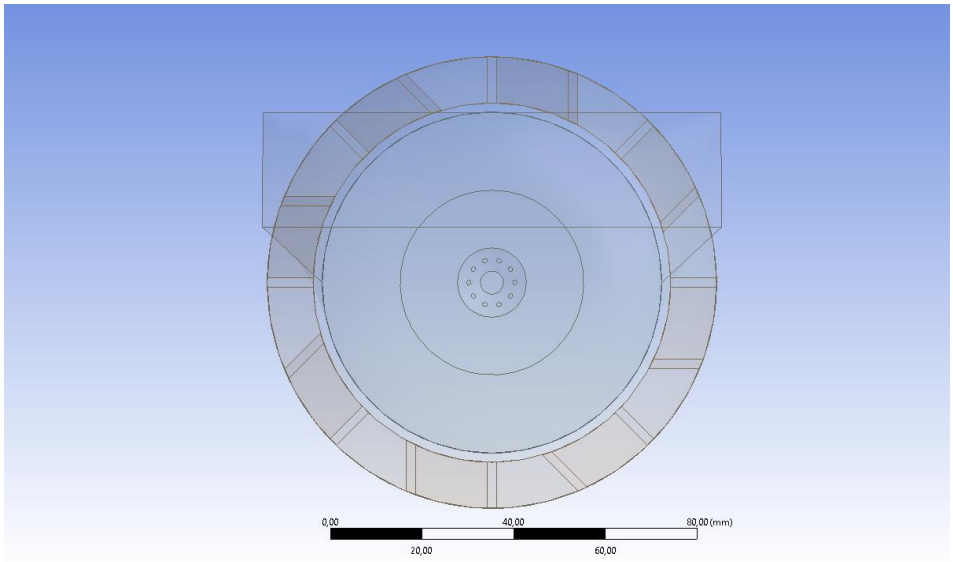

Figure 4.29 reverse air combustor left view.

4.5 Mesh generation

Since the CFD solver uses the finite-volume philosophy to numerically solve the flow and turbulence equations, the domain needs to be discretized into finite volumes, which is the essence of grid generation. The conservation equations of continuity, momentum, energy, etc. are then satisfied for each cell and for the entire domain. Grid generation procedures follow the same hierarchy as the geometrical entities.

This chapter focuses on the complexity of grid generation involved in meshing two combustor geometries. It also provides a quick overview of the different components used in grid generation.

4.5.1 Grid independence study-overview

It becomes imperative to establish grid independence if one needs to verify that the simulation's numbers are accurate. This research helps determine a grid size that might work well for a particular issue. The following is the process used in grid independence analysis:

1-Construct a grid A for a given problem.
2-Obtain the results for the same and study the variation of a critical parameter (e.g., static temperature) on a fixed geometrical entity (e.g., the centerline) of the domain.

3-Refine grid A to obtain grid B and plot the variation of the same parameter on the same entity.

4-If there is a negligible variation between the plots obtained by grids A and B, then the solution is said to have become grid-independent.

5-If both plots have a considerable variation between them, repeat the entire procedure until a match is obtained.

for our study, the variation of exit temperature along the center line of nozzle outlet will be considered in the grid independence analysis.

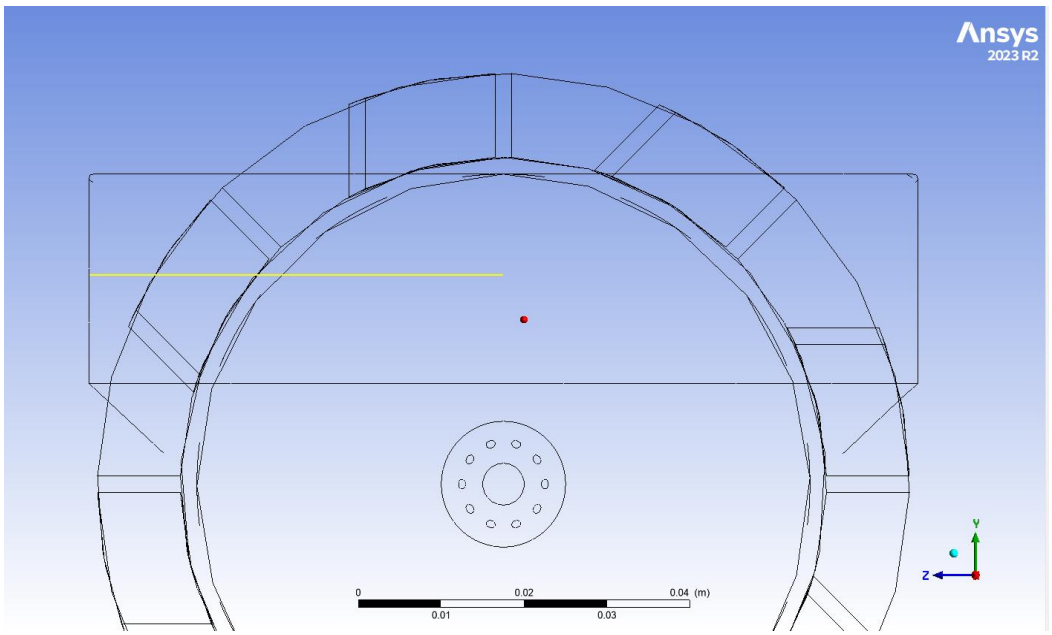

Figure 4.30 centerline position for our grid independence study, convergent nozzle outlet.

Generally speaking, all excellent CFD studies include a methodical search for grid-independent results. Understanding the predicted features of the flow is crucial for designing a good first grid. It is undoubtedly helpful to have prior knowledge of the fluid dynamics of the specific problem, and gridding experience with related situations is also quite beneficial.

4.5.2 Mesh generation for the combustors

4.5.2.1 Conventional combustor

Final grid size achieved is 1770535 non structured tetrahedral elements.

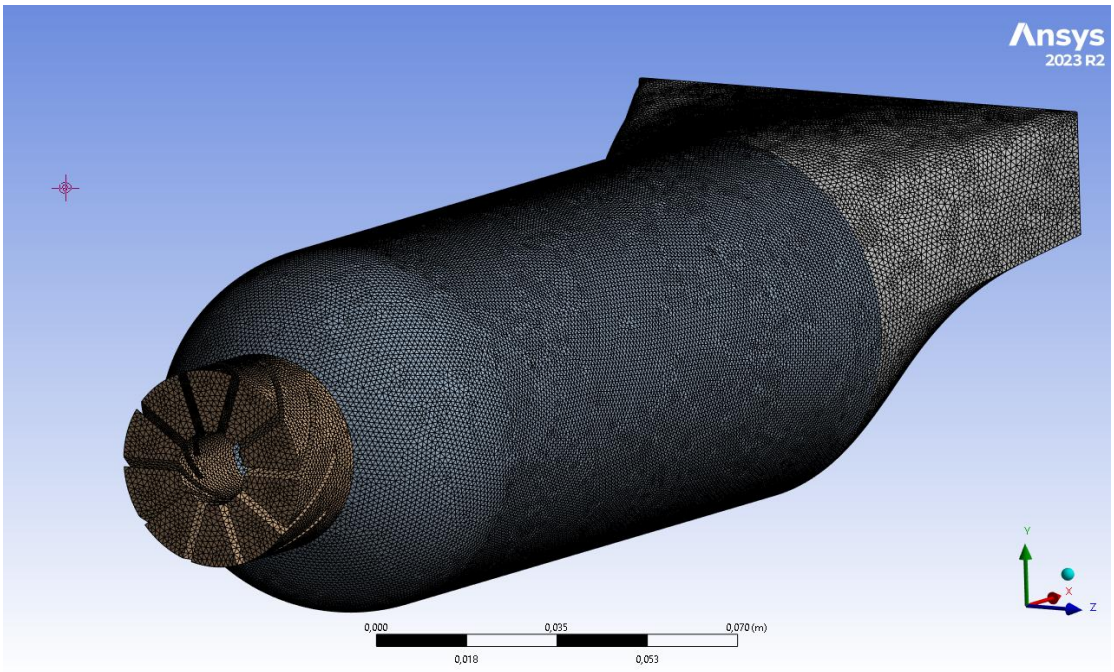

Figure 4.31 conventional combustor isometric front view mesh.

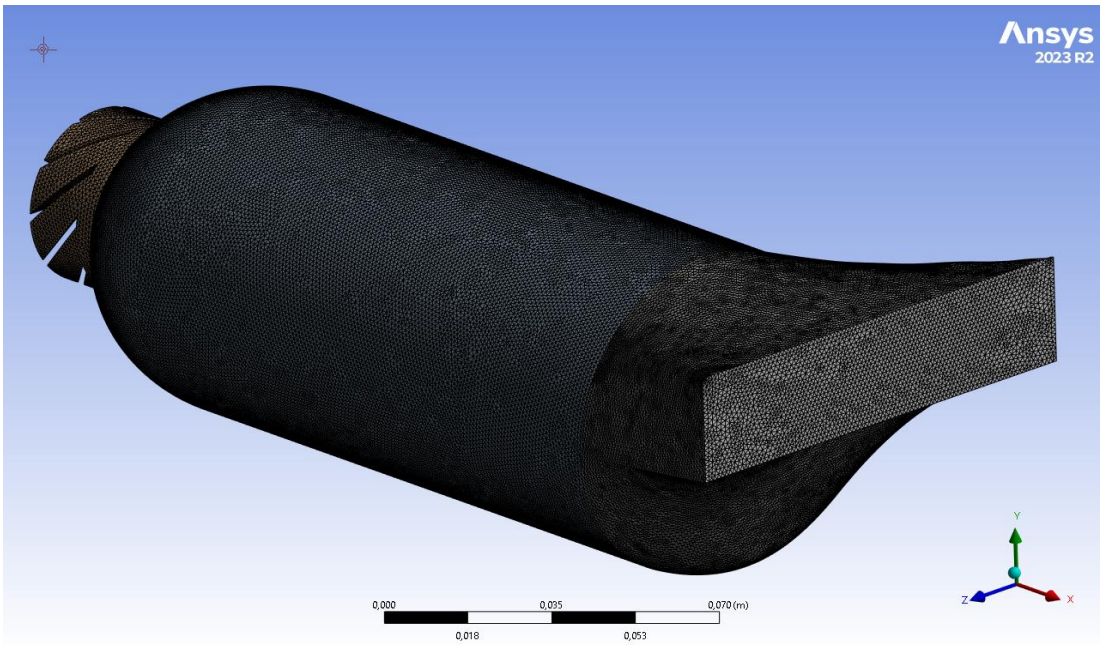

Figure 4.32 conventional combustor isometric back view mesh.

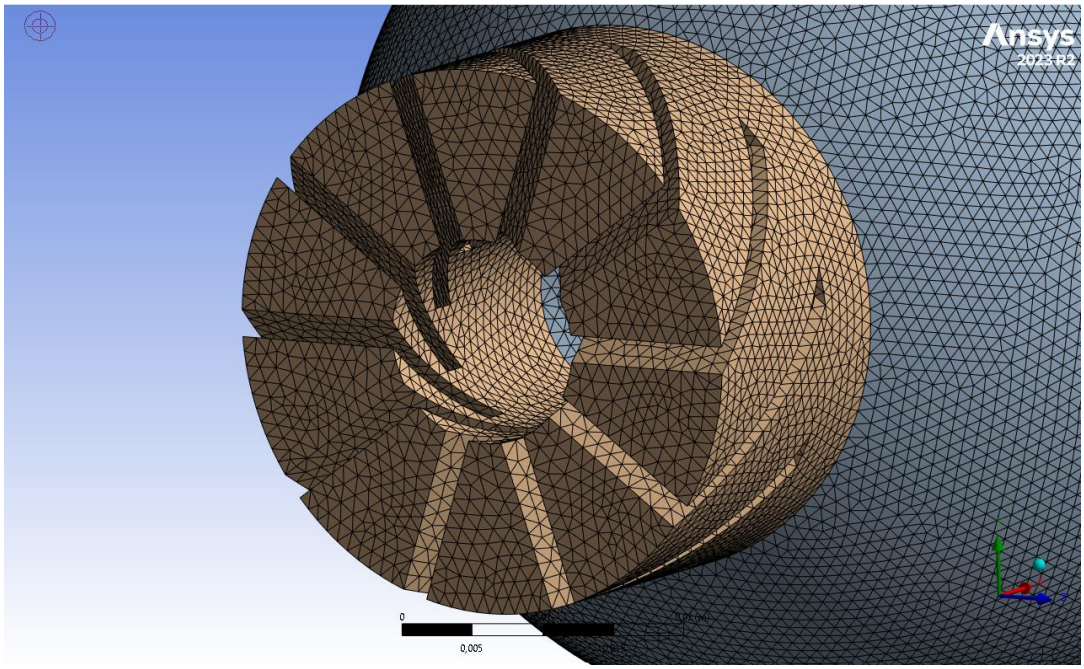

Figure 4.33 conventional combustor swirler mesh.

4.5.2.2 Reverse air combustor

Final grid size achieved is 2404038 non structured tetrahedral elements.

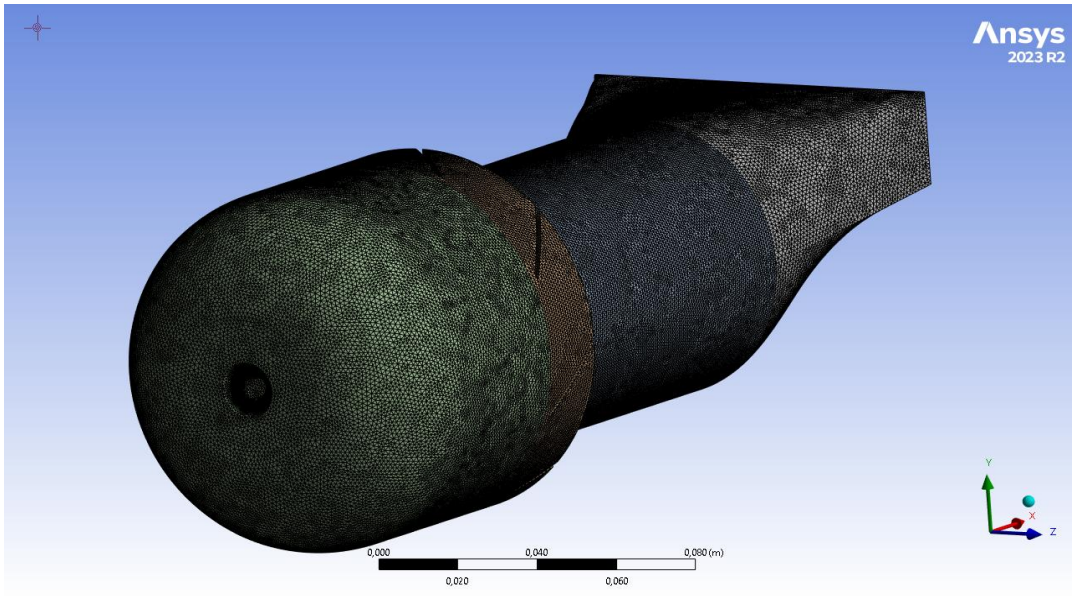

Figure 4.34 reverse air combustor isometric front view mesh.

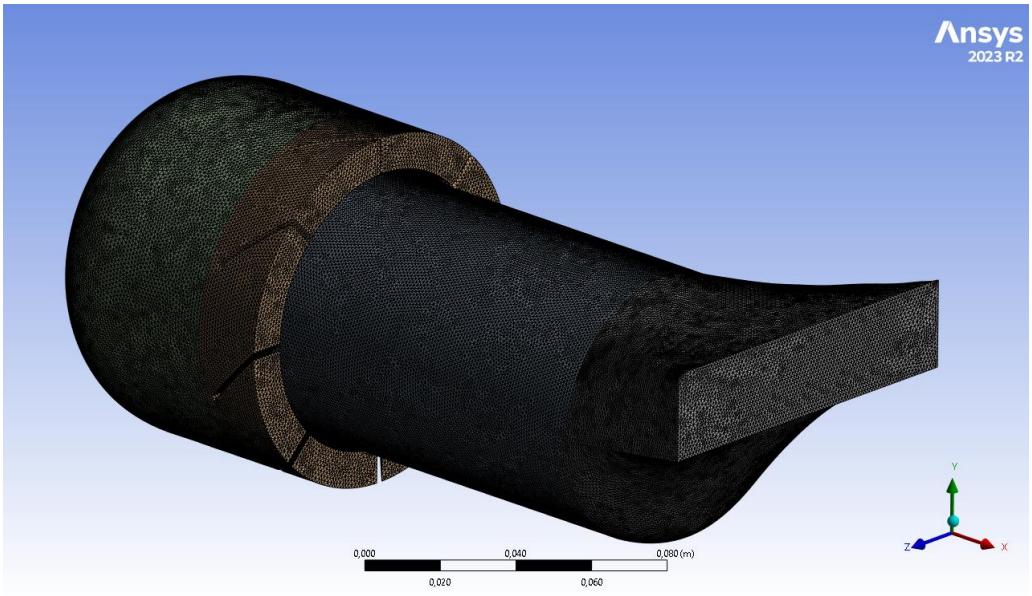

Figure 4.35 reverse air combustor isometric back view mesh.

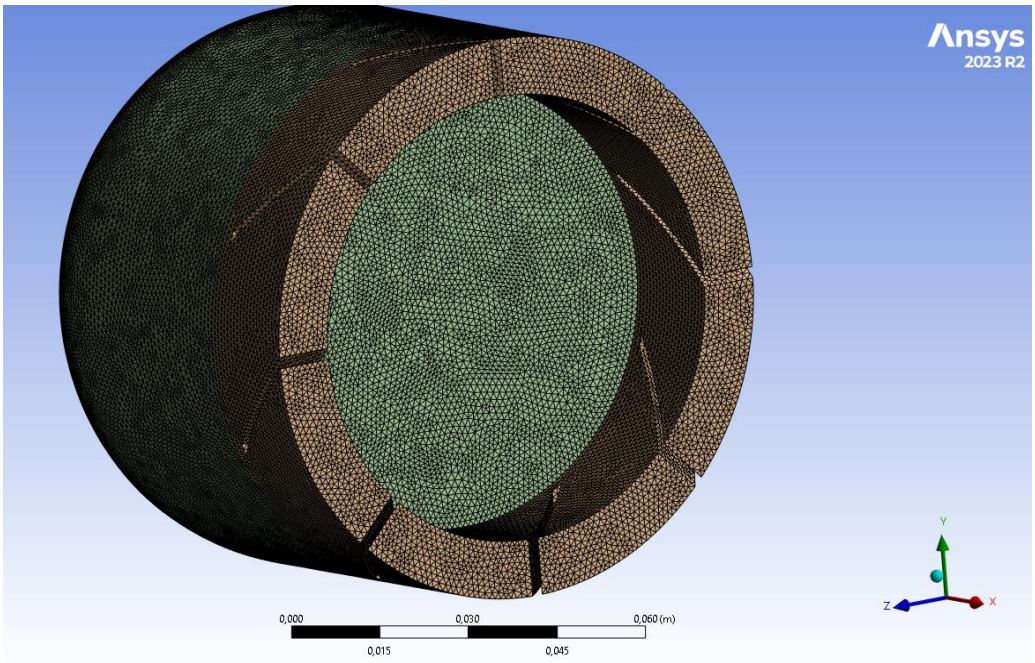

Figure 4.36 reverse air combustor swirler mesh.

4.5.3 Mesh quality

4.5.3.1 Skewness

A good grid quality means the absence of large distortions of elements (good skewness).

Excellent	Very good	Good	Acceptable	Bad	Unacceptable
0-0.25	0.25-0.50	0.50-0.80	0.80-0.94	0.95-0.97	0.98-1.00

Figure 4.37 skewness mesh spectrum. [57]

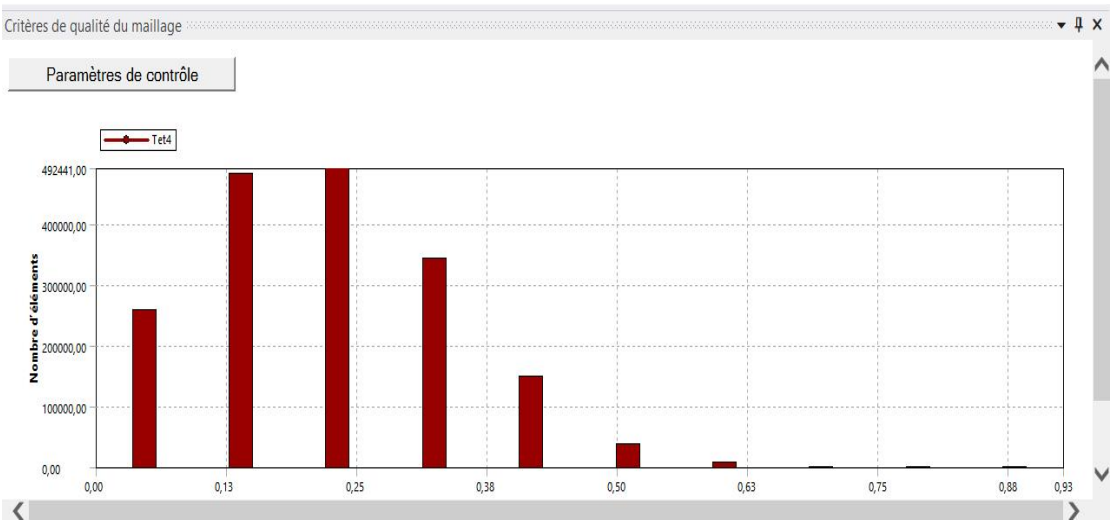

Figure 4.38 skewness quality for conventional combustor.

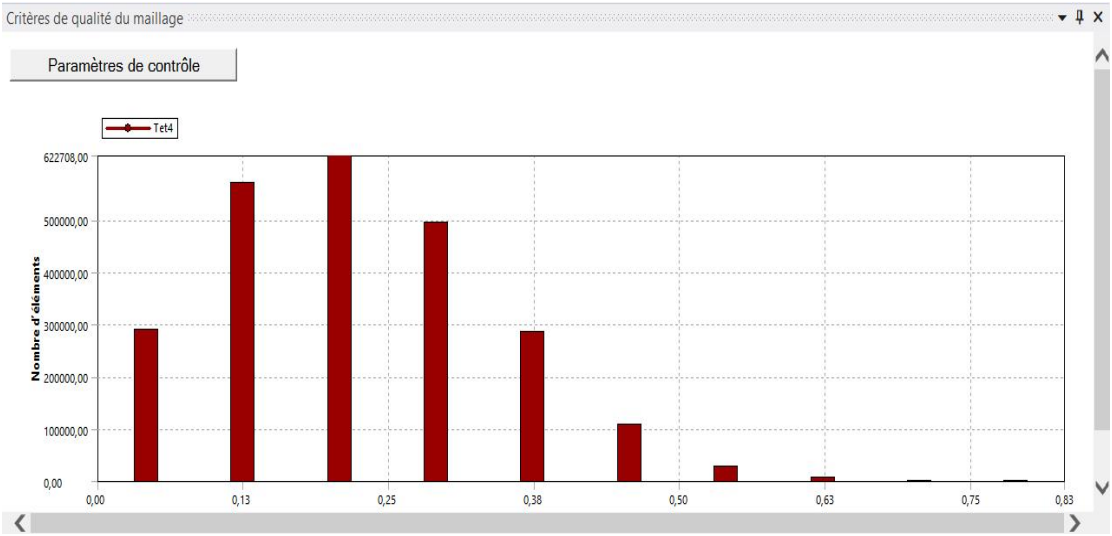

Figure 4.39 skewness quality for reverse air combustor.

4.5.3.2 Orthogonal quality

The non-orthogonality of a mesh is defined as the angle formed by the vector connecting two adjacent cell centers through their common face and the normal face.

Unacceptable	Bad	Acceptable	Good	Very good	Excellent
0-0.001	0.001-0.14	0.15-0.20	0.20-0.69	0.70-0.95	0.95-1.00

Figure 4.40 orthogonal quality mesh spectrum. [57]

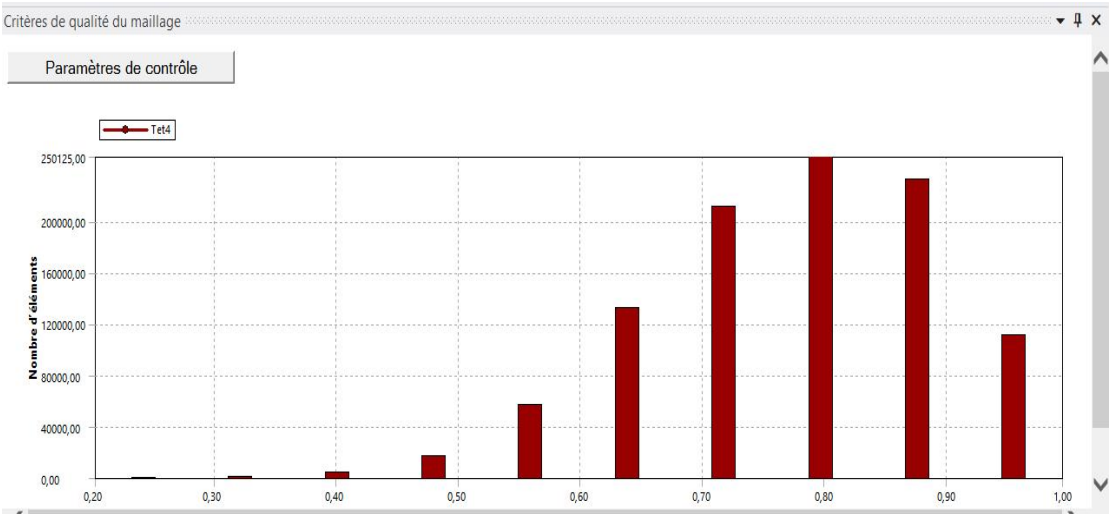

Figure 4.41 conventional combustor orthogonal quality.

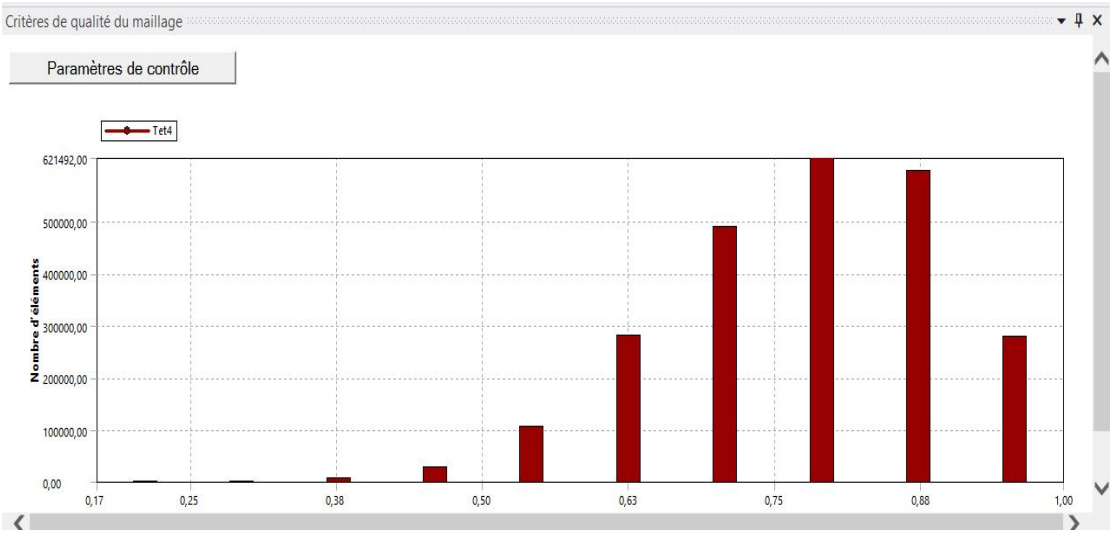

Figure 4.42 reverse air orthogonal quality.

To conclude, we can consider that our meshing for both combustors is a good mesh because most of the elements are in the acceptable limits for mesh qualities.

4.6 Boundary conditions

4.6.1 Section naming

4.6.1.1 Conventional can-type combustor

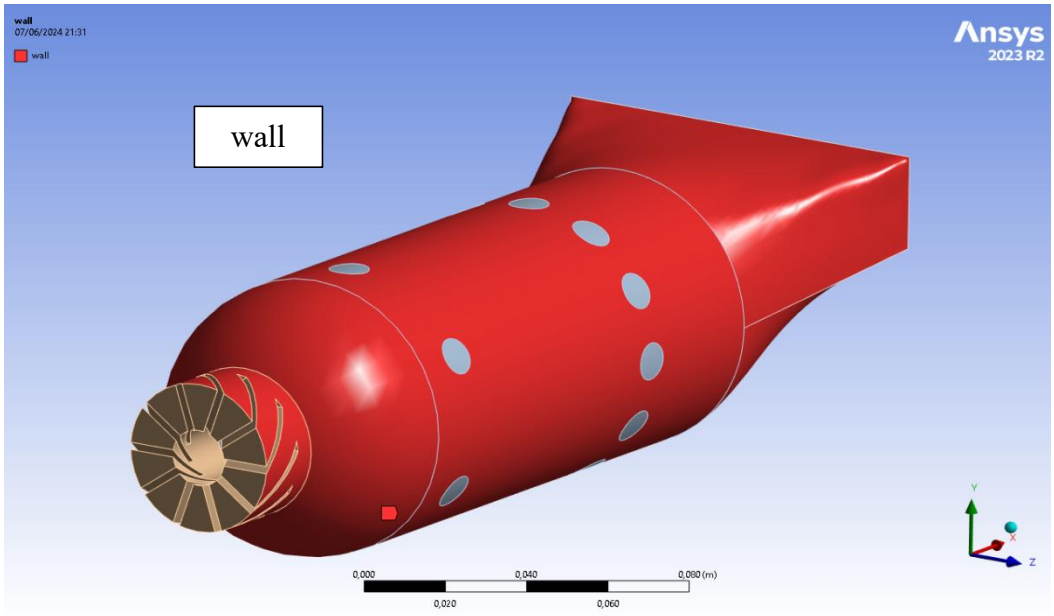

Figure 4.43 conventional combustor wall section BC.

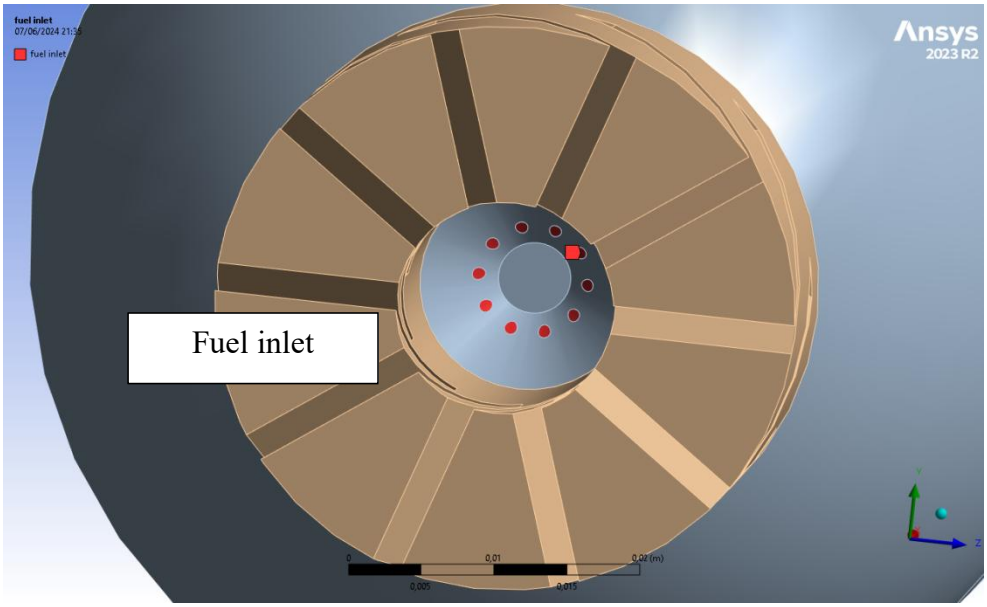

Figure 4.44 conventional combustor fuel inlet section BC.

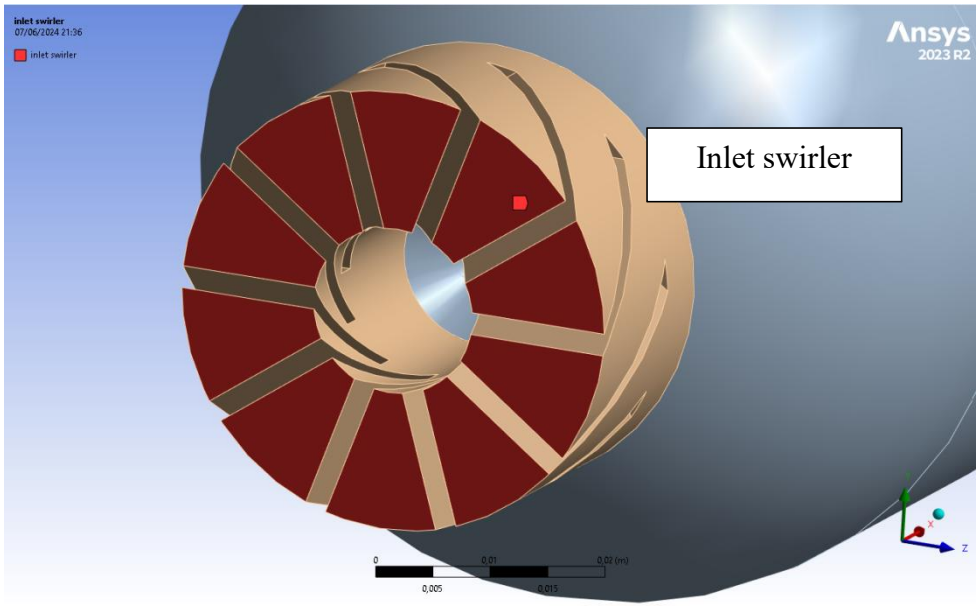

Figure 4.45 conventional combustor inlet swirler section BC.

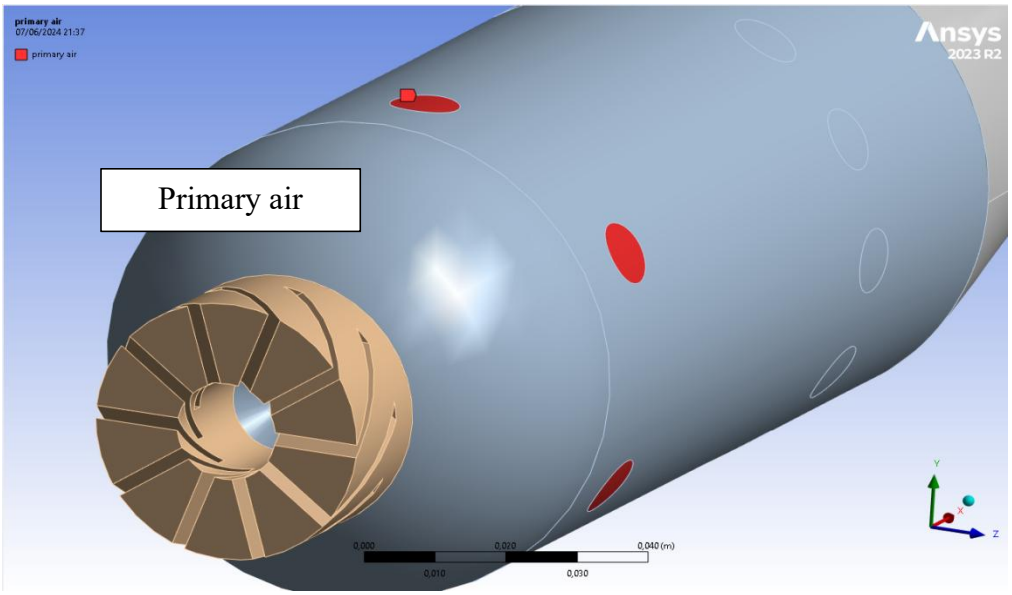

Figure 4.46 conventional combustor primary air BC.

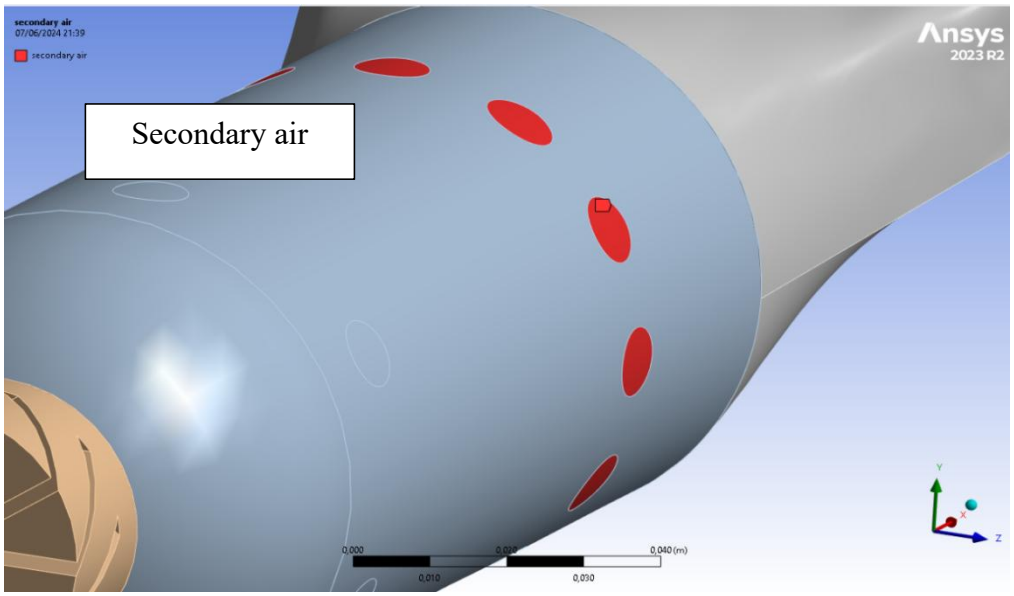

Figure 4.47 conventional combustor secondary air section BC.

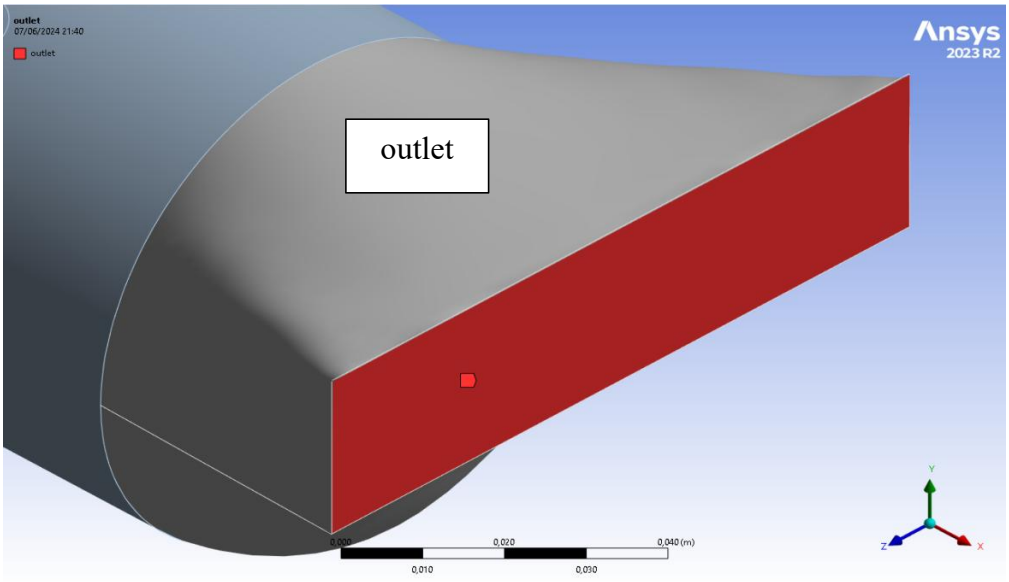

Figure 4.48 conventional combustor outlet section BC.

4.6.1.2 Reverse air can-type combustor

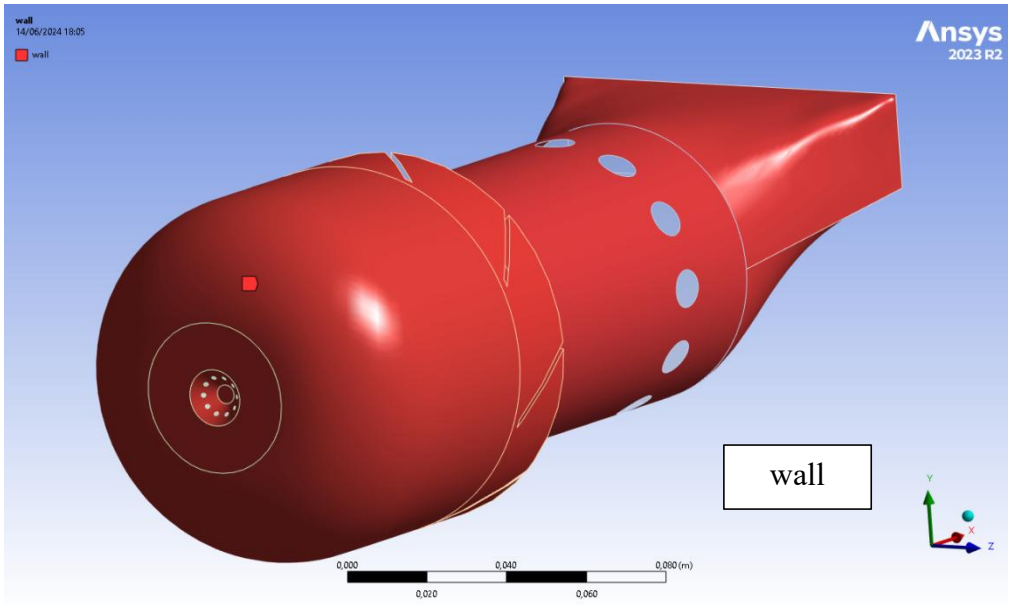

Figure 4.49 reverse air combustor wall section BC.

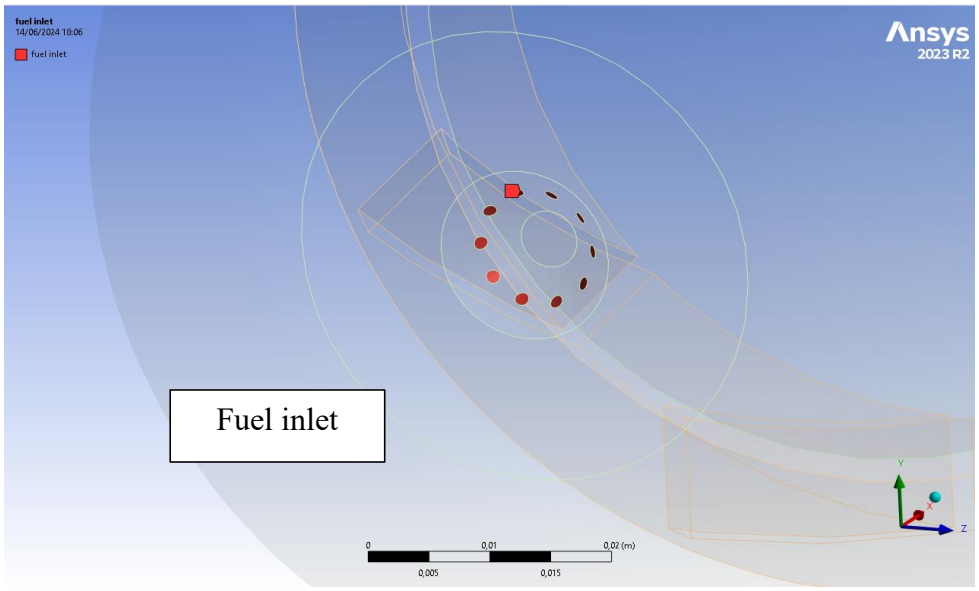

Figure 4.50 reverse air combustor fuel inlet section BC.

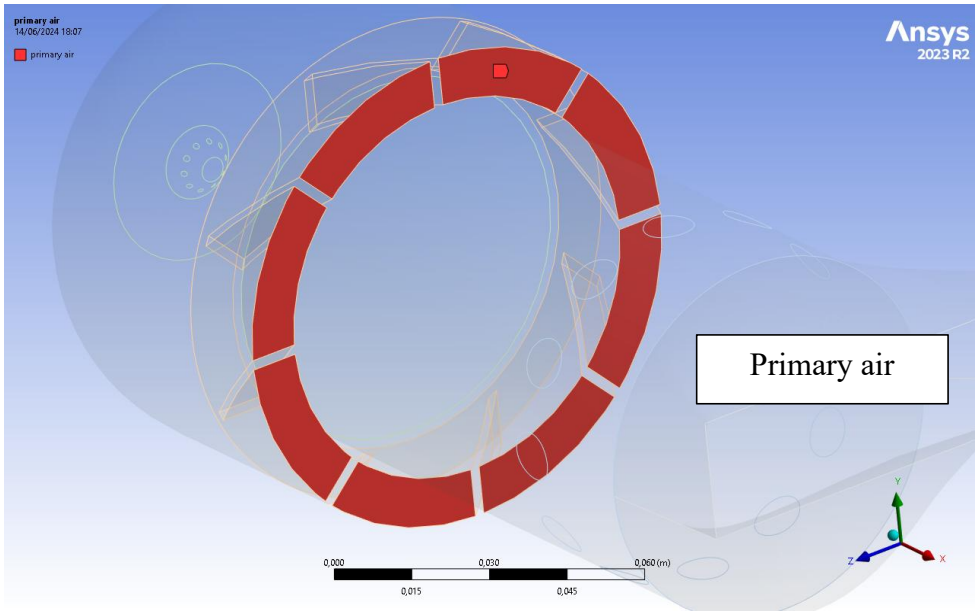

Figure 4.51 reverse air combustor primary air section BC.

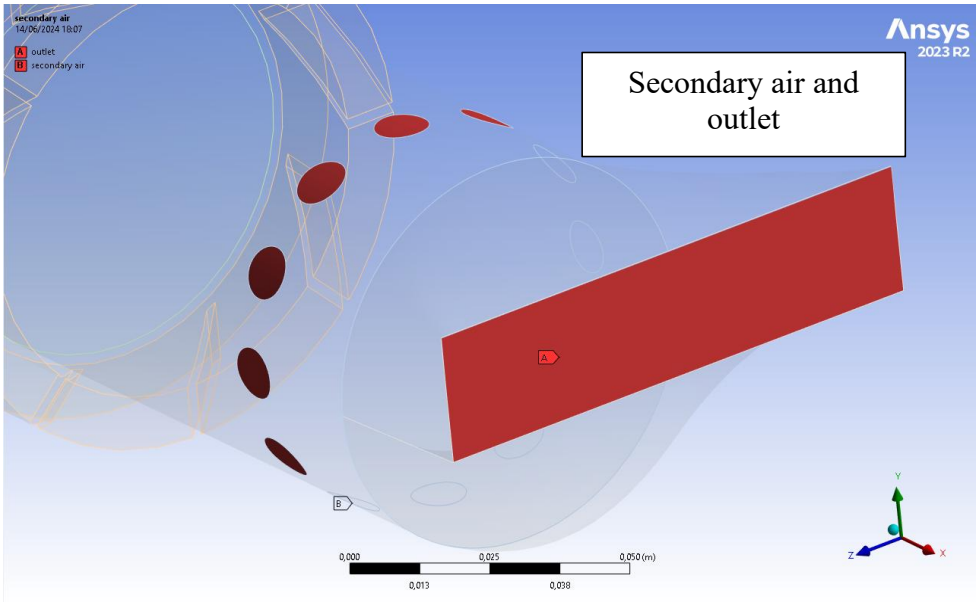

Figure 4.52 reverse air combustor secondary and outlet sections BC.

4.6.2 Boundary conditions identification

The initial air and fuel temperatures used in the computations are 300K. A mass flow inlet is defined as any inlet surface. At the combustor exit, a pressure boundary condition is assigned. Airflow mass flow rate is fixed at 0.07 kg/s. Fuel made of methane is utilized. In the simulations, the air-fuel ratio (AFR) is ranging between 50 to 70 by setting the equivalent fuel flow rate. Based on the idea of area resistance to flow, the total air mass flow provided at the combustor input is distributed to the swirler and dilution holes. **[24-38]**

4.6.2.1 Conventional combustor

Sections calculation for inlet air:

$\dot{m}_{tot}$=0.07 kg/s

$A_{inlet\ swirler}$= $\pi(r_2^2-r_1^2)$= $\pi(20^2-7.5^2)-(2\times12.5\times10)=830mm^2$.

$A_{primary\ air}=\pi r^2=\pi\times5^2\times6=471.24mm^2$.

$A_{secondary\ air}=\pi r^2=\pi\times5^2\times12=942.47mm^2$.

$A_{tot}=A_{inlet\ swirler}+A_{primary\ air}+A_{secondary\ air}=2243.71mm^2$.

From the continuity law:

$$\frac{A_{inlet\ swirler}}{A_{tot}}=\frac{\dot{m}_{inlet\ swirler}}{\dot{m}_{tot}}=0.37\Rightarrow\dot{m}_{inlet\ swirler}=\dot{m}_{tot}\times0.37=0.0259\ \text{kg/s}.$$

$\frac{A_{primary\ air}}{A_{tot}} = \frac{\dot{m}_{primary\ air}}{\dot{m}_{tot}}$=0.21⇒$\dot{m}_{primary\ air}$=$\dot{m}_{tot}$×0.21= 0.0147 kg/s.

$\frac{A_{secondary\ air}}{A_{tot}} = \frac{\dot{m}_{secondary\ air}}{\dot{m}_{tot}}$=0.42⇒$\dot{m}_{secondary\ air}$=$\dot{m}_{tot}$×0.37= 0.0294 kg/s.

Since the primary air and the air in inlet swirler are dedicated directly to taking part in the principal process of combustion, and the dilution air is introduced just to get a proper mixing and an acceptable distribution of the temperature at the outlet of the nozzle, All that means is that the mass flow rate of dilution holes is not considered in the calculation of AFR (air fuel ratio), and since the air mass flow rate is a constant, we will variate the fuel mass flow rate for a range of AFR between 50 and 70.

So, for the fuel mass flow rate:

$$\text{AFR}=\frac{\dot{m}_{primary\ air+inlet\ swirler}}{\dot{m}_{fuel\ inlet\ combustor}} \Rightarrow \dot{m}_{fuel\ inlet\ combustor} \frac{\dot{m}_{primary\ air+inlet\ swirler}}{\text{AFR}} = \frac{0.0406}{AFR}$$

For AFR=50:

$\dot{m}_{fuel\ inlet\ combustor}$=0.000812 kg/s.

For AFR=60:

$\dot{m}_{fuel\ inlet\ combustor}$=0.00067 kg/s.

For AFR=70:

$\dot{m}_{fuel\ inlet\ combustor}$=0.00058 kg/s.

Table 4-1 boundary conditions for conventional combustor.

entity	type	value	Hydraulic diameter(m)
Inlet swirler	Mass flow rate	0.0259 kg/s	0.025
Primary air	Mass flow rate	0.0147 kg/s	0.06
Secondary air	Mass flow rate	0.0294 kg/s	0.12
Fuel inlet (AFR 50)	Mass flow rate	0.000812 kg/s	0.017
Fuel inlet (AFR 60)	Mass flow rate	0.00067 kg/s	//
Fuel inlet (AFR 70)	Mass flow rate	0.00058 kg/s	//
Outlet	Pressure outlet	0	0.04

4.6.2.2 Reverse air combustor

Sections calculation for inlet air:

$\dot{m}_{tot}$=0.07 kg/s

$A_{primary\ air}$= π(r_2^2-r_1^2)= π(49^2-39^2)-(2×10×8)=2604.6mm^2.

$A_{secondary\ air}$=πr^2=π×5^2×12=942.47mm^2.

A_{tot}=$A_{primary\ air}$+$A_{secondary\ air}$ = 3547.07mm^2.

$\frac{A_{primary\ air}}{A_{tot}} = \frac{\dot{m}_{primary\ air}}{\dot{m}_{tot}}$=0.73⇒$\dot{m}_{primary\ air}$=$\dot{m}_{tot}$×0.73= 0.0511 kg/s.

$\frac{A_{secondary\ air}}{A_{tot}} = \frac{\dot{m}_{secondary\ air}}{\dot{m}_{tot}}$=0.27⇒$\dot{m}_{secondary\ air}$=$\dot{m}_{tot}$×0.27= 0.0189 kg/s.

Same thing as the conventional combustor, only the primary air is dedicated directly to taking part in the principal process of combustion.

So, for the fuel mass flow rate:

$$\text{AFR}=\frac{\dot{m}_{primary\ air+inlet\ swirler}}{\dot{m}_{fuel\ inlet\ combustor}} \Rightarrow \dot{m}_{fuel\ inlet\ combustor} \frac{\dot{m}_{primary\ air+inlet\ swirler}}{\text{AFR}} = \frac{0.0511}{AFR}$$

For AFR=50:

$\dot{m}_{fuel\ inlet\ combustor}$=0.0001022 kg/s.

For AFR=60:

$\dot{m}_{fuel\ inlet\ combustor}$=0.000852 kg/s.

For AFR=70:

$\dot{m}_{fuel\ inlet\ combustor}$=0.00073 kg/s.

Table 4-2 reverse air combustor boundary conditions.

entity	type	value	hydraulic diameter
Primary air	Mass flow rate	0.0511 kg/s	0.01
Secondary air	Mass flow rate	0.0189 kg/s	0.12
Fuel inlet (AFR 50)	Mass flow rate	0.0001022 kg/s	0.017
Fuel inlet (AFR 60)	Mass flow rate	0.000852 kg/s	//
Fuel inlet (AFR 70)	Mass flow rate	0.00073 kg/s	//
Outlet	Pressure outlet	0	0.04

4.6.2.3 Thermal boundary condition for wall- outer wall-

The material that we used it for our simulation is steel considering its resistance to high temperature.

Table 4-3 steel proprieties.

property	value
Thermal conductivity (k)	16.27 W/m k
Specific heat (C_p)	502.48
Density (ρ)	8030 kg/m^3

Where we will take the characteristic length for both combustors L_c is the hydraulic diameter of the cylinder where the most of the phenomena take a big place in it.

So, L_c =74mm.

Now we can determine the convective heat transfer coefficient and external emissivity of radiation .

Table 4-4 thermal wall boundary conditions for convection.

Wall condition	value
convective heat transfer coefficient (h)	219.86 W/m^2k

4.6.2.4 Equivalence ratio

The stiochiometric combustion reaction for methane/air mixture can be expressed by:

$$\underbrace{CH_4}_{16} + \underbrace{2(O_2 + 3.76\ N_2)}_{274.56} \rightarrow CO_2 + 2H_2O + 7.52\ N_2 \qquad (4.1)$$

To estimate the equivalence ratio for the mixture we will take the equation has been mentionned in chapter 01 -equation (1.12)-

$$\phi = \frac{\left(\frac{\text{fuel quantity}}{\text{air quantity}}\right)_{\text{actual}}}{\left(\frac{\text{fuel quantity}}{\text{air quantity}}\right)_{\text{stiochiometric}}}$$

$$\left(\frac{\text{fuel quantity}}{\text{air quantity}}\right)_{\text{actual}} = \frac{1}{50} = 0.02$$

$$\left(\frac{\text{fuel quantity}}{\text{air quantity}}\right)_{\text{stiochiometric}} = \frac{1}{17.16} = 0.058.$$

$$\phi = \frac{\left(\frac{\text{fuel quantity}}{\text{air quantity}}\right)_{\text{actual}}}{\left(\frac{\text{fuel quantity}}{\text{air quantity}}\right)_{\text{stiochiometric}}} = 0.34.$$

Since $\phi < 1$, we can consider that our combustion is lean non-premixed combustion .

4.7 Combustion simulation

4.7.1 Cold flow analysis

Once grid independence is achieved, cold flow analysis is conducted, taking into consideration that the flow regime inside the chamber is turbulent. The local Reynolds number reaches significantly high values near the dilution and primary hole regions, as well as inside the nozzle. **[44]**

Therefore, it becomes necessary to treat the flow as highly turbulent. In such cases, a single-equation turbulence model is not sufficient. Instead, the k-e realizable turbulence model is used for both cold and combusting flow simulations. This model solves two transport equations, one for turbulence kinetic energy and one for its dissipation within the domain, as discussed in Chapter 2.

4.7.2 Reactive flow analysis

The combustion flow analysis is carried out after the cold flow simulations are completed and a firm understanding of the flow regime is obtained. The independent grid obtained from the cold flow simulation is used to simulate the combustion regime. Combustion modeling is performed using a non-premixed approach, as the gas turbine combustor is essentially a non-premixed system **[44]**. Premixed systems, like the Bunsen burner, cannot be simulated using the non-premixed model. The non-premixed modeling approach is best suited for reacting flows that involve strong turbulence, chemistry interactions, and are mixing-driven. The governing chemical reactions are never single-step, as they are sometimes shown to avoid complexities. In

reality, a large number of intermediate species are formed during the combustion process, which must be accounted for by the solver. The present investigation also considers the intermediate species formed during the combustion process of natural gas and air.

4.8 Fluent setup

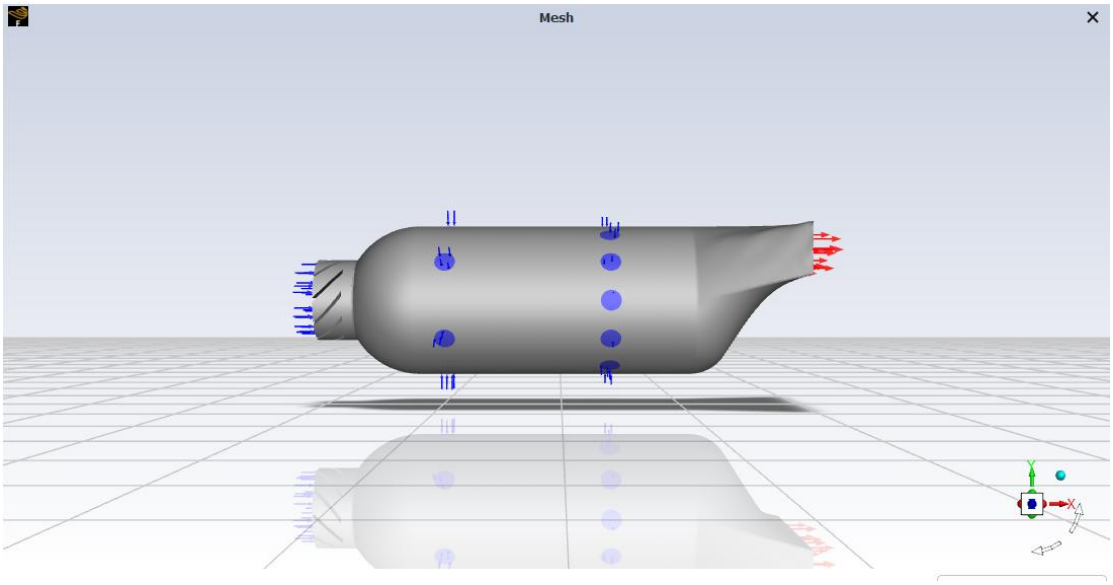

Figure 4.53 front view of conventional combustor in Ansys-Fluent with boundary conditions indication.

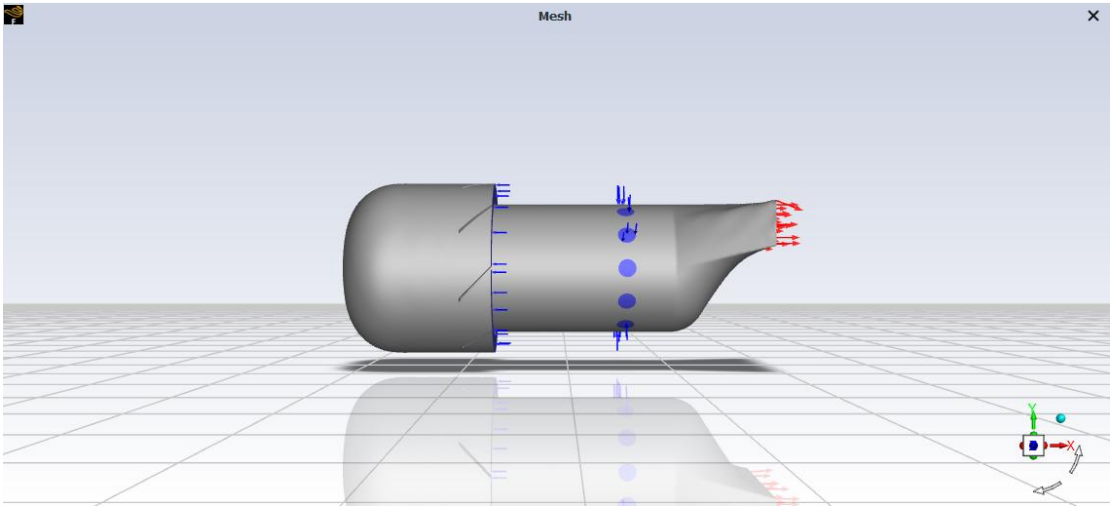

Figure 4.54 front view of reverse air combustor in Ansys-Fluent with boundary conditions indication.

In order to handle both combustion process and compressible flow simulations, the pressure-based solver type has been selected. This solver is also the only one compatible with the non-premixed combustion model. Since the combustion reaction occurs rapidly and instantaneously, the entire event can be captured by considering a stationary second. The goal of steady-state simulation is to compute a solution that remains constant over time. Mean values are used to achieve this. Steady-state simulation is much faster than transient simulation.

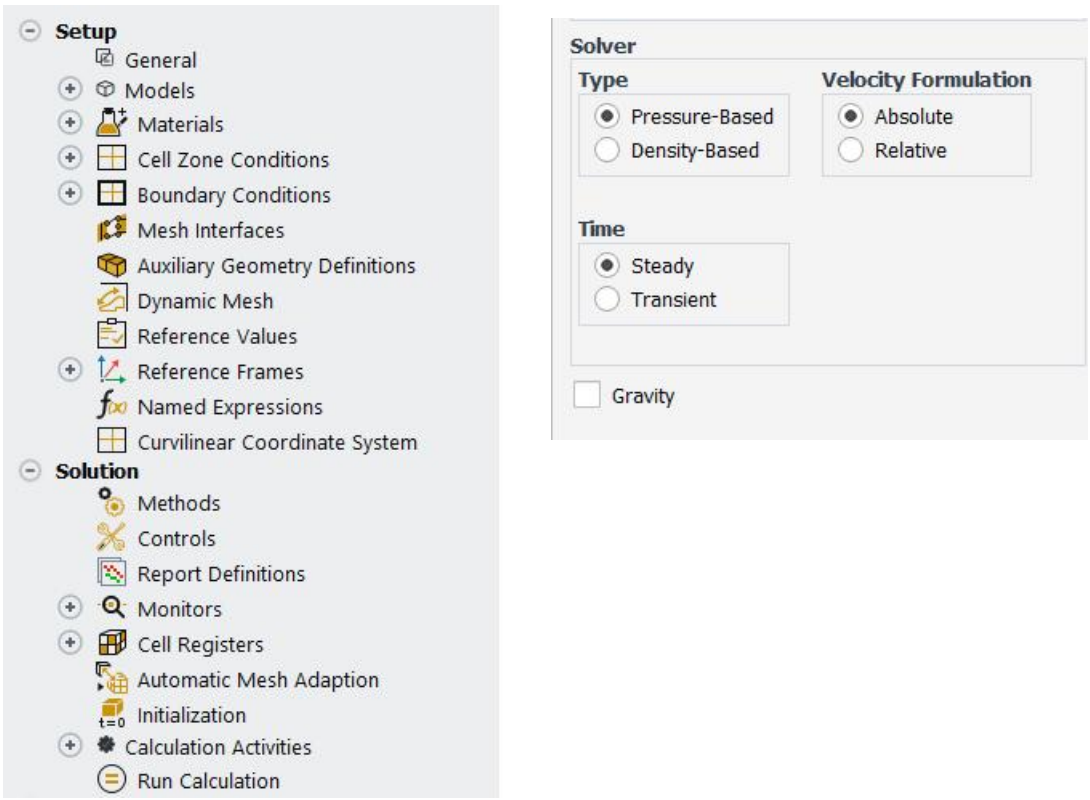

Figure 4.55 pressure based solver selection.

4.8.1 Energy equation activation

You must find the solution to the energy equation because heat transfer takes place in the system under consideration.

Figure 4.56 energy equation selection.

4.8.2 Turbulence model

The k-ε realizable model with non-equilibrium wall function for near-wall treatment has been selected for its advantages.

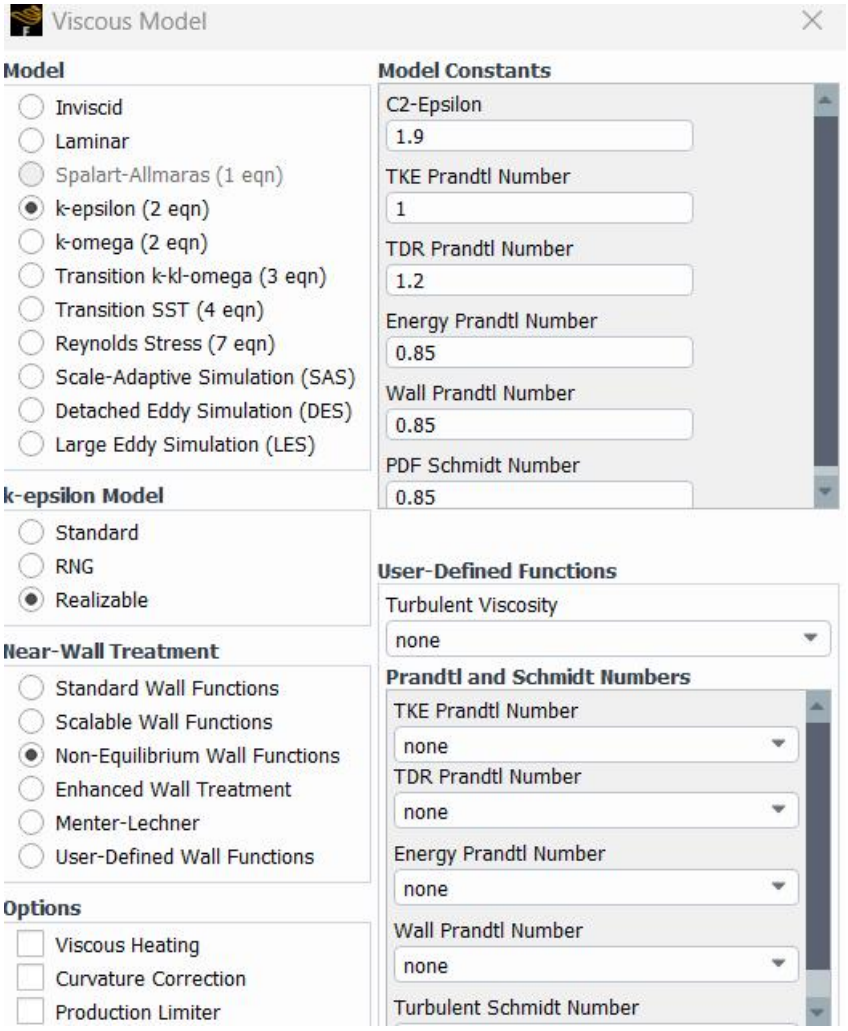

Figure 4.57 turbulence model selection with wall function.

4.8.3 Species model

we will left the species model off for our cold flow analysis.

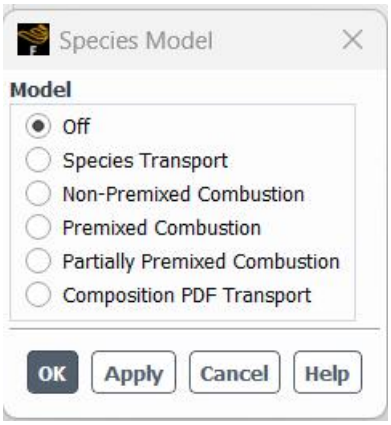

Figure 4.58 species model off for cold flow analysis.

For the combustion chemistry model we will go for the non-premixed combustion model according to the specification of our combustors in this study.

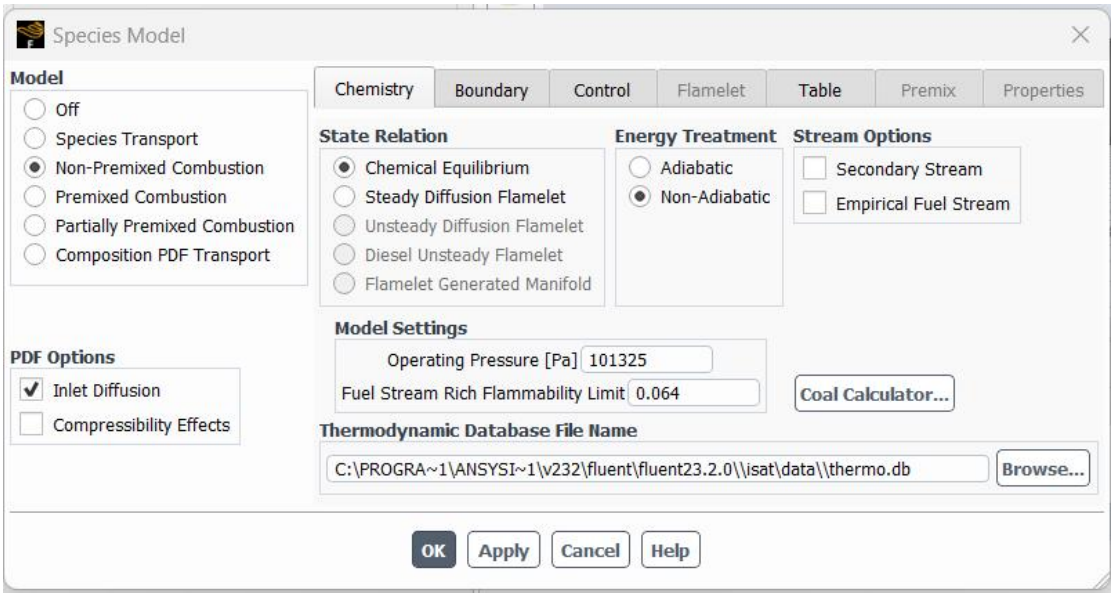

Figure 4.59 species model selection for reactive flow analysis.

To use the non-premixed combustion model, a Probability Density Function (PDF) table needs to be created. This table discusses the Thermochemistry and its relationship to turbulence. ANSYS FLUENT interpolates the PDF when solving the non-premixed combustion model.

The mixed fraction can diffuse out of the domain through inlets and outlets by using the Inlet Diffusion option.

It is recommended to use the equilibrium chemistry model in most non-premixed combustion simulations. The Steady Flamelets option can model local chemical non-equilibrium caused by turbulent strain.
In combustion scenarios, the rich flammability limit of the fuel stream can be set to a value greater than 10% to 50% of the stoichiometric mixture fraction. Since the stoichiometric fraction in this case is 0.058, a number that is 10% higher would be 0.064.

You can perform a "partial equilibrium" calculation using the Fuel Stream Rich Flammability Limit, which stops equilibrium calculations when the mixture fraction exceeds the designated rich limit. This makes the PDF computation more efficient and allows you to avoid performing complex equilibrium calculations in the fuel-rich area.

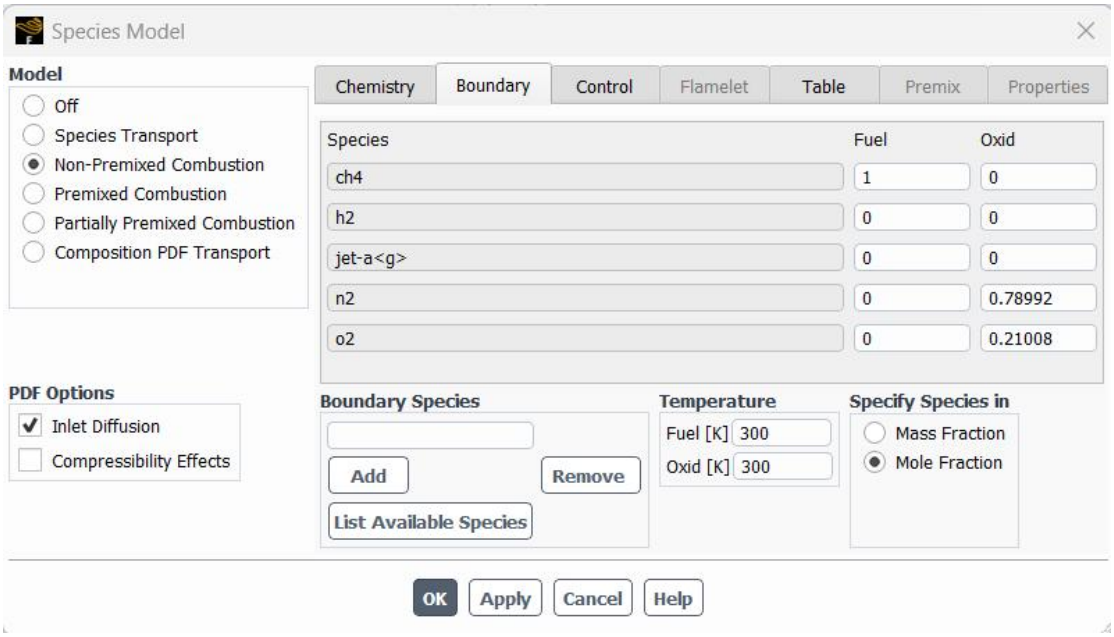

Figure 4.60 boundaries for non-premixed model.

The fuel and air initial temperature used for this simulation is 300k, we are simulating the flow using a pure CH4 that's why the mole fraction of it is 1.

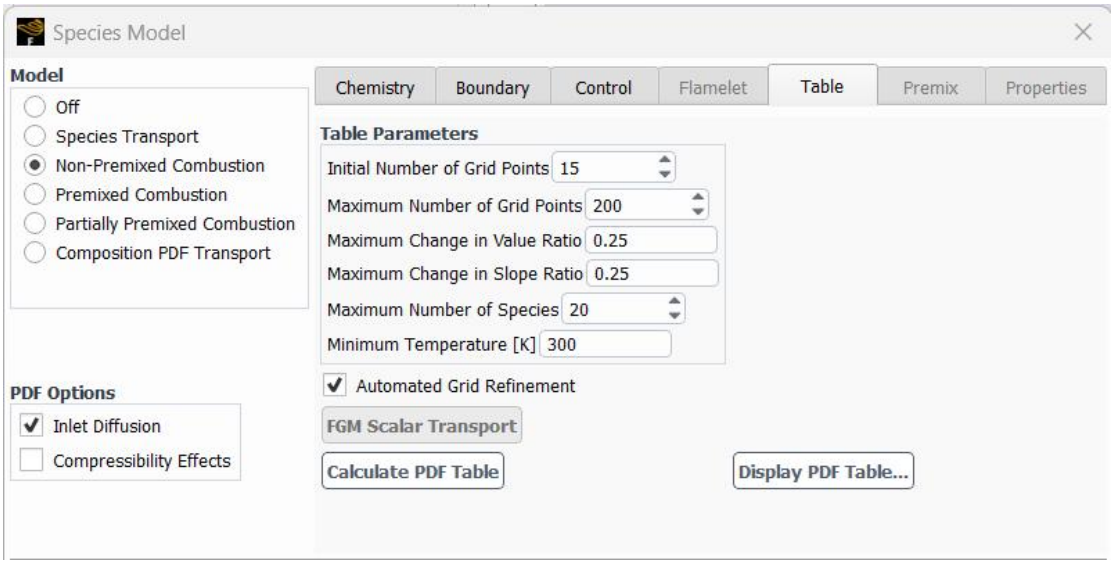

Figure 4.61 PDF table generation for non-premixed model.

After calculating the PDF table, save the formatted (ASCII or text) file. To save an unformatted binary file, enable the "Write Binary Files" option in the Select File dialog box.

4.8.4 Materials editing:

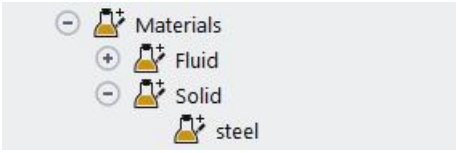

For the fluid, we have air as the main reactant in the combustion reaction with the methane CH4.

For the solid material, we are going to use steel to ensure thermal resistance and to protect the outer wall of our combustors. Due to its high thermal conductivity, steel can efficiently manage heat in processes like cooling systems and manufacturing operations, affecting performance and safety.

all the species existing in the PDF table are mentioned in material's mixture field

Figure 4.62 materials indication, fluid, mixture, solid.

4.8.5 Boundary conditions setup

The boundary conditions, particularly the entering mass flow rate field and the heat transfer through the walls, can have an impact on the CFD solution for reacting flows.

For all the necessary boundary conditions for our computational calcul we have calculated and estimated all of them in the section of boundary conditions above and the figures below show how to enter them properly for all the sections.

You must specify the input Mean Mixture Fraction and Mixture Fraction Variance in the Species tab for fuel inlet, primary and secondary air also for the inlet swirler (conventional combustor case) in order to do the non-premixed combustion calculation. For primary, secondary air and inlet swirler have a zero mean mixture fraction and mixture fraction variance. For the fuel inlet we will set the mean mixture fraction to be equal to 1.

All the boundary conditions for inlet fuel, inlet swirler, primary air, secondary air and also the thermal wall conditions for both combustors are sited in the previous tables 4-1, 4-2, 4-4

Note: The system pressure at the exit is defined as the operating pressure when the exit gauge pressure is zero. Temperature, mixture fraction, and turbulence parameters are the scalar backflow conditions that will only be applied if flow is entrained into the domain through the exit.

4.8.6 Solution methods

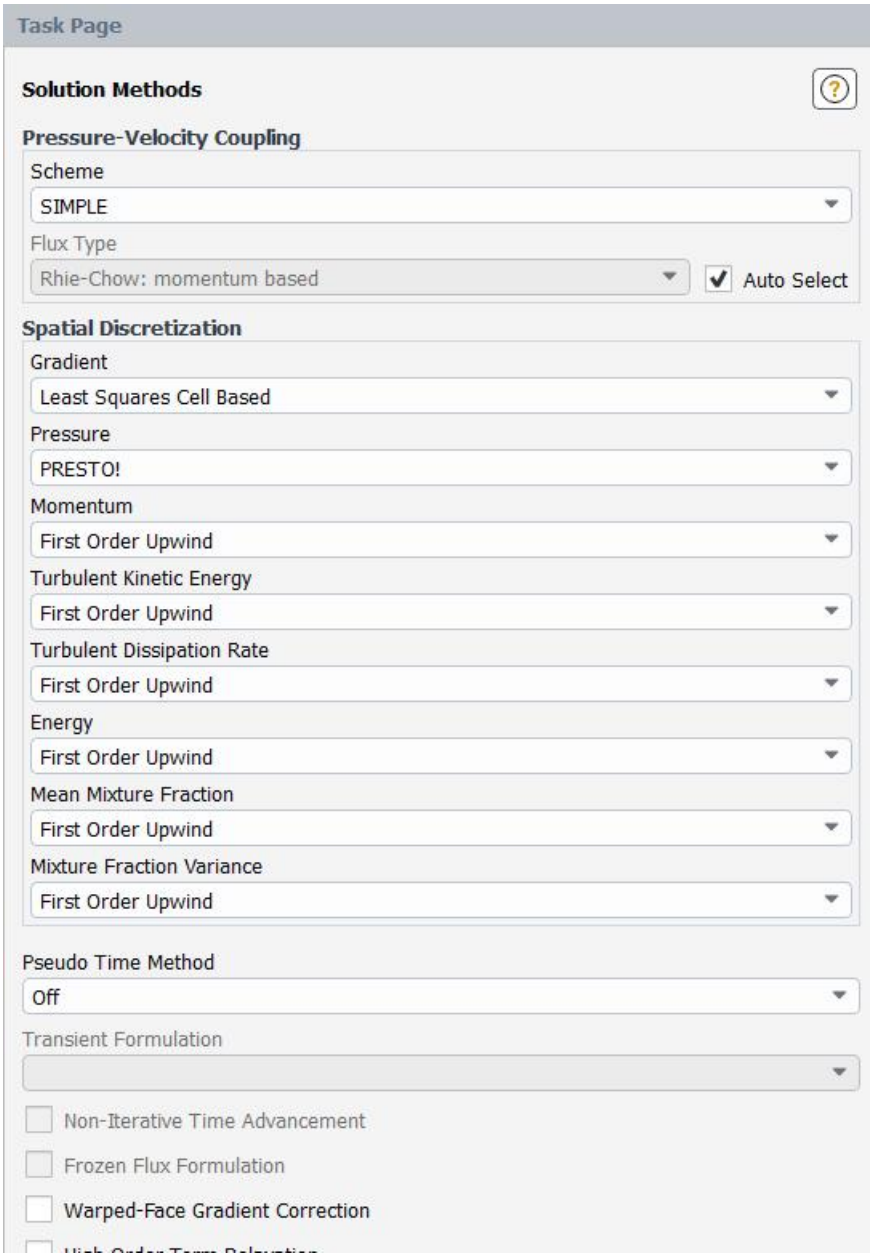

Figure 4.63 solution methods.

4.8.7 Solution controls

Table 4-5 under-relaxation factors values for non-premixed combustion. [63]

Under-relaxation factor	value
density	0.8
momentum	0.3
Turbulent kinetic energy	0.7
Turbulent kinetic rate	0.7

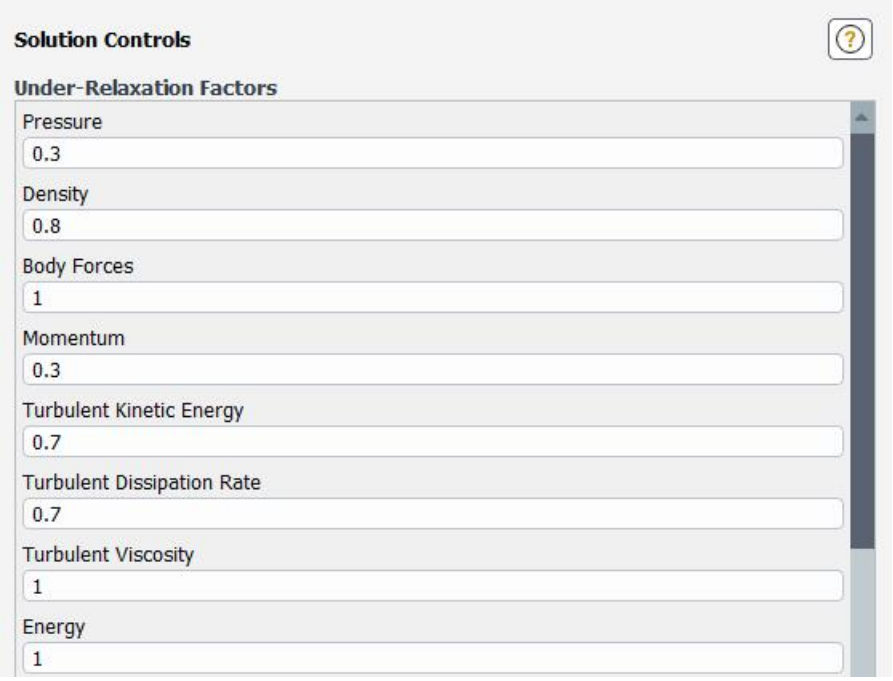

Figure 4.64 solution controls-under-relaxation factors.

The default under-relaxation factors are considered to be too aggressive for reacting flow cases with high swirl velocity and turbulence.

4.8.8 Solution initialization

We initialize the solution using the hybrid initialization.

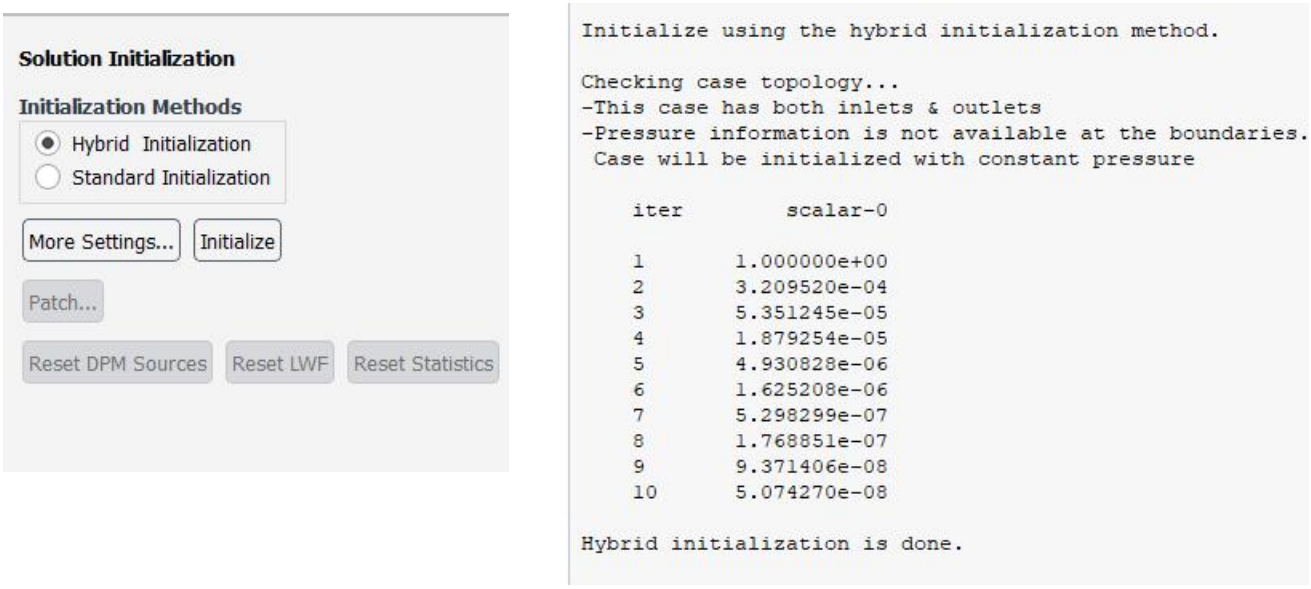

Figure 4.65 solution initialization- hybrid initialization.

Then we will calculate the solution.

4.9 NOx simulation

4.9.1 Thermal NOx

Formed by nitrogen present in the air.

4.9.2 Prompt NOx

produced by reactions at the flame front.

4.9.3 intermediate NOx

During high pressure low temperature conditions.

Using a custom field function to compute NO parts per million (ppm), NO ppm will be calculated from the following equation **[64]**:

$$\text{NO ppm} = \frac{\text{NO mole fraction} \times 10^6}{1 - \text{H}_2\text{O mole fraction}} \quad (4.2)$$

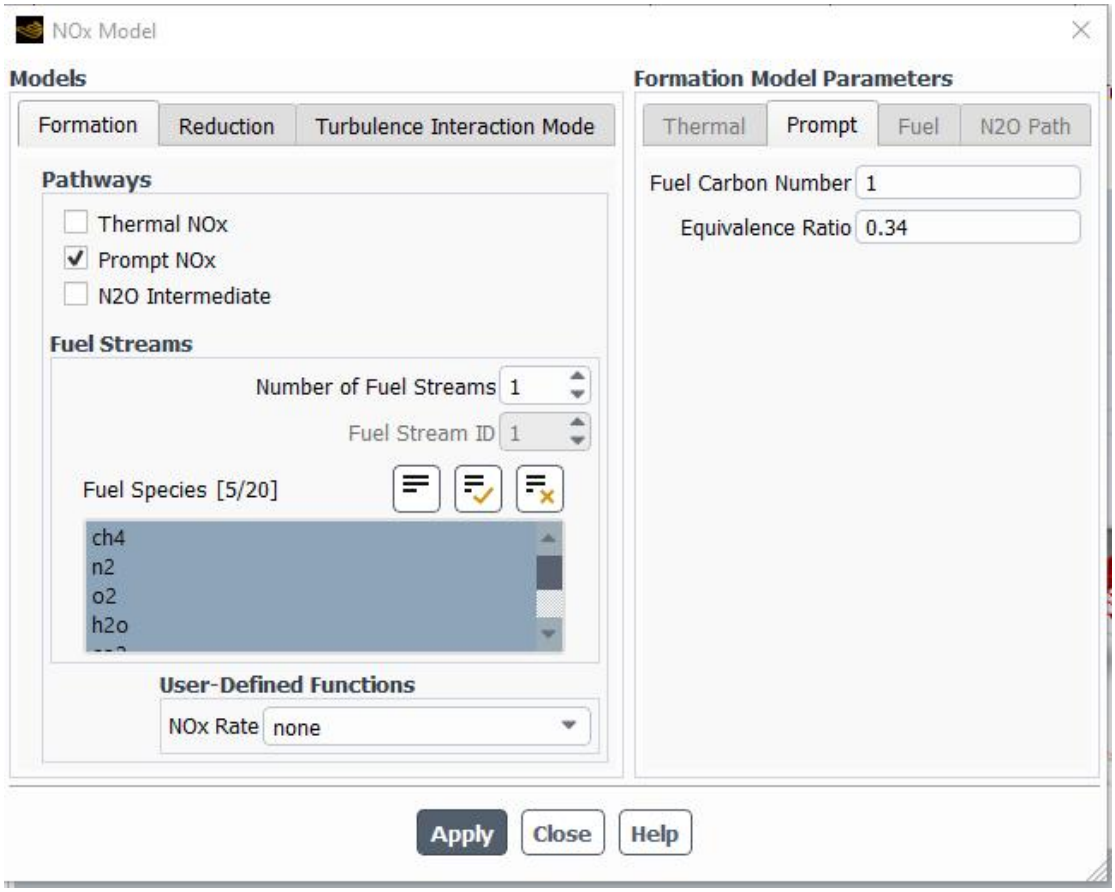

Figure 4.66 NOx model setup.

CHAPTER 05:

Results and discussion

Summary:

Chapter 05: results and discussion

5.1 Introduction

This chapter presents the analysis of flow behavior for both geometries, comparing and highlighting the main differences. It also provides specifications for each combustor under different cases, such as AFR and preheating temperature, using visual aids like contours, streamlines, and charts. Various contour plots of different variables will be displayed to enhance our understanding of the model's physics and chemistry.

5.2 Grid independence study results

5.2.1 Conventional can-type combustor independence study results

The grid independence study for different meshes for the conventional combustor is presented in Table (5-1) with the different specifications and characterizations involved in these meshes.

Table 5-1 Grid independence study results for conventional combustor under an AFR 50.

Mesh	Element size(m)	Number of elements	Tmax(K)	T exit max(K)
Mesh 1	0.003	280244	2094	1353.65
Mesh 2	0.0014	1016061	2050	1224.6
Mesh 3	0.0012	1445780	2034.36	1207.36
Mesh 4	0.0011	1777755	2034.44	1191.64

The chart below shows the variation of the exit temperature in the nozzle's outlet for the conventional combustor along its center line (as described in chapter 04). It also illustrates the variation of exit temperature for different mesh configurations.

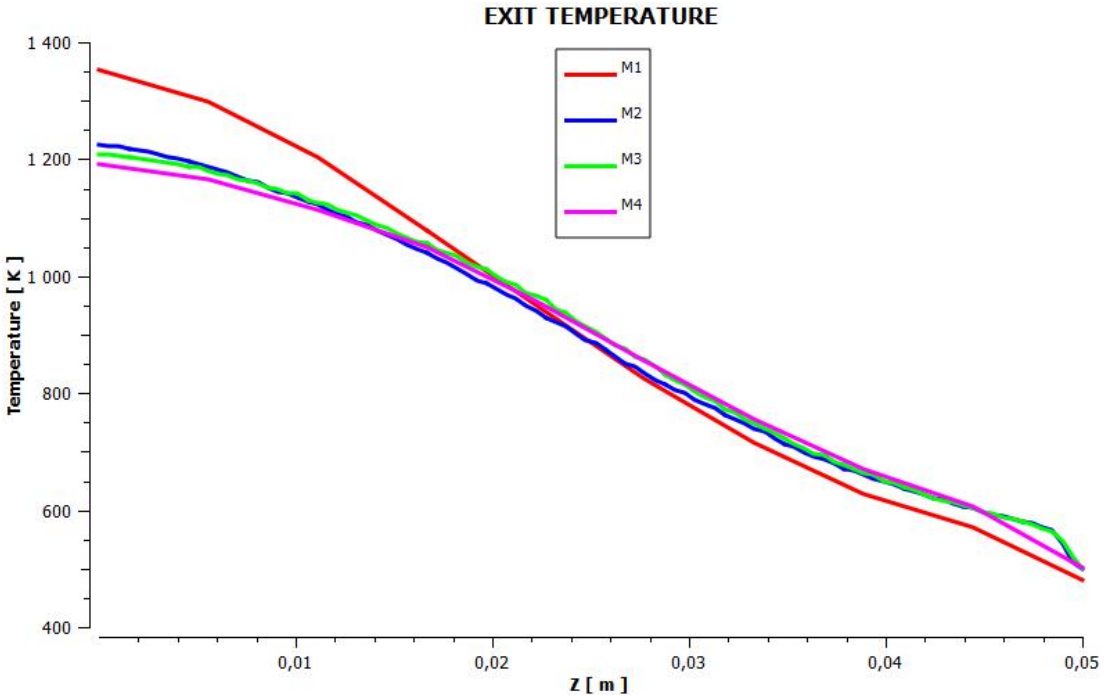

Figure 5.1 exit temperature charts for conventional combustor grid in dependence study, $\dot{m}_f$=0.000812 kg/s, $\dot{m}_{pa}$=0.0147 kg/s, $\dot{m}_{sa}$= 0.0294 kg/s, $\dot{m}_{IS}$=0.0259 kg/s.

Table (5-2) shows a comparison between our result and the previous numerical results **[24]** for the conventional combustor, the mesh 4 with a number of elements of 1777755 gives us the most suitable result comparing to the previous results.

Table 5-2 comparison with numerical previous results for conventional combustor . [24]

Tmax(K)	T exit max(K)	T max num[24]	T exit max num [24]	T exit max exper[24]
2034.44	1191.64	≈ 2166	≈1190	≈ 1000

The table above shows that the numerical simulation result for exit temperature (1991.64 k) is higher than the experimental result (1000 k) with an error of 19% for an AFR 50.

5.2.2 Reverse air can-type combustor independence study

The grid independence study for different meshes for the reverse air combustor is presented in Table (5-3) with the different specifications and characterizations involved in these meshes.

Table 5-3 Grid independence study results for reverse air combustor -AFR 50-

Mesh	Element size(m)	Number of elements	Tmax(K)	T exit max(K)
Mesh 1	0.003	302460	1890	1539.32
Mesh 2	0.0015	1153651	1860	1598.08
Mesh 3	0.0013	1614538	1890	1688.92
Mesh 4	0.0011	2404038	1899.30	1759.58

The chart below shows the variation of the exit temperature in the nozzle's outlet for the reverse air combustor along its center line (as described in chapter 04). It also illustrates the variation of exit temperature for different mesh configurations.

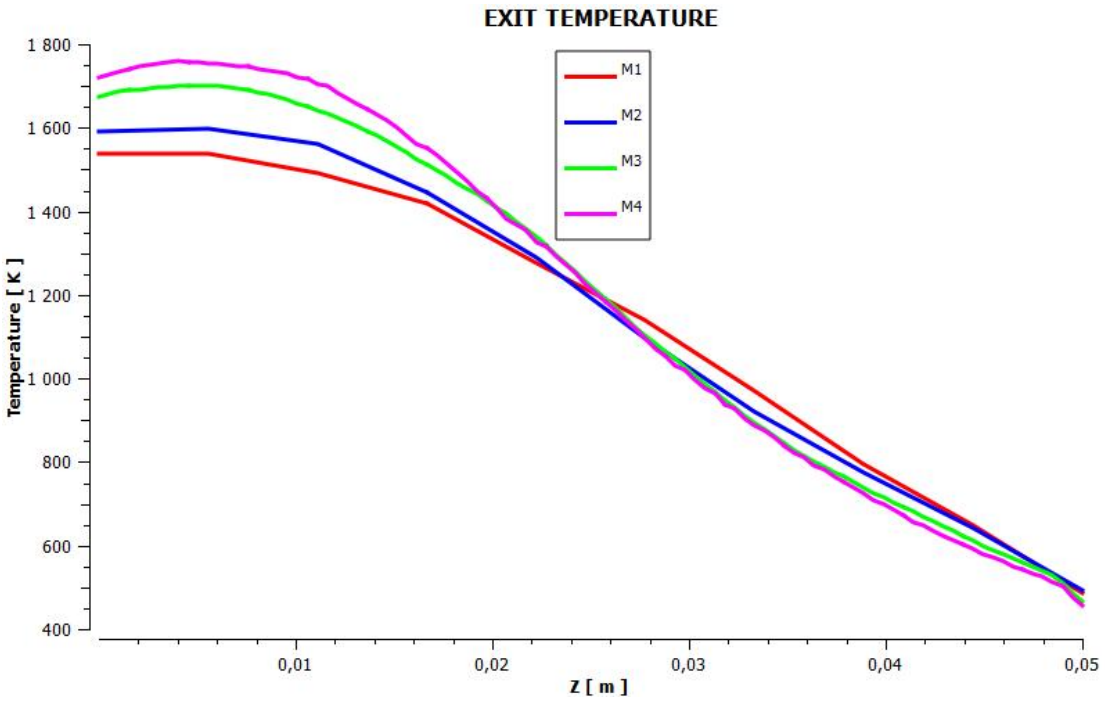

Figure 5.2 exit temperature charts for reverse air combustor grid independence study, $\dot{m}_f$=0.0001022 kg/s, $\dot{m}_{pa}$=0.0511 kg/s, $\dot{m}_{sa}$= 0.0189 kg/s.

Table 5-4 comparison with numerical of previous results for reverse air combustor. [24]

Tmax(K)	T exit max (K)	T max num[24]	T exit max num [24]	T exit exper [24]
1899.30	1759.58	≈ 2152	≈1770	≈ 1400

Table (5-4) shows a comparison between our result and the previous numerical **[24]** results for the conventional combustor, the mesh 4 with a number of elements of 2404038 gives us the most suitable result comparing to the previous results.

The table above shows that the numerical simulation result for exit temperature (1759.58 k) is higher than the experimental result (1400 k) with an error of 25% for an AFR 50.

The tables 5-2 and 5-4 highlight a discrepancy between the numerical and experimental results. This discrepancy is due to many possible reasons notably the simplifications for some aspects in combustors physics or chemistry also there could be some uncertainty in the experiments measurements.

The comparison with experimental data is shown in figure (5.3) .

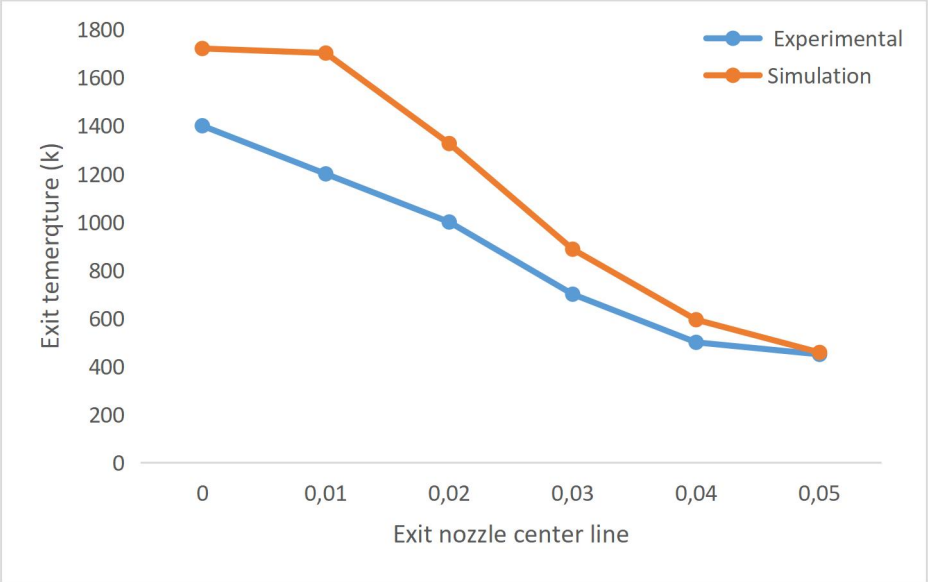

Figure 5..3 comparison of experimental and simulation results of exit temperature for reverse air combustor. [26]

5.3 Reacting flow analysis results

5.3.1 residual and convergence study

Before using the simulation results, we need to ensure that the computations have converged. One way to verify convergence in the fluent program is by examining the graph of residuals, which should consistently decrease.

Figure (5.4) displays the residuals for a converged solution. Based on this figure, we can conclude that our solution has converged and obtained a final result.

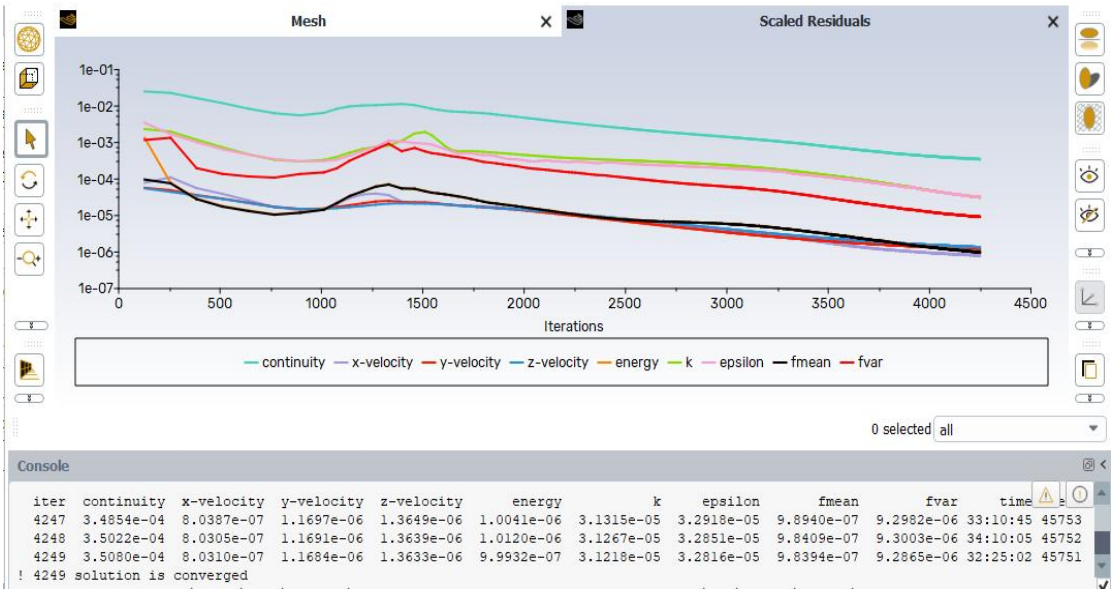

Figure 5.4 residual's graph for converged solution.

5.3.2 Temperature contours

The most effective visual aid for understanding the dynamics of flame front travel inside the chamber is the static temperature contour.

The temperature distribution for both geometries is shown in the figures from (5.5) to (5.10) below. At first, it is immediately apparent that when the geometry is changed , the flame dynamics alter significantly.

5.3.2.1 reverse air combustor

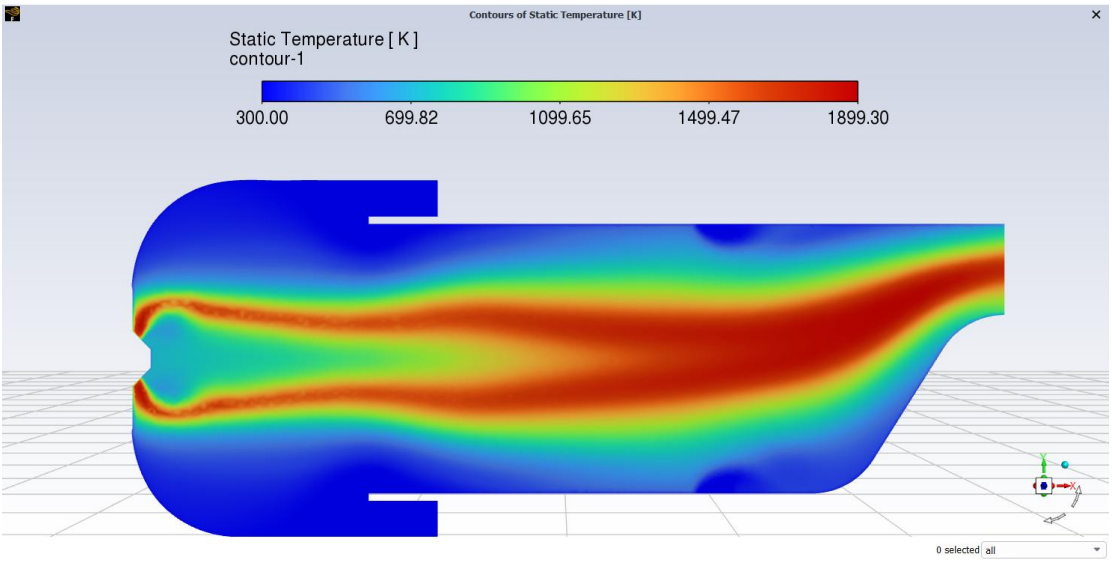

Figure 5.5 static temperature contour for reverse air combustor (xy plan),$\dot{m}_f$=0.0001022 kg/s, $\dot{m}_{pa}$=0.0511 kg/s, $\dot{m}_{sa}$= 0.0189 kg/s.

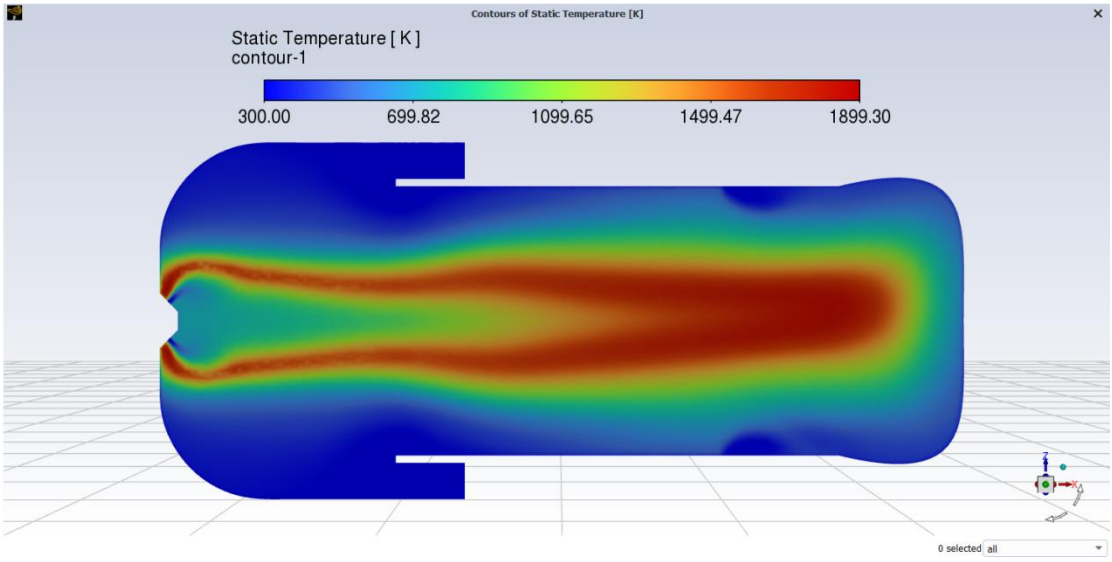

Figure 5.6 static temperature contour for reverse air combustor (xz plan), $\dot{m}_f$=0.0001022 kg/s, $\dot{m}_{pa}$=0.0511 kg/s, $\dot{m}_{sa}$= 0.0189 kg/s.

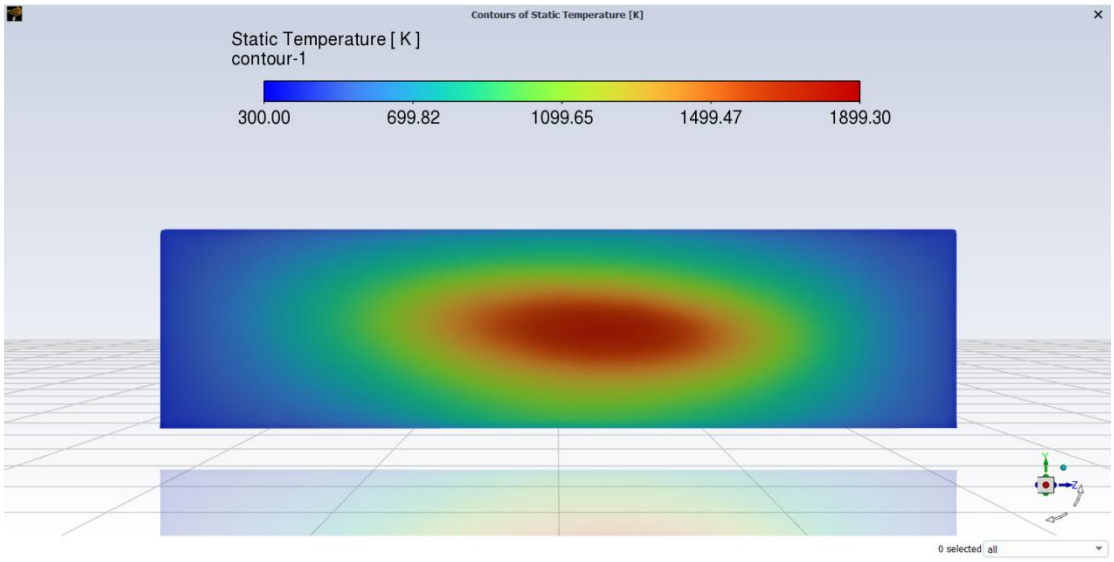

Figure 5.7 static temperature contour for reverse air combustor (outlet).

5.3.2.2 conventional combustor

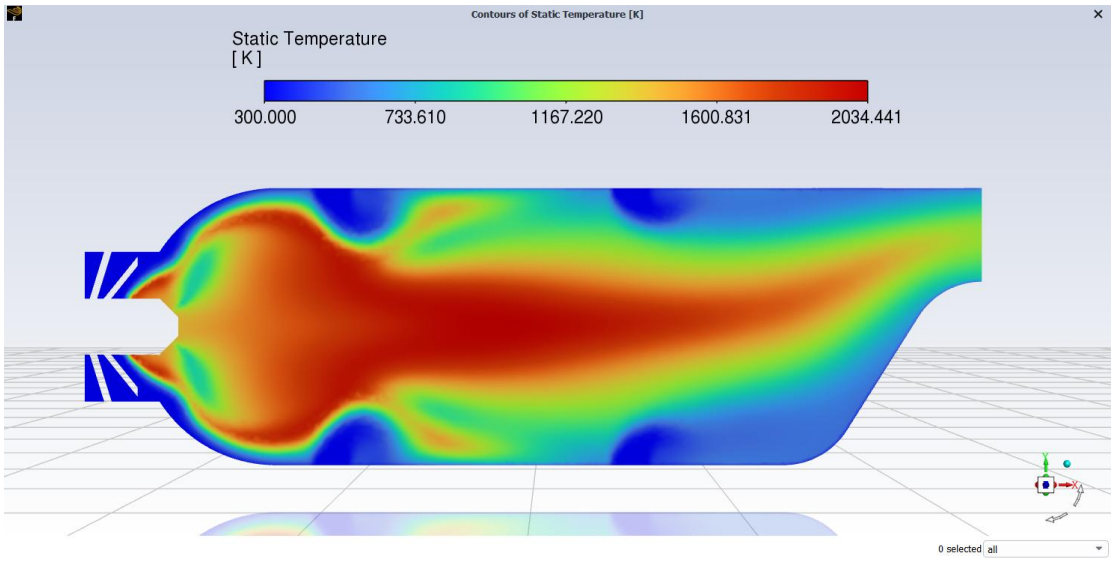

Figure 5.8 static temperature contour for conventional combustor (xy plan), $\dot{m}_f$=0.000812 kg/s, $\dot{m}_{pa}$=0.0147 kg/s, $\dot{m}_{sa}$= 0.0294 kg/s, $\dot{m}_{IS}$=0.0259 kg/s.

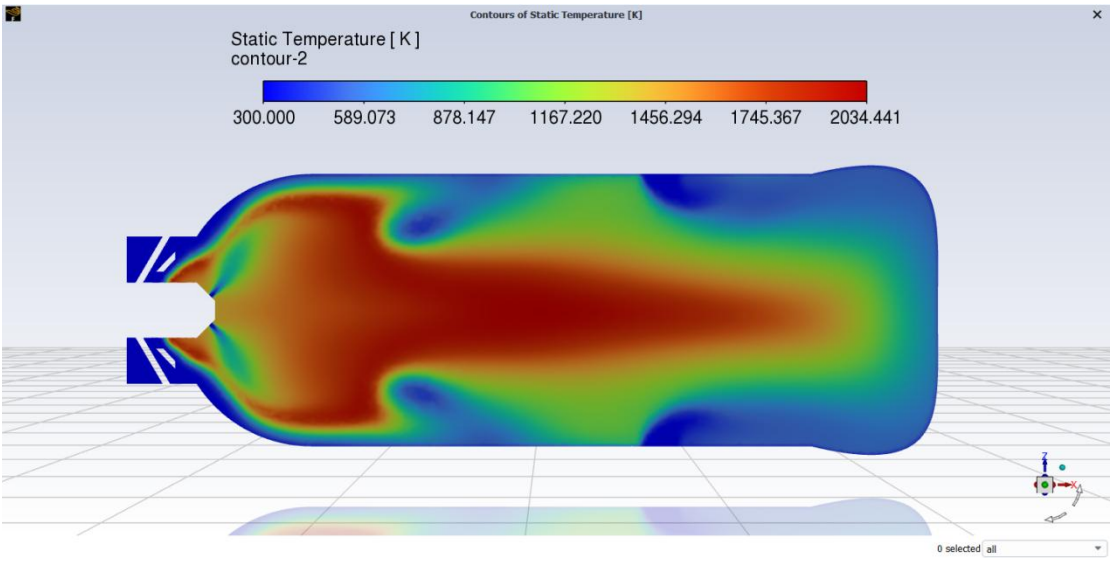

Figure 5.9 static temperature contour for conventional combustor (xz plan), $\dot{m}_f$=0.000812 kg/s, $\dot{m}_{pa}$=0.0147 kg/s, $\dot{m}_{sa}$= 0.0294 kg/s, $\dot{m}_{IS}$=0.0259 kg/s.

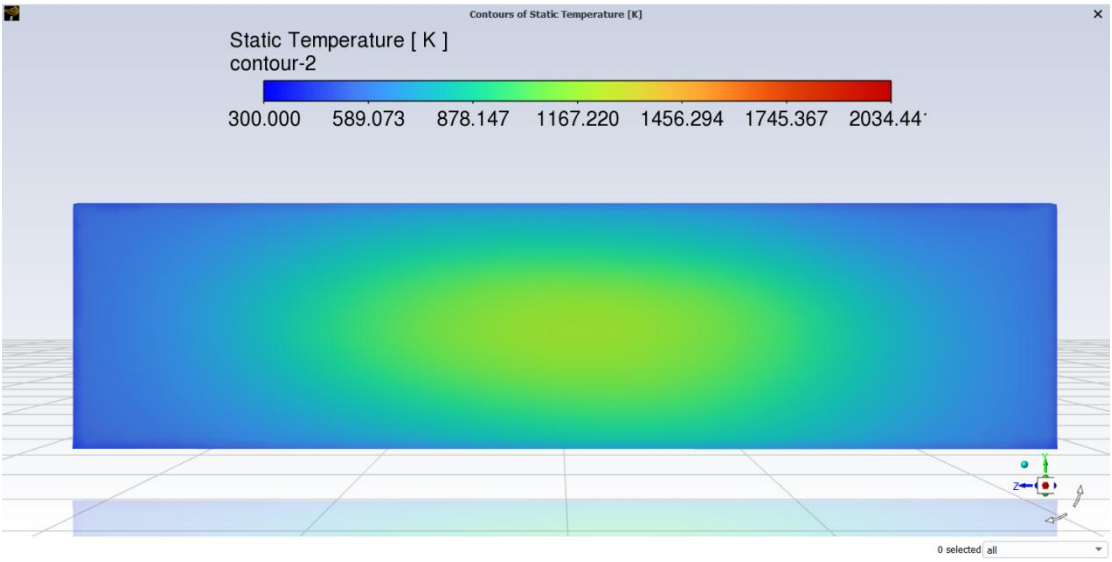

Figure 5.10 static temperature contour for reverse air combustor (outlet).

For the reverse air combustor, The flame temperature is highest at the center of the combustor up to the exit, where it reaches a threshold of about 1900K. However, in the central zone after the fuel injectors, the temperature is much lower due to a high concentration of fuel. Conversely, the temperature is relatively low in areas near the walls where dilution air cools the reactive combustion mixture and protects the wall against thermal stress and erosion. This also brings the combustor exit temperature to appropriate limits for gas turbine.

The maximum temperature reached in the conventional combustor exceeds 2000 K (shown in red color). The walls of the cylinder show excessive heating due to confinement of the flame in this region. Since most of the high enthalpy flow is confined to the walls of the chamber, this design is unfavorable. The contours also indicate a rapid fuel consumption inside the chamber.

In the reverse air combustor, the maximum temperature reached globally is lower than that of the conventional combustor. In this case, it is clear that the hot spot propagates from the injector to the nozzle, demonstrating flame stability.

For the exit temperature in the conventional combustor (1191.64 K) is much lower than the reverse air one (1759.58 K) with a difference of 47%. what makes the reverse air combustor have an improved performances and a greater efficiency.

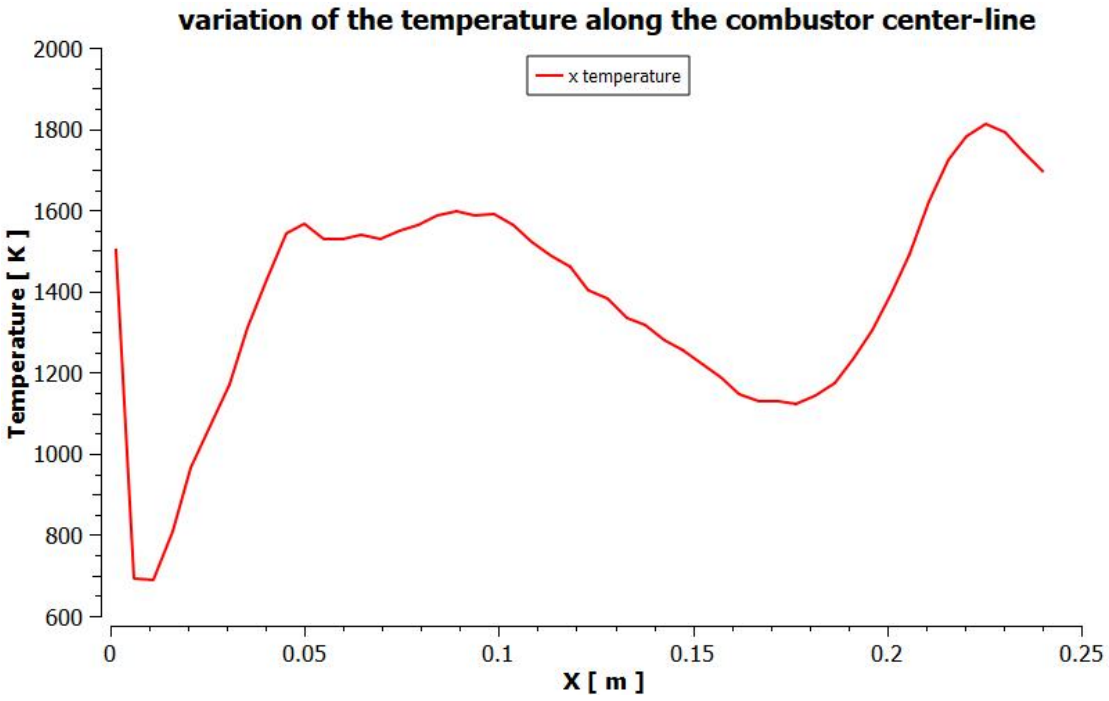

Figure 5.11 temperature variation along combustor center-line (from inlet fuel to the outlet) for reverse air combustor.

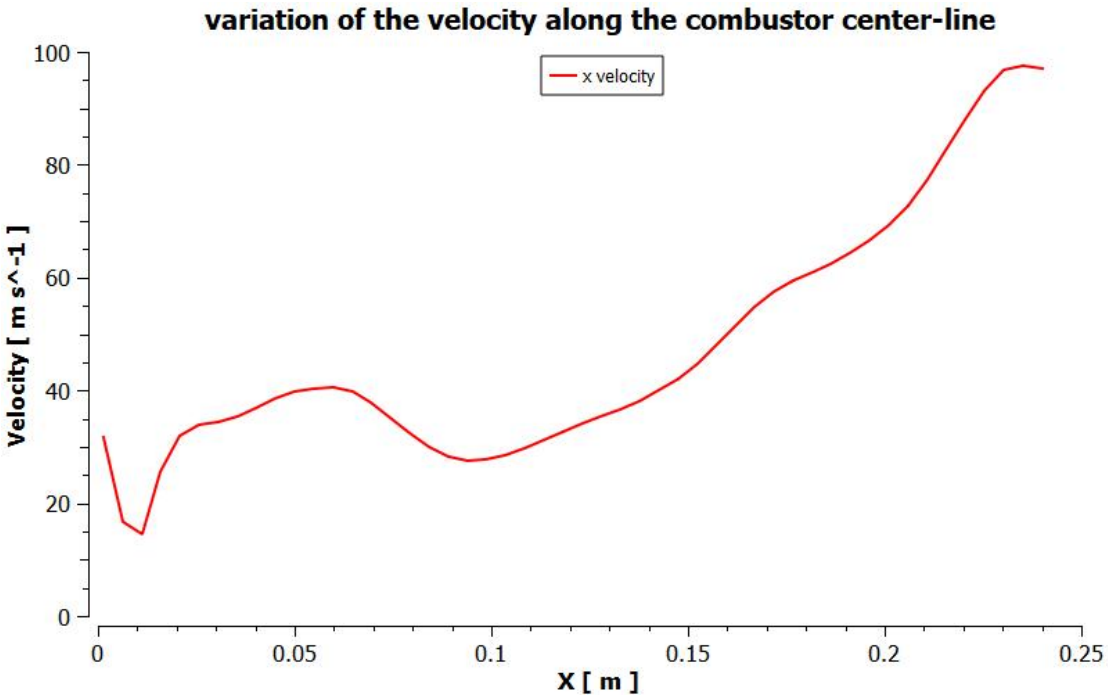

Figure 5.12 velocity variation along combustor center-line (from inlet fuel to the outlet) for reverse air combustor.

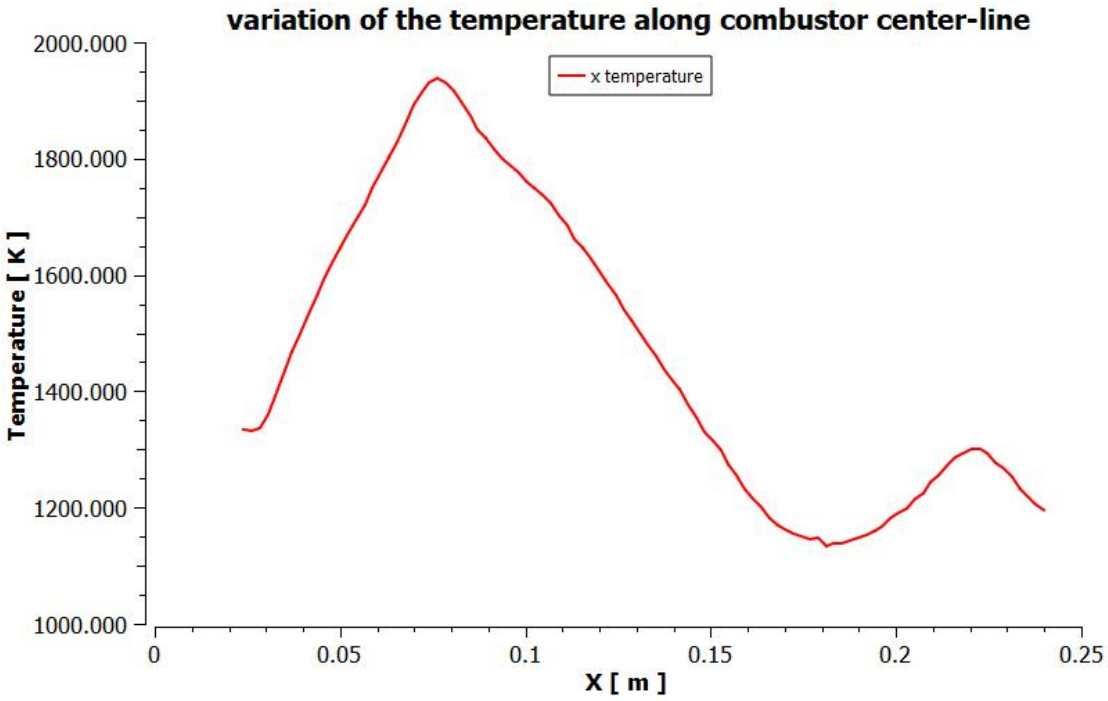

Figure 5.13 temperature variation along combustor center-line (from inlet fuel to the outlet) for conventional combustor.

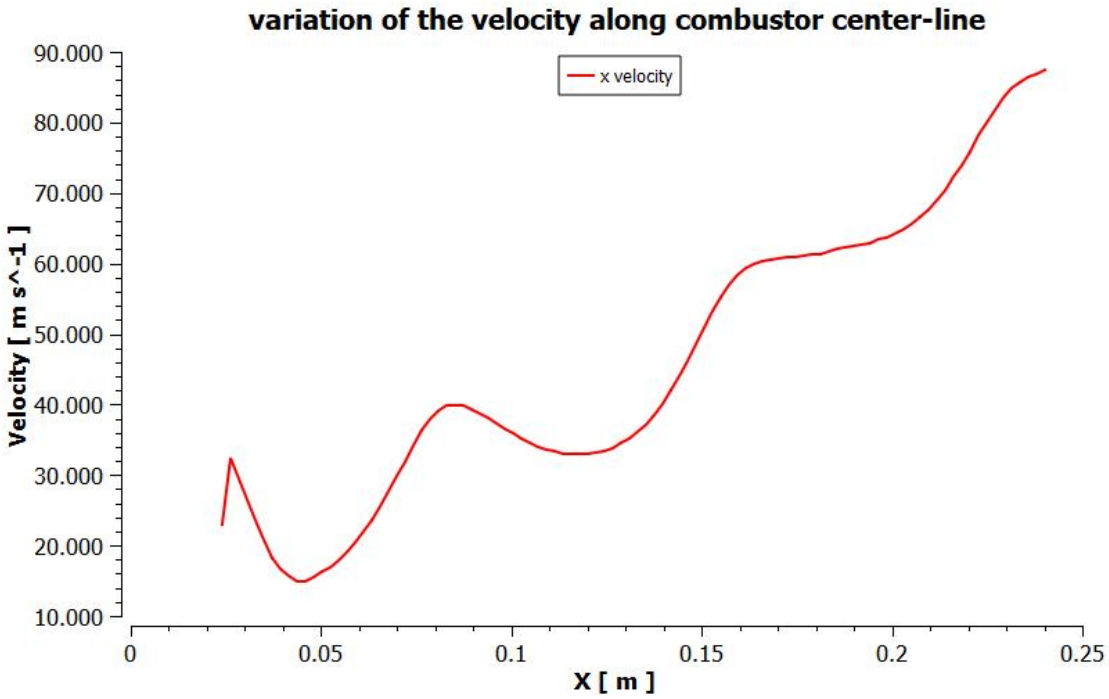

Figure 5.14 velocity variation along combustor center-line (from inlet fuel to the outlet) for conventional combustor.

5.3.3 Section temperature contours and charts

5.3.1 reverse air combustor

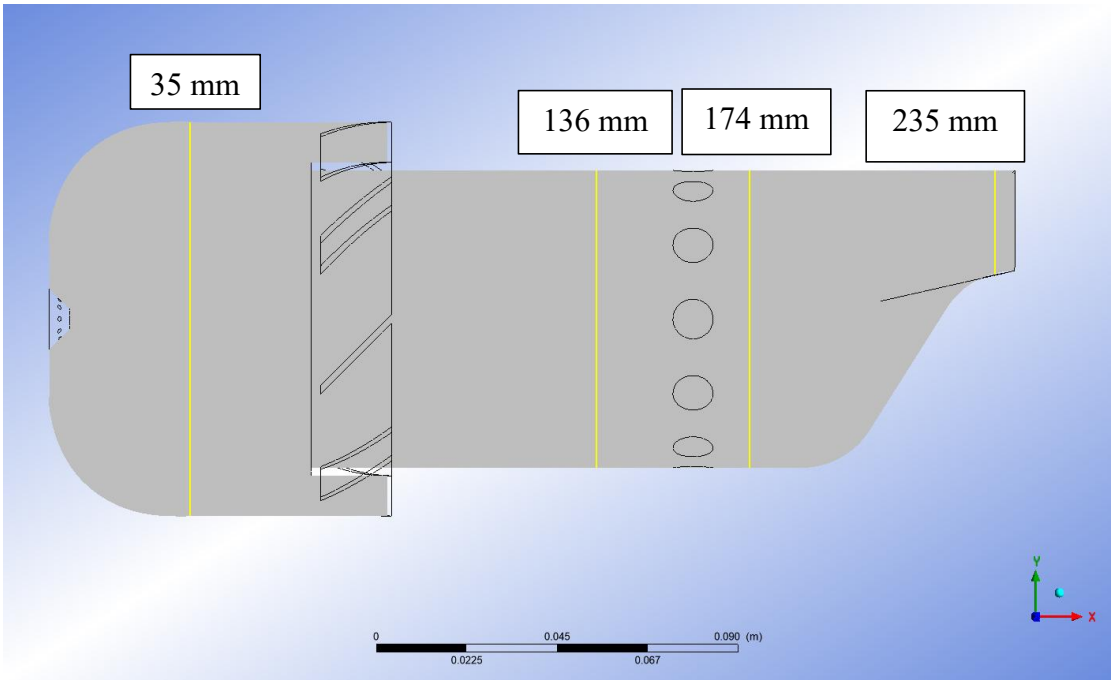

Figure 5.15 sections placement for temperature contours in front face for reverse air combustor.

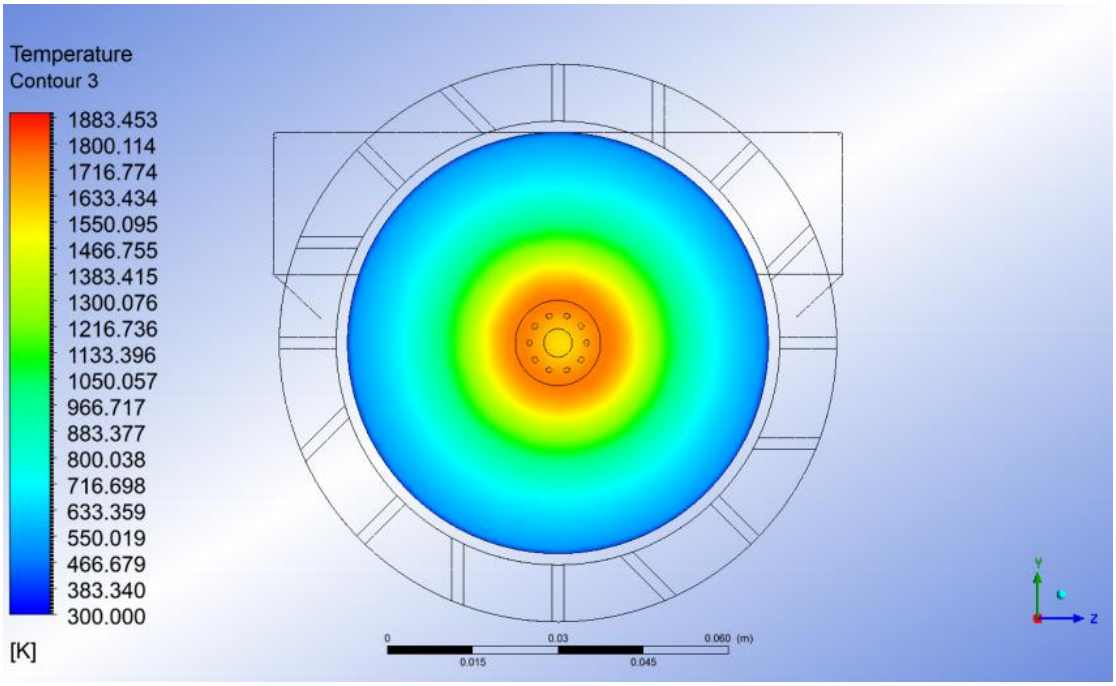

Figure 5.16 temperature contour for x=35 mm from reference.

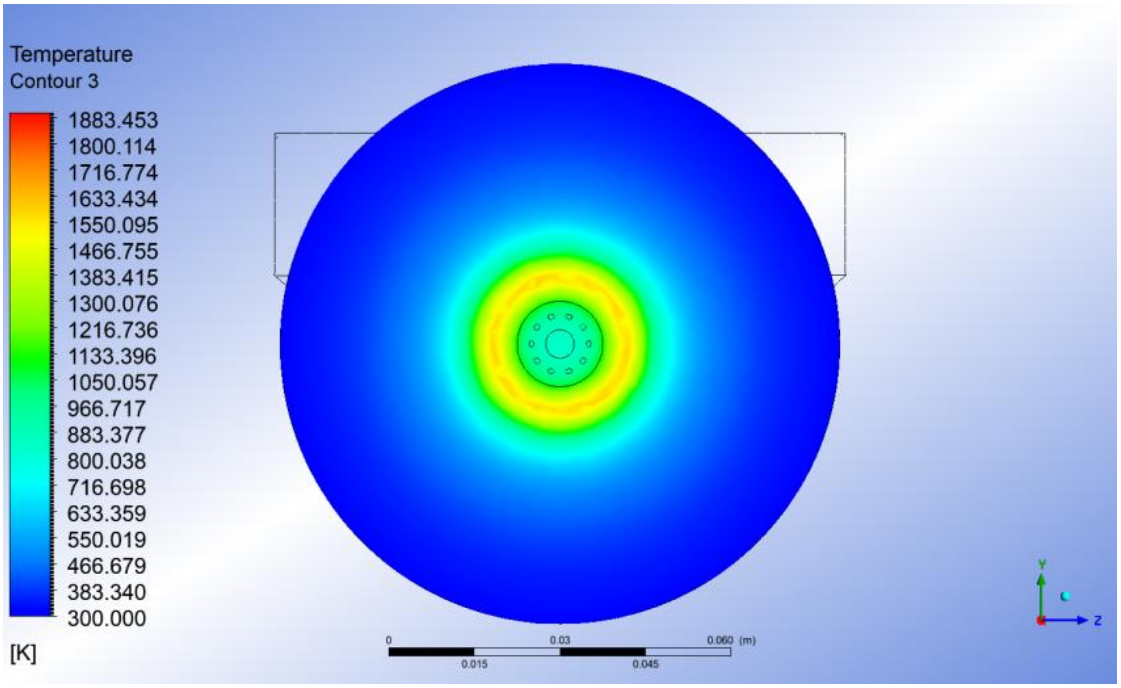

Figure 5.17 temperature contour for x=136 mm from reference.

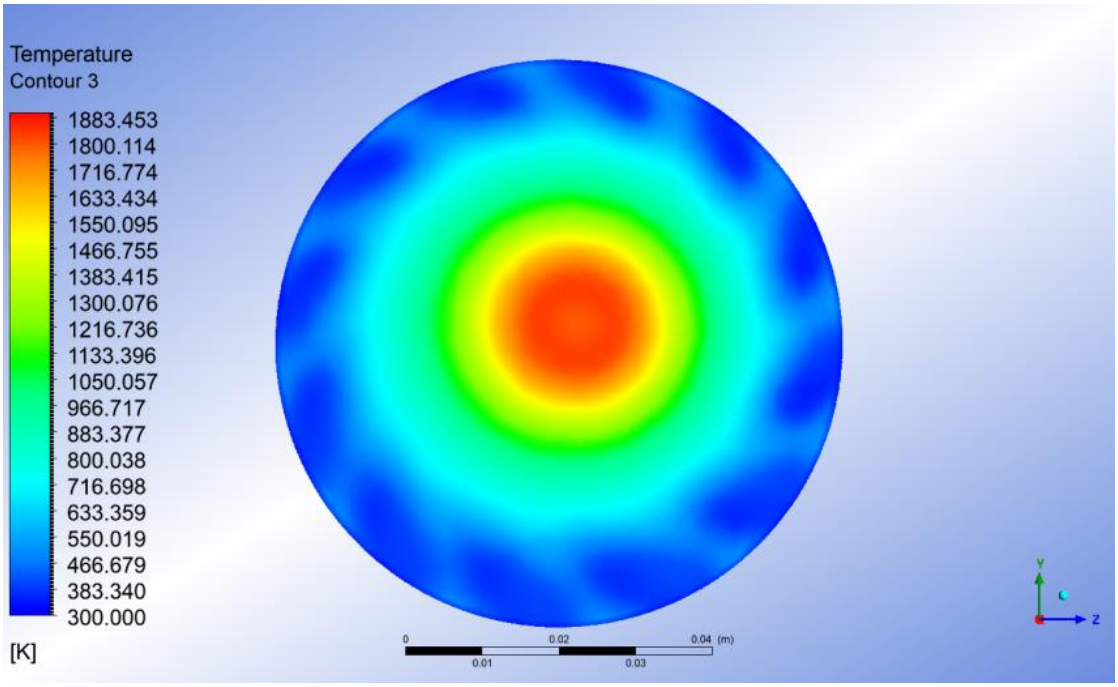

Figure 5.18 temperature contour for x= 174mm from reference.

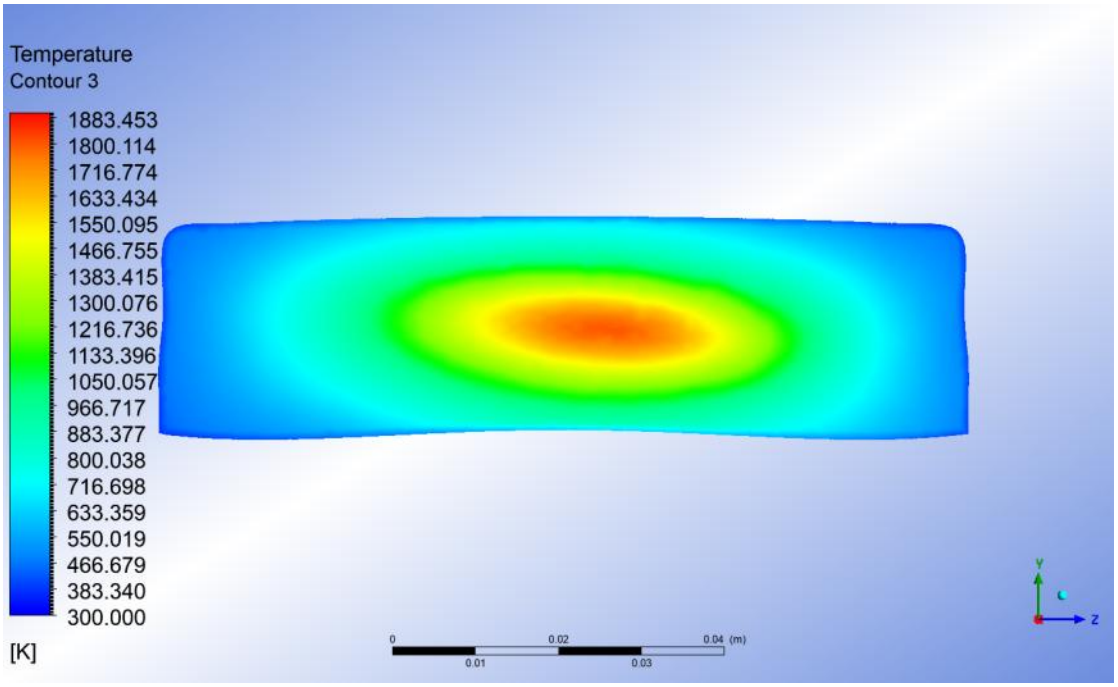

Figure 5.19 temperature contour for x=235mm from reference.

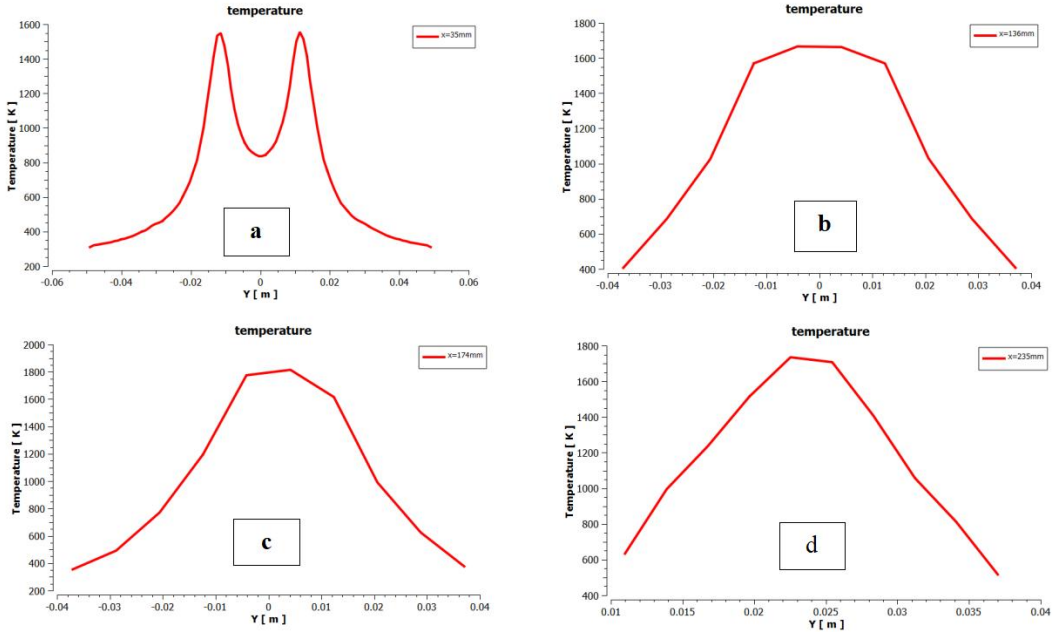

Figure 5.20 charts display for temperature in different sections from reference

a=35 mm, b=136 mm, c=174 mm, d=235mm

5.3.3.2 conventional combustor

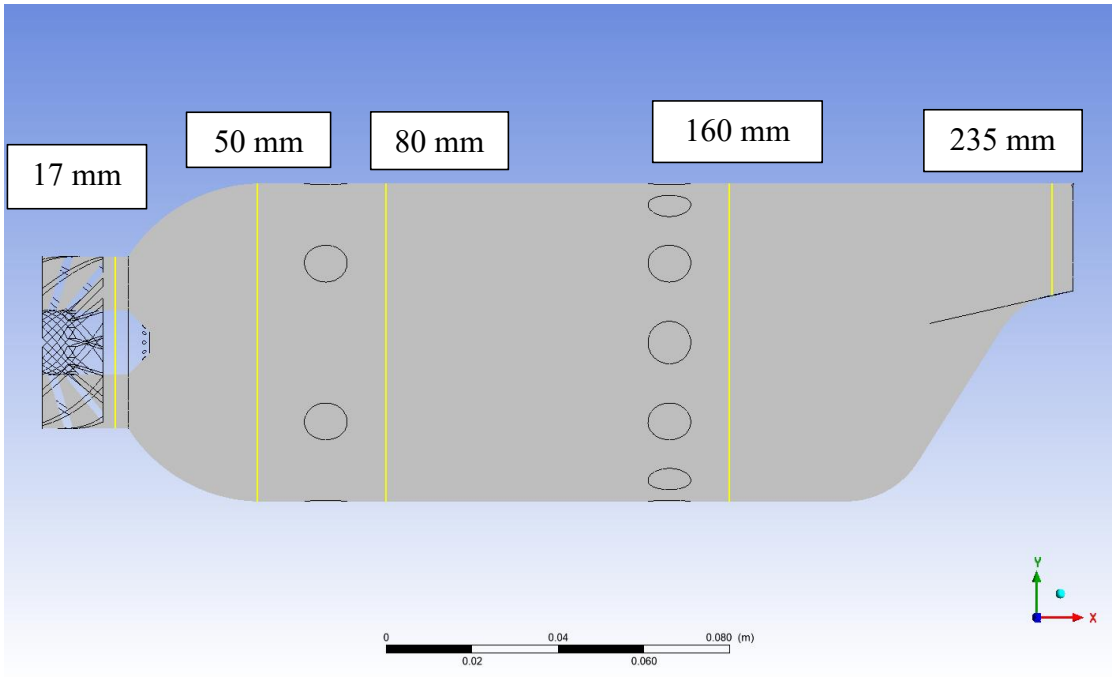

Figure 5.21 sections placement for temperature contours in front face for conventional combustor.

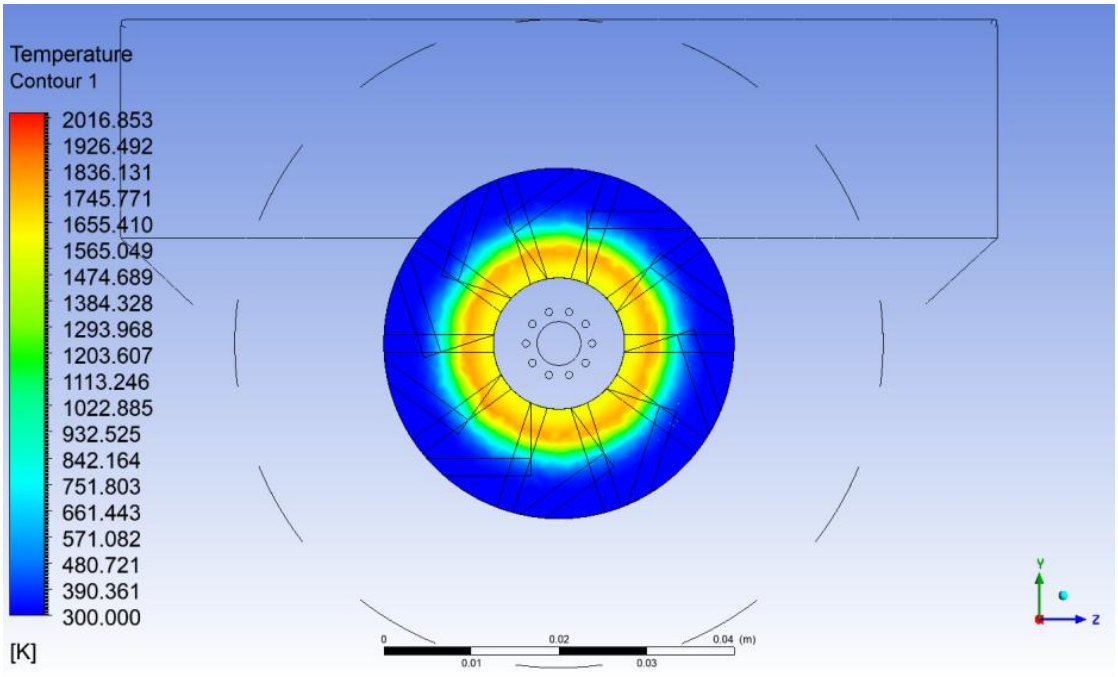

Figure 5.22 temperature contour for x=17 mm from reference.

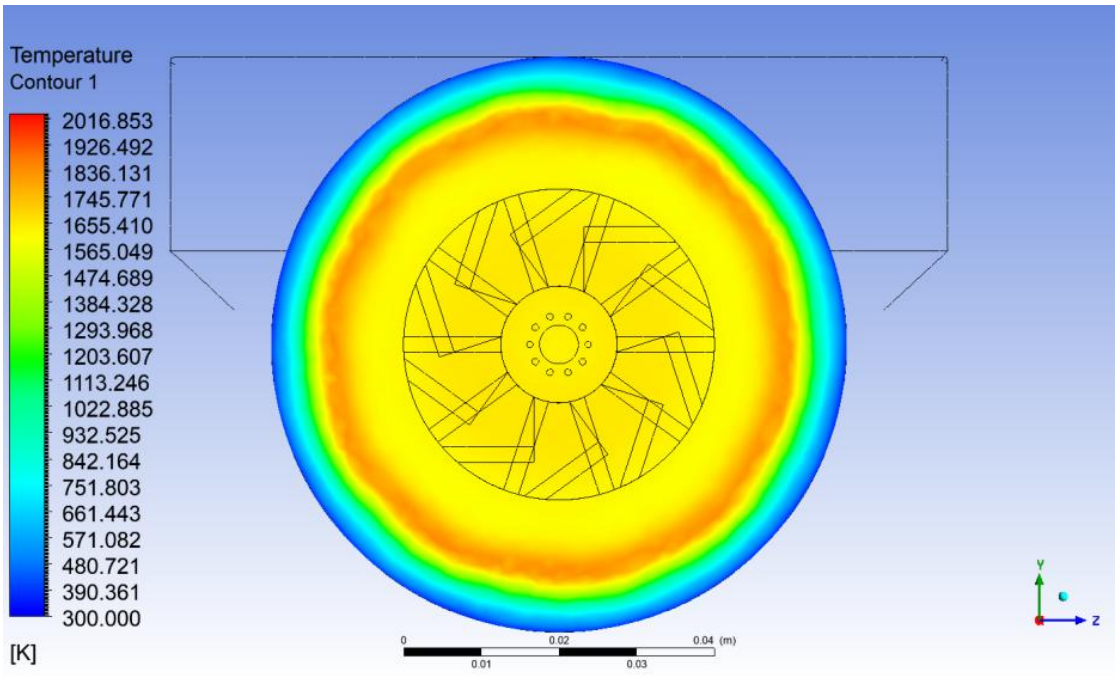

Figure 5.23 temperature contour for x=50 mm from reference.

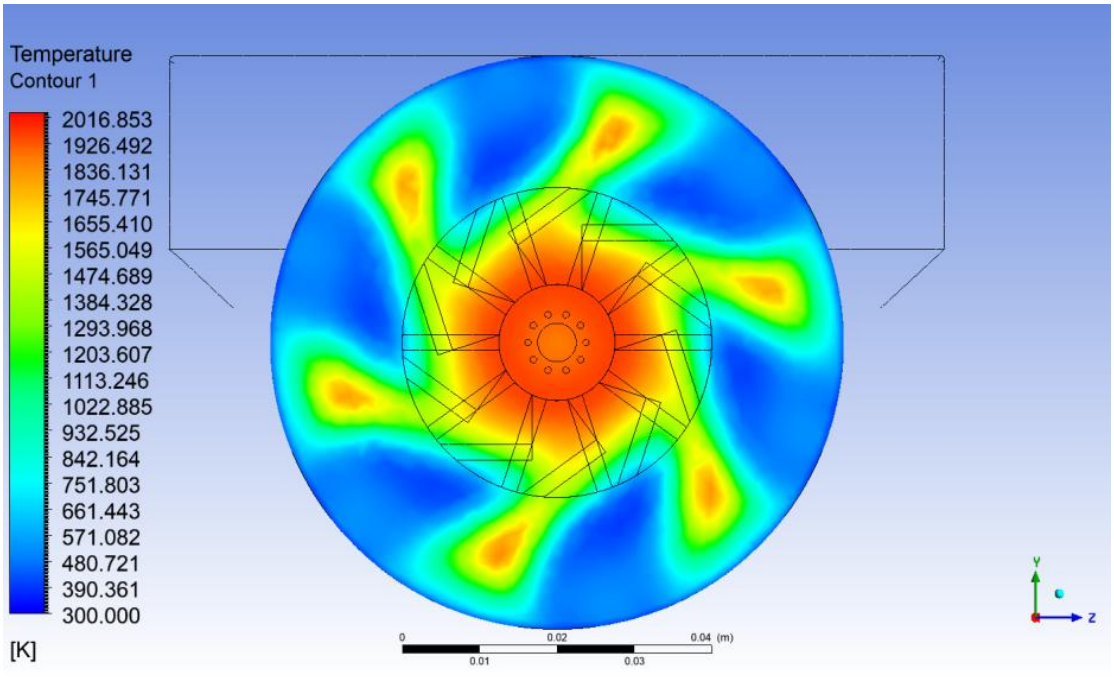

Figure 5.24 temperature contour for x=80 mm from reference.

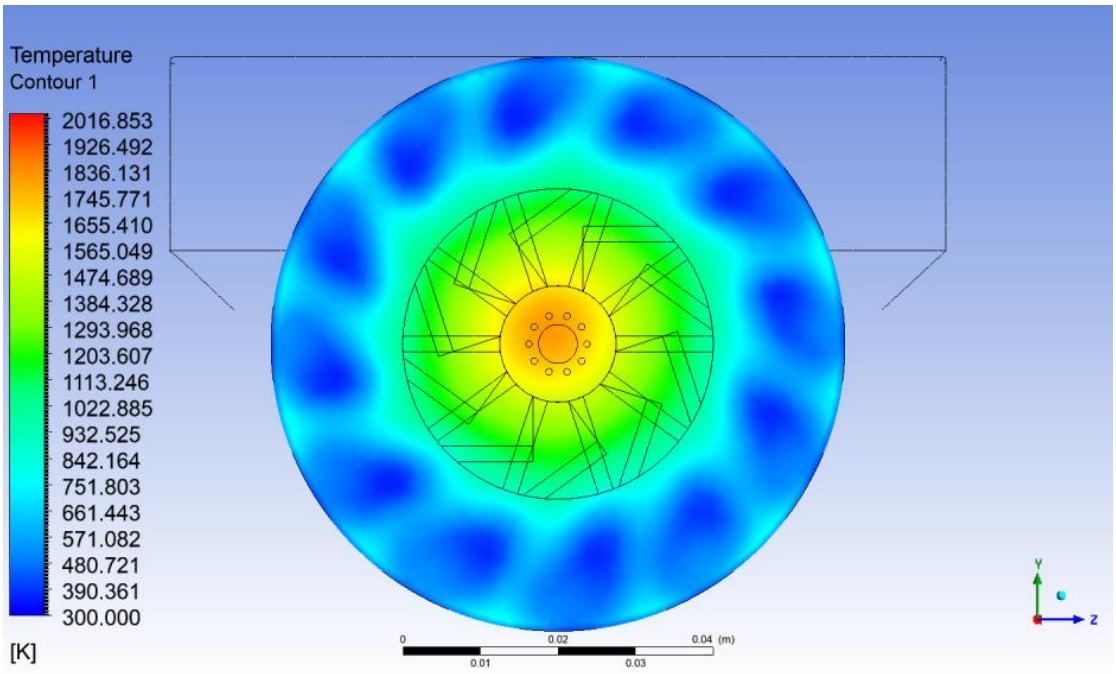

Figure 5.25 temperature contour for x=160 mm from reference.

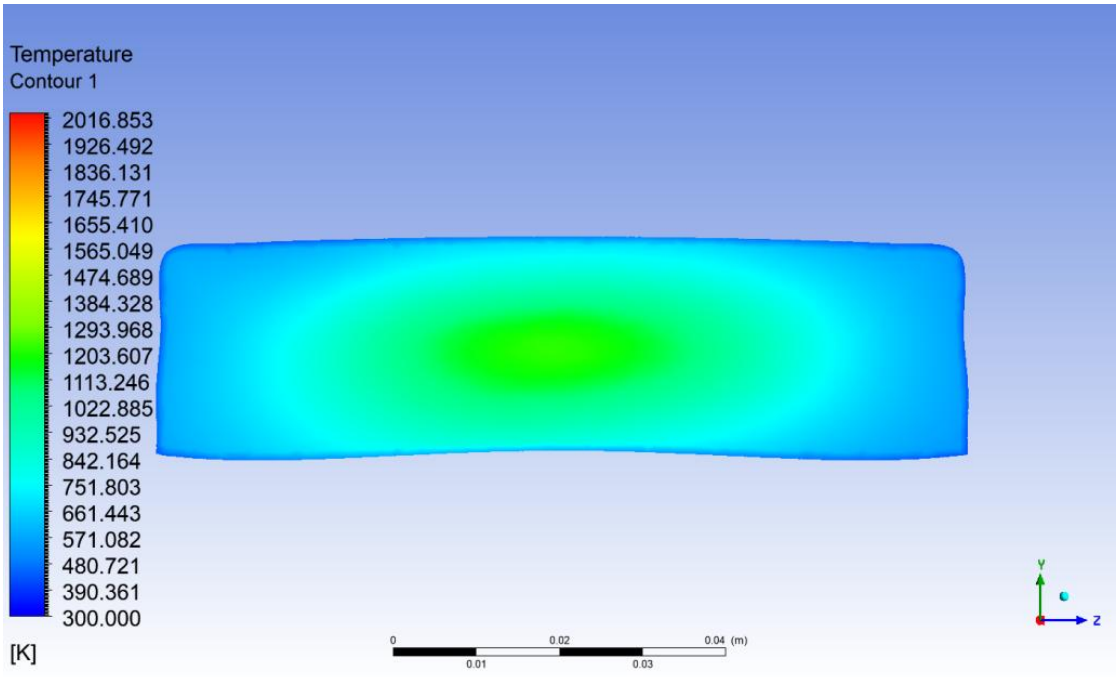

Figure 5.26 temperature contour for x=235 mm from reference.

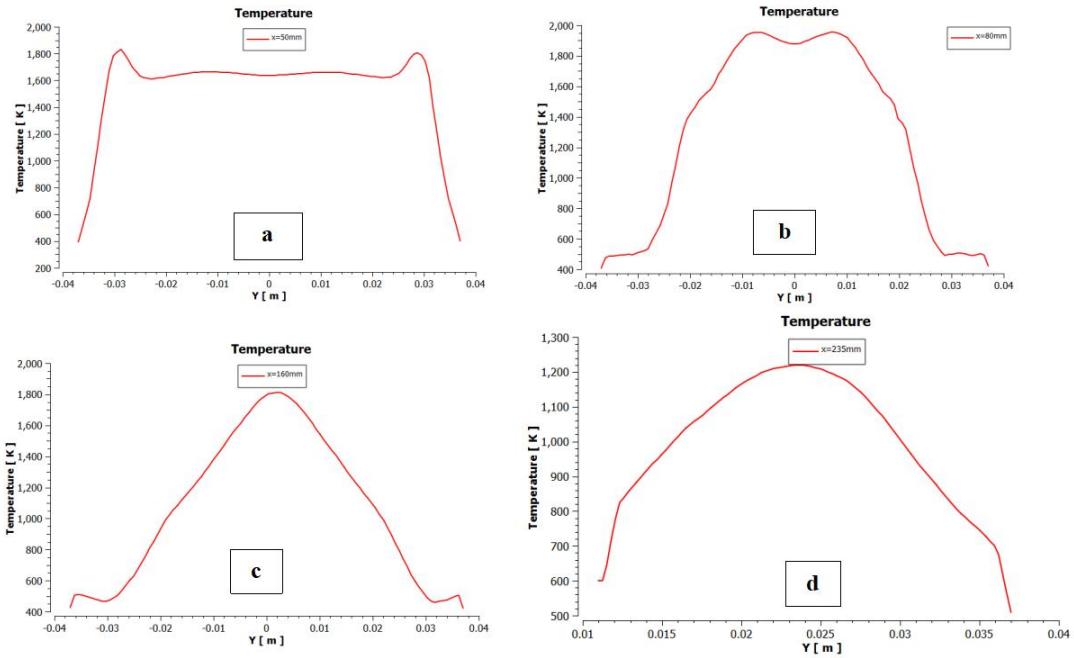

Figure 5.27 charts display for temperature in different sections from reference

a=50 mm, b=80 mm, c=160 mm, d=235 mm

5.3.4 Pressure contours

5.3.4.1 reverse air combustor

The static pressure contour for reverse air combustor is shown in figure (5.24) below.

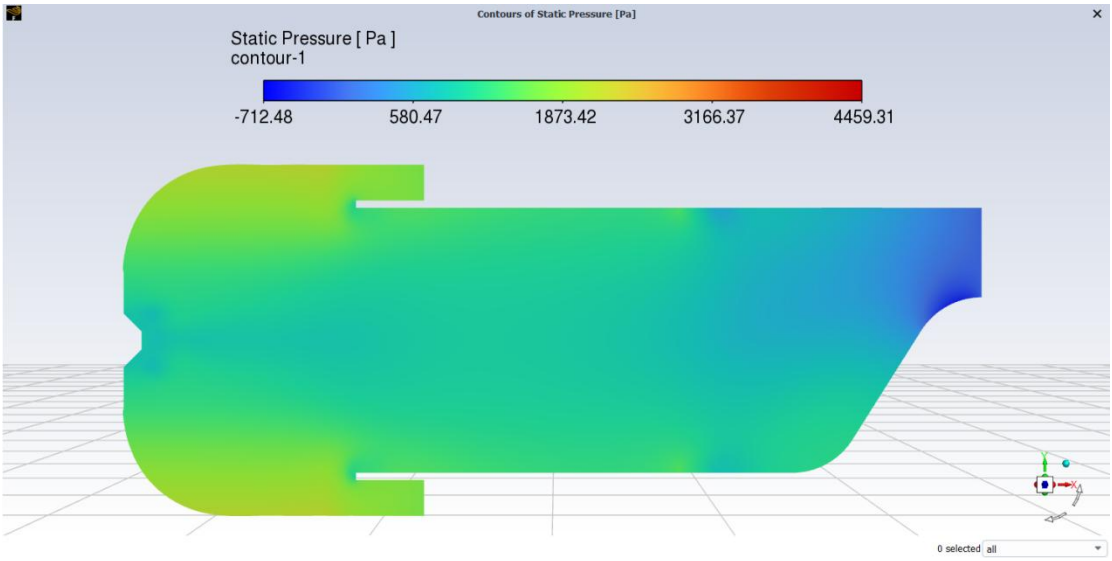

Figure 5.28 static pressure contour for reverse air combustor (xy plan).

5.3.4.2 conventional combustor

The static pressure contour for conventional combustor is shown in figure (5.25) below.

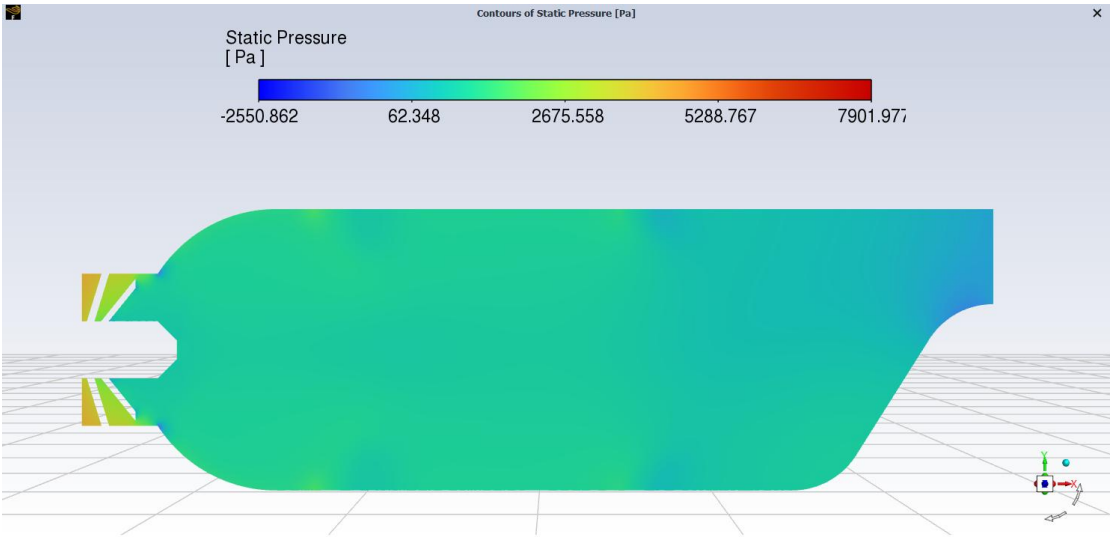

Figure 5.29 static pressure contour for conventional combustor (xz plan).

For both geometries, we can see that the highest pressure value captured in the domain was located in the primary zones, with the pressure falling to almost atmospheric value in the nozzle's outlet. This is because the flow is subsonic and the nozzle leads to an increase in velocity, resulting in a decrease in pressure.

5.3.5 Velocity contours and charts of exit velocity

The velocity variation inside the domain for both cases has been studied in this section. The maximum velocities are attained inside the nozzle of the combustor, but the values show a huge discrepancy. The figures from (5.26) to (5.29) below show the contours of velocity's variation for magnitude velocity and velocity in direction x.

5.3.5.1 reverse air combustor

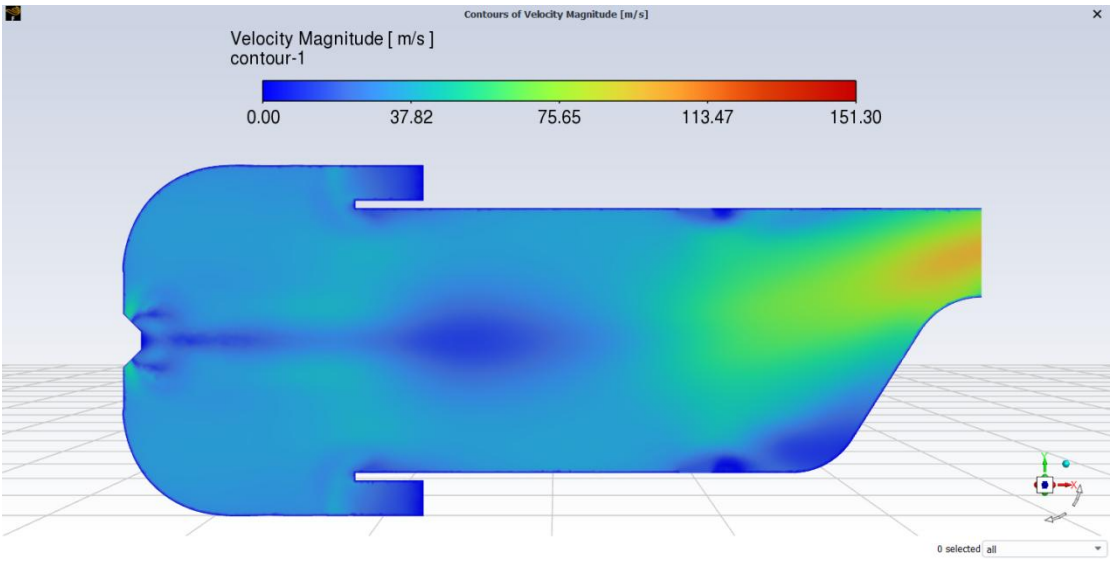

Figure 5.30 magnitude velocity contour for reverse air combustor (xy plan).

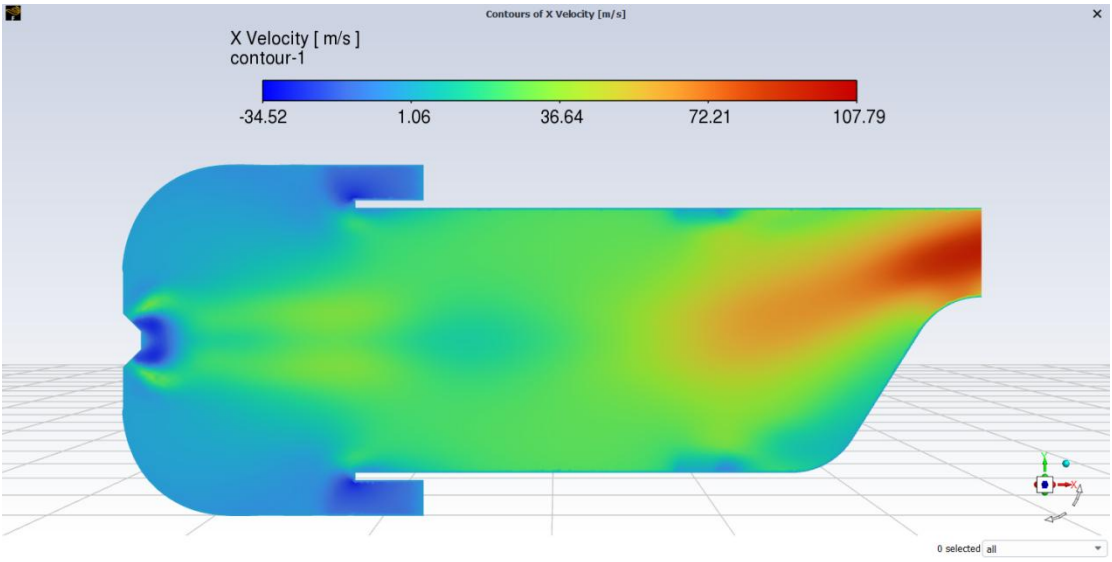

Figure 5.31 x velocity contour for reverse air combustor (xy plan).

5.3.5.2 conventional combustor

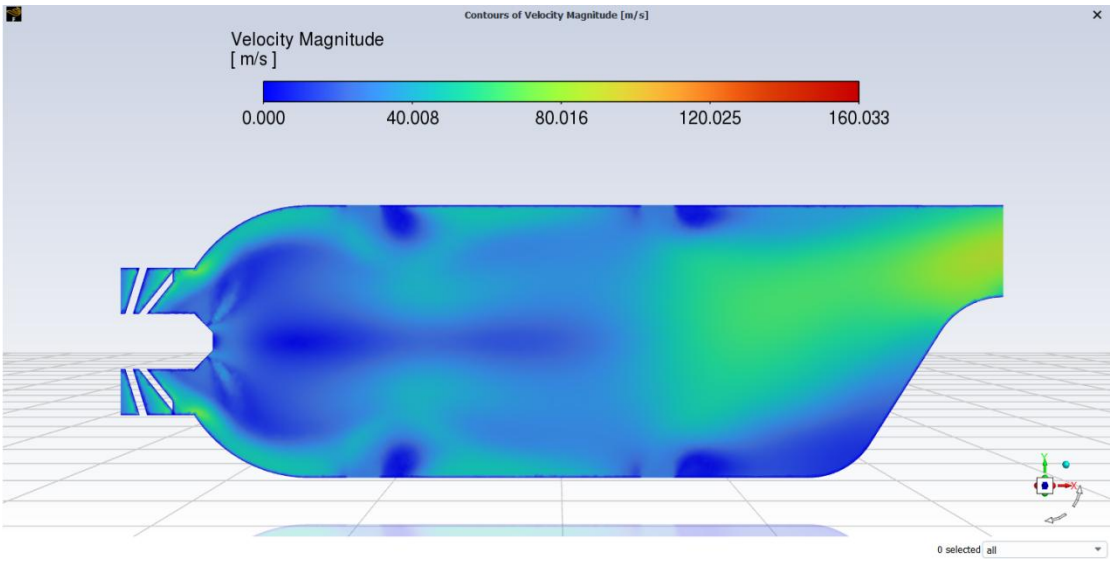

Figure 5.32 magnitude velocity contour for conventional combustor (xy plan).

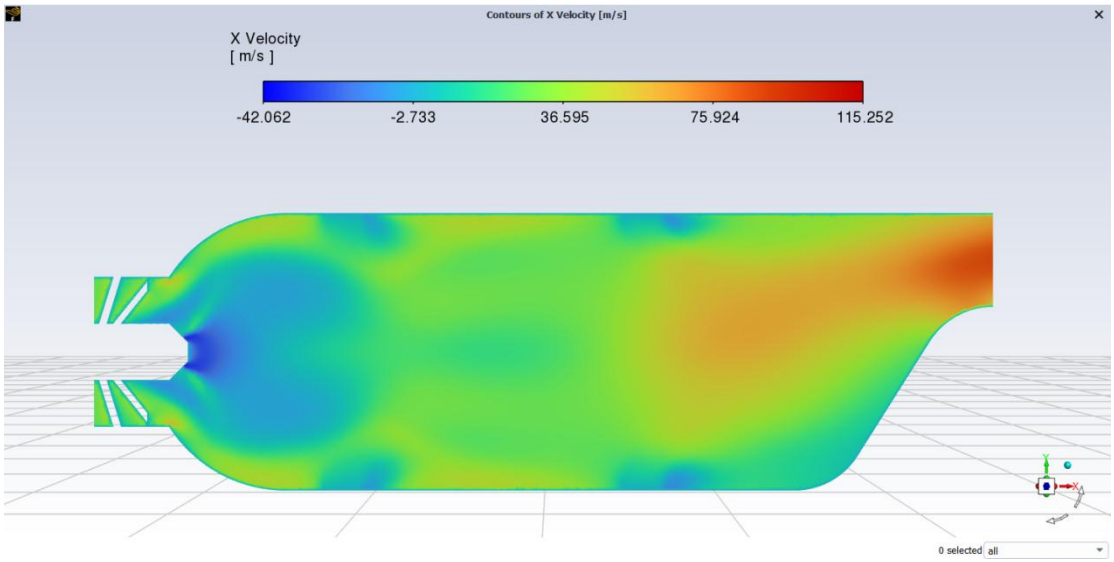

Figure 5.33 x velocity contour for conventional combustor (xy plan).

The velocity value (highlighted in red color in the above figures) is highest at the nozzle's outlet for both combustors. However, the reverse air combustor has a higher velocity value compared to the conventional one. This indicates that the gases leaving the chamber in the reverse air combustor have a relatively higher energy content. Additionally, we can observe that there is less recirculation in the primary zone for the reverse air combustor, whereas the conventional combustor shows the opposite effect.

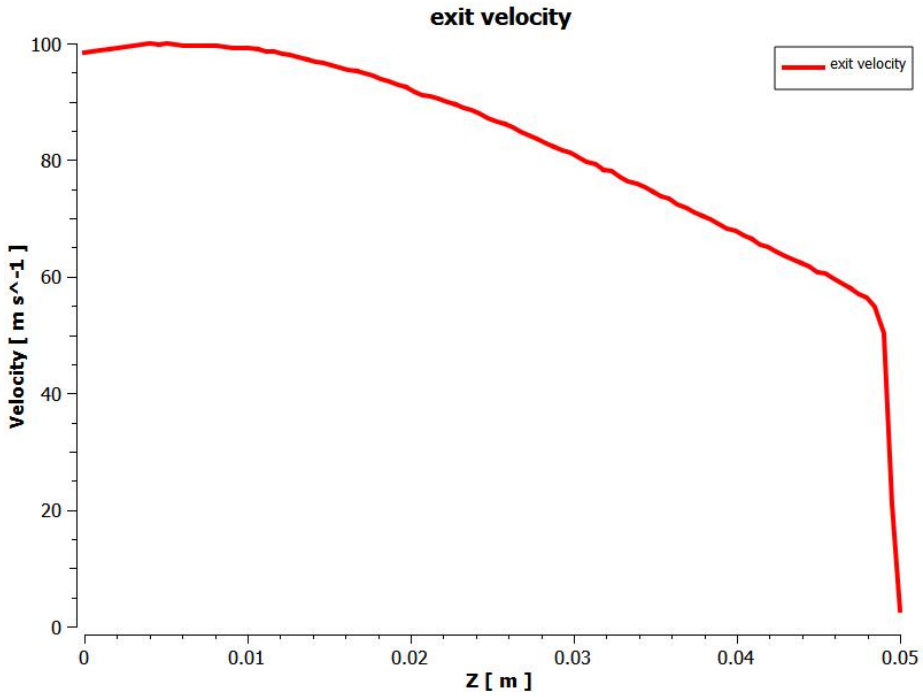

Figure 5-34 exit velocity chart for reverse air combustor.

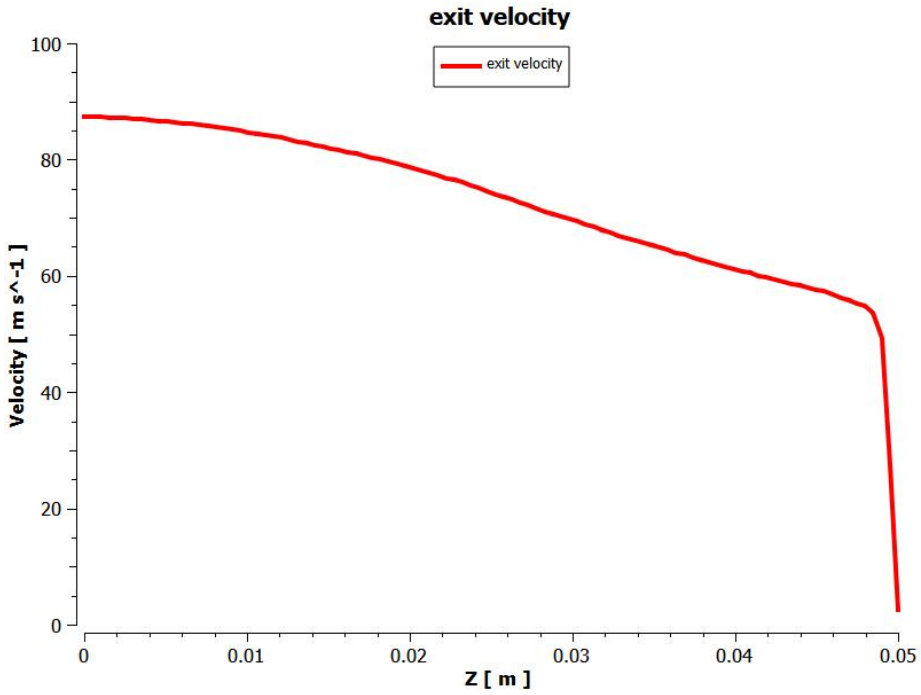

Figure 5.35 exit velocity chart for conventional combustor.

Table 5-5 maximum velocity values in the nozzle's outlet.

	Reverse air combustor	Conventional combustor
Velocity (m/s)	100	87

5.3.6 Density contours

The density of air inside the combustors can be seen in figures (5.32) and (5.33) for reverse air and conventional combustors, respectively.

5.3.6.1 reverse air combustor

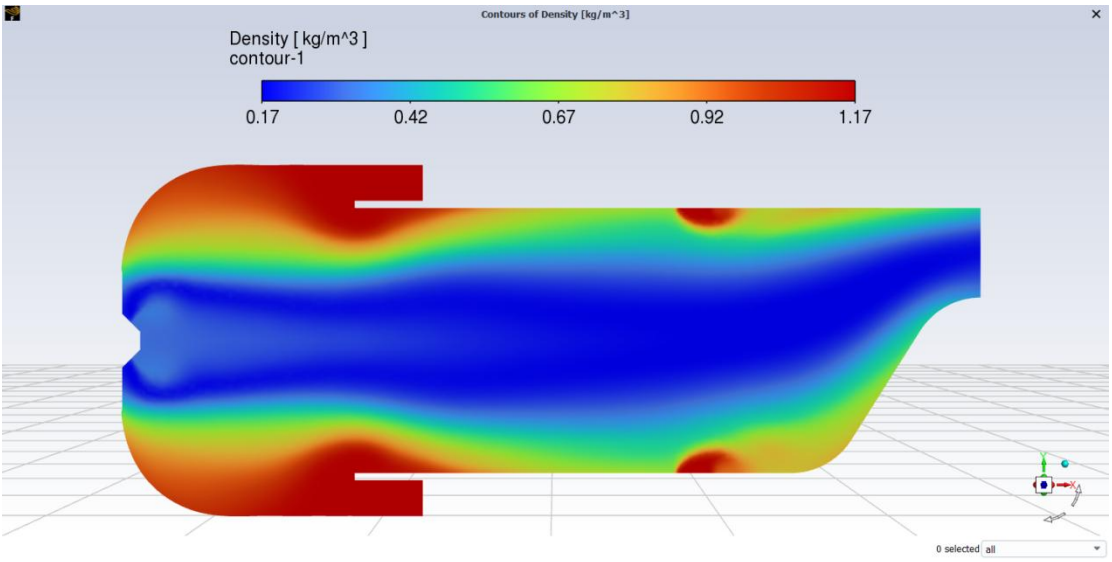

Figure 5.36 density contour for reverse air combustor (xy plan).

5.3.6.2 conventional combustor

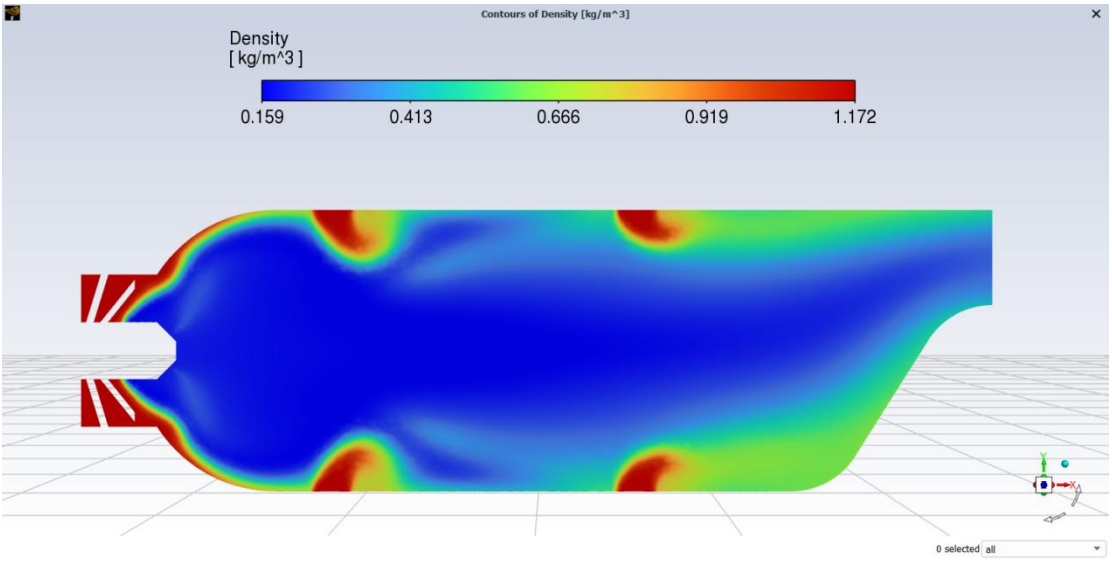

Figure 5.37 density contour for conventional combustor (xy plan).

From the above figures it's obvious where the zones have higher air density located in where the air enter the combustor (inlet swirler, primary air and secondary air), and this is presented in the figures where the color of the contour is red.

5.3.7 Mass fraction

To comprehend the interaction between turbulence and chemistry, it is crucial to monitor the consumption and generation of species within the combustor. This monitoring also aids in confirming the distribution of different intermediate species formed during the reaction.

5.3.7.1 Ch4 mass fraction

Figures (5.34), (5.35) below show the variation of CH4 inside the two combustors.

5.3.7.1.1 reverse air combustor

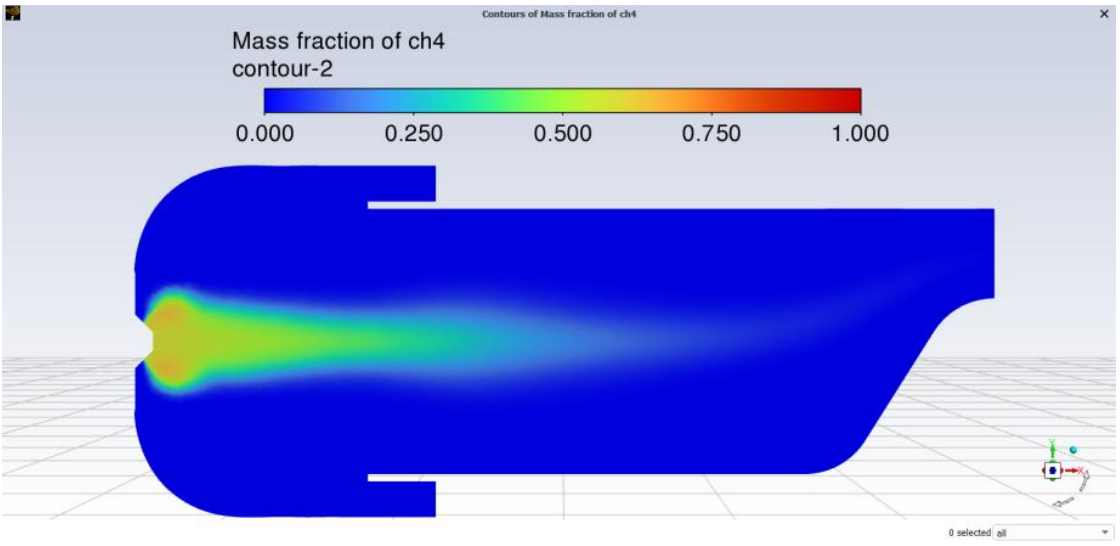

Figure 5.38 Ch4 mass fraction contour for reverse air combustor (xy).

5.3.7.1.2 conventional combustor

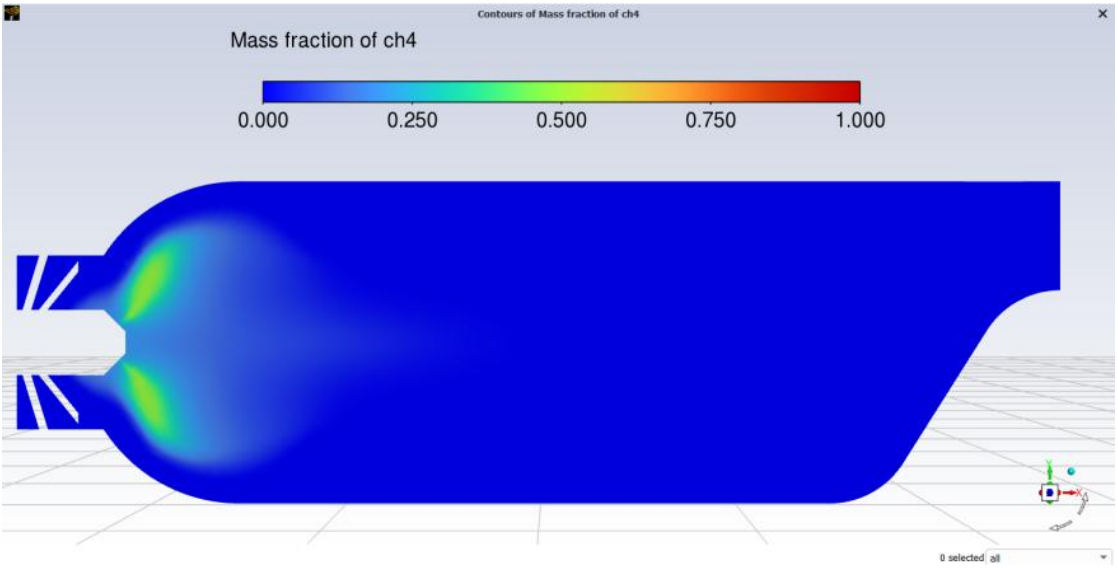

Figure 5.39 Ch4 mass fraction contour for conventional combustor (xy plan).

From the figures above, it can be observed that excessive levels of turbulence in the conventional combustor lead to quick dissipation of fuel with the swirl and primary air. This primarily occurs along the chamber's centerline, where the flame is expected to be. Consequently, under such conditions, excessive heating of the annulus becomes unavoidable. However, in the reverse air combustor, the fuel is available along the centerline for combustion, thereby maintaining the flame. This stream of fuel can only be sustained in the absence of highly turbulent regions and dissipation along the flame path, which is precisely achieved in the reverse air combustor.

5.3.7.2 O2 mass fraction

the variation of O2 mass fraction fraction is shown in the figures below for reverse air and conventional combustor.

5.3.7.2.1 reverse air combustor

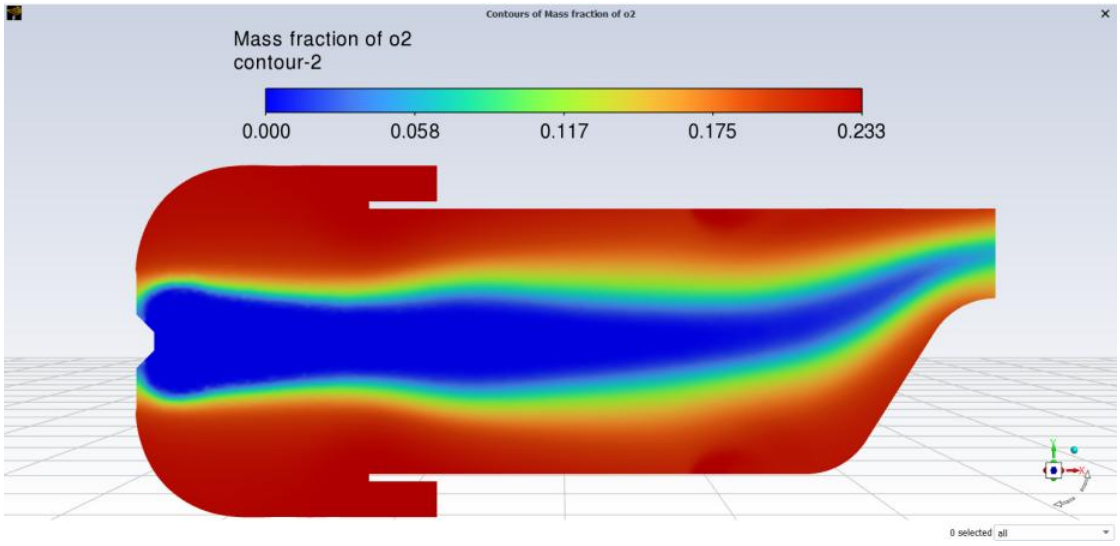

Figure 5.40 O2 mass fraction contour for reverse air combustor (xy plan).

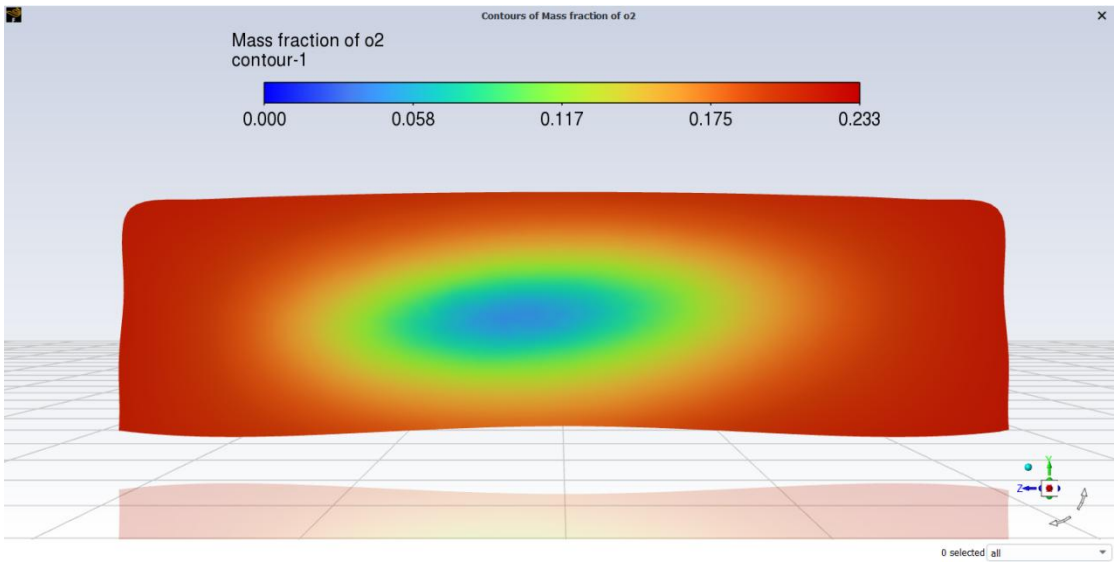

Figure 5.41 O2 mass fraction contour for reverse air combustor (exit nozzle section).

5.3.7.2.2 conventional combustor

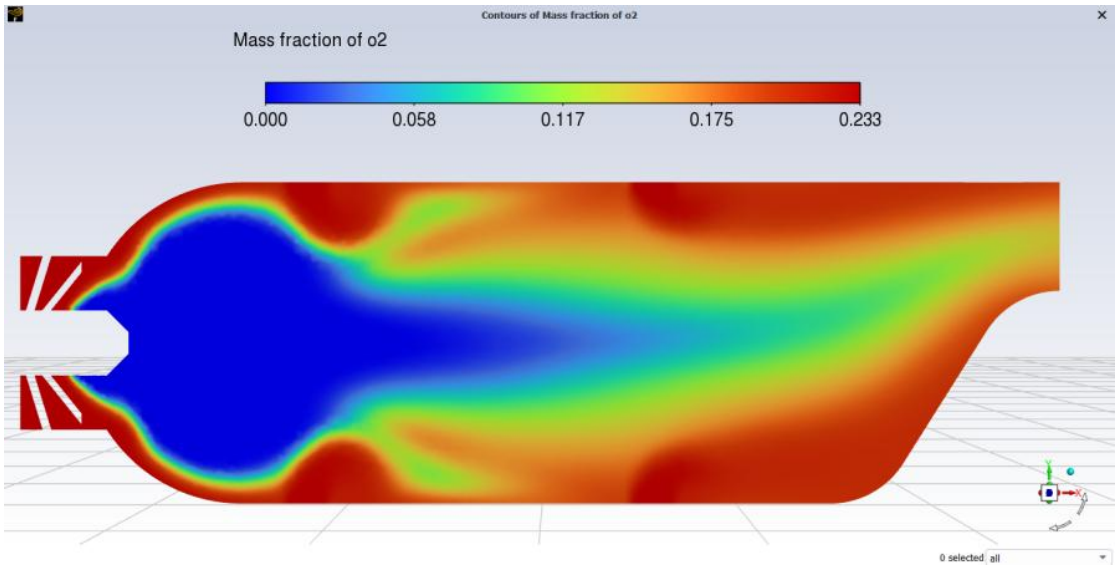

Figure 5.42 O2 mass fraction contour for conventional combustor (xy plan).

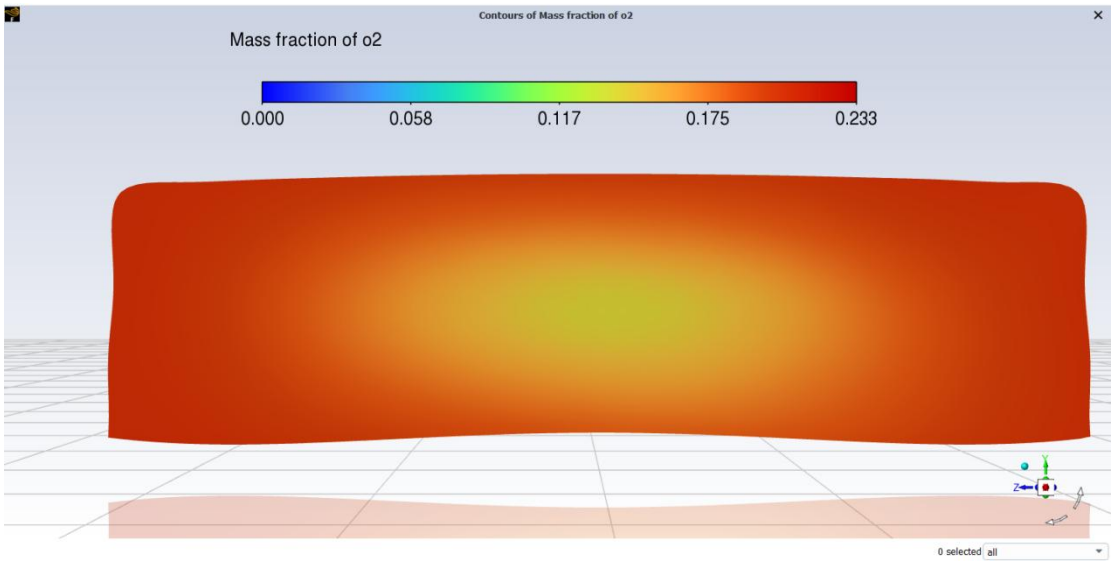

Figure 5.43 O2 mass fraction contour for conventional combustor (exit nozzle section).

In the previous contours, we can observe two areas:

Areas with a low O2 mass fraction represent a zone where the fuel is rich (blue area), as fuel and combustion mix to reduce the O2 concentration.

The area where the O2 concentration is high (the red area) is where the air that contains O2 enters the combustors and also refers to no combustion in this zone.

5.3.7.3 Co2 mass fraction

As shown below, the variation of the CO2 mass fraction is represented in these figures.

5.3.7.3.1 reverse air combustor

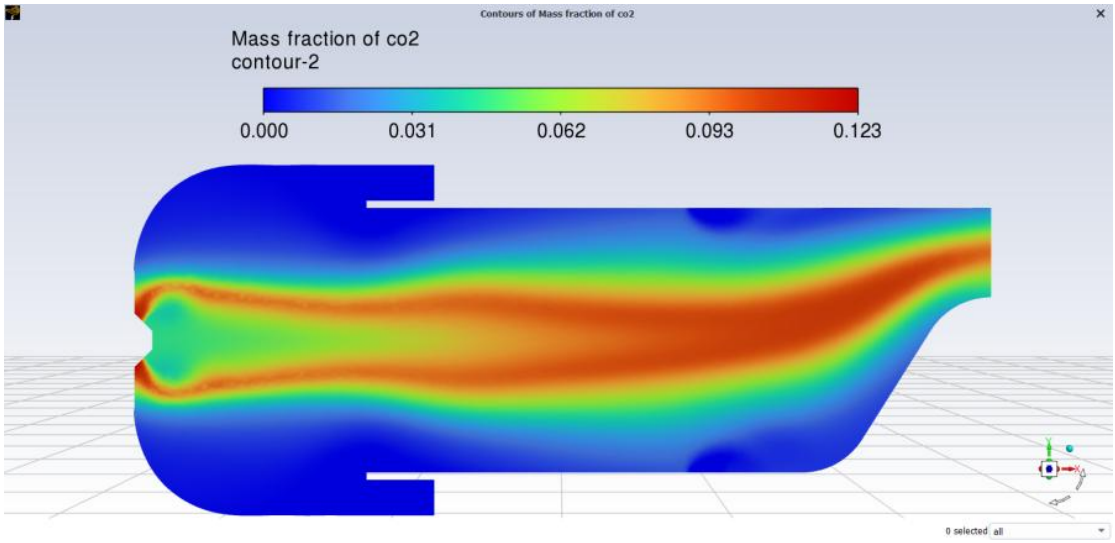

Figure 5.44 CO2 mass fraction contour for reverse air combustor (xy plan).

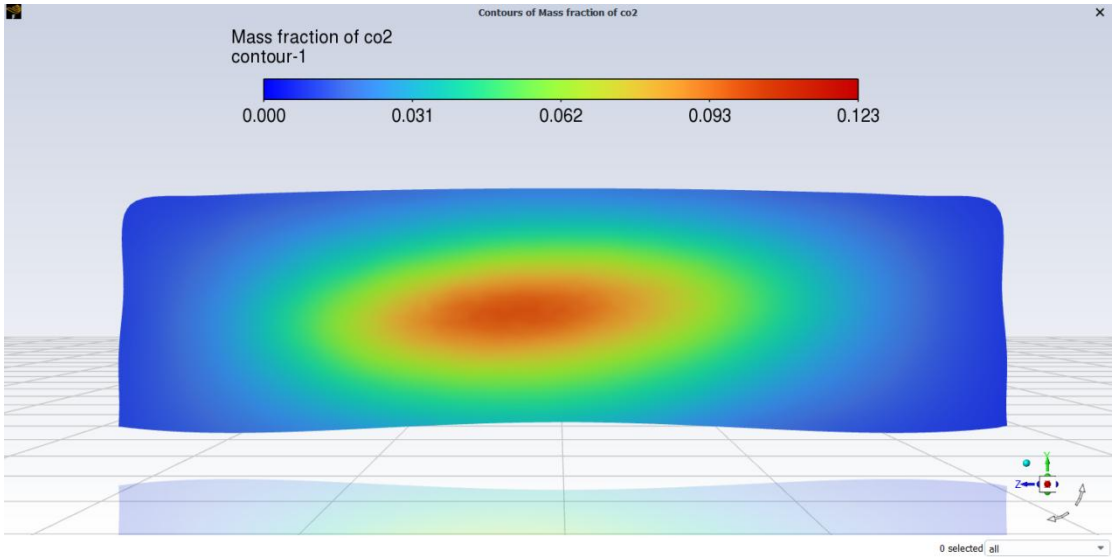

Figure 5.45 CO2 mass fraction contour for reverse air combustor (exit nozzle section).

5.3.7.3.2 conventional combustor

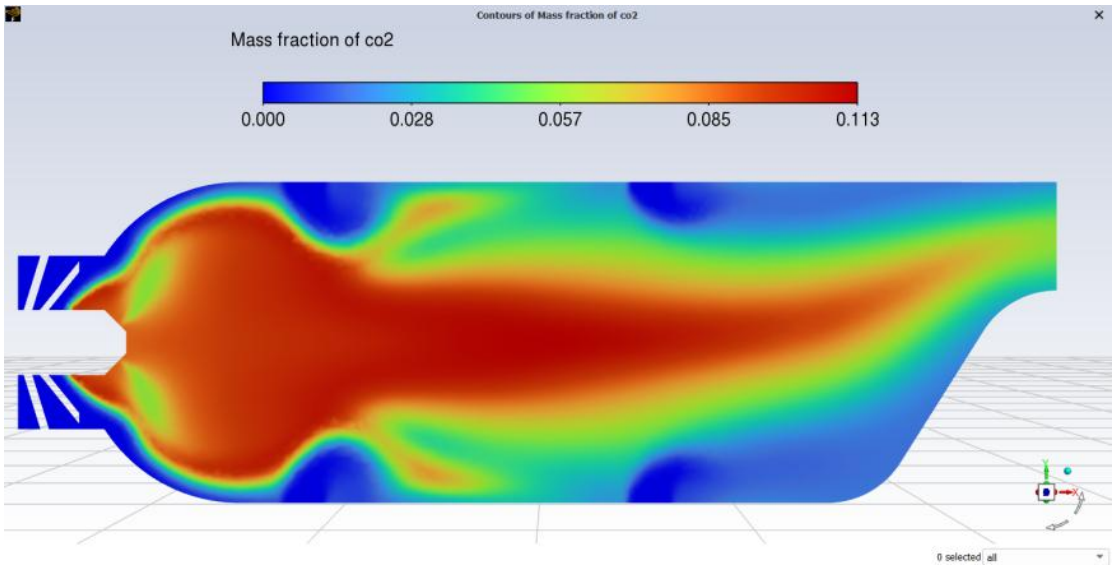

Figure 5.46 CO2 mass fraction contour for conventional combustor (xy plan).

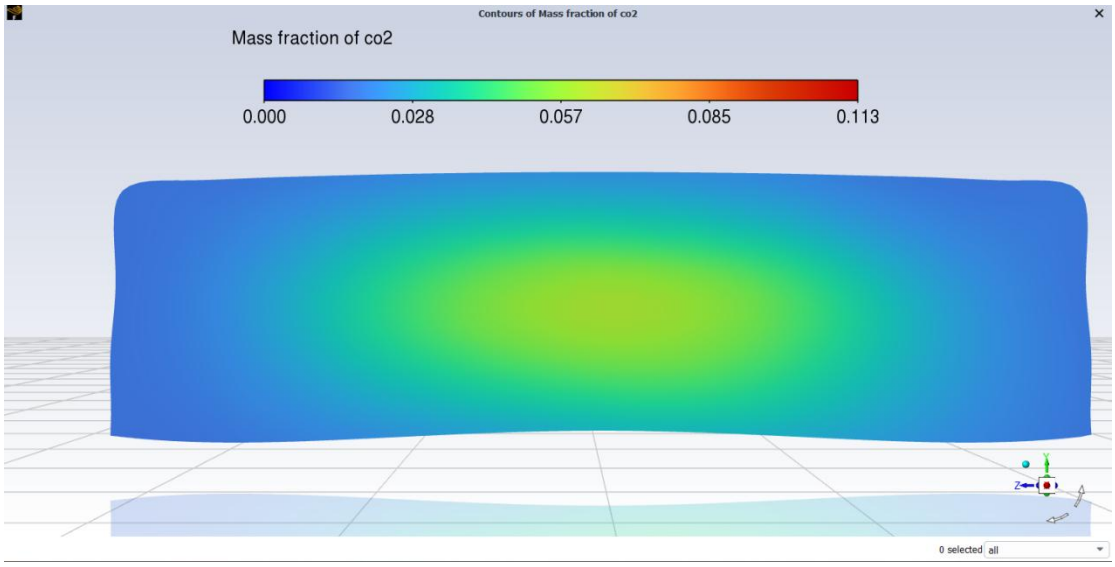

Figure 5.47 CO2 mass fraction contour for conventional combustor (exit nozzle section).

The CO2 mass fraction can represent the combustion efficiency. A high CO2 concentration shows that most of the fuel has been burned and transformed into CO2 (orange and red zones). A low CO2 concentration reveals that there is incomplete combustion, which can form pollutants such as carbon monoxide (CO) (blue zones).

5.3.7.4 Co mass fraction

Figures (5.44) and (5.45) below represent the variation of CO for both combustors.

5.3.7.4.1 reverse air combustor

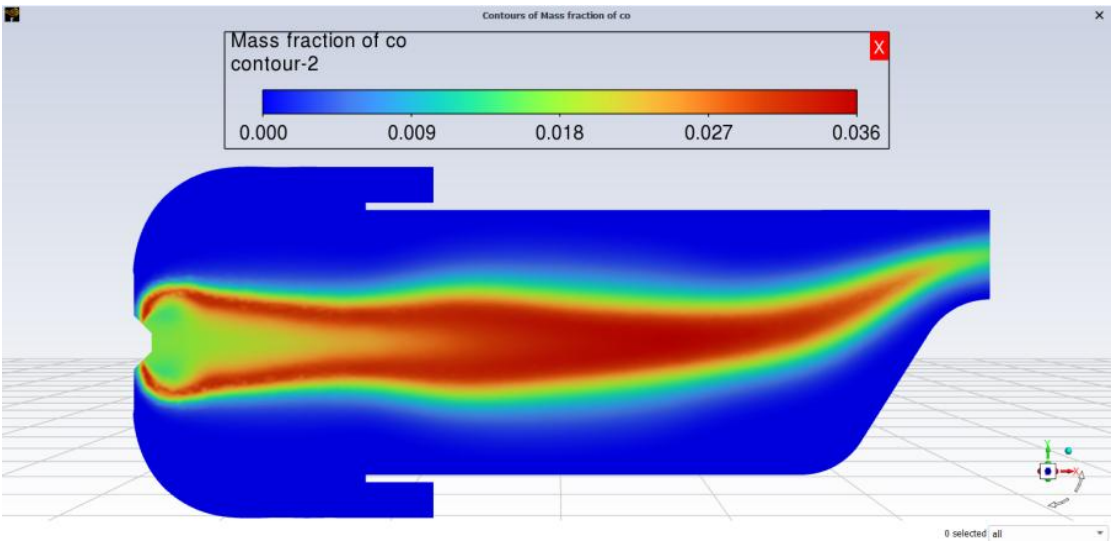

Figure 5.48 CO mass fraction contour for reverse air combustor (xy plan).

5.3.7.4.2 conventional combustor

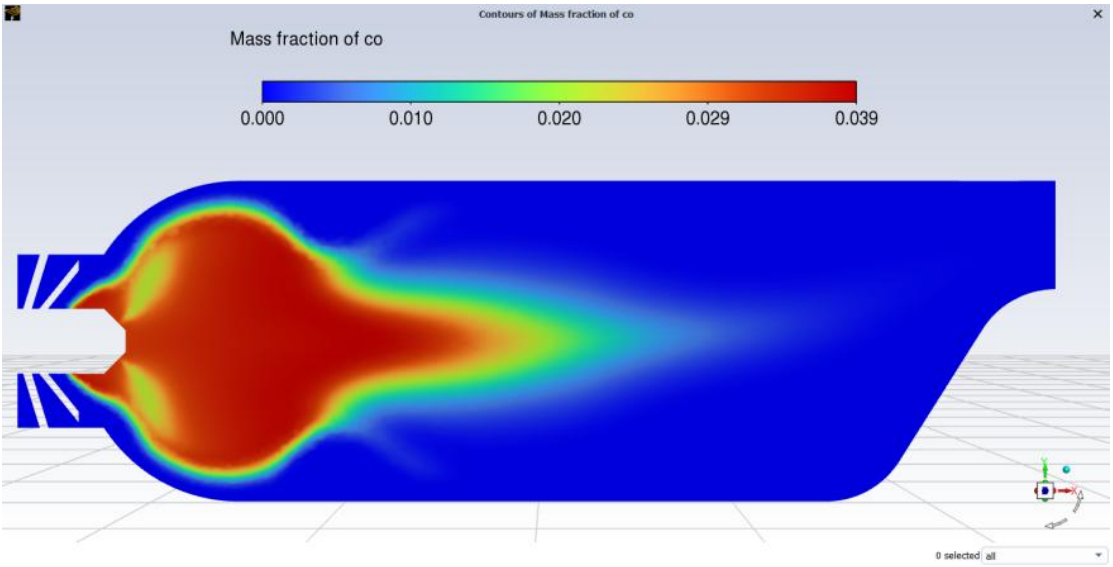

Figure 5.49 CO mass fraction contour for conventional combustor (xy plan).

The geometry of conventional combustor yielded more favorable levels of carbon monoxide. The significant turbulence within the dome region facilitated the complete conversion of carbon to carbon monoxide. This outcome was not achieved

in reverse air combustor, where higher levels of carbon monoxide were observed at the outlet.

5.3.8 Vectors of velocity

The velocity vectors in the two combustion chambers play a crucial role in analyzing and optimizing the performance of the combustion system. They allow for the visualization of the fluid flow direction and magnitude at different points in the combustion chamber and show how fuel and air mix, which is essential for efficient and complete combustion. Velocity vectors help identify recirculation zones where the fuel-air mixture can be improved to promote more stable combustion. They also reveal regions of turbulence, which are essential for mixing and flame propagation. The vector of magnitude velocity are shown in figures (5.46) and (5.47).

5.3.8.5 .1 reverse air combustor

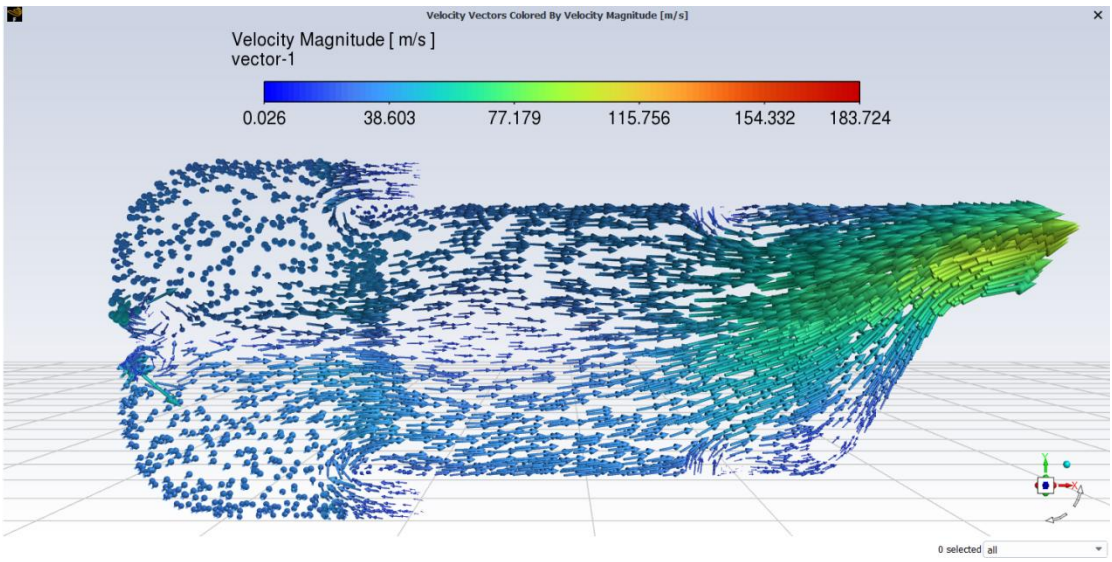

Figure 5.50 magnitude velocity vector for reverse air combustor (xy plan).

5.3.8.5 .2 conventional combustor

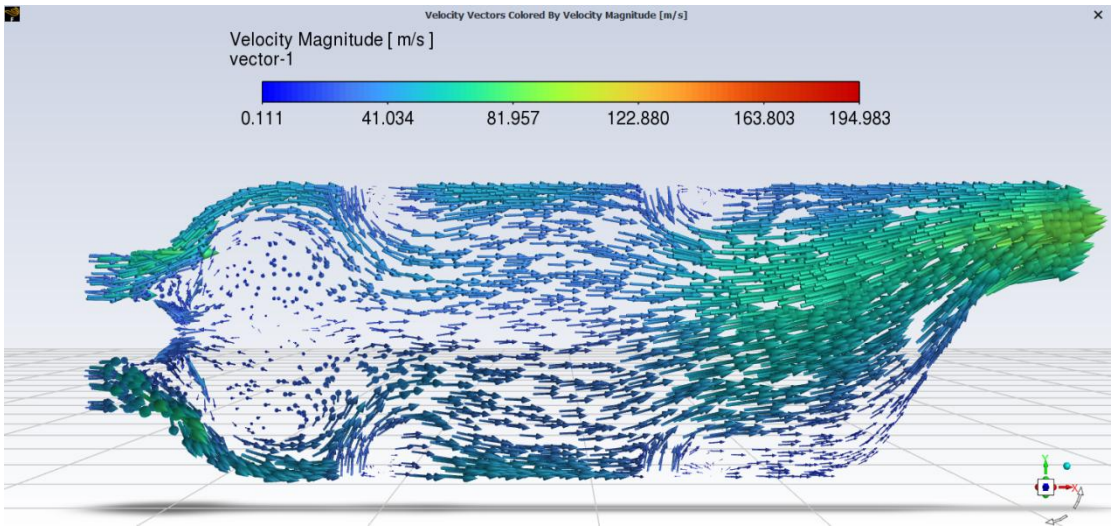

Figure 5.51 magnitude velocity vector for conventional combustor (xy plan).

For the reverse air combustor (Fig. 5.46), the velocity vectors have a reverse direction compared to the flow in the first dome zone and near the wall. In this same zone and in the central part, the reverse air mixes with the fuel coming from the injectors at high speed, creating a zone of turbulence and recirculation at about one-third of the dome wall. This turbulence zone decelerates the flow, improves the fuel-air mixing, and promotes flame anchoring for more stable combustion. The hot reactive mixture continues its movement towards the chamber exit, passing through a dilution zone to control the turbine inlet temperature (TIT), which should not exceed certain limits. Additionally, the flow magnitude informs us that the exit velocity is around 110 m/s.

In contrast, regarding the conventional chamber (Fig. 5.47), the chamber is subdivided into three zones: primary, secondary, and dilution. In the first dome zone, the air follows the dome wall, driven by the pressure of the fuel injected via the angular injectors. A dilution air ramp intervenes to change the direction of the wall flow, creating a zone of turbulence and recirculation that slows and improves the fuel-air mixing and promotes flame anchoring and combustion stability. After the secondary zone, the high-temperature reactive mixture is diluted again with a second air ramp, which better controls the TIT. A narrowing of the chamber towards the exit accelerates the flow to a limit of about 105 m/s.

In terms of comparison between the two types of chambers, an improvement in speed of about 4 to 5% is noted in favor of the reverse-flow combustion chamber.

5.3.9 Pathlines

Figures (5.48) to (5.53) illustrate the pathlines for both the conventional and reverse burner chambers. Pathlines represent the trajectories followed by individual fluid particles within the combustion chamber over time. These pathlines provide a visual representation of the fluid particles' movements as they flow through the chamber. Each pathlines shows the route taken by a single particle from its origin to its exit. Pathlines are particularly useful for understanding the behavior of fluid particles in turbulent or unstable flows, such as the turbulence and recirculation zones studied here. They reveal the precise paths of particles, highlighting complex flow patterns and interactions within the flame zone.

Pathlines are essential for obtaining a comprehensive understanding of the flow in both geometries. They allow for a clear visualization of the three dimensions associated with most combustor flows, including the fuel inlet, inlet swirler, primary and secondary air. In Figure (5.47) to (5.52), the fluid flow within the domain for both geometries is depicted as pathlines

5.3.9.1 conventional combustor

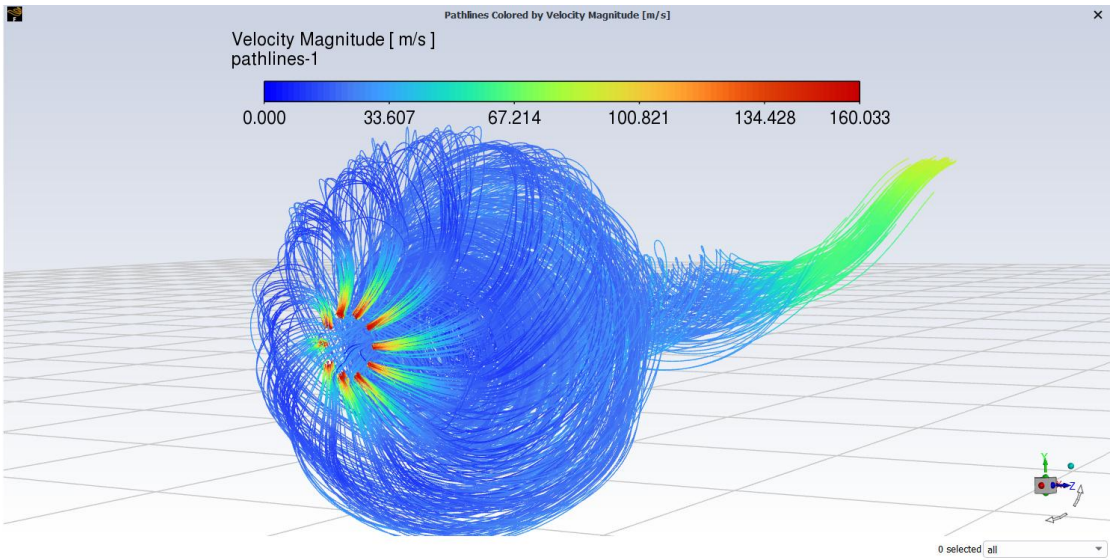

Figure 5.52 Pathlines for magnitude velocity from fuel inlet for conventional combustor.

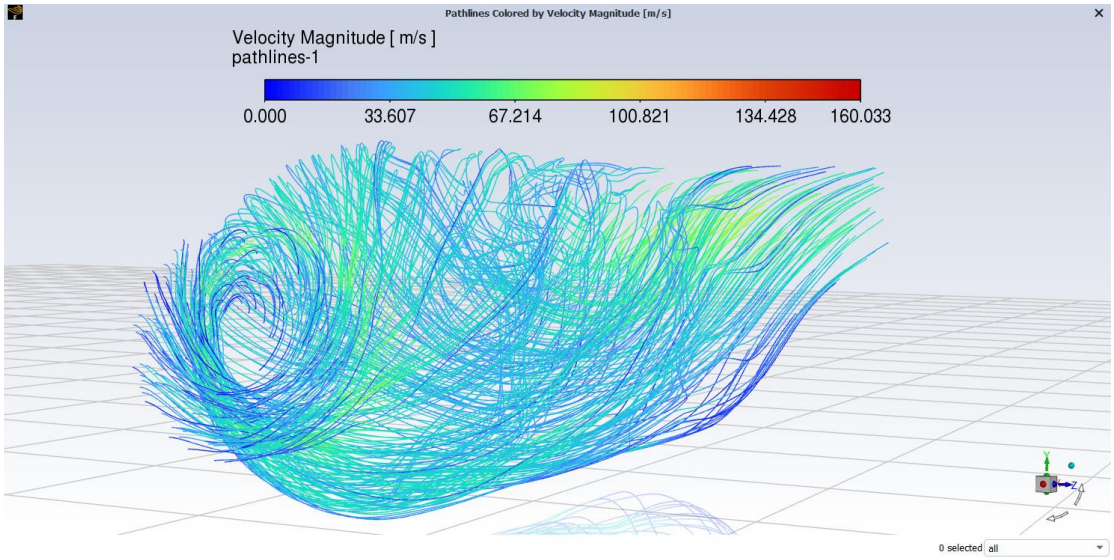

Figure 5.53 Pathlines for magnitude velocity from inlet swirler for conventional combustor.

From figures (5.48) and (5.49) we can see that the swirler and injector flow migrate towards the dome's edge, Because of the toroidal recirculation zone inside the primary region.

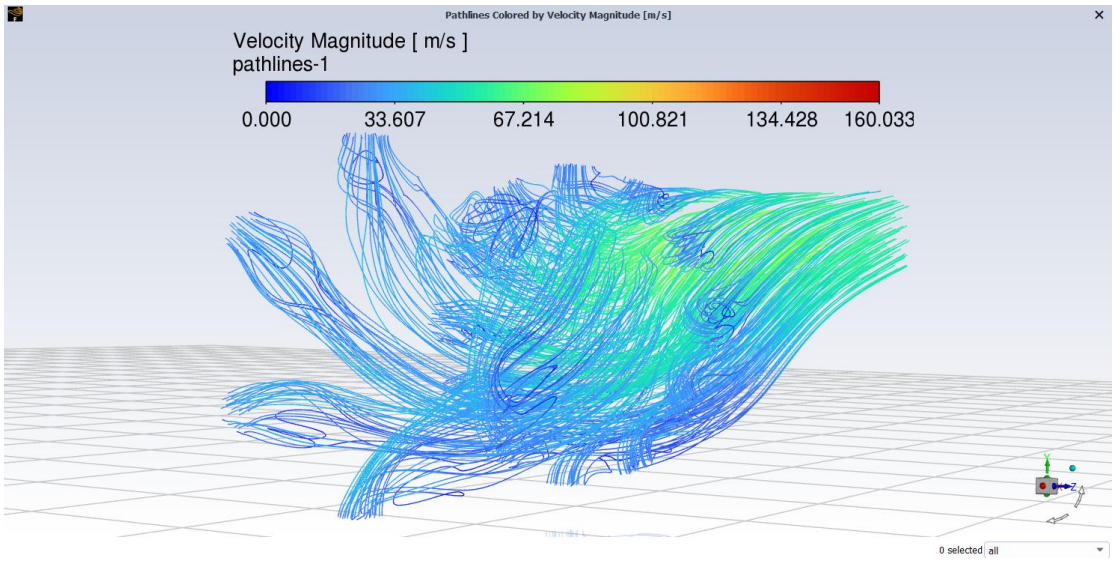

Figure 5.54 Pathlines for magnitude velocity from primary and secondary air for conventional combustor.

5.3.9.2 reverse air combustor

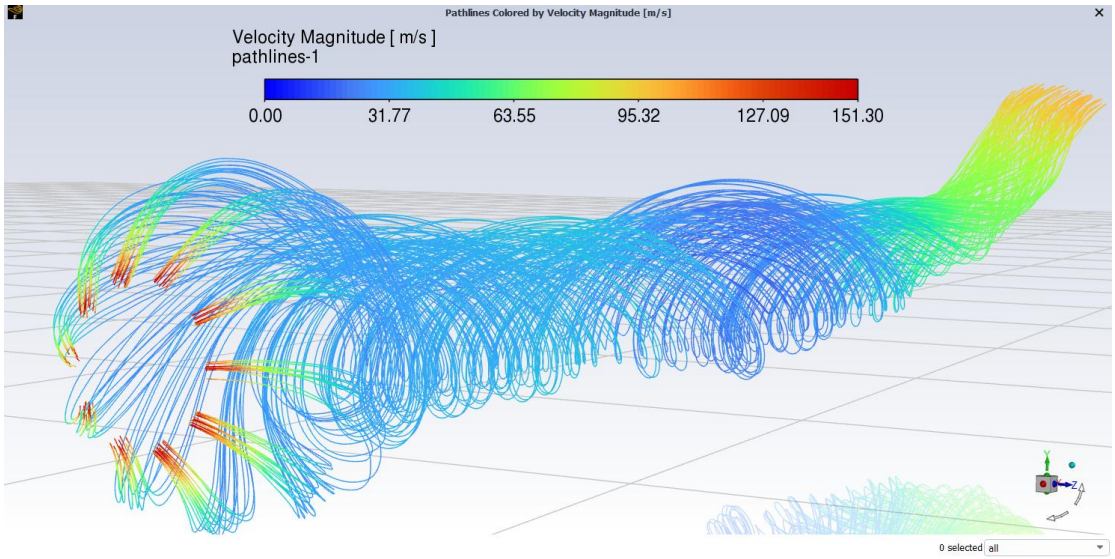

Figure 5.55 Pathlines for magnitude velocity from fuel inlet for reverse air combustor.

The fuel flow from the injector does not get stretched towards the dome periphery. The fuel jets remain distinct as they are released from the injector, which is observable from the figure (5.51).

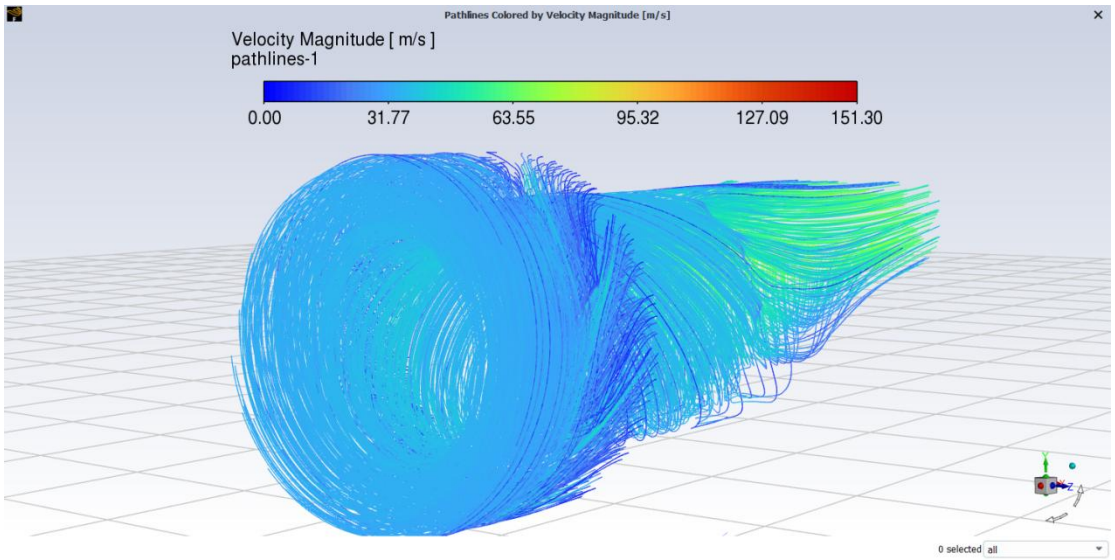

Figure 5.56 Pathlines for magnitude velocity from primary air for reverse air combustor.

Figure (5.52) shows pathlines released from the primary air inlet. Due to the contour of the dome, the flow regime forms an umbrella-like structure which surrounds the fuel injector. Such a behavior leads to the generation of a high amount of turbulence only near the fuel injection area.

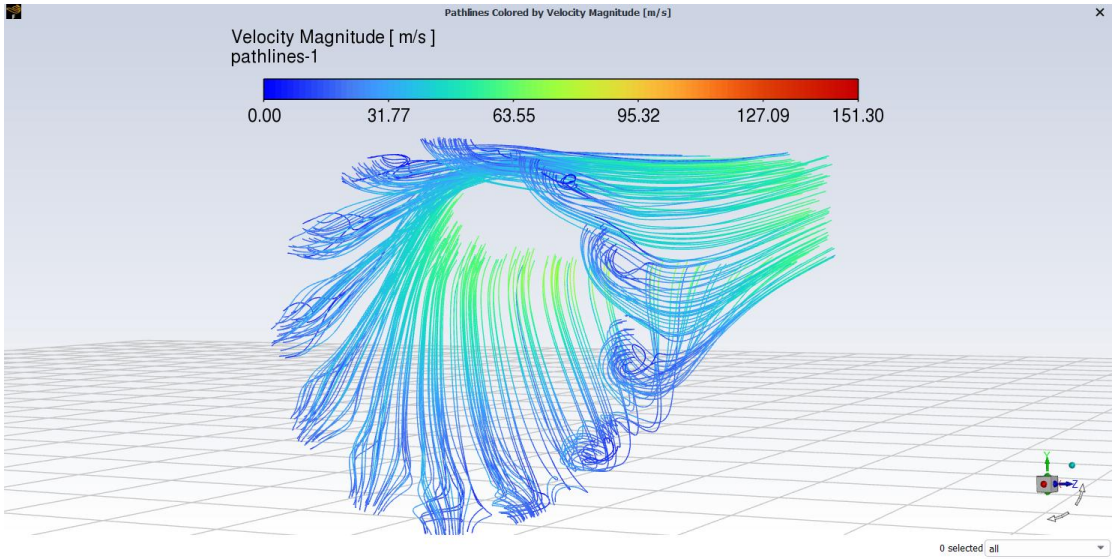

Figure 5.57 Pathlines for magnitude velocity from secondary air for reverse air combustor.

The dilution air from secondary air getting dragged inside the nozzle by the mean flow is clearly observable.The central flame present inside the nozzle is clearly observable. The dilution air is heated up as it gets dragged along by the combusting flow.

5.4 AFR influence on maximum temperature and exit temperature

This section shows the influence of Air-Fuel Ratio on the maximum temperature of combustion and exit temperature of both combustors presented in figures below.

The Air-Fuel Ratio (AFR) plays a critical role in determining the maximum temperature within a combustion chamber. As the AFR increases, it acts as a dilution factor, making the fuel-air mixture leaner. This reduction in fuel concentration leads to a decrease in the exit temperature of the combustion chamber.

5.4.1 reverse air combustor

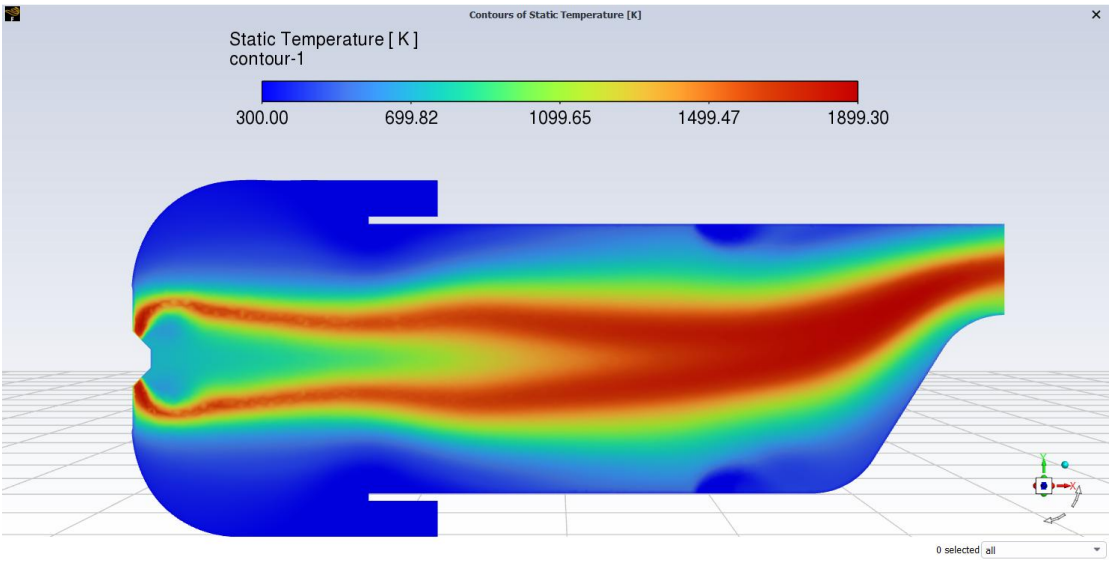

Figure 5.58 static temperature contour for reverse air combustor AFR 50.

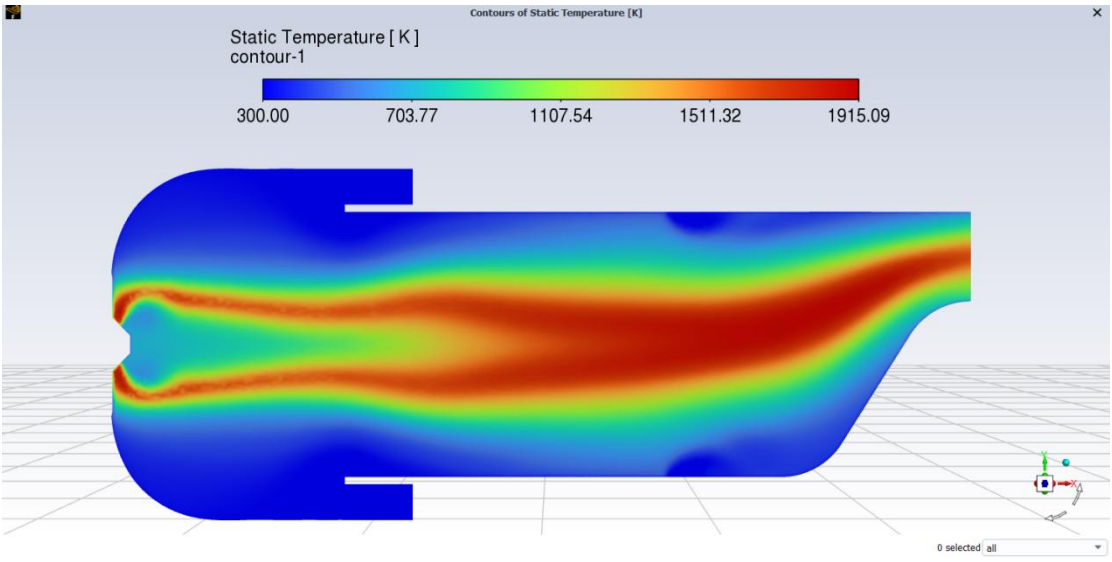

Figure 5.59 static temperature contour for reverse air combustor AFR 60.

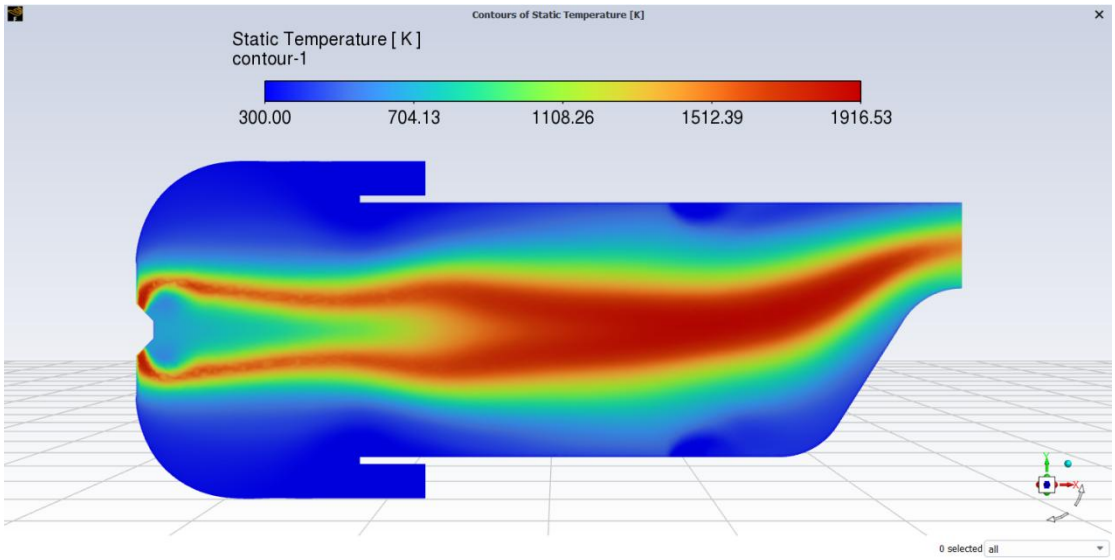

Figure 5.60 static temperature contour for reverse air combustor AFR 70.

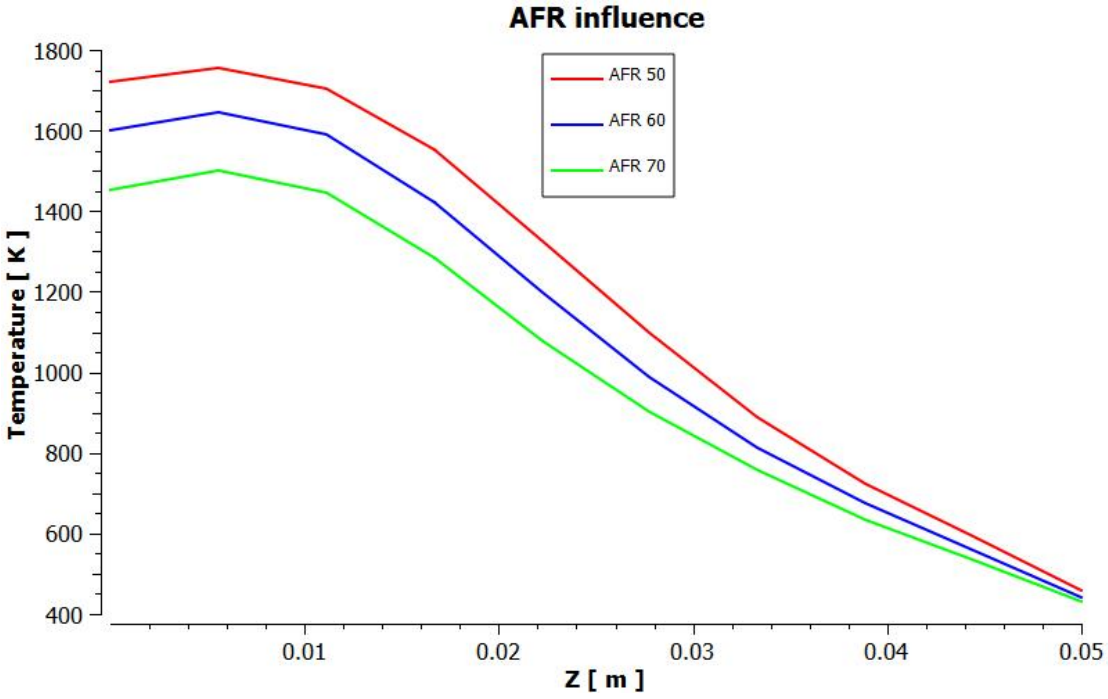

Figure 5.61 AFR influence on exit temperature charts for reverse air combustor.

Table 5-6 results of Tmax and T exit max under difference Air fuel ratio.

AFR	T max (k)	T exit (k)
50	1899.30	1753.69
60	1915.05	1645.09
70	1916.53	1499.89

5.4.2 conventional combustor

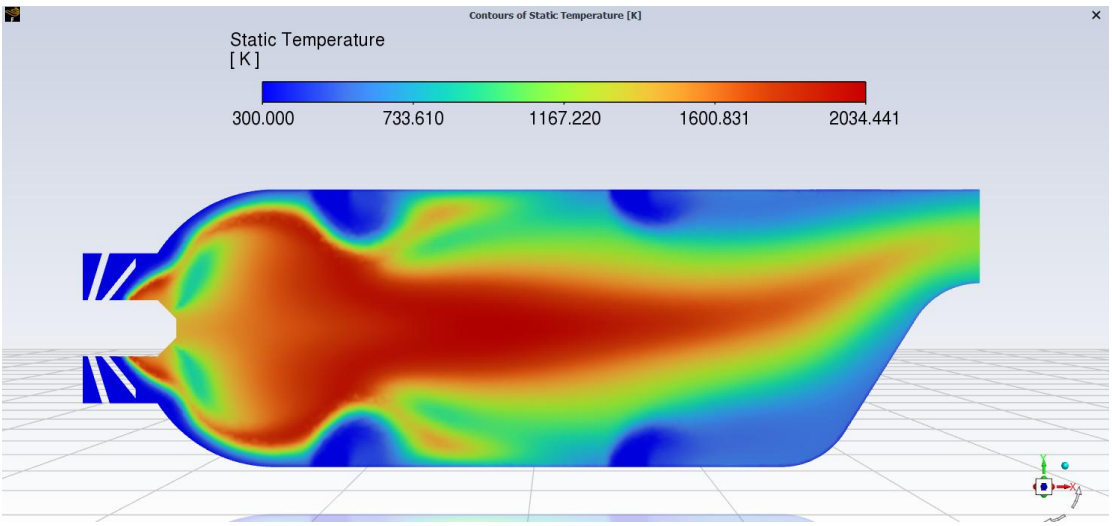

Figure 5.62 static temperature contour for conventional combustor AFR 50.

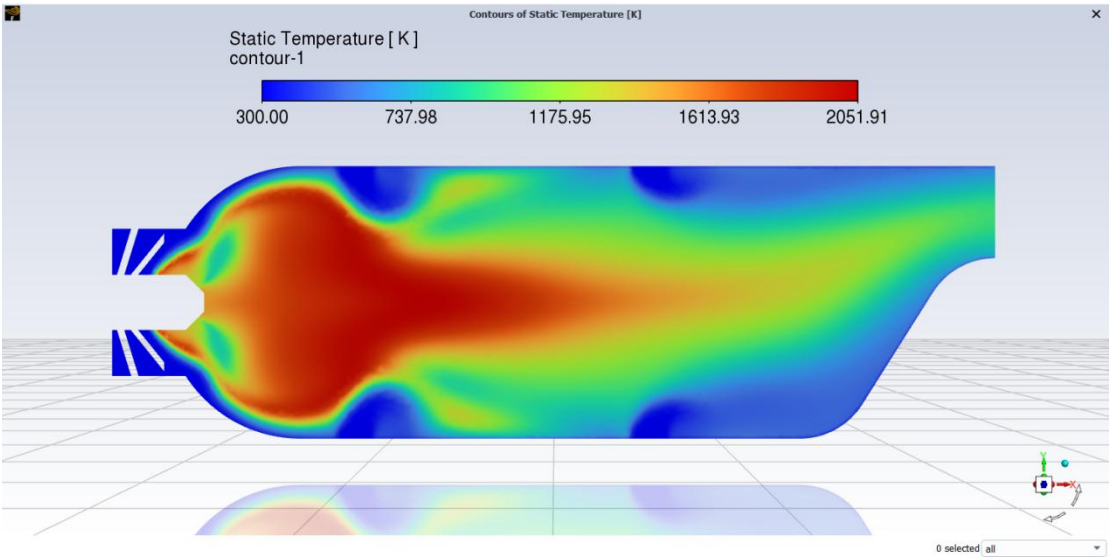

Figure 5.63 static temperature contour for conventional combustor AFR 60.

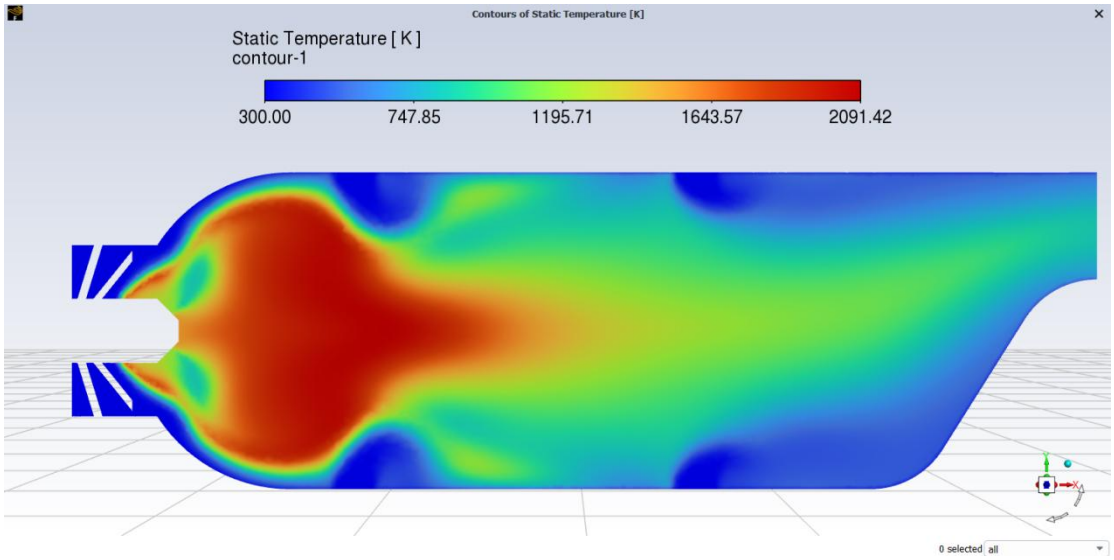

Figure 5.64 static temperature contour for conventional combustor AFR 70.

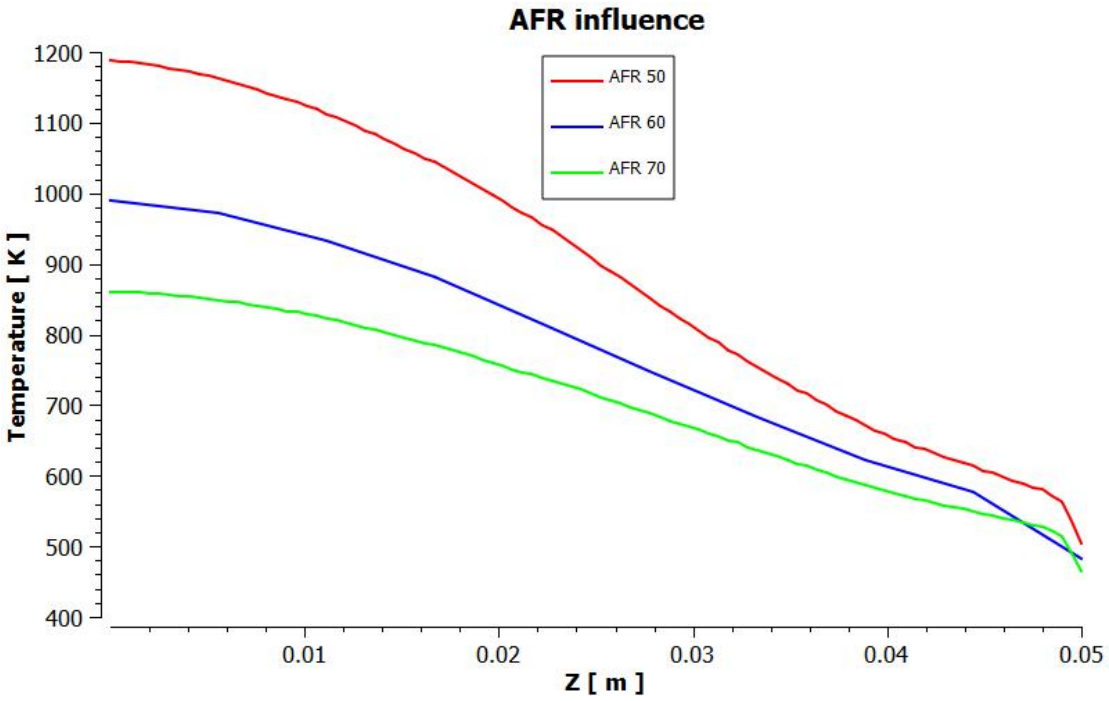

Figure 5.65 AFR influence on exit temperature charts for conventional combustor.

Table 5-7 results of Tmax and T exit max under difference Air fuel ratio.

AFR	T max (k)	T exit (k)
50	2034.44	1187.97
60	2061.91	989.70
70	2091.42	860.92

According to Figures (5.54) to (5.56) corresponding to reverse air combustor results, which correspond to AFR of 50, 60, and 70 respectively, the maximum temperature increases progressively. Specifically, the maximum temperatures are 1899 K, 1915 K, and 1916 K for AFR of 50, 60, and 70. The exit temperatures decreases, dropping from 1753 K to 1645 K and finally to 1499 K as the AFR increases.

Similarly to the conventional combustor results in figures from (5.58) to (5.61) for AFR of 50,60,70 respectively where it follows the same process for the variation of AFR. In addition, we can see in the charts the value of exit temperature with an AFR of 70 for the conventional combustor is under the limit of auto-inflammatory for methane because of the high fuel consumption of this combustor.

This logic is presented in Table 5-7 and table 5-6, further demonstrating that as the AFR increases, the exit decreases accordingly. In summary, a higher AFR results in a lower exit temperature, which highlights the significant impact of AFR on combustion efficiency and thermal management.

5.5 preheating influence on maximum temperature and exit temperature

The influence of preheating temperature for fuel and air is studied in this section, the results for maximum and exit temperatures are presented in the figures below.

5.5.1 reverse air combustor

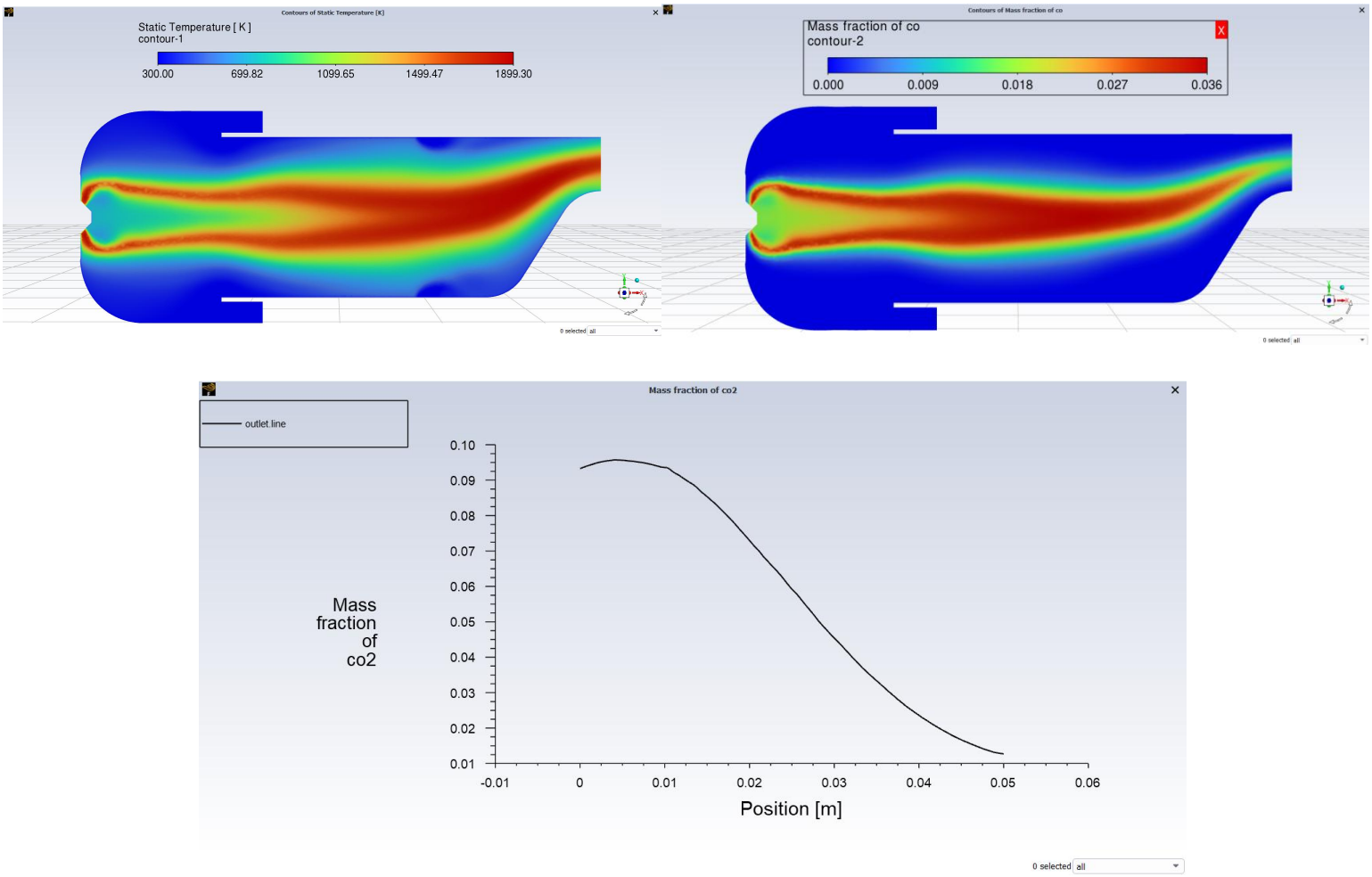

Figure 5.66 static temperature contour, C mass fraction contour, CO2 mass fraction plot for preheating of 300k -reverse air combustor-

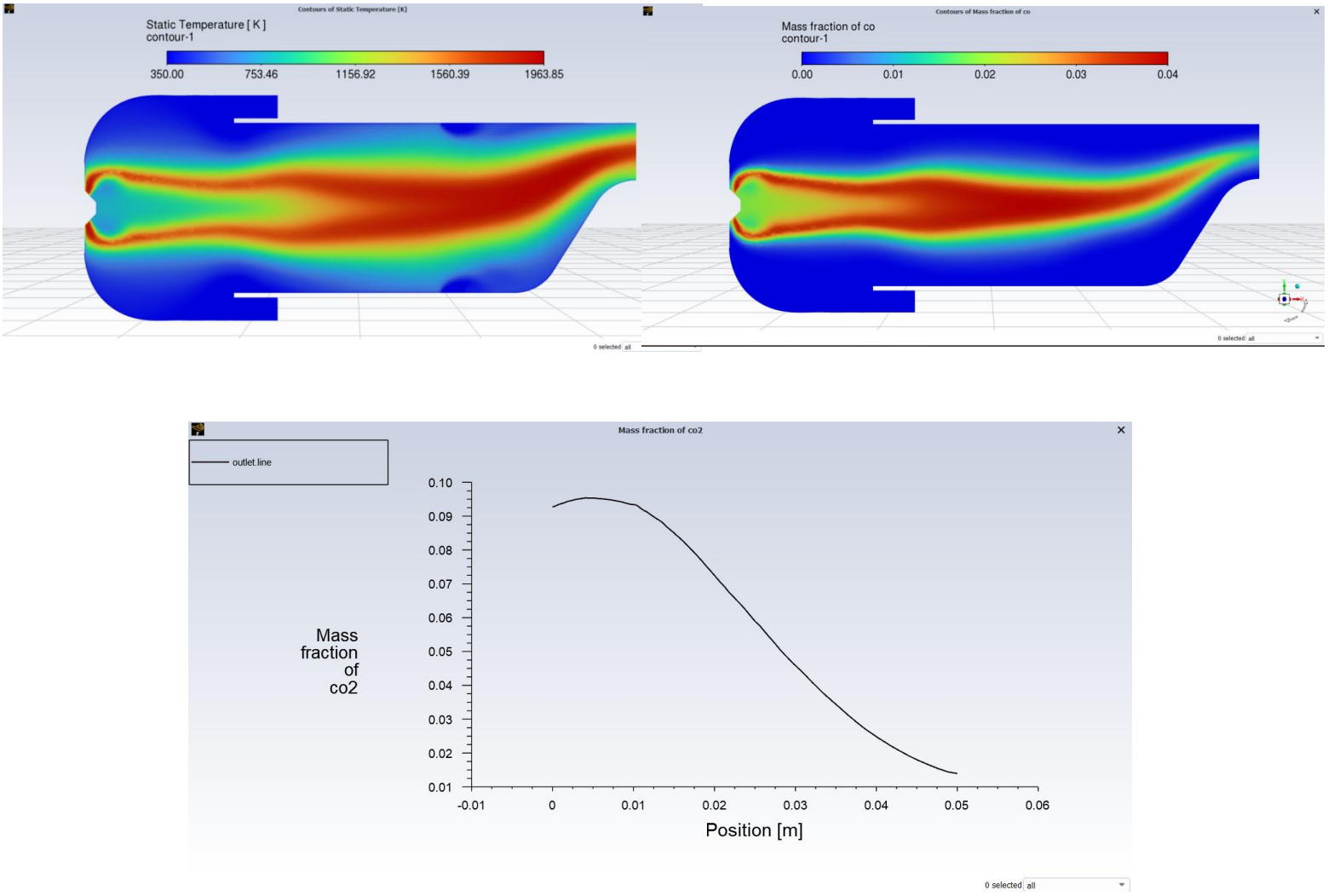

Figure 5.67 static temperature contour, CO mass fraction contour, CO2 mass fraction plot for preheating of 350k -reverse air combustor-

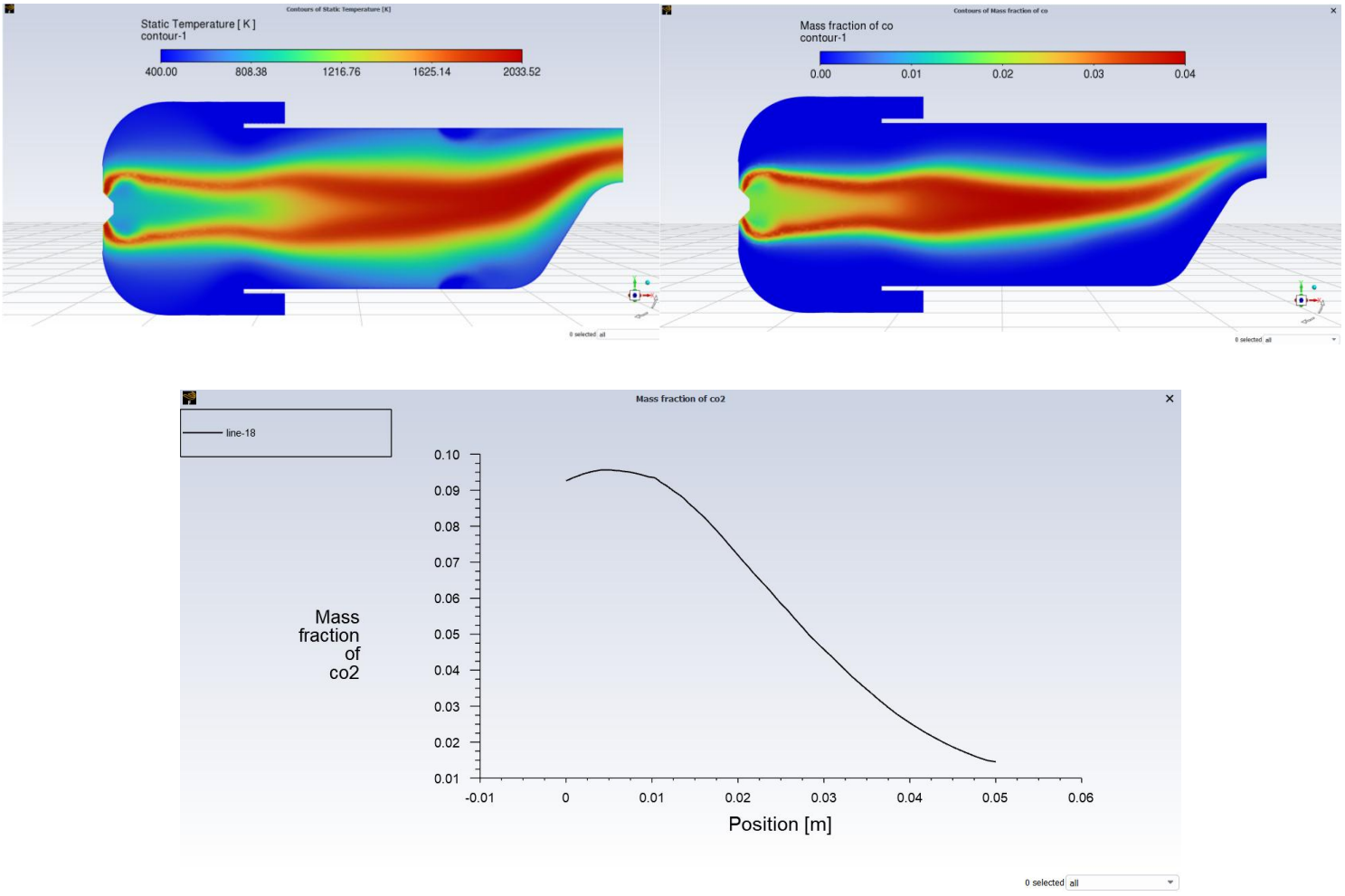

Figure 5.68 static temperature contour,CO mass fraction contour, CO2 mass fraction plot for preheating of 400k -reverse air combustor-

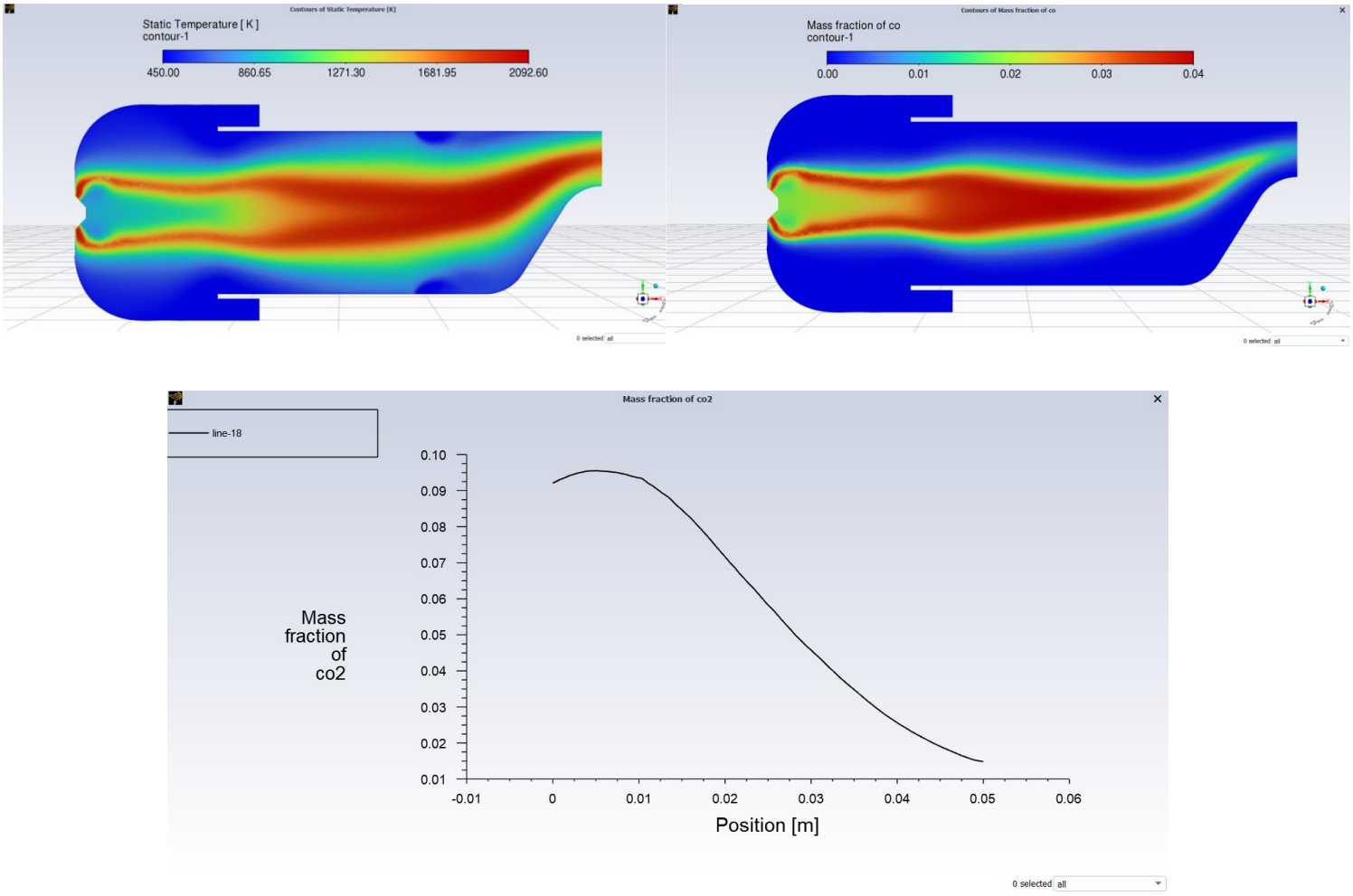

Figure 5.69 static temperature contour, CO mass fraction, CO2 mass fraction plots for preheating of 450k -reverse air combustor-

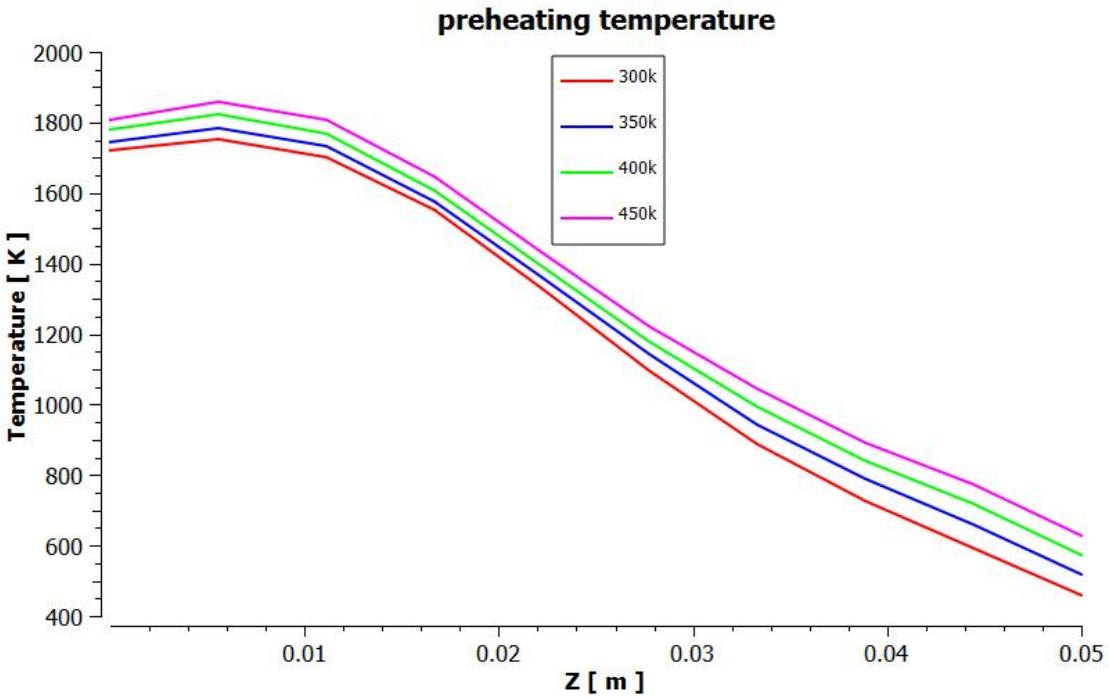

Figure 5.70 preheating influence on exit temperature for reverse air combustor charts .

Table 5-8 preheating influence for Tmax and T exit max.

Preheat temperature (k)	T max (k)	T exit (k)
300	1899.30	1753.69
350	1963.85	1782.77
400	2033.52	1821.64
450	2092.60	1857.73

5.5.2 conventional combustor

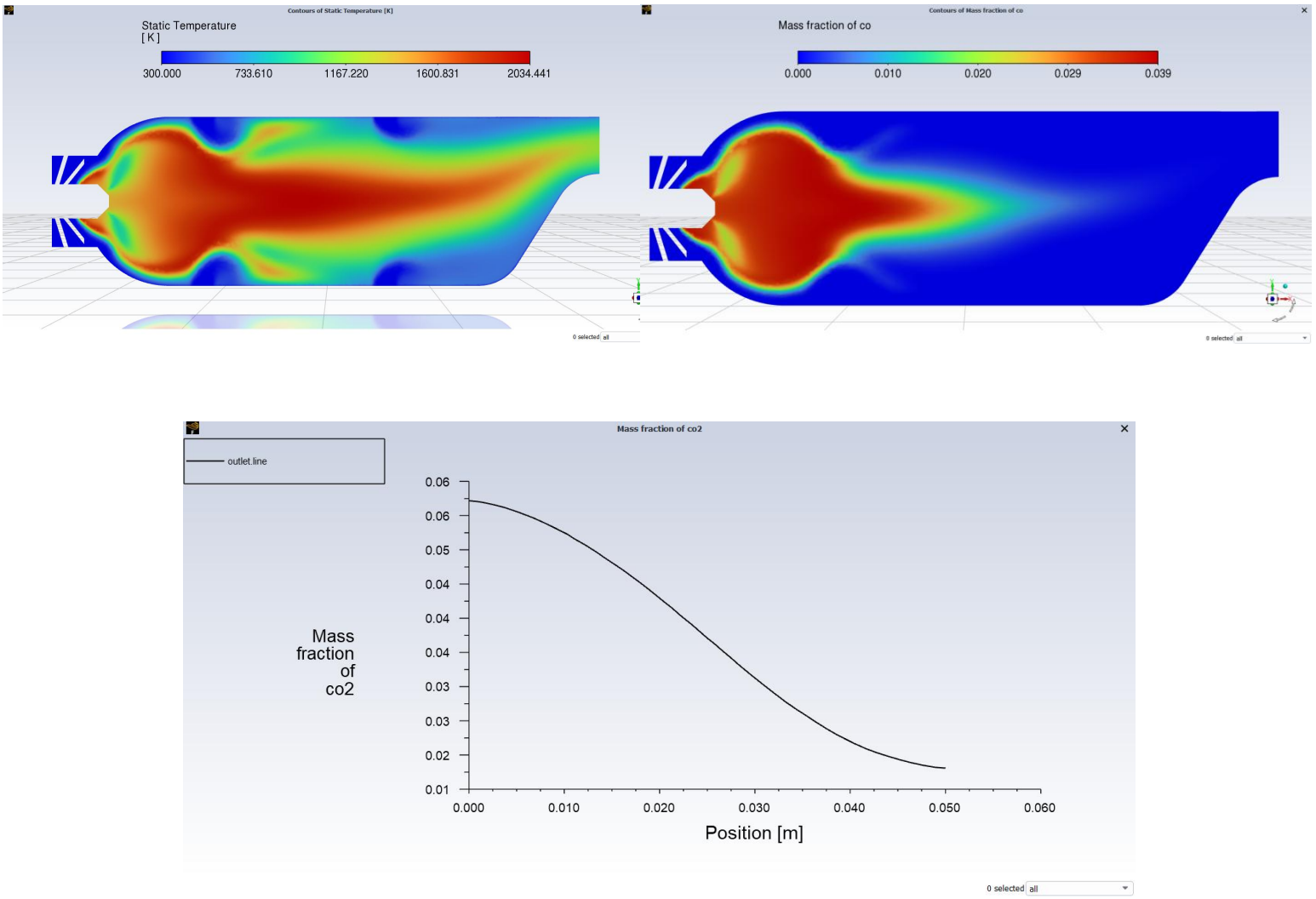

Figure 5.71 static temperature contour, CO mass fraction contour, CO2 mass fraction plot for preheating of 300k -conventional combustor-

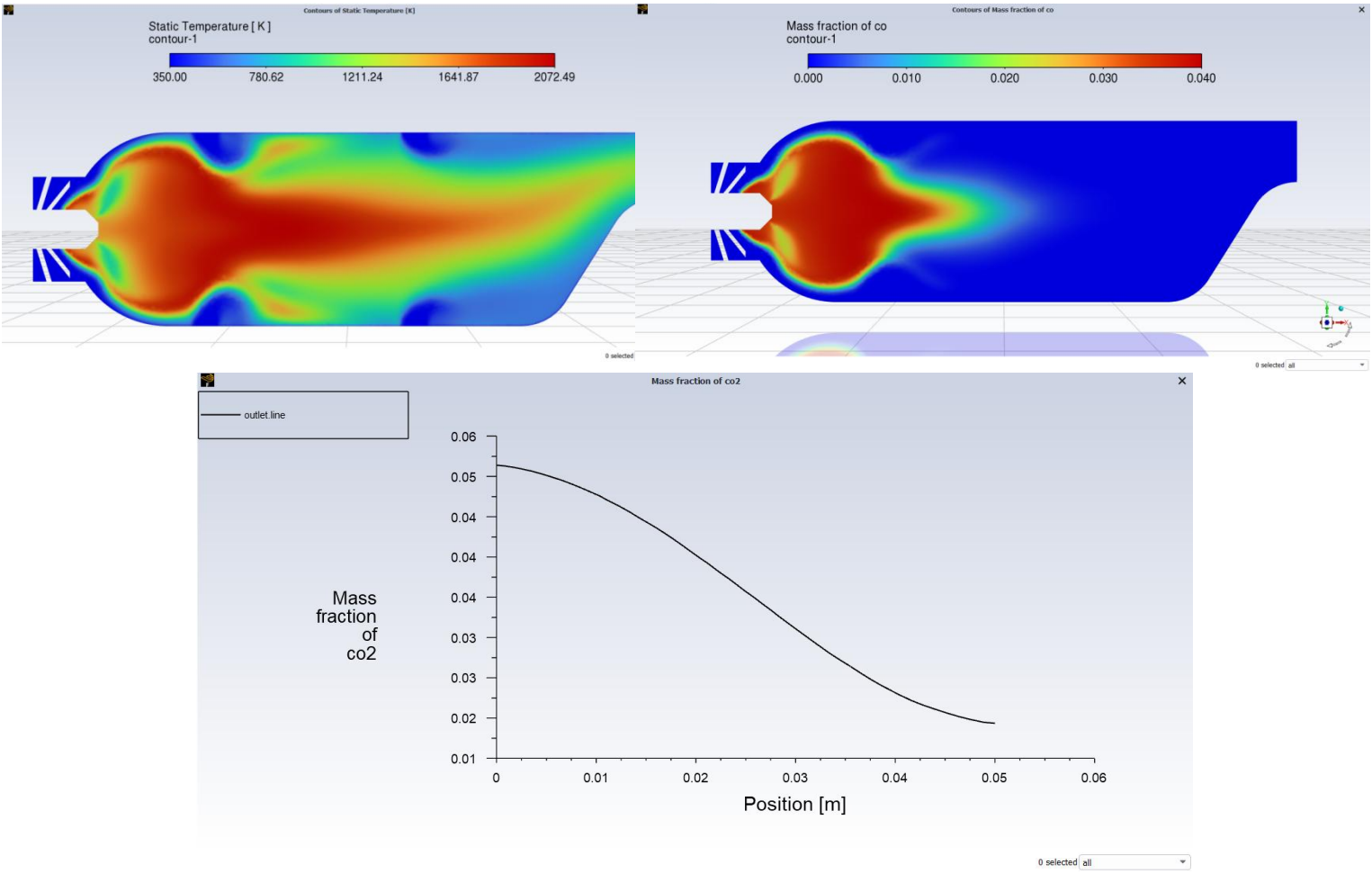

Figure 5.72 static temperature contour, CO mass fraction contour, CO2 mass fraction plot for preheating of 350k -conventional combustor-

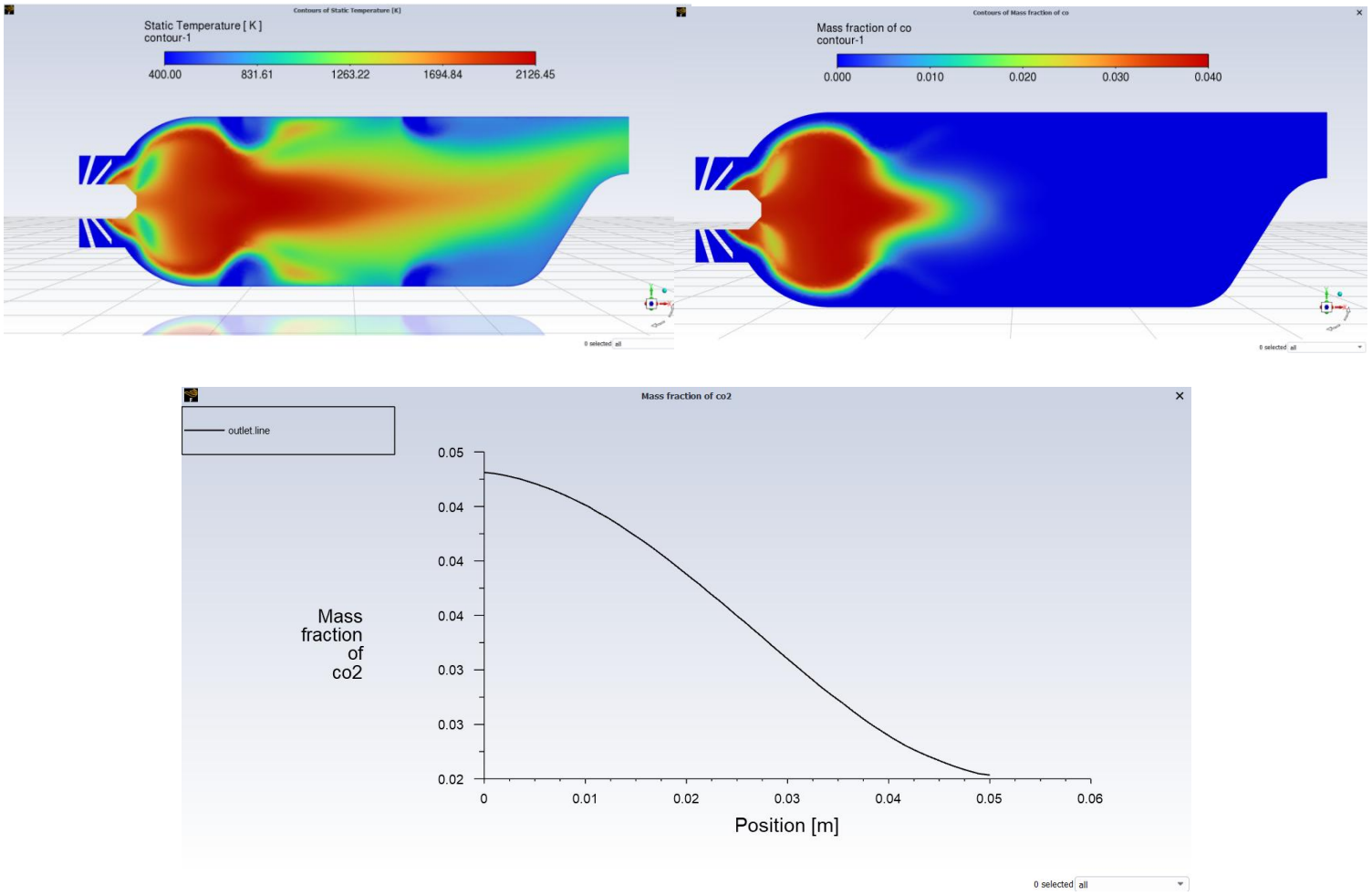

Figure 5.73 static temperature contour, CO mass fraction, CO2 mass fraction plot contour for preheating of 400k -conventional combustor-

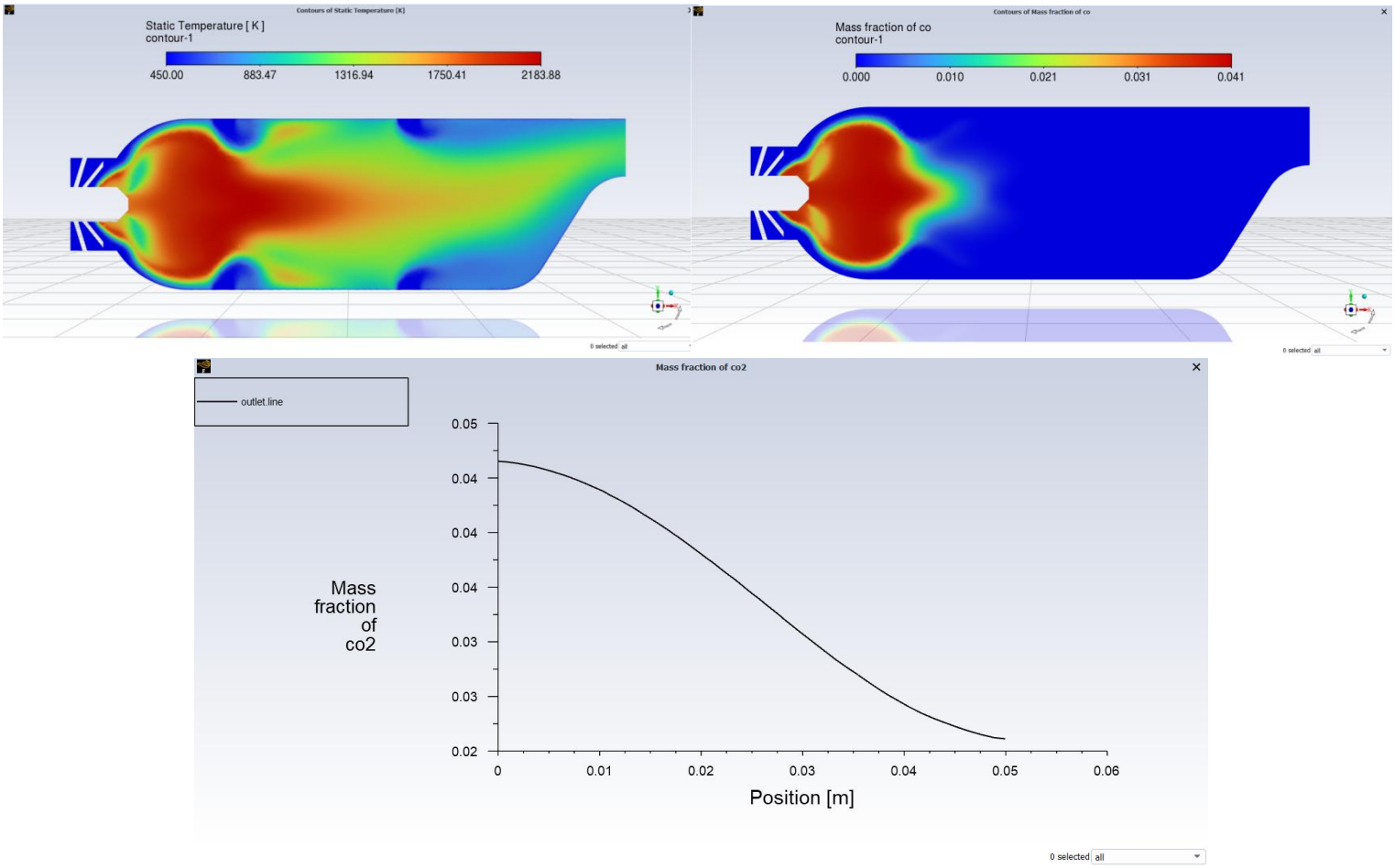

Figure 5.74 static temperature contour, CO mass fraction contour, CO2 mass fraction plot for preheating of 450k -conventional combustor-

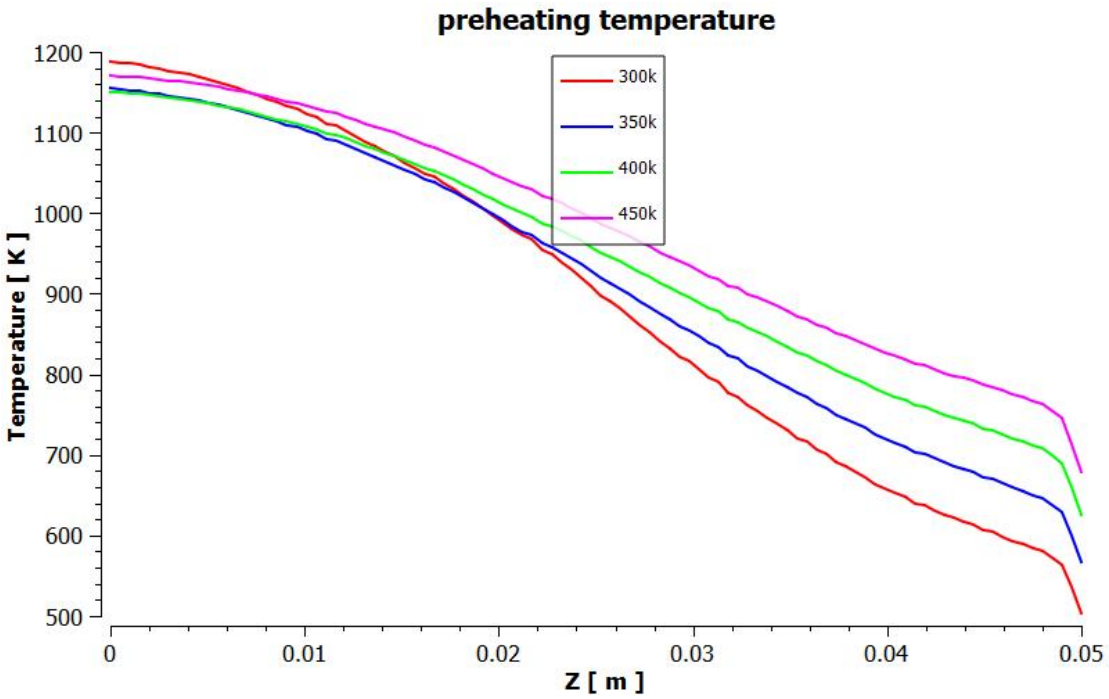

Figure 5.75 preheating influence on exit temperature charts for conventional combustor.

Table 5-9 preheating influence for Tmax and T exit max.

Preheat temperature (k)	T max (k)	T exit (k)
300	2034.44	1150.70
350	2072.49	1154.48
400	2126.45	1170.61
450	2183.88	1187.97

Figures (5.62) to (5.66) show the effect of preheating the reactive mixture in the reverse air combustion chamber at temperatures of 300 k, 350 k, 400 k, and 450 k. As a result, the maximum temperatures increase from 1899 k to 1963 k, 2033k, and finally 2092 k. This leads to an increase in the exit temperature of the chamber to 1753 k, 1782 k, 1821 k, and finally 1857 k. same process is adopted in the conventional combustor as well presented in figures from (5.67) to (5.71). Preheating the mixture before entering the combustion zone is an essential process. It offers several advantages, including improved overall performance and combustion process efficiency. Preheating the mixture also reduces ignition delay and ensures more complete fuel combustion.

The figures above show that preheating allows for the reduction of pollutant emissions by promoting more complete combustion. It also helps in reducing the formation of pollutants such as carbon monoxide (CO) and nitrogen oxides (NOx), thus reducing exhaust emissions and complying with environmental regulations. The same process occurs in the conventional chamber presented in figures (5.67) to (5.71).

5.6 NOx emissions simulation results

The residual for converged solution with NOx emissions is shown in figure (5.71).

Figure 5.76 residual solution converged for NOx simulation.

The pollutant no mass fraction contour is represented in figures (5.73) and (5.74).

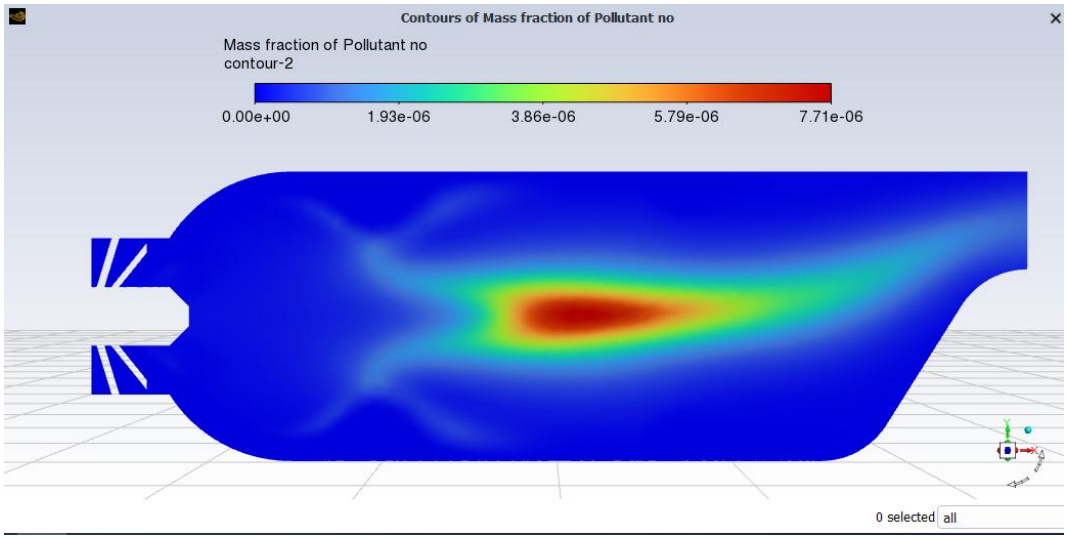

Figure 5.77 pollutant no mass fraction contour for conventional combustor.

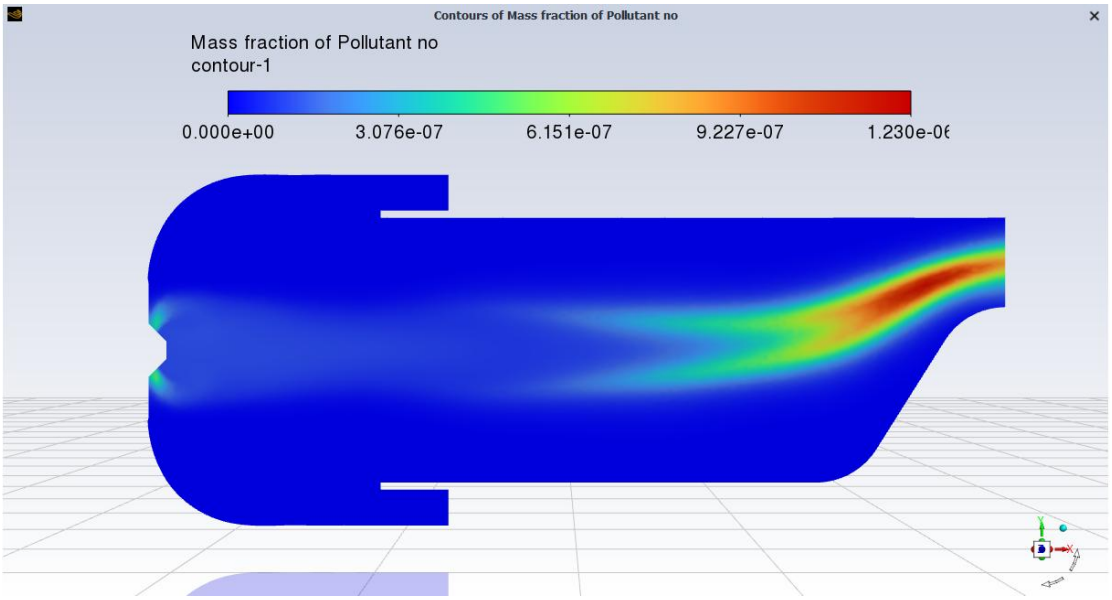

Figure 5.78 pollutant no mass fraction contour for reverse air combustor.

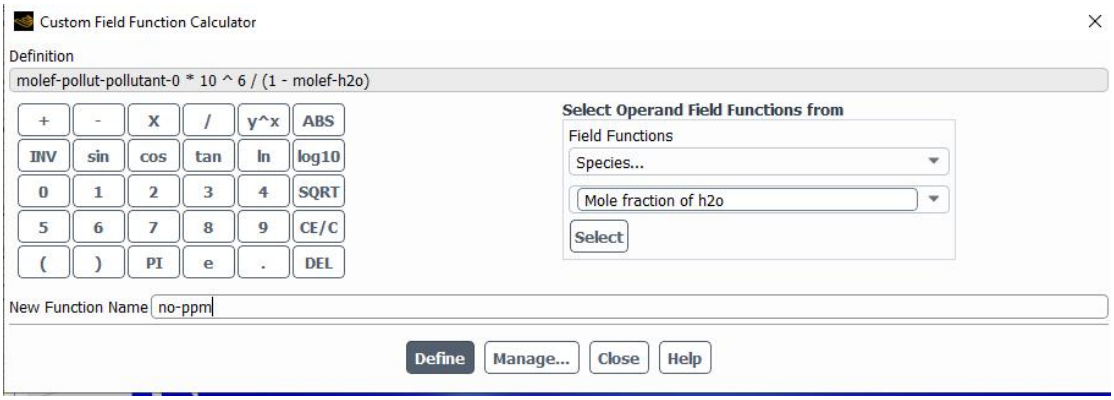

Figure 5.79 no-ppm field customizing.

Figures (5.76) and (5.77) show the no parts per million contour for both combustion.

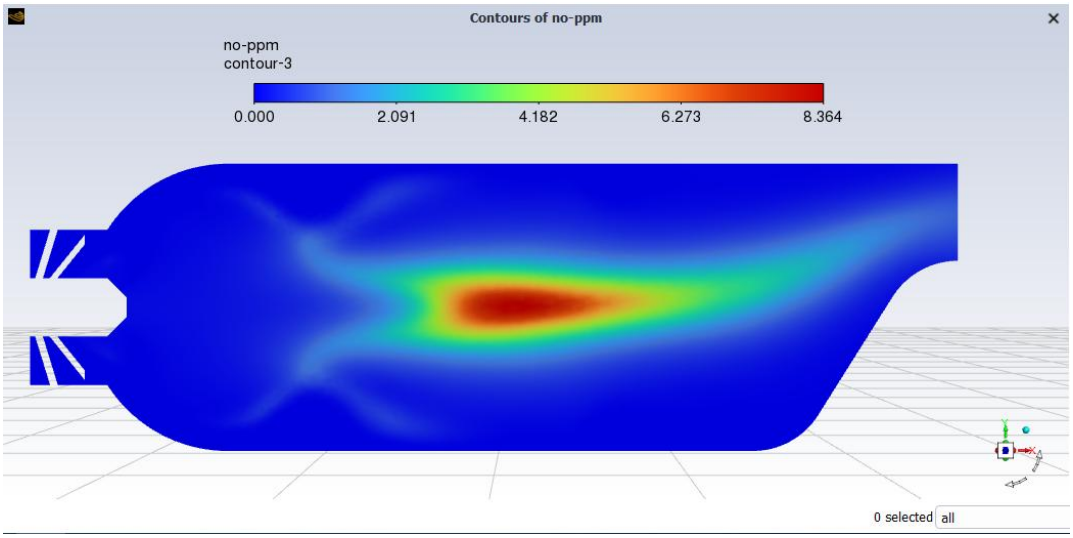

Figure 5.80 no-ppm contour for conventional combustor.

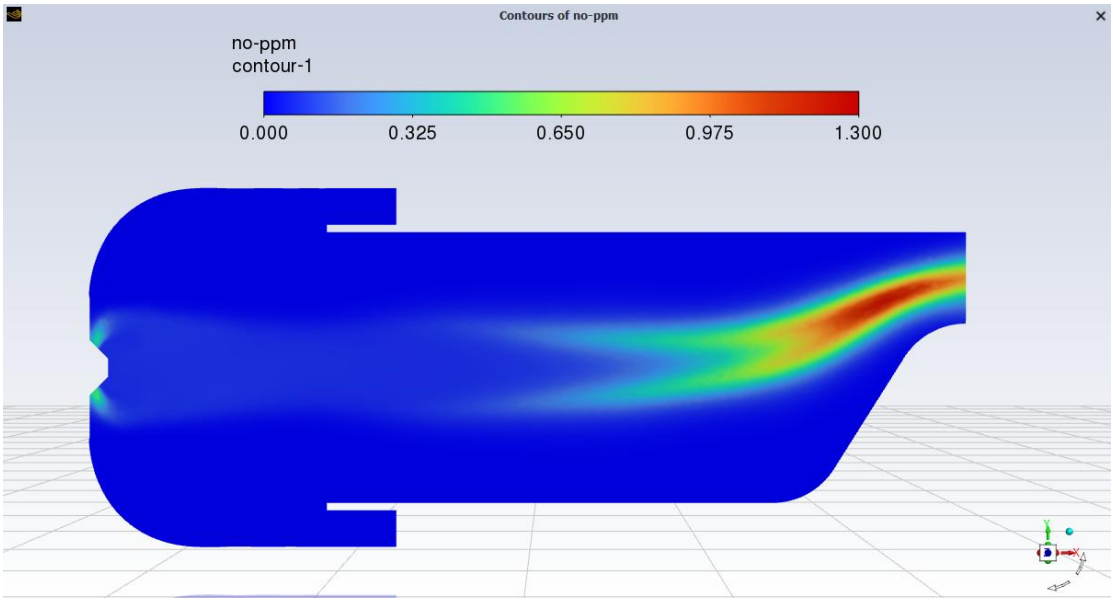

Figure 5.81 no-ppm contour for reverse air combustor.

Table 5-10 comparison of NO-ppm between the two combustors.

	Conventional combustor	Reverse air combustor
NO-ppm	8.364	1.3

From the previous results, we can observe that the NOx emissions for the reverse air combustor are lower than the NOx emissions for the conventional one with a difference of 84%, and this is an important advantage of the reverse air.

The highest value of NOx mass fractions and no parts per million are located in the center of the cylinder for a conventional combustor versus the reverse air, where it's located in the nozzle section.

Conclusion and outlook

Conclusion

This work focuses on numerically simulating turbulent methane combustion in can-type combustors, specifically conventional and reverse air combustors, using CFD techniques. The aim is to comprehensively analyze the flow behavior, compare the specifications and performances of both combustors, investigate the complex interactions between turbulent flows and chemical reactions in methane combustion, and ultimately determine which combustor is most suitable for future use in combustion chambers.

The following findings can be reached by comparing the different results obtained in this study for the two cases:

1. flame temperature is highest at the center, reaching 1900K. However, it is lower in the central zone after fuel injectors. The combustor exit temperature is suitable for gas turbines. This is advantageous as conventional combustor designs often exceed 2000K, leading to excessive heating and rapid fuel consumption. The reverse air combustor has a lower maximum global temperature, demonstrating flame stability.
2. The velocity value at the nozzle's outlet is highest for both combustors, with the reverse air combustor having a higher velocity value of around 100 m/s. This is due to its higher energy content and less recirculation in the primary zone.
3. Excessive turbulence in conventional combustors leads to fuel dissipation along the flame path, causing annulus heating. In contrast, in a reverse air combustor, fuel remains available along the centerline for combustion. This ensures flame sustainment without highly turbulent regions and dissipation along the flame path.
4. The reverse air combustor has a reversed flow direction, which causes turbulence and recirculation in the central part of the dome wall. This decelerates the flow, improves fuel-air mixing, and promotes flame anchoring for stable combustion. The hot reactive mixture moves towards the chamber exit, passing through a dilution zone to control the turbine inlet temperature (TIT). The exit velocity is around 110 m/s. On the other hand, the conventional chamber is divided into three zones: primary, secondary, and dilution. The first zone follows the dome

wall, while the second zone's dilution air ramp controls the TIT. The chamber narrows towards the exit, accelerating the flow to a limit of about 105 m/s.

5. The maximum temperature progressively increases with an air fuel ratio (AFR) of 50, 60, and 70. The resulting maximum temperatures are 1899K, 1915K, and 1916K, respectively. As the AFR increases, the exit temperatures decrease, dropping from 1753K to 1499K.
6. Preheating the reactive mixture in both the reverse air combustion chamber and the conventional combustor at various temperatures (300K-450K) leads to an increase in maximum temperatures from 1899K to 2092K. This results in an increase in the chamber's exit temperature. This process improves performance and efficiency, reduces ignition delay, and ensures complete fuel combustion.
7. From the study of NOx emissions, it was found that the reverse air combustor has lower NOx emissions, around 1.3, compared to the conventional combustor, which has emissions around 8.36 with a difference between the two values of 84%. This is a significant advantage of the reverse air combustor.

In summary, this study demonstrates that the reverse air flow arrangement of a conventional CAN combustor effectively addresses the issues of liner wall heating and high NOx emissions. Additionally, it improves performance by increasing the exit velocity, which subsequently enhances the kinetic energy at the turbine inlet.

Outlook

The study presented here provides a general overview of the possible modifications that can be applied to a can-type combustor numerical simulation. Deeper research into the domain can provide a clearer explanation for the results. Therefore, the following has been suggested:

1. Simulate the combustion in a transient flow using the LES turbulence model; a comparison with the previous results could be made.
2. In addition to the NOx emissions study of this work, a simulation of SOx inside the combustors could be studied.
3. Including the effect of the radiation model on the propagation of the temperature inside the domain.

4. Using the species transport model to simulate the global reaction of methane air with hydrogen addition, a detailed mechanism for the reaction can be included.
5. Study the influence of various fuel injections angle on flame characteristics.

References

[1] :YATHIS GIOVANNI DELICAT « étude de la réactivité de l'iode transporte dans un mélange H2/H2O en conditions de combustion dans des flammes basse pression prémélangées ». -Thèse doctorat-2012.

[2] :R. BORGHI & M. DESTERIAU La combustion et les flammes, TECHNIP (1975).

[3] :J. Warnatz, U. Maas and R. W. Dibble. "Combustion – Introduction, Fundamental Definitions and Phenomena". Springer-Verlag Berlin Heidelberg 2006.

[4] :« étude et simulation numérique de la combustion des flammes premelanges suspendus de méthane-air pour des bruleurs a faible nombre de swirl » thèse de doctorat, université de Boumardas-2013

[5] :Memoire: Simulation de flamme de diffusion pour la combustion du mélange méthane/air Encadré par : Dr R.RENANE (IAES) et Dr R.ALLOUCHE (IAES) Réalisé par : ABDELAZIZ Mourad

[6] : YAKHOT.A ORSZAG S., « Numerical simulation of turbulent flow in the inlet region of a smooth pipe», J. Sci. Comput. (USA), 8, 2, 111 - 21, (1993).

[7] :"Damköhler numbers" Retrieved from https://en.wikipedia.org/wiki/Damk%C3%B6hler_numbers [Accessed: June 14, 2023].

[8] :MOUANGUE RUBEN MARTIN « Contribution à la modélisation de la combustion turbulente non-prémélangée avec prise en compte de l'autoallumage»- thèse de doctorat- 2011

[9] :Ludovic Landry « Etude expérimentale des modes de combustion essence sous forte pression et forte dilution » archives –ouverts

[10] :Cindy Merlin, "Simulation numérique de la combustion turbulente : Méthode de frontières immergées pour les écoulements compressibles, application à la combustion en aval d'une cavité", Institut National des Sciences Appliquées de Rouen, le 8 décembre 2011.

[11] :DENIS VEYNANTE "modélisation et simulation numérique de la combustion turbulente" WWW.idris.fr/docs/journal/pdf_N.3/N3veynam.pdf.

[12] :N. I. Durrani, “Numerical simulations of separated reactive flow using an hybrid RANS-LES approach”, University of Sheffield, March 2009.

[13] :Theodore L. Brown; H. Eugene LeMay, Jr.; and Bruce E. Bursten, “Chapter 14 Chemical Kinetics”, Chemistry, The Central Science, 10th edition, 2006.

[14] :R. Borghi and M. Destriau. "Combustion and flame: chemical and physical principles". Editions Technip, 1998.

[15] :G. Godel, "Modélisation de sous-maille de la combustion turbulente : développement d’outils pour la prédiction de la pollution dans une chambre aéronautique. PhD thèse, INSA de Rouen, 2010.

[16] : thesis: “Numerical Simulation of Methane Turbulent Premixed Combustion with Hydrogen Addition” supervised by : Dr R.RENANE (IAES) et Dr R.ALLOUCHE (IAES) Realized by : OUARMIM Alaa Eddine and AMRATE Soheib.

[17] :Chemtalk, "Enthalpy of Reaction, Formation, and Combustion."

[18] :A. E. Azzouz and L. Aliouat, "Simulation de la combustion turbulente dans une chambre de combustion tubulaire pour le mélange kérosène/air et méthane/air," Blida Saad Dahleb University, 2022.

[19] :Dr. C. Badarinath. “Development of Aero gas turbine Annular Combustor: An Overview”. Combustion group, GTRE, Bangalore – 93.

[20] :Shah RD, Banerjee J (2014) Development of an upward swirl CAN type combustor. Ph. D. thesis. National Institute of Technology Surat; 2014.

[21] :J. J. McGuirk and J. M. L. M. Palma. “Experimental investigation of flow Inside a Water model of a Gas Turbine Combustor : Part 1 – Mean and turbulent flow-field”. Transactions of the ASME, 450 – 458 (117) 1995

[22] :J. J. McGuirk and J. M. L. M. Palma. “Experimental investigation of flow Inside a Water model of a Gas Turbine Combustor : Part 2 - Higher Order moments and flow visualization”. Transactions of the ASME, 459 – 467 (117) 1995

[23] :J. J. McGuirk and J. M. L. M. Palma. “The flow inside a model Gas Turbine Combustor : Calculations”. Transactions of the ASME, 594 – 602 (115) 1993

[24] :Rajpara, P., International Journal of Thermal Sciences (2018), https://doi.org/10.1016/j.ijthermalsci.2017.12.00

[25] :Tomohiko Furuhata, Shunsuke Amano, Kousaku Yotoriyama, Masataka Arai. “Development of can – type low NOx combustor for micro gas turbine

(fundamental characteristics in a primary combustion zone with upward swirl". Fuel 86 (2007) 2463 – 2474. Elsevier.

[26] : Rajpara P, Dekhatawala A, Shah R, Banerjee J (2018) Influence of fuel injection method on performance of upward swirl can-type combustor. Appl Therm Eng 130. https://doi.org/10. 1016/j.applthermaleng.2017.11.017

[27] :Koutmos, P., & McGuirk, J. J. (1989, April 1). Investigation of Swirler/Dilution Jet Flow Split on Primary Zone Flow Patterns in a Water Model Can-Type Combustor. *Journal of Engineering for Gas Turbines and Power*, *111*(2), 310–317. https://doi.org/10.1115/1.3240253

[28] :Gopinath, R., & Ganesan, V. (1994, March). Numerical investigation of the combined effect of swirler and primary jets on the recirculation zone of a can-type combustor by means of an orthogonal array technique. *International Journal of Numerical Methods for Heat & Fluid Flow*, *4*(3), 207–227. https://doi.org/10.1108/eum0000000004039

[29] :Ghenai, C. (2010, January). Combustion of Syngas Fuel in Gas Turbine Can Combustor. *Advances in Mechanical Engineering*, *2*, 342357. https://doi.org/10.1155/2010/342357

[30] : F.H. Pathan, N.K Patel and M.V. Tadvi, ‚Numerical Investigation of the Combustion of the Methane-Air Mixture in Gas Turbine Can-Type Combustion Chamber'. International Journal of Scientific & Engineering Research. Volume 3, Issue10, October-2012 ISSN-2229-5518.

[31] :Shah, R. D., & Banerjee, J. (2015, April 22). Thermal and emission characteristics of a CAN combustor. *Heat and Mass Transfer*, *52*(3), 499–509. https://doi.org/10.1007/s00231-015-1572-9

[32] :F.H. Pathan, N.K Patel and M.V. Tadvi,Comparative analysis of the Combustion in Gas Turbine Can-Type Combustion Chamber'. International Journal of Scientific & Engineering Research. Volume 3, Issue 4, April-2016 e-ISSN: 2393-9877, p-ISSN: 2394-2444.

[33] :Shreekala N, & S. N. Sridhara. (2018, November). Combustion Characteristics In a Can Combustor Fueled with surrogates of Gasoline and Jet-A using Numerical Methods . *International Journal of Pure and Applied Mathematics*, *Volume 119 No. 14 2018, 187-192*.

[34] :ARAI, M., AMANO, S., & FURUHATA, T. (2007). Combustion Characteristics in a Micro Gas Turbine Combustor with a Recirculation Zone Induced by an

Upward Swirl. *Journal of Environment and Engineering*, *2*(1), 124–135. https://doi.org/10.1299/jee.2.124.

[35] :R.D. Shah, J. Banerjee, Development of an upward swirl CAN type combustor, Ph.D. Thesis National Institute of Technology Surat, India, 2014.

[36] :Rajpara, P., Dekhatawala, A., Shah, R. D., & Banerjee, J. (2017, December 27). *COMBUSTION CHARACTERISTICS OF A CAN COMBUSTOR WITH DIFFERENT FUEL INJECTOR CONFIGURATIONS*. ResearchGate. https://www.researchgate.net/publication/322163214_COMBUSTION_CHARACTERISTICS_OF_A_CAN_COMBUSTOR_WITH_DIFFERENT_FUEL_INJECTOR_CONFIGURATIONS.

[37] : Rajpara P, et al., Effect of hydrogen addition on combustion and emission characteristics of methane fuelled upward swirl can combustor, International Journal of Hydrogen Energy (2018), https://doi.org/10.1016/j.ijhydene.2018.07.111.

[38] : Rajpara, P., Shah, R., & Banerjee, J. (2021). Performance Evaluation of Upward Swirl Combustor with Reverse Fuel Injector and Hydrogen Blending. In *Green energy and technology* (pp. 383–410). https://doi.org/10.1007/978-981-16-2648-7_17

[39] :Williams, F. A. (2018, March 5). *Combustion Theory*. https://doi.org/10.1201/9780429494055

[40] : FLUENT 6.2 User Guide. January 2005

[41] :SHASWAT SAINCHER; thesis"Numerical Simulation of Gas Turbine Combustion Chamber (Prelims)", guided by: Mr. RUPESH SHAH; December 2008. DOI: 10.13140/RG.2.2.11285.91360.

[42] :Memoire: Analyse et simulation de la structure de la flamme de diffusion turbulente et son impact sur la paroi d'une chambre de combustion aéronautique Encadré par : Dr R.RENANE (IAES), Dr R.ALLOUCHE (IAES) et Dr S.LAAZAB Réalisé par : MOKHTARI Ahlem.

[43] :Memoire:" Simulation de la combustion turbulente du kérosène et du méthane dans un modèle de chambre de combustion d'un moteur d'avion" Encadré par : Dr R.RENANE (IAES) , Dr R.ALLOUCHE (IAES) et Dr S.LAAZAB Réalisé par : BOUKACEM Abdeslamet NASSAR Abderrahmen.

[44] :Yann MARCHESSE (Mécanique et Energétique) Année universitaire 2009-2010

[45] : DAVID WILCOX C., « Turbulence Modeling for CFD »; DCW Industries, Inc. La Cafiada, California 91011; November 1994

[46] :YAKHOT.A ORSZAG S., Numerical simulation of turbulent flow in the inlet region of a smooth pipe, J. Sci. Comput. (USA), 8, 2, 111 - 21, (1993).

[47] :FLUENT INC. FLUENT12.0 User Guide.

[48] : https://www.afs.enea.it/project/neptunius/docs/fluent/

[49] : MAGNUSSEN B, HJERTAGER BH 16th symposium (int.) on combustion, 719-729, The Combustion Institute, Pittsburgh. (1976).

[50] : Magnussen, B.: On the structure of turbulence and generalized eddy dissipation concept for chemical reaction in turbulent flow. In : Nineteeth AIAA Meeting , St Louis (1981)

[51] : www.abbesazzi.com (Methodes Numeriques Appliquees aux Calculs des Ecoulements et du Transfert de Chaleur)

[52] : Guest. (n.d.). An introduction to computational fluid dynamics - PDF Free Download. *epdf.tips*. https://epdf.tips/an-introduction-to-computational-fluid-dynamics.html

[53] :Serrano, M. I. R. (2016). Computational Fluid Dynamics in Green Design. In *Green energy and technology* (pp. 25–38). https://doi.org/10.1007/978-3-319-45883-0_3

[54] :Dadvand, A., & Motlagh, S. Y. (2022). Introduction on principle of computational fluid dynamics. In *Elsevier eBooks* (pp. 1–26). https://doi.org/10.1016/b978-0-12-822294-2.00006-0

[55] :Xamán, J., Zavala-Guillén, I., Aguilar, J., Álvarez, G., López-Mata, C., & Arce, J. (2014b). Conjugate heat transfer in a room with a laminated glazing with CuS or CuS–Cu2−xSe. *Solar Energy*, *105*, 36–47. https://doi.org/10.1016/j.solener.2014.03.008

[56] :Parabajinkya. (2012, March 27). *Introduction to cfd*. SlideShare. https://www.slideshare.net/slideshow/introduction-to-cfd/12173131

[57] :Andre Bakker, “Lectures on Applied computational fluid dynamics”, 2008.

[58] :M. Bidabadi, H. B. Dizaji, F. F. Dizaji, and S. A. Mostafavi, "A parametric study of Icypodium dust flame."

[59] :M. A. Hossain, "Design of a High Intensity Turbulent Combustion System."

[60] :Wang J, Huang Z, Tang C, Miao H, Wang X (2009) Numerical study of the effect of hydrogen addition on methane–air mixtures combustion. Int J Hydrogen Energy 34. https://doi.org/10. 1016/j.ijhydene.2008.11.010.

[61] :Larsson, A., Zettervall, N., Hurtig, T., Nilsson, E. J. K., Ehn, A., Petersson, P., Alden, M., Larfeldt, J., & Fureby, C. (2017). Skeletal Methane–Air Reaction Mechanism for Large Eddy Simulation of Turbulent Microwave-Assisted Combustion. *Energy & Fuels*, *31*(2), 1904–1926. https://doi.org/10.1021/acs.energyfuels.6b02224.

[62] :Tutorial 15. Using the Non-Premixed Combustion Model Release 12.0 c ANSYS, Inc. March 12, 2009.

[63] :H. K. Versteeg and W. Malalasekera. "An introduction to computational fluid dynamics – The finite volume method ". Longman Scientific and Technical 1995.

[64] :Engineering Nature. (2021, September 14). *ANSYS-Fluent Tutorial|| Species transport modelling || NOx modelling (Methane combustion 2/2)* [Video]. YouTube. https://www.youtube.com/watch?v=eZIE0h-zP6I